Uncovering Wnt signaling mechanisms in control of cell migration in *C. elegans*

Remco A. Mentink

The research described in this thesis was performed at the Hubrecht Institute for Developmental Biology and Stem Cell Research within the framework of the Cancer, Stem Cells and Developmental Biology graduate school of the Utrecht University.

ISBN: 978-90-393-6212-9

Cover: "*C. elegans* wordle" by Remco A. Mentink

Layout: Remco A. Mentink

Printing: Gildeprint - www.gildeprint.nl

Uncovering Wnt signaling mechanisms in control of cell migration in *C. elegans*

Ontdekking van Wnt signalerings mechanismen die
cel migratie in *C. elegans* reguleren
(met een samenvatting in het Nederlands)

Proefschrift

ter verkrijging van de graad van doctor aan de Universiteit Utrecht op gezag van de rector magnificus, prof.dr. G.J. van der Zwaan, ingevolge het besluit van het college voor promoties in het openbaar te verdedigen op woensdag 29 oktober 2014 des middags te 12.45 uur

door

Remco Anton Mentink

geboren op 10 februari 1986
te Apeldoorn

Promotor:

Prof. dr. H.C. Korswagen

Table of contents

Scope of this thesis

The Wnt signaling pathway has important roles during all stages of nervous system development. Wnt ligands have for example recently been shown to act as guidance factors during the migration of neurons and growth cones. The presence of a large number of genetically encoded Wnt ligand and receptor homologues, combined with the ability of Wnts to activate multiple downstream pathways has however complicated research into the specific functions of these proteins. This was an important reason for us to choose to study how Wnt signaling controls cell migration in *Caenorhabditis elegans*, a simplified model organism.

Chapter 1 introduces both the canonical Wnt/ß-catenin pathway and the more recently identified collection of non-canonical Wnt pathways. We will then discuss the role of these respective pathways during nervous system development of vertebrates and *C. elegans*. Special emphasis is put on describing the migration of the QL and QR neuroblasts and their descendants during *C. elegans* L1 development, as this system was our prime subject of study. Additionally we point out one of the burning questions in the Wnt field, which asks how signaling specificity is achieved amongst the various Wnt proteins and the different downstream pathways they activate that may have signaling components in common.

Chapters 2 to 5 contain our experimental work regarding the role of Wnt signaling during cell migration in *C. elegans*. In **Chapter 2** we describe how non-canonical Wnt signaling controls anterior QR.d migration and how the timed expression of *mig-1*/*Fz* is crucial for the activation of a canonical Wnt/ß-catenin pathway that stops migration. Furthermore, we describe a Planar Cell Polarity (PCP)-like pathway that controls the dorsoventral migration of the final QR descendants. In **Chapter 3** we identify a role for the PCP component *vang-1* as a negative regulator of canonical Wnt/ß-catenin in both Q cell lineages. In **Chapter 4** we describe how intricately linked positive and negative transcriptional feedback loops result in the robust activation of *mab-5*/*Hox* expression in the QL lineage. In **Chapter 5** the genetic role of Wnt signaling components in controlling the migration of ALM, HSN, CAN and BDU neurons during embryogenesis is described.

Chapter 6 explains in detail the single molecule Fluorescence *in situ* hybridization (smFISH) protocol that was instrumental in studying how the various Wnt pathways operate during cell migration in *C. elegans* for all experimental chapters. Finally, a summarizing discussion is provided in **Chapter 7**, followed by Addendum I on the role of *lin-17*/*Fz* in shaping the EGL-20/Wnt secretion gradient.

Chapter 1

General introduction

During embryonic development, the tightly controlled patterning of cells, tissues and organs is crucial to shape a functional animal. Furthermore, once a working organ has been formed, it is important to maintain it as such throughout the animal's life. The Wnt signal transduction pathway is one of the major developmental signaling pathways that may orchestrate these events. Wnts are secreted lipid-modified glycoproteins that may either act as short range signaling molecules or function as morphogens in longer distance secreted gradients that inform cells in developing tissues about their respective positions (Alexandre et al., 2014; Cadigan and Nusse, 1997; Zecca et al., 1996). Wnt signaling has major roles during processes such as gastrulation, neural tube formation and anteroposterior axis specification and may control stem cell maintenance, cell fate and proliferation (Niehrs, 2010; van Amerongen and Nusse, 2009; Wend et al., 2010). Deficits in Wnt signaling during embryogenesis may lead to a wide range of developmental defects (Sugimura and Li, 2010). Moreover, malfunction of the Wnt pathway during adult life has been implicated in human disease, such as colon cancer or melanoma, as well as neurodegenerative diseases (Clevers and Nusse, 2012; Polakis, 2012).

Initial clues indicating that Wnt signaling could have such a dramatic influence on animal development and disease came with the discovery of the first Wnt genes. In 1982 it was found that the MMTV retrovirus, when integrated at a specific locus in the genome, causes mammary carcinomas to develop in mice through activation of a proto-oncogene termed *Integrated 1* (*Int1*) at the time (Nusse and Varmus, 1982). Around the same time genetic screens were performed in *Drosophila* embryos with the goal to identify mutants harboring patterning defects. This led to the identification of a group of mutants affecting segment number and polarity such as *armadillo, arrow* and *wingless* (Nusslein-Volhard and Wieschaus, 1980). Later, it was discovered that both *Int1* and *wingless* belonged to a family of evolutionarily conserved, extracellularly secreted signaling molecules (Rijsewijk et al., 1987). These gene family members were then renamed "Wnt" genes, referring to both founding members. A receptor for the secreted Wnt ligands was long sought after, but was finally identified in the seven-pass transmembrane Frizzled (Fz) proteins (Bhanot et al., 1996; Sawa et al., 1996). Fz's appeared to be part of a large and conserved gene family as well and posses an extracellular cysteine-rich domain (CRD) which is used for the interaction with Wnt (Janda et al., 2012; Wang et al., 1996). After these discoveries, the families of Wnt and Fz proteins expanded as members were identified in all multicellular animals, representing an ancient feature of animal development (Niehrs, 2010).

Wnt signaling can be recognized as inherently complex with 19 Wnts and 10 Frizzleds making up the vertebrate gene families. The amount of possible receptor-ligand interactions therefore becomes bewildering (Kikuchi et al., 2009). To add to this complexity, there is a range of different downstream signaling cascades that can be initiated by Wnt signaling. These responses are broadly categorized as "canonical" and "non-canonical" Wnt signaling pathways. The canonical pathway is the most thoroughly studied and uses the co-receptor LRP5/6, together with Fz, to allow for stabilization of ß-catenin, which subsequently complexes with DNA-binding TCF proteins to elicit downstream transcriptional activity (Clevers and Nusse, 2012). Non-canonical Wnt signaling comprises any pathway that does not involve ß-catenin and may lead to a wide range of cellular responses, among which are the activation of intracellular calcium fluxes, Jnk or Src kinases and members of small GTPase families (Angers and Moon, 2009). Non-canonical signaling does not require LRP5/6, but may use alternative Wnt (co)-receptors such as Ror or Ryk to transduce downstream

signaling (Clark et al., 2012).

Originally, a distinction between canonical or transforming Wnts (e.g. Wnt1, Wnt3A and Wnt8) and non-canonical or non-transforming Wnts (e.g. Wnt4, Wnt5A and Wnt11) was made, based on their ability to induce formation of an ectopic axis in *Xenopus* embryos or to act as oncogenes (McMahon and Moon, 1989; Shimizu et al., 1997). This led to the idea of categorized Wnt signaling pathways having their own distinct signaling outcomes. More recently, however, it has become clear that the downstream pathway that is activated by specific Wnts is dependent on the receptors that are currently expressed by the receiving cell (van Amerongen et al., 2008). For example, the classical non-transforming Wnt5A may activate canonical Wnt/ß-catenin signaling *in vitro* if LRP5/6 and Fz4 receptors are over expressed upon treatment with recombinant protein (Mikels and Nusse, 2006).

One of the developmental processes that may benefit from all facets of Wnt signaling outcomes is the complex wiring of the central nervous system (CNS) and the brain. On a large scale, Wnts are involved in defining the anteroposterior axis of the nervous system as well as regulating the closure of the neural tube and migration of neural crest cells (Kiecker and Niehrs, 2001; Matthews et al., 2008; Wallingford and Harland, 2002). And on a smaller scale, Wnt signaling regulates neuronal polarity, neural cell fate specification, as well as axonal guidance, neuronal migration and synapse formation (Castelo-Branco et al., 2003; Hall et al., 2000; Lyuksyutova et al., 2003; Vivancos et al., 2009). Wnts function chiefly as specification and guidance factors along the anteroposterior axis. This is consistent with their differential expression pattern across this very axis that is highly conserved across the animal kingdom (Petersen and Reddien, 2009).

Here, I will first discuss the canonical and non-canonical Wnt signaling pathways and subsequently their respective roles in nervous system development. I will focus on those aspects of Wnt signaling that regulate anteroposterior specification of the nervous system, as well as the guidance of axons, commissures and cell migrations required for formation and wiring of the neural network. Subsequently, I will discuss the conservation of these processes in the small nematode *C. elegans*, our model organism of choice for the study of Wnt signaling in neuronal migration.

The canonical Wnt/ß-catenin pathway

The output of the canonical Wnt pathway consists exclusively of transcriptional responses. Some of the processes it is involved in are cell proliferation, differentiation and stem cell self-renewal (Clevers and Nusse, 2012). In the absence of Wnt ligands, cytoplasmic ß-catenin is engaged by a destruction complex of scaffold proteins adenomatous polyposis coli (APC) and Axin, which promote the constant phosphorylation of ß-catenin by the serine-threonine kinases GSK3ß and CK1α/δ (Amit et al., 2002; Liu et al., 2002; Yanagawa et al., 2002). Phosphorylation occurs at a so-called “phosphodegron” site that is recognized by the F-box protein ß-TrCP, which in turn recruits an E3 ubiquitin ligase complex. Subsequent ubiquitination of ß-catenin and targeting to the proteasome leads to its rapid degradation, preventing any transcriptional activity (Figure 1A) (Aberle et al., 1997).

When Wnt binds to its receptor Fz and co-receptor LRP5/6, the destruction complex dissociates and degradation of ß-catenin is inhibited (Figure 1A). The exact mechanism of destruction complex inhibition is uncertain and currently several models exist to describe this phenomenon. One model describes that upon Wnt binding the cytoplasmic scaffold

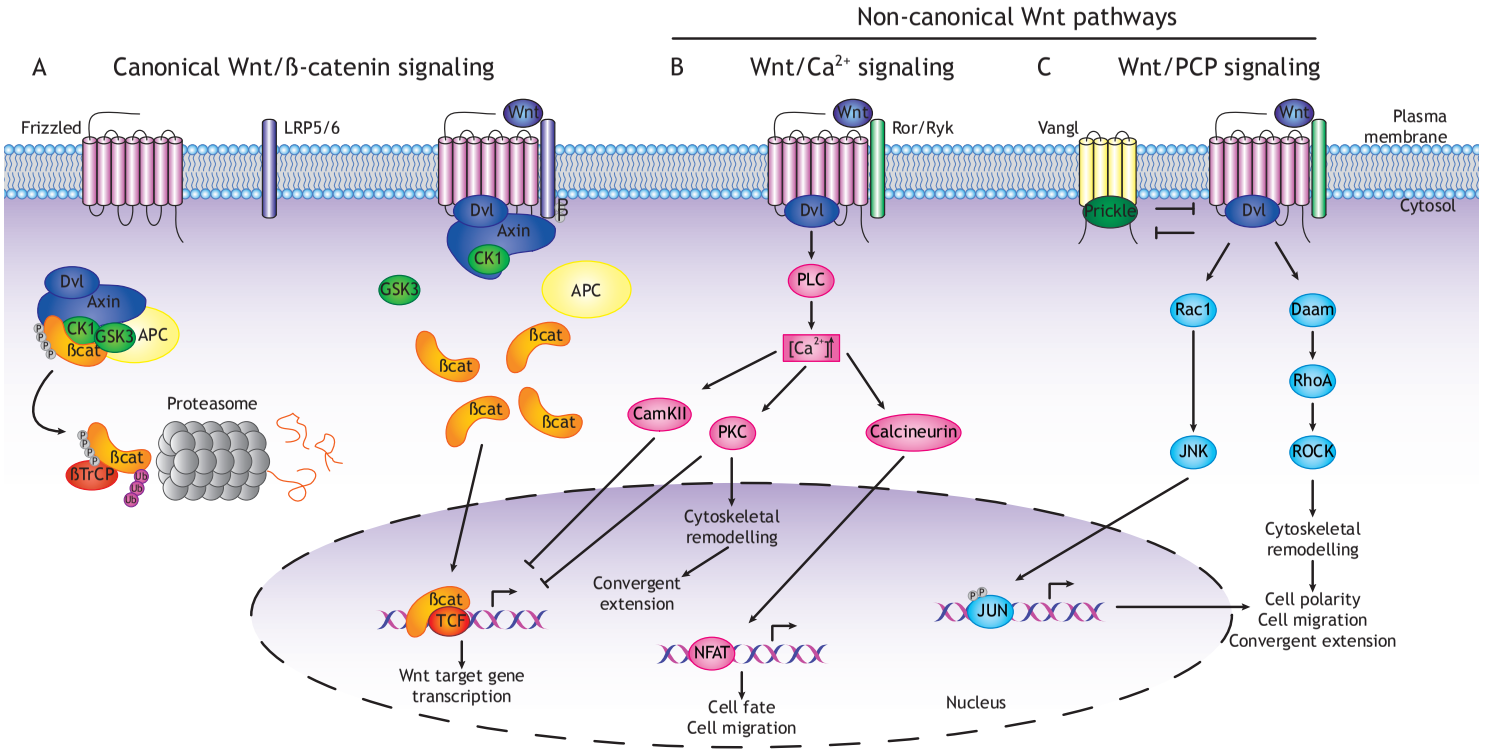

Figure 1. Schematic overview of both canonical and non-canonical Wnt signaling pathways. (**A**) The canonical Wnt/ß-catenin pathway: In the absence of Wnt, ß-catenin is bound to the destruction complex consisting of scaffold proteins APC and Axin and phosphorylated by kinases CK1 and GSK3ß. This leads to binding of E3 ubiquitin ligase ßTrCP to ß-catenin and its subsequent ubiquitination and proteasomal degradation. When Wnt binds to plasma membrane receptor Frizzled and co-receptor LRP5/6, the destruction complex is inhibited through sequestration by Dishevelled, which allows ß-catenin to accumulate and translocate to the nucleus, where it initiates target gene transcription. (**B, C**) Non-canonical Wnt/Ca^{2+} and Wnt/PCP signaling: Wnt binds to plasma membrane receptor Frizzled and/or co-receptors Ror or Ryk to initiate signaling via the cytoplasmic protein Dishevelled. Downstream responses are varied and often involve the activation of different kinases, such as JNK, PKC, CamKII or ROCK to for example modulate the cell cytoskeleton or influence transcription of target genes.

protein Disheveled (Dvl) is recruited to the plasma membrane and binds the Fz-LRP5/6 receptor complex. This leads to clustering of the receptors and the recruitment of Axin and GSK3β, which promotes LRP5/6 phosphorylation and internalization of the receptor-scaffold complexes in so-called "signalosomes" (Bilic et al., 2007). The destruction complex now no longer targets β-catenin for degradation and it is allowed to accumulate in the cytoplasm. Subsequently, it translocates to the nucleus, where it initiates target gene transcription together with the transcription co-factor TCF (Buechling and Boutros, 2011). More recently, a model has been proposed where β-catenin remains associated with the destruction complex, but ubiquitination is inhibited by plasma membrane recruitment. This sequesters all components away from the cytoplasm, allowing newly synthesized β-catenin to accumulate and translocate to the nucleus (Li et al., 2012).

An interesting feature of canonical Wnt signaling is that many of its constituent components are also themselves target genes of the pathway, either by up- or downregulation (Logan and Nusse, 2004). For example, one of the best-described direct target genes in vertebrates is Axin2, a negative regulator of the pathway that is upregulated in response to Wnt signaling and is now used as a general indicator of pathway activity (Clevers and Nusse, 2012; Jho et al., 2002). Self-targeting by transcriptional regulation indicates that the modulation of pathway output by feedback mechanisms is a key feature of canonical Wnt signaling (Logan and Nusse, 2004).

Non-canonical Wnt signaling pathways

Non-canonical Wnt pathways do not involve the protein β-catenin and may elicit both transcriptional and non-transcriptional responses in cells. Furthermore, in contrast to the co-receptor LRP5/6, alternative Wnt receptors Ror and Ryk may be engaged for downstream signaling (Niehrs, 2012). The best-described non-canonical pathways are the Wnt/PCP and the Wnt/Ca^{2+} pathways, which have major roles in the regulation of cell and tissue polarity (Clark et al., 2012).

Wnt/Ca^{2+} signaling

Ca^{2+} functions as a second messenger in Wnt signaling pathways that control cell fate, migration and axon guidance (Clark et al., 2012). It was originally identified by the effect of Wnt5A on intracellular Ca^{2+} fluxes in developing zebrafish embryos (Slusarski et al., 1997). Briefly, binding of Wnt to Fz may activate phospholipase C through Dvl, which results in the production of diaceylglycerol (DAG) and IP_3 from phosphatidylinositol 4,5-bisphosphate (PIP_2), in turn leading to Ca^{2+} fluxes within the cell. Ca^{2+} sensing proteins such as calcium calmodulin kinase II (CAMKII), calcineurin and protein kinase C (PKC) may then be activated, resulting in downstream signaling (Figure 1B) (De, 2011). One of the described consequences of Wnt/Ca^{2+} signaling involves activation of the transcriptional regulator nuclear factor associated with T cells (NFAT), a pathway that is involved in cancer, inflammation and neurodegeneration (De, 2011). Furthermore, at a cytoskeletal level, local increases in Ca^{2+} concentration may stimulate the formation of actin fibers, leading to filopodial protrusion formation (Lau et al., 1999).

Downstream events in the Wnt/Ca^{2+} signaling pathway in *Xenopus* provide an illustrative example of Wnt pathway crosstalk. In this model system, canonical Wnt/β-catenin signaling is required for proper CE, as it activates transcription of Xnr-3, a protein that modulates

cell migration (Kuhl et al., 2000). It was demonstrated that the Ca^{2+} pathway may inhibit CE movements by blocking canonical signaling, a process that occurs via the Dvl protein (Kuhl et al., 2000). In Ca^{2+} signaling Dvl is required for PKC activation, yet PKC in turn phosphorylates Dvl, making it unavailable for Wnt/ß-catenin signaling. Furthermore, Dvl activates CAMKII, which functions to inhibit TCF mediated transcription (Kuhl et al., 2000). Dvl thus functions as a hypothetical switch between the two pathways, modulated by its phosphorylation status.

Dvl's switch-like behavior between these two Wnt signaling cascades indicates that it may act as an important mediator between different responses downstream of Wnt (Gao and Chen, 2010). We have already seen that Dvl is involved in Wnt/ß-catenin, Wnt/PCP and Wnt/Ca^{2+} signaling, making it an ideal mediator of crosstalk between the pathways. Furthermore, its three distinct domains (DEP, DIX and PDZ) facilitate interactions with a wide range of intracellular components, which can result in activation of specific signaling outcomes (Gao and Chen, 2010). For example, the DIX domain mediates Dvl polymerization and localization to intracellular punctae, a process that is crucial for Wnt/ß-catenin signaling (Schwarz-Romond et al., 2005; Smalley et al., 2005). In contrast, a Dvl lacking the DIX domain is sufficient to activate both Wnt/PCP and Wnt/Ca^{2+} signaling (Sheldahl et al., 2003; Tada and Smith, 2000). Specificity could be achieved by different upstream Wnt signals activating distinct parts of the Dvl protein to elicit a particular downstream response (Gao and Chen, 2010).

Wnt/PCP signaling

Planar Cell Polarity (PCP) signaling was originally identified in *Drosophila* and regulates the adopted polarity of cells in an epithelial sheet, for example during the establishment of wing hair polarity in the developing fly wing. An analogous mechanism is required in vertebrates to regulate convergence and extension (CE) during embryonic gastrulation and neural tube closure (reviewed in Roszko et al., 2009). PCP signaling requires communication between neighboring cells and is not exclusively mediated by intracellular mechanisms. Upon the establishment of PCP in the fly wing epithelium, the proximal and distal sides of the cell are polarized through the differential localization of the two PCP core complexes. On the proximal side, Prickle (Pk) is recruited to the membrane by Strabismus/Van Gogh (Vang) and antagonizes the membrane recruitment of Dsh (Disheveled in invertebrates) by Fz (Jenny et al., 2003; Tree et al., 2002). On the distal side, a complex is formed between Fz, Dsh and Diego (Dgo, Diversin in vertebrates), a cytoplasmic component that promotes Fz-Dsh binding (Feiguin et al., 2001). Finally, the atypical cadherin Flamingo (Fmi) localizes to both ends of the cell and promotes asymmetry between the two complexes (Chen et al., 2008; Usui et al., 1999). Both in flies and vertebrates, signaling can be abrogated by either gain or loss of different PCP components, emphasizing the molecular balance that is required between the different factors (Adler, 2002; Goto and Keller, 2002; Jessen et al., 2002; Strutt, 2003). In vertebrates, no complete picture yet exists in any one tissue that describes the exact localization and interactions of all core components. However, some examples do exist that hint at similar localization patterns as can be found in flies. These include the asymmetric localization of Dvl to the posterior of mesodermal cells undergoing CE in *Xenopus* and the anterior localization of Vangl1 and Pk2 versus the posterior localization of Dvl2 and Dvl3 in the mouse node (the LR asymmetry organ) (Antic et al., 2010; Hashimoto and Hamada, 2010).

The upstream events that coordinate global localization of PCP components are still not well known. Remarkably, in flies there has been no convincing evidence showing that Wnts are involved (Chen et al., 2008). On the contrary, in vertebrates Wnt5A and Wnt11 have been shown to function in PCP signaling during CE (Heisenberg et al., 2000; Wallingford et al., 2001). Downstream signaling involves the recruitment of Dvl to the cytoplasmic domain of membranous Fz. At the plasma membrane Daam1, a formin homology domain-containing adaptor, mediates the interaction of Dvl with the small Rho GTPase RhoA (Figure 1C) (Habas et al., 2001). Dvl and Daam1 interact with WGEF (weak-similarity GEF) to activate RhoA, which in turn activates ROCK kinase, leading to the formation of actin stress fibers (Habas et al., 2001). Cytoskeletal rearrangements that occur via the regulation of actin dynamics may influence cellular polarity and migration. Dvl may also activate a different Rho GTPase, Rac1. Activation of Rac1 stimulates c-Jun N-terminal kinase (JNK), which may regulate cell polarization and movement during for example *Xenopus* gastrulation (Figure 1C) (Habas et al., 2003). The effects of JNK activation during CE are most likely mainly mediated transcriptionally, via its phosphorylation of transcription factors c-Jun or ATF2 (Lyu and Joo, 2005; Ohkawara and Niehrs, 2011; Park and Moon, 2002; Schambony and Wedlich, 2007).

Wnt/Ror signaling

Rors are evolutionarily conserved, single-pass transmembrane receptor tyrosine kinases that contain an extracellular immunoglobulin (Ig), CRD (similar to the Fz Wnt binding domain) and Kringle (Kg) domain. Intracellularly, they posses a tyrosine kinase (TK) domain (Green et al., 2008b). Vertebrate genomes code for two Ror receptor homologues, Ror1 and Ror2, yet the function of the Ror2 homologue is best described (Green et al., 2008b). The mouse Ror2 homologue is one of the few Ror receptors for which catalytic activity has been demonstrated (Kani et al., 2004; Mikels and Nusse, 2006).

Rors have been demonstrated to function in multiple Wnt-dependent pathways, often having mechanistically distinct effects in signal transduction. It has therefore been difficult to generally define signaling components downstream of Ror signaling (Green et al., 2008b; Petrova et al., 2014). In mice, the main ligand for Ror2 signal transduction is Wnt5A. The gross morphological phenotypes of both *Ror2* and *Wnt5A* mutant mice are very similar, displaying facial abnormalities, dwarfism and shortened limbs (Takeuchi et al., 2000; Yamaguchi et al., 1999).

Evidence from *Xenopus* shows that Wnt5A and Ror2 interact and function in a common pathway to activate JNK in order to regulate CE, a Wnt/PCP process (Hikasa et al., 2002). This is corroborated by studies performed in mouse fibroblasts (MEFs), which show that Ror2 and Wnt5A, but not Wnt3A, physically interact and synergistically activate JNK (Oishi et al., 2003). However, subsequently it was demonstrated that this Wnt5A-Ror2-JNK pathway in *Xenopus* functions separately of the Wnt11/PCP mediated CE movements (Schambony and Wedlich, 2007). Moreover, a recent study where they simultaneously knocked out Ror1 and Ror2 in mice, shows that Wnt5A may activate JNK in the absence of any Ror receptor. These same authors found that the double Ror knockout has no neural tube closure defects, such as can be seen in *Vangl1*; *Vangl2* double knockouts (Ho et al., 2012). The role of Ror2 in PCP signaling therefore seems inconsistent and may depend on the cellular contexts involved.

In vitro studies have provided insight into the Ror2 signaling mechanism. Wnt5A binding to Ror2 may induce its homodimerization or formation of a heterodimeric complex with Fz receptors (Grumolato et al., 2010; Liu et al., 2008; Sato et al., 2010). Ror2 is then activated

by GSK3ß mediated phosphorylation, which leads to phosphorylation of Dvl by CK1ε and further downstream events (Kani et al., 2004; Nishita et al., 2010; Witte et al., 2010; Yamamoto et al., 2007). Ror2 may also associate with the actin binding protein filamin A, which leads to filopodia formation by cytoskeletal rearrangements. Binding to filamin A, together with JNK activation, is required for Wnt5A mediated formation of lamellipodia and cell migration (Nishita et al., 2006; Nomachi et al., 2008). Indeed, Wnt5A/Ror2 signaling promotes metastasis of melanoma cells and stimulates migration of primordial germ cells during mouse embryonic development (Lai et al., 2012; Laird et al., 2011; O'Connell et al., 2010).

In addition to its effects on PCP signaling and cell migration, Ror2 may modulate the Wnt/ß-catenin pathway. Wnt5A and Ror2 inhibit canonical signaling at the receptor level by competing for Fz receptors, preventing their interaction with Wnt3A and LRP5/6 (Grumolato et al., 2010; Sato et al., 2010). Wnt5A/Ror2 signaling may also directly inhibit canonical signaling at the transcriptional level (Mikels and Nusse, 2006). Remarkably, the *C. elegans* homologue of Ror2, CAM-1, sequesters Wnts to dampen signaling output in order to regulate vulval patterning and cell migration during development (Green et al., 2007; Kim and Forrester, 2003; Modzelewska et al., 2013).

Wnt/Ryk signaling

Similar to Ror, Ryk is a single-pass transmembrane tyrosine kinase receptor, which was originally identified in *Drosophila* for its role in axon guidance in the nerve cord (Yoshikawa et al., 2003). Another feature that Ryk shares with the Ror receptor is its involvement in many different Wnt signaling pathways (Niehrs, 2012). Ryk is known to function in Wnt/ß-catenin, Wnt/PCP and Wnt/Ca^{2+} pathways (Li et al., 2009; Lu et al., 2004; Macheda et al., 2012). In contrast to Ror though, the tyrosine kinase domain of Ryk is non-functional due to several amino acid substitutions (Clark et al., 2012). Yet it might still be able to transduce a phosphorylation signal due to its interaction with Src tyrosine kinases (Wouda et al., 2008).

Although Ryk signaling has mainly been studied in the context of nervous system development, as it has been implicated in axon guidance, neural tube closure, neural cell fate specification and neuron migration (Kamitori et al., 2005; Kim et al., 2008; Lu et al., 2004; Zhong et al., 2011), it most likely has roles outside of the nervous system as well. Ryk is expressed in many developing tissues and mice that are mutant for Ryk show skeletal malformations and cardiac defects (Andre et al., 2012; Halford et al., 2000). In addition, in the *C. elegans* ventral epithelium, the Ryk orthologue LIN-18 controls the polarity of the P7.p vulval precursor cell to regulate proper vulva development (Green et al., 2008a).

Wnt signaling in vertebrate nervous system development

Development of the central nervous system (CNS) is a highly coordinated process during which different regions of the brain and spinal cord are shaped and specified and innumerable connections are formed by neurons through the guidance of their projected processes and subsequent formation of synaptic contacts. Wnt signaling has been implicated in all steps of CNS development studied to date and has important functions in anteroposterior specification and guidance (Mulligan and Cheyette, 2012). Below the mechanisms of Wnt signaling required for specification and formation of the neural tube, as well as for growth cone and neuronal cell migration will be discussed.

Canonical Wnt signaling controls anteroposterior specification of the neural plate

The primary event in CNS development is the specification of neural tissue from ectodermal tissue, which leads to the formation of the neural plate, the basis of the vertebrate nervous system (Mulligan and Cheyette, 2012).

Studies performed in *Xenopus* showed that Wnt signaling has a key role in the proper specification of the anteroposterior axis of the neural plate. Ectopic expression of Wnt3A or β-catenin in *Xenopus* animal caps leads to the induction of posterior neural markers and inhibition of anterior neural markers (McGrew et al., 1995). In an opposite experiment, expression of a dominant negative Wnt8 suppresses the emergence of posterior neural markers (Bang et al., 1999; McGrew et al., 1997). In zebrafish, loss of the transcriptional repressor of canonical Wnt signaling Tcf3, as it occurs in the *headless* mutant, leads to a complete lack of anterior neural structures such as eyes and forebrain (Kim et al., 2000). These findings suggested a gradient of Wnt activity during specification of the neural plate that is high posteriorly and low anteriorly. Indeed, later it was shown that increasing doses of Wnt8 protein induce progressively posterior neural fates in *Xenopus* animal cap explants and that the amount of nuclear β-catenin declines from posterior to anterior (Kiecker and Niehrs, 2001).

To achieve a posterior high to anterior low Wnt signal, it is crucial that signaling activity is inhibited from the anterior. Loss of anterior expression of the secreted Wnt inhibitor Dickkopf1 (Dkk1) in *Xenopus* results in posteriorization of neural fates (Glinka et al., 1998; Kazanskaya et al., 2000). Conversely, overexpression of Dkk1 has potent head-inducing activity and suppresses the Wnt signal (Glinka et al., 1998). Moreover, the anteriorly expressed transmembrane protease Tiki1 is required for head formation in *Xenopus*, as it truncates Wnt ligands N-terminally, strongly reducing their receptor binding affinity (Zhang et al., 2012). Further evidence of anterior Wnt inhibition comes from zebrafish and chicken, where a strong case has been made for the requirement of Wnt antagonistic Secreted Frizzled proteins (Sfrps) during anterior neural tube specification (Figure 2) (Esteve et al., 2000; Houart et al., 2002).

From these results it can be concluded that Wnt inhibition in the anterior and Wnt activation in the posterior are critical for the proper specification of the neural tube and thus CNS development. A comparison across the different animal phyla learns that posterior Wnt expression and anterior expression of Wnt inhibitors such as Dkk and Sfrp is a highly conserved phenomenon, which controls anteroposterior axis specification in organisms ranging from sea anemones to vertebrates (Petersen and Reddien, 2009).

Neural tube formation is controlled by Wnt/PCP signaling

The second major event in CNS development is the formation of the neural tube by a well-coordinated series of cell movements. During neurulation, cells from the overlying neural plate and epidermis, as well as the underlying mesoderm migrate inwards from dorsolateral regions towards the dorsal midline. The neural plate folds in on itself while lengthening and narrowing by a CE process, decreasing the amount of cell layers through cell intercalation. Finally, the dorsal tips of the folded tissue approach the midline and fuse, which results in neural tube closure (Figure 2) (Keller et al., 2000). The Wnt/PCP pathway controls the mediolateral directionality and polarity of the migrating cells (Roszko et al., 2009). Abrogation of the PCP pathway prevents migration towards the dorsal midline and subsequent cell intercalation, causing the neural tube to remain open, a root cause

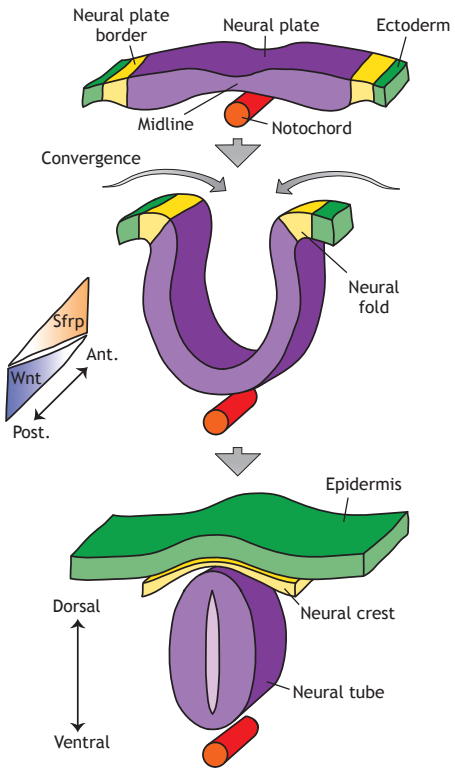

Figure 2. Schematic representation of the major morphological events leading to formation of the neural tube during vertebrate embryonic development. Specification of the neural plate (purple) from the ectoderm (green) requires a posterior high to anterior low gradient of Wnt activity. This is achieved by secretion of Wnt ligands from the animal posterior, while Wnt antagonists, such as Secreted Frizzled (Sfrp) or Dickkopf1 (DKK1), are secreted from the animal anterior. The neural plate is separated from the ectoderm by the neural plate border (yellow). Factors secreted by the notochord (red) induce the neural plate to fold in on itself, joining its two ends (now called neural crest) on the dorsal side. The neural plate detaches from the ectoderm to form the neural tube. The neural crest cells will specify different components of the nervous system later in development. In Wnt/PCP mutants, a defect in cell intercalation and migration leads to a broadened neural plate midline area, which results in a failure of the dorsal folds to join together and causes the neural tube to remain open.

of congenital defects such as anencephaly, spina bifida or craniorachischisis (Copp, 2005).

In *Xenopus* and zebrafish, a core PCP pathway driven by the activity of non-canonical signaling through Wnt5a/Wnt11 and Fz3/Fz7 to downstream effectors Dvl and GTPases RhoA and Rac affects cytoskeletal arrangements and mediolateral cell polarity, resulting in directed CE movements and neural tube closure (Djiane et al., 2000; Heisenberg et al., 2000; Kilian et al., 2003; Wallingford et al., 2000). Vang and Pk are involved as well and it is suggested that by removal of membranous Dvl, mediated through Pk, they counteract Dvl-induced GTPase activity and thereby fine-tune the cellular control over filopodial extensions and polarity (Carreira-Barbosa et al., 2003; Roszko et al., 2009; Takeuchi et al., 2003). Vang and Pk are also known to activate the downstream PCP effector JNK, which may regulate transcriptional responses (Park and Moon, 2002; Veeman et al., 2003).

In mammals, mutating PCP pathway homologues may lead to failure of neural tube closure. Mice that harbor mutations in core PCP genes such as *Vangl2*, *Celsr1*/*Fmi*, *Dvl1; Dvl2* double mutants and *Fz3* or *Fz6* all display varying degrees of neural tubes that remain open at the hindbrain and spinal cord levels, also known as craniorachischisis (Curtin et al., 2003; Etheridge et al., 2008; Kibar et al., 2001; Wang et al., 2006). In humans, DNA sequencing revealed that mutations in *Vangl1* and *Vangl2* are linked to neural tube defects (Kibar et al., 2007; Lei et al., 2010). These results provide compelling evidence that a PCP pathway is operating to regulate CE movements during neural tube closure in mammals.

In the mammalian inner ear, correct hair bundle orientation on sensory cells is regulated by PCP signaling. Several studies have shown that PCP components such as Vangl2, Fz3

and Fz6 are asymmetrically localized in hair cells and that this distribution is lost in PCP pathway mutants (Montcouquiol et al., 2006; Wang et al., 2006). Whether similar patterns of localization operate during neural tube closure remains to be established.

Wnts guide the migration of neurons in vertebrates

Following the initiating events of neural plate specification and neural tube formation, development of the mature CNS also requires guidance of neurons and growth cones to their correct destinations in order to set up an intricately wired, functional neuronal network. Secreted long- or short-range guidance cues establish concentration gradients along the path of migration to indicate directionality. Interaction of guidance cues with membrane-bound guidance receptors may trigger intracellular signaling cascades that rearrange the cytoskeleton, causing the cell or growth cone to move in the right direction, up or down the gradient (Song and Poo, 2001). Many different guidance cues have been described, and it is now clear that the family of secreted Wnt ligands also displays potent guidance activity.

The best-described example of Wnt-directed neuronal migration in vertebrates can be found in the hindbrain, where facial branchiomotor (FBM) neurons migrate across a neuroepithelium in a caudal direction between different rhombomeres (Chandrasekhar et al., 1997). Components of the Wnt/PCP pathway such as Vang, Pk, Fz and Celsr/Fmi are required for migration of the FBM neurons to their normal extent in zebrafish (Bingham et al., 2002; Carreira-Barbosa et al., 2003; Jessen et al., 2002; Wada et al., 2006). PCP signaling functions cell autonomously in FBM neurons, yet also acts to correctly polarize the neuroepithelium across which these neurons migrate (Jessen et al., 2002; Wada et al., 2006; Walsh et al., 2011). Apparently, FBM neurons use two different modes of migration; one involving interactions between the neurons and their planar-polarized environment, the other being a collective mode of migration, involving interactions amongst the neurons themselves (Walsh et al., 2011).

In mice, FBM neuron migration is similarly regulated by Wnt/PCP signaling. It was found that Wnt7A and Wnt5A regulate migration and that Wnt5A is expressed in a caudal high, rostral low gradient (Vivancos et al., 2009). Application of Wnt5A-coated beads to hindbrain explants demonstrated its function as a chemo attractant (Vivancos et al., 2009). Remarkably, in *Celsr1/Fmi* mutant mice a subset of FBM neurons migrates rostrally, where a lower amount of the Wnt5A chemo attractant is expressed (Qu et al., 2010). Rostral migration is suppressed when either *Vangl2* or *Dvl2* is disrupted, indicating that PCP signaling can modulate the sensitivity to the Wnt chemo attractant (Glasco et al., 2012).

Wnts guide growth cone migrations in vertebrates

Wnt signaling also has an important function in directing the outgrowth of neurites during CNS development. A prime example of this is found in the mammalian spinal cord, where Wnts control the migration of growth cones along the corticospinal tract (CST) and the ascending somatosensory tract (Figures 3A and 3B) (Clark et al., 2012).

In the embryonic vertebrate spinal cord, somatosensory commissural neurons located near the dorsal roof plate initially project axons ventrally towards the floor plate, which then turn and cross the midline. On the opposite lateral side the axons turn anteriorly and migrate towards their destinations in the brain. A Wnt signaling pathway acting through Wnt4 and Fz3 controls the anterior turning of these post-crossing commissural axons (Figure 3A) (Lyuksyutova et al., 2003). Wnt4 is expressed in the spinal cord floor plate in an anterior

high to posterior low gradient and acts as an instructive chemo attractant cue. Application of recombinant Wnt4 protein in an open book spinal cord explant assay showed that commissural axons turn towards the applied Wnt4 source (Lyuksyutova et al., 2003). Mutants for *Fz3* showed a random orientation of post-crossing axons, indicating that Wnt4 might use Fz3 as its receptor (Lyuksyutova et al., 2003). Downstream of Wnt4 and Fz3 a Wnt/Ca^{2+} pathway is activated, which requires the catalytic activity of PKC and Phosphatidylinositol-3-Kinase (PI3K) (Wolf et al., 2008). An interesting finding is that, whereas blocking PI3K catalytic activity resulted in random axon orientation, overexpressing active PI3K resulted in precocious turning of pre-crossing axons, indicating that PI3K might function as a switch to activate responsiveness to Wnt signaling (Wolf et al., 2008). Anterior turning of commissural axons is also controlled by Wnt5a signaling, which is similarly expressed in an anterior high to posterior low gradient (Shafer et al., 2011). A PCP pathway is activated when Wnt5a binds to Fz3, which leads to internalization of Fz3 and subsequent activation of JNK via Dvl (Shafer et al., 2011). Fz3 endocytosis is regulated by its level of phosphorylation. A negative feedback loop driven by Dvl1 increases Fz3 phosphorylation and prevents Fz3 internalization. Vangl2 counteracts Dvl1 activity and decreases Fz3 phosphorylation levels (Shafer et al., 2011). Interestingly, Vangl2 is localized specifically to the tips of filopodia and areas of the plasma membrane where filopodia will emerge in commissural growth cones. This suggests that Vangl2 may cell autonomously and locally promote Fz3 induced actin dynamics (Shafer et al., 2011).

The role of Wnt signaling in the anterior turning of commissural axons clearly shows that Wnts can function as bona fide chemo attractants. Evidence also exists however,

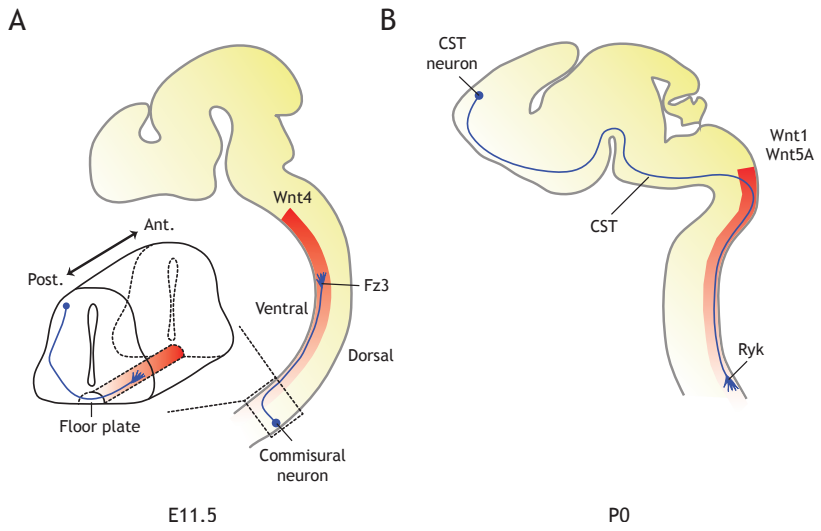

Figure 3. Schematic overview of Wnt directed axonal guidance during mouse spinal cord development. (**A**) Somatosensory commissural neurons located on the dorsal roof plate of the spinal cord send out their growth cones ventrally to eventually cross the midline near the floor plate. On the opposite lateral side the growth cones turn anteriorly and are guided by a Wnt signaling pathway operating via Wnt4 and receptor Fz3. The growth cones migrate up an attractive anterior high to posterior low Wnt4 expression gradient. (**B**) Pyramidal corticospinal tract (CST) neurons reside in the neocortex of the brain and send out growth cones posteriorly along the CST. In the spinal cord the growth cones pass a domain with high Wnt1 and Wnt5A expression, after which they are guided further posteriorly by repulsive anterior high to posterior low Wnt expression gradients. The repulsive signal is transmitted via the alternative Wnt receptor Ryk.

that demonstrates a role for Wnt ligands as chemo repellants, which appears to be mainly mediated through the alternative Wnt receptor Ryk (Clark et al., 2014). Ryk was first discovered to function as a chemo repulsive guidance receptor in the *Drosophila* embryonic CNS. The *Drosophila* ventral nerve cord consists of two parallel axon tracts that connect via an anterior and posterior commissure. The *Drosophila* Ryk orthologue *derailed* (*Drl*) is expressed in neurons that project axons through the anterior commissure. In *derailed* mutants, however, axons are projected through the posterior commissure as well (Bonkowsky et al., 1999). *Wnt5* is expressed only in this region and acts as a chemo repellant through the *Drl* receptor, preventing axon entrance (Yoshikawa et al., 2003).

In the murine spinal cord, Ryk mediates the descent of axons along the CST, which originate from pyramidal corticospinal neurons in the neocortex (Figure 3B) (Liu et al., 2005). The pyramidal neurons first send their axons sub cortically, after which they travel posteriorly to the hindbrain and finally project into the spinal cord (Canty and Murphy, 2008). Further guidance of CST axons down the spinal cord is mediated by chemo repellants Wnt1 and Wnt5A, which signal through the Ryk receptor (Liu et al., 2005). *Wnt1* and *Wnt5A* are expressed along the spinal cord in an anterior high posterior low gradient, while *Ryk* is expressed in descending CST axons (Liu et al., 2005). In *ex vivo* explant assays, as well as *in vivo*, anti-Ryk antibodies could block the repellent activity of Wnt1 and Wnt5A (Liu et al., 2005).

Collectively these data demonstrate that Wnt gradients can act instructively to either attract or repel migrating neurons or growth cones during embryonic development.

A role for Wnt signaling in *C. elegans* neural development

Wnt signaling does not only play a part during the wiring of the vertebrate nervous system, but is also heavily involved in similar processes in the small nematode *C. elegans*. The many advantages that *C. elegans* offers in terms of its size, simplicity (both in genetic and cellular makeup), transparency and reproductive cycle make it an ideal model organism for studying the biology of development (Brenner, 1974). On top of this come the many tools that have been developed over the years to generate mutants, knock down genes by RNAi and introduce foreign DNA sequences by microinjection.

For these reasons *C. elegans* was our organism of choice for the study of Wnt regulated cell migration. I will now describe the role of Wnt signaling in *C. elegans* during the guidance of growth cone and neuron migration, starting with an overview of the different Wnt genes in *C. elegans* and their expression along the anteroposterior axis. The migration of the Q neuroblasts and their descendants will be described in more detail, as these were the subject of study during the making of this thesis.

Expression of the C. elegans Wnt genes

Compared to vertebrates, the *C. elegans* genome codes for a modest number of five different Wnt genes: *lin-44*, *egl-20*, *cwn-1*, *cwn-2* and *mom-2* (Korswagen, 2002; Sawa and Korswagen, 2013). The number of Wnt receptors is equally small, with four Frizzleds (*mig-1*, *lin-17*, *mom-5* and *cfz-2*) and single Ror and Ryk homologues (*cam-1*/*Ror* and *lin-18*/*Ryk*) (Forrester et al., 1999; Inoue et al., 2004; Korswagen, 2002; Sawa and Korswagen, 2013). The Wnt expression pattern of *C. elegans* has recently been described in detail, using a quantitative single molecule fluorescence *in situ* hybridization protocol, a method that is

explained in **Chapter 6** of this thesis as well (Harterink et al., 2011; Raj et al., 2008). The Wnts are expressed in partially overlapping domains along the anteroposterior axis, with the most prominent expression in the animal posterior (Figure 4) (Harterink et al., 2011). In the anterior, the secreted Wnt inhibitor *sfrp-1* is expressed and likely functions to dampen Wnt signaling (Harterink et al., 2011). Posterior Wnt expression opposed by anterior expression of Wnt inhibitors is similar to what is observed during anteroposterior specification of the vertebrate nervous system and again underscores the evolutionary conservation of this expression pattern (Petersen and Reddien, 2009).

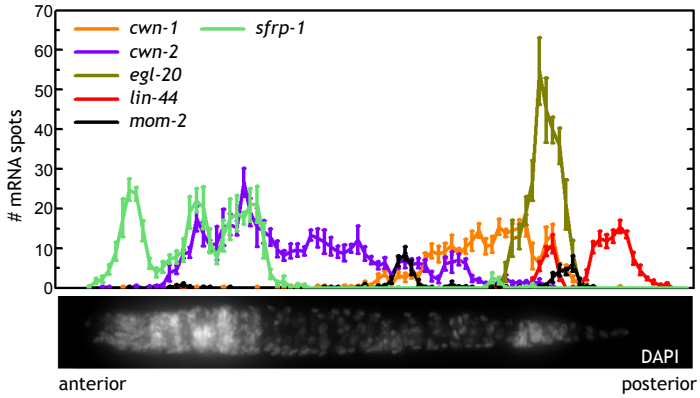

Figure 4. Anteroposterior expression domains of the *C. elegans* Wnts and *sfrp-1* as determined in early L1 larvae by single molecule mRNA FISH (smFISH). The graph denotes the quantification of mRNA molecules for each gene, as represented by single fluorescent spots, along the entire anteroposterior axis. Note the staggered and mostly posterior expression domains of the different Wnts, while *sfrp-1* is expressed in the anterior. Adapted from (Harterink et al. 2011).

As has been well described in vertebrates and *Drosophila*, Wnts are known to act as secreted morphogens that may provide concentration dependent information to cells across tissues (Cadigan and Nusse, 1997). The expression of *egl-20* in only a few cells in the posterior, combined with its described functions in the midbody region such as regulation of vulva development, seems very suggestive of such gradients existing in *C. elegans* as well (Green et al., 2008a; Harterink et al., 2011). Indeed, expression of a tagged version of EGL-20 showed that it forms a concentration gradient that is high in the posterior and declines slowly towards the midbody region (Coudreuse et al., 2006). Whether any of the other Wnts form gradients as well is currently unknown.

During my discussion on the role of Wnts as guidance factors in *C. elegans* it will become clear that oftentimes they function as instructive cues, consistent with the idea of secreted morphogen gradients. However, perhaps paradoxically, they may also function permissively in some processes.

Wnts guide growth cone migrations in C. elegans

By now several reports have demonstrated that Wnts have an important role in guiding the outgrowth of neuronal processes in *C. elegans*. Neurons on different locations along the nematode anteroposterior axis require different Wnts as guidance factors for their extended processes, which seems to be generally consistent with their described expression domains (Figures 5A-5F) (Harterink et al., 2011).

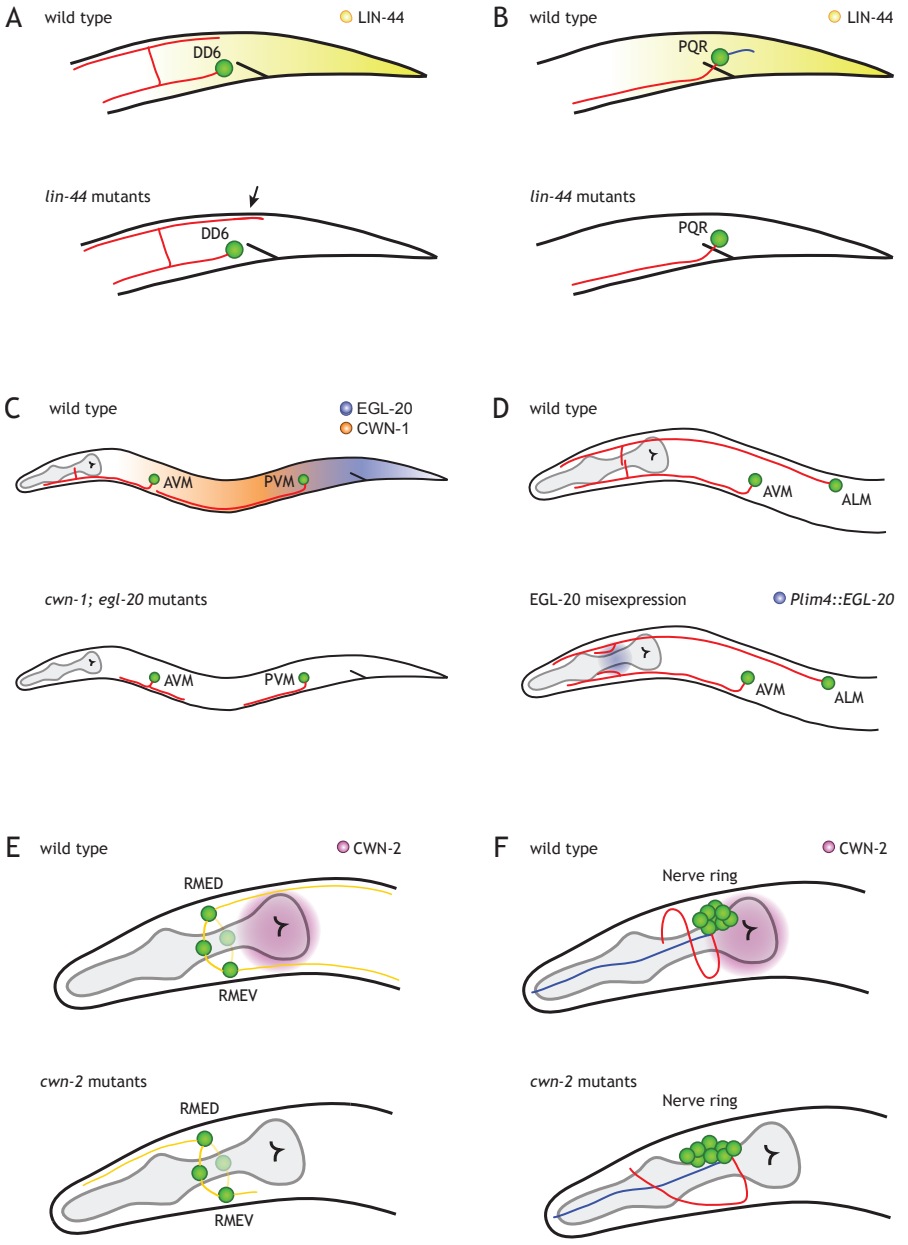

Figure 5. Anteroposterior neurite outgrowth is controlled by Wnt signaling in *C. elegans*. (**A-F**) Schematic representations of various neuronal cell bodies (green) and their extended processes - either axons (red), dendrites (blue) or neurites (yellow) - in wild type (top) and Wnt mutant or ectopic Wnt expression conditions (bottom). The arrowhead in panel **A** denotes an extended axon in *lin-44* mutants. Defects shown for *lin-44* mutants in panel **B**, *cwn-1; egl-20* mutants in panel **C** and for *cwn-2* mutants in panel **F** represent only one of the various possible phenotypes. Worms are depicted at various stages of magnification. Presumed Wnt secretion gradients are represented by a color gradient. The pharynx is shaded in gray. Adapted from (Sawa and Korswagen et al. 2013).

In the animal posterior, the GABAergic motoneuron DD6, located in the ventral nerve cord, projects an axon dorsally, which then further extends posteriorly and terminates at an anteroposterior position opposite its cells body. The two most posteriorly expressed Wnts, EGL-20 and LIN-44, control the extent of its posterior outgrowth, with a minor role for EGL-20 (Figure 5A) (Maro et al., 2009). The Wnts act as instructive chemo repellants and activate a canonical Wnt pathway through the Fz receptor LIN-17. In *lin-44* mutants the axon over extends posteriorly, whereas in wild type animals expressing ectopic *lin-44* in the posterior, under extension is observed (Maro et al., 2009).

LIN-44 also has a major role in controlling dendrite outgrowth from the oxygen sensing neuron PQR (Figure 5B) (Kirszenblat et al., 2011). During L1 development, the PQR neuron differentiates in the animal posterior and extends a single axon anteriorly, as well as a single dendrite posteriorly. It was found that LIN-44 provides an attractive cue through its receptor LIN-17 and controls outgrowth of the PQR dendrite specifically (Kirszenblat et al., 2011). In *lin-44* mutants, dendrite outgrowth is often stunted or even rerouted to the anterior, while rerouting defects are enhanced when LIN-44 is ectopically expressed anterior of the PQR cell body in *lin-44* mutants.

Further towards the anterior, mechanosensory neurons AVM and PVM send out a single axon that enters the ventral nerve cord and then turns anteriorly; the AVM process extends into the head to connect to the nerve ring, while the PVM process stops in the midbody region (White et al., 1986). Axon growth and branching is redundantly regulated by EGL-20 and CWN-1, as in double mutants axon outgrowth may stop prematurely, show ectopic branching or reverse direction entirely towards the posterior (Figure 5C) (Pan et al., 2006; Prasad and Clark, 2006). The Wnts signal via Fz receptors MIG-1 and MOM-5 in the AVM neurons, whereas in PVM the LIN-18 Ryk orthologue is required in addition to the two Fz's (Pan et al., 2006). EGL-20 functions instructively to repel axon growth as expression from anterior head neurons in *cwn-1; egl-20* double mutants enhanced misrouting defects to the posterior, while expression in a posterior body region was able to rescue most of the guidance defects (Pan et al., 2006).

When the AVM axon enters the head region ventrally, it sends out a single branch that connects in the nerve ring to a mirrored branch of the dorsally located axon that belongs to ALM, a third mechanosensory neuron (White et al., 1986). Branch formation in the nerve ring is redundantly regulated by CWN-1 and CWN-2, which is consistent with the anterior expression domain of CWN-2 (Pan et al., 2006; Prasad and Clark, 2006). The chemo repellent function of EGL-20 could be confirmed, as ectopic expression in head neurons near the nerve ring was able to repel the branches and prevent their connection (Figure 5D) (Pan et al., 2006). The exact role of CWN-2 in this process remains to be determined.

Two different studies have looked more closely at how CWN-2 may act to control neuronal process outgrowth in the head region. The RMED/V GABAergic motoneurons are situated anterior of the pharyngeal bulb, close to the nerve ring. Both send out processes that connect to the nerve ring, as well as a long posterior process that extends into the midbody region. CWN-2 is expressed in the pharynx and functions as an attractive cue specifically for the posteriorly projected RMED/V neurites (Figure 5E) (Song et al., 2010). In *cwn-2* mutant animals, most processes are completely eliminated and ectopic expression of CWN-2 anterior to the nerve ring results in rerouting to the anterior (Song et al., 2010). CWN-2 signals via CAM-1/Ror, which may use MIG-1 and CFZ-2 Fz's as co-receptors to signal downstream to DSH-1. Interestingly, ectopic expression of other Wnts could only partially

rescue the *cwn-2* mutant defects, indicating that some specificity exists in Wnt receptor interactions (Song et al., 2010).

A second study found that CWN-2 directs the placement of the nerve ring, again via CAM-1/Ror and MIG-1/Fz (Figure 5F) (Kennerdell et al., 2009). Loss of *cwn-2* function results in anterior displacement of the nerve ring. Remarkably, even though CWN-2 is expressed posterior to the nerve ring, where it could act as an attractive cue on nerve ring placement, it acts permissively in this process. This can be concluded from the rescue that is observed in *cwn-2* mutants either by anterior or heat-shock driven uniform expression of CWN-2 (Kennerdell et al., 2009). The authors then go on to show that the CAM-1 and MIG-1 receptors are required in SIA and SIB motoneurons for proper nerve ring positioning. These neurons extend axons that are directed by CWN-2 to follow a complex trajectory along the nerve ring and subsequently enter the dorsal or ventral nerve cord posteriorly. This suggests an intriguing model where CWN-2 controls neurite outgrowth in SIA and SIB neurons, which in turn influences placement of the nerve ring (Kennerdell et al., 2009).

In summary, it can be concluded that in *C. elegans* Wnts function mostly as instructive cues that direct growth cones along the A/P axis. Growth in the D/V direction was mostly left unaffected in Wnt mutants, such as the short ventral projections of AVM and PVM neurons or the dorsoventral projections to the nerve ring of RMED/V neurons (Pan et al., 2006; Prasad and Clark, 2006; Song et al., 2010). This is in agreement with the role of Wnts as A/P guidance factors in the mammalian spinal cord (Liu et al., 2005; Lyuksyutova et al., 2003).

Wnts guide the migration of neurons during embryogenesis in C. elegans

Several neurons are known to migrate under the influence of Wnt signaling in *C. elegans*, among which are the embryonic migrations of the bilateral pairs of BDU, ALM, CAN and HSN neurons, as well as the migration of the Q neuroblast descendants that occurs during the L1 stage of larval development (Figures 6A-6D) (Hedgecock et al., 1987; Silhankova and Korswagen, 2007; Sulston et al., 1983). Again there are examples of Wnts acting either instructively or permissively during these processes. An interesting conclusion that can be drawn from these studies is that each cell requires the concerted action of a different set of Wnt ligands and receptors for their proper migration.

The HSN motoneurons are born in the tail and migrate anteriorly during embryogenesis towards the middle of the embryo, where, later in development, they will innervate the vulval muscles to stimulate contraction and to induce egg laying (Figure 6D) (Desai et al., 1988). EGL-20 stimulates HSN anterior migration through cell autonomously required MIG-1, yet all the other Wnts and Fz's seem to play minor roles as well (Pan et al., 2006; Zinovyeva et al., 2008). Curiously, mutation of *lin-17* suppresses the under migration phenotype of *mig-1* mutants, indicating an antagonizing role (Pan et al., 2006). Anterior migration of the HSN neuron is terminated when it reaches a position that is close to the CAN neuron (Forrester and Garriga, 1997). The CAN neuron expresses CAM-1/Ror that may act as a sink for EGL-20 and inhibits its signaling activity (Forrester et al., 2004; Kim and Forrester, 2003). Recently it was shown that CAM-1 localizes to punctate structures in the CAN posterior axon and there sequesters EGL-20 to regulate vulval development (Modzelewska et al., 2013). To properly test a putative role for EGL-20 as a repulsive cue, Pan et al. used *vab-8/kinesin* mutants that suffer impaired CAN migration. In *vab-8* mutants the HSN neurons migrate beyond their normal stopping point, as they no longer encounter the CAN neuron blockade. They could now demonstrate that ectopic posterior EGL-20 expression enhanced the HSN

over migration phenotype of *vab-8* mutants (Pan et al., 2006). Finally, in a reciprocal experiment, the authors found that anterior expression of EGL-20 in *vab-8* mutants reduced the over migration phenotype, firmly establishing EGL-20 as a chemo repellent (Pan et al., 2006).

The CAN neurons are born in the head and migrate posteriorly to the middle of the embryo (Figure 6D) (Sulston et al., 1983). Migration is mainly controlled by CWN-2, with minor roles for CWN-1 and EGL-20 (Zinovyeva and Forrester, 2005; Zinovyeva et al., 2008). CAM-1 is required cell autonomously, while the Frzs MOM-5 and CFZ-2 contribute to proper migration as well (Forrester et al., 1999; Zinovyeva et al., 2008). Interestingly, mutating Wnts may cause CAN neurons to migrate too far, whereas mutating Fz's only results in under migration (Zinovyeva et al., 2008).

The BDU neurons are born in the anterior body region and move a short distance anteriorly, stopping just before the terminal bulb of the pharynx (Figure 6D) (Sulston et al., 1983). Correct migration requires the redundant action of CWN-1 and CWN-2, as well as

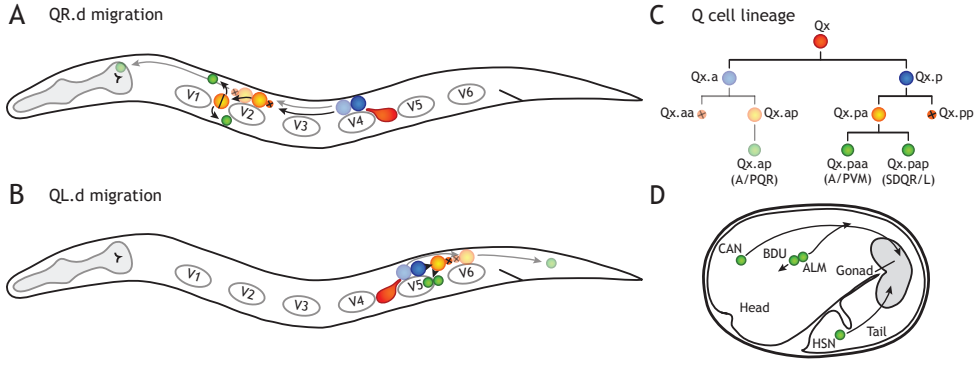

Figure 6. Wnt signaling controls cell migration along the anteroposterior axis in *C. elegans*. (**A-C**) Schematic representation of the migration of the Q cells and their descendants along the anteroposterior axis during L1 development, as well as of their cell lineage. QL and QR each have an identical cell lineage. The Qx.a cells and their daughters are lightly shaded to distinguish them from the Qx.p lineage. Apoptotic cells are depicted as smaller cells with a cross. (**A**) Immediately after hatching in the L1 larva, the QR neuroblast (red) is located on the right lateral side between seam cells V4 and V5, polarizes anteriorly and migrates over seam cell V4. On top of V4 QR divides into QR.a and QR.p neuroblasts (blue), which proceed to migrate anteriorly. After a certain distance both QR.a and QR.p divide, generating QR.ap and QR.pa neuroblasts (yellow), as well as QR.aa and QR.pp apoptotic cells. QR.ap continues its anterior migration into the head region near the pharynx (gray), where it stops and differentiates into the AQR sensory neuron (green). QR.pa migrates a short distance anteriorly and divides a final time to generate the QR.paa and QR.pap neuroblasts (green). QR.paa then migrates a short distance posteriorly and ventrally where it differentiates into the AVM mechanosensory neuron, while QR.pap migrates a short distance anteriorly and dorsally to finally differentiate into the SDQR interneuron. (**B**) The QL neuroblast (red) is located between seam cells V4 and V5 on the left lateral side, polarizes posteriorly and migrates over seam cell V5. On top of V5 QL divides into QL.a and QL.p neuroblasts (blue). QL.a then migrates posteriorly over QL.p, while QL.p stays localized on V5, after which both cells divide to generate QLap and QL.pa neuroblasts (yellow), as well as QL.aa and QL.pp apoptotic cells. QL.ap continues to migrate posteriorly into the tail and differentiates into the PQR sensory neuron (green). QL.pa remains near the V5 seam cell and divides to generate QL.paa and QL.pap neuroblasts (green), which subsequently differentiate into the SDQL interneuron and PVM mechanosensory neuron respectively. (**D**) Schematic representation of the migration of HSN, ALM, CAN and BDU neurons (green) during embryogenesis. The ALM and CAN neurons migrate posteriorly, with CAN migrating from the head towards the midbody region near the future gonad (gray) and ALM migrating from near seam cell V1 to seam cell V3. The BDU (sister cell of ALM) and HSN neurons migrate anteriorly, with BDU migrating a very short distance anteriorly and HSN migrating from the tail towards the midbody region, stopping just before the CAN final position.

both Fz receptors MOM-5 and LIN-17 (Zinovyeva et al., 2008). CAM-1 has a minor role as an inhibitor of BDU migration (Forrester et al., 1999).

The final pair of neurons known to migrate a longer distance during embryogenesis consists of the two mechanosensory ALM neurons. They are born close to where the BDU neurons emerge, but migrate a short distance posteriorly (Figure 6D) (Sulston et al., 1983). The Wnts CWN-1 and CWN-2 control posterior migration and functional CFZ-2 is required as well (Zinovyeva et al., 2008). The receptors MOM-5 and MIG-1 seem to inhibit migration and antagonize CFZ-2 function (Zinovyeva et al., 2008). Increasing anterior Wnt levels by removing the secreted inhibitor SFRP-1 also interferes with ALM migration (Harterink et al., 2011).

Wnts guide the post-embryonic migration of the Q neuroblasts and their descendants

At the end of embryonic development, a bilateral pair of Q neuroblasts is generated, which occupy equivalent left right positions along the anteroposterior axis (Sulston and Horvitz, 1977). During L1 larval development, both cells polarize and migrate in opposite directions, with the left neuroblast (QL) migrating posteriorly, whereas the right (QR) migrates anteriorly (Figures 6A and 6B) (Sulston and Horvitz, 1977). As they migrate, both Q neuroblasts generate an identical set of three descendant cells (Q.d), which differentiate into neurons and occupy well-defined positions along the anteroposterior axis (Figure 6C) (Sulston and Horvitz, 1977). A conserved canonical Wnt signaling pathway controls posterior migration of the QL.d (Korswagen, 2002; Silhankova and Korswagen, 2007). EGL-20 signals to Fz receptors MIG-1 and LIN-17 to initiate downstream signaling. In **Chapter 4** of this thesis, we find that *mig-1* is the initially expressed receptor in QL, which is subsequently downregulated, whereas *lin-17* is upregulated. We proceed to show that an intricate network of interlocked negative and positive feedback loops initiated by the Wnt signal mediates these transcriptional events and is crucial to ensure robust expression of target Antennapedia-like Homeobox (Hox) gene *mab-5* (Ji et al., 2013). Downstream, the receptors signal to MIG-5/Dsh to allow inhibition of a destruction complex consisting of PRY-1/Axin, APR-1/APC and GSK-3. This results in BAR-1/ß-catenin and POP-1/TCF activating expression of the target gene *mab-5* in the QL neuroblast (Harris et al., 1996; Korswagen et al., 2002; Korswagen et al., 2000; Maloof et al., 1999; Whangbo and Kenyon, 1999). MAB-5 expression is necessary and sufficient to induce posterior migration of the QL.d (Harris et al., 1996; Maloof et al., 1999; Salser and Kenyon, 1992; Whangbo and Kenyon, 1999). EGL-20 does not induce the expression of *mab-5* in the QR neuroblast, which results in the QR.d migrating in the default anterior direction. Similarly, if canonical Wnt signaling is abrogated in any way by genetic mutations, the QL.d will migrate anteriorly as well.

It was shown that an inherently different sensitivity to the EGL-20 ligand, with QL having a lower threshold for canonical Wnt signaling activation, underlies the asymmetric response of the Q neuroblasts (Whangbo and Kenyon, 1999). In addition to this, the initial posterior polarization of QL might expose it to higher levels of the posteriorly secreted Wnt gradient, resulting in the activation of canonical signaling (Coudreuse et al., 2006; Middelkoop et al., 2012). Over-activating the canonical pathway either by removal of the negative regulator PRY-1, or heat shock mediated expression of EGL-20 will result in *mab-5* expression in QR as well (Maloof et al., 1999; Whangbo and Kenyon, 1999).

Lower exposure to EGL-20 allows QR and its descendants to migrate anteriorly under the control of a non-canonical Wnt pathway. The extent of anterior migration is also controlled

by EGL-20, but here it acts redundantly with CWN-1 and CWN-2 (Whangbo and Kenyon, 1999; Zinovyeva et al., 2008). Importantly, EGL-20 acts permissively in QR.d migration, as ubiquitous expression from a heat shock promoter (to levels below those required to activate canonical signaling in QR.d) may rescue the under migration defects in *egl-20* mutants (Whangbo and Kenyon, 1999). At the receptor level, undermigration of the QR.d is clearly observed in *mom-5* mutants, a phenotype that is seemingly enhanced in *mom-5;cfz-2* double mutants (Zinovyeva et al., 2008). CAM-1 is required for wild type QR.d migration as well and this depends at least in part on its kinase activity (Kim and Forrester, 2003). In **Chapter 2** of this thesis, we describe that CWN-1, like EGL-20, functions permissively and that both Wnts signal through parallel non-canonical pathways, using the receptors MOM-5 and CAM-1 respectively, to regulate different aspects of anterior migration. Furthermore, we demonstrate that a cell intrinsic timing mechanism regulates the dynamic upregulation of the MIG-1 receptor, resulting in the activation of canonical Wnt signaling and termination of anterior migration (Mentink et al., 2014).

Besides the non-canonical Wnt signaling pathway, anterior QR.d migration is also dependent on the activity of the Sex Combs Reduced-like Hox gene *lin-39*, as well as on the LDL receptor repeat-containing transmembrane protein *mig-13* (Clark et al., 1993; Sym et al., 1999). The Hox co-factors CEH-20 and UNC-62 are required for the QR.d cells to respond to the MIG-13 signal (Yang et al., 2005). Despite previous reports that MIG-13 functions cell non-autonomously, recently it was demonstrated that LIN-39 directly binds the *mig-13* promotor to drive expression in the QR.d and promote anterior migration (Sym et al., 1999; Wang et al., 2013). Interestingly, expression of *mab-5* in QL suppresses *lin-39* and prevents anterior migration (Wang et al., 2013). MIG-13 drives migration in parallel to the non-canonical Wnt signal and exactly how these two pathways relate to each other is currently unknown (Sym et al., 1999; Yang et al., 2005).

Concluding remarks

Wnts are crucial mediators of anteroposterior patterning and regulate many different processes during embryonic development, from vertebrates to small nematodes like *C. elegans*. Although some advances have been made in unraveling the different downstream signaling cascades that can be initiated by Wnts (Angers and Moon, 2009), many questions remain unanswered. We may ask for instance how signaling specificity is achieved in cells? Or how is the Wnt gradient interpreted and translated into the required response? Important clues come from studies that show that the expressed receptor repertoire may determine which downstream Wnt pathway is activated (Grumolato et al., 2010; Sato et al., 2010); or results that demonstrate domain specificity in the Dvl protein for activation of a particular downstream pathway (Gao and Chen, 2010). Future research will have to determine the mechanisms that cells use to regulate their active surface receptors or downstream Wnt components or if these will even be the prime methods that cells may use to adapt to the Wnt signal.

1

References

Aberle, H., Bauer, A., Stappert, J., Kispert, A., and Kemler, R. (1997). beta-catenin is a target for the ubiquitin-proteasome pathway. The EMBO journal *16*, 3797-3804.

Adler, P.N. (2002). Planar signaling and morphogenesis in Drosophila. Developmental cell *2*, 525-535.

Alexandre, C., Baena-Lopez, A., and Vincent, J.P. (2014). Patterning and growth control by membrane-tethered Wingless. Nature *505*, 180-185.

Amit, S., Hatzubai, A., Birman, Y., Andersen, J.S., Ben-Shushan, E., Mann, M., Ben-Neriah, Y., and Alkalay, I. (2002). Axin-mediated CKI phosphorylation of beta-catenin at Ser 45: a molecular switch for the Wnt pathway. Genes & development *16*, 1066-1076.

Andre, P., Wang, Q., Wang, N., Gao, B., Schilit, A., Halford, M.M., Stacker, S.A., Zhang, X., and Yang, Y. (2012). The Wnt coreceptor Ryk regulates Wnt/planar cell polarity by modulating the degradation of the core planar cell polarity component Vangl2. The Journal of biological chemistry *287*, 44518-44525.

Angers, S., and Moon, R.T. (2009). Proximal events in Wnt signal transduction. Nature reviews Molecular cell biology *10*, 468-477.

Antic, D., Stubbs, J.L., Suyama, K., Kintner, C., Scott, M.P., and Axelrod, J.D. (2010). Planar cell polarity enables posterior localization of nodal cilia and left-right axis determination during mouse and Xenopus embryogenesis. PloS one *5*, e8999.

Bang, A.G., Papalopulu, N., Goulding, M.D., and Kintner, C. (1999). Expression of Pax-3 in the lateral neural plate is dependent on a Wnt-mediated signal from posterior nonaxial mesoderm. Developmental biology *212*, 366-380.

Bhanot, P., Brink, M., Samos, C.H., Hsieh, J.C., Wang, Y., Macke, J.P., Andrew, D., Nathans, J., and Nusse, R. (1996). A new member of the frizzled family from Drosophila functions as a Wingless receptor. Nature *382*, 225-230.

Bilic, J., Huang, Y.L., Davidson, G., Zimmermann, T., Cruciat, C.M., Bienz, M., and Niehrs, C. (2007). Wnt induces LRP6 signalosomes and promotes dishevelled-dependent LRP6 phosphorylation. Science *316*, 1619-1622.

Bingham, S., Higashijima, S., Okamoto, H., and Chandrasekhar, A. (2002). The Zebrafish trilobite gene is essential for tangential migration of branchiomotor neurons. Developmental biology *242*, 149-160.

Bonkowsky, J.L., Yoshikawa, S., O'Keefe, D.D., Scully, A.L., and Thomas, J.B. (1999). Axon routing across the midline controlled by the Drosophila Derailed receptor. Nature *402*, 540-544.

Brenner, S. (1974). The genetics of Caenorhabditis elegans. Genetics *77*, 71-94.

Buechling, T., and Boutros, M. (2011). Wnt signaling signaling at and above the receptor level. Current topics in developmental biology *97*, 21-53.

Cadigan, K.M., and Nusse, R. (1997). Wnt signaling: a common theme in animal development. Genes & development *11*, 3286-3305.

Canty, A.J., and Murphy, M. (2008). Molecular mechanisms of axon guidance in the developing corticospinal tract. Progress in neurobiology *85*, 214-235.

Carreira-Barbosa, F., Concha, M.L., Takeuchi, M., Ueno, N., Wilson, S.W., and Tada, M. (2003). Prickle 1 regulates cell movements during gastrulation and neuronal migration in zebrafish. Development *130*, 4037-4046.

Castelo-Branco, G., Wagner, J., Rodriguez, F.J., Kele, J., Sousa, K., Rawal, N., Pasolli, H.A., Fuchs, E., Kitajewski, J., and Arenas, E. (2003). Differential regulation of midbrain dopaminergic neuron development by Wnt-1, Wnt-3a, and Wnt-5a. Proceedings of the National Academy of Sciences of the United States of America *100*, 12747-12752.

Chandrasekhar, A., Moens, C.B., Warren, J.T., Jr., Kimmel, C.B., and Kuwada, J.Y. (1997). Development of branchiomotor neurons in zebrafish. Development *124*, 2633-2644.

Chen, W.S., Antic, D., Matis, M., Logan, C.Y., Povelones, M., Anderson, G.A., Nusse, R., and Axelrod, J.D. (2008). Asymmetric homotypic interactions of the atypical cadherin flamingo mediate intercellular polarity signaling. Cell *133*, 1093-1105.

Clark, C.E., Liu, Y., and Cooper, H.M. (2014). The Yin and Yang of Wnt/Ryk axon guidance in development and regeneration. Science China Life sciences *57*, 366-371.

Clark, C.E., Nourse, C.C., and Cooper, H.M. (2012). The tangled web of non-canonical Wnt signalling in neural migration. Neuro-Signals *20*, 202-220.

Clark, S.G., Chisholm, A.D., and Horvitz, H.R. (1993). Control of cell fates in the central body region of C. elegans by the homeobox gene lin-39. Cell *74*, 43-55.

Clevers, H., and Nusse, R. (2012). Wnt/beta-catenin signaling and disease. Cell *149*, 1192-1205.

Copp, A.J. (2005). Neurulation in the cranial region--normal and abnormal. Journal of anatomy *207*, 623-635.

Coudreuse, D.Y., Roel, G., Betist, M.C., Destree, O., and Korswagen, H.C. (2006). Wnt gradient formation requires retromer function in Wnt-producing cells. Science *312*, 921-924.

Curtin, J.A., Quint, E., Tsipouri, V., Arkell, R.M., Cattanach, B., Copp, A.J., Henderson, D.J., Spurr, N., Stanier, P., Fisher, E.M., *et al.* (2003). Mutation of Celsr1 disrupts planar polarity of inner ear hair cells and causes severe neural tube defects in the mouse. Current biology : CB *13*, 1129-1133.

De, A. (2011). Wnt/Ca2+ signaling pathway: a brief overview. Acta biochimica et biophysica Sinica *43*, 745-756.

Desai, C., Garriga, G., McIntire, S.L., and Horvitz, H.R. (1988). A genetic pathway for the development of the Caenorhabditis elegans HSN motor neurons. Nature *336*, 638-646.

Djiane, A., Riou, J., Umbhauer, M., Boucaut, J., and Shi, D. (2000). Role of frizzled 7 in the regulation of convergent extension movements during gastrulation in Xenopus laevis. Development *127*, 3091-3100.

Esteve, P., Morcillo, J., and Bovolenta, P. (2000). Early and dynamic expression of cSfrp1 during chick embryo development. Mechanisms of development *97*, 217-221.

Etheridge, S.L., Ray, S., Li, S., Hamblet, N.S., Lijam, N., Tsang, M., Greer, J., Kardos, N., Wang, J., Sussman, D.J.,

et al. (2008). Murine dishevelled 3 functions in redundant pathways with dishevelled 1 and 2 in normal cardiac outflow tract, cochlea, and neural tube development. PLoS genetics *4*, e1000259.

Feiguin, F., Hannus, M., Mlodzik, M., and Eaton, S. (2001). The ankyrin repeat protein Diego mediates Frizzled-dependent planar polarization. Developmental cell *1*, 93-101.

Forrester, W.C., Dell, M., Perens, E., and Garriga, G. (1999). A C. elegans Ror receptor tyrosine kinase regulates cell motility and asymmetric cell division. Nature *400*, 881-885.

Forrester, W.C., and Garriga, G. (1997). Genes necessary for C. elegans cell and growth cone migrations. Development *124*, 1831-1843.

Forrester, W.C., Kim, C., and Garriga, G. (2004). The Caenorhabditis elegans Ror RTK CAM-1 inhibits EGL-20/Wnt signaling in cell migration. Genetics *168*, 1951-1962.

Gao, C., and Chen, Y.G. (2010). Dishevelled: The hub of Wnt signaling. Cellular signalling *22*, 717-727.

Glasco, D.M., Sittaramane, V., Bryant, W., Fritzsch, B., Sawant, A., Paudyal, A., Stewart, M., Andre, P., Cadete Vilhais-Neto, G., Yang, Y., *et al*. (2012). The mouse Wnt/PCP protein Vangl2 is necessary for migration of facial branchiomotor neurons, and functions independently of Dishevelled. Developmental biology *369*, 211-222.

Glinka, A., Wu, W., Delius, H., Monaghan, A.P., Blumenstock, C., and Niehrs, C. (1998). Dickkopf-1 is a member of a new family of secreted proteins and functions in head induction. Nature *391*, 357-362.

Goto, T., and Keller, R. (2002). The planar cell polarity gene strabismus regulates convergence and extension and neural fold closure in Xenopus. Developmental biology *247*, 165-181.

Green, J.L., Inoue, T., and Sternberg, P.W. (2007). The C. elegans ROR receptor tyrosine kinase, CAM-1, non-autonomously inhibits the Wnt pathway. Development *134*, 4053-4062.

Green, J.L., Inoue, T., and Sternberg, P.W. (2008a). Opposing Wnt pathways orient cell polarity during organogenesis. Cell *134*, 646-656.

Green, J.L., Kuntz, S.G., and Sternberg, P.W. (2008b). Ror receptor tyrosine kinases: orphans no more. Trends in cell biology *18*, 536-544.

Grumolato, L., Liu, G., Mong, P., Mudbhary, R., Biswas, R., Arroyave, R., Vijayakumar, S., Economides, A.N., and Aaronson, S.A. (2010). Canonical and noncanonical Wnts use a common mechanism to activate completely unrelated coreceptors. Genes & development *24*, 2517-2530.

Habas, R., Dawid, I.B., and He, X. (2003). Coactivation of Rac and Rho by Wnt/Frizzled signaling is required for vertebrate gastrulation. Genes & development *17*, 295-309.

Habas, R., Kato, Y., and He, X. (2001). Wnt/Frizzled activation of Rho regulates vertebrate gastrulation and requires a novel Formin homology protein Daam1. Cell *107*, 843-854.

Halford, M.M., Armes, J., Buchert, M., Meskenaite, V., Grail, D., Hibbs, M.L., Wilks, A.F., Farlie, P.G., Newgreen, D.F., Hovens, C.M., *et al*. (2000). Ryk-deficient mice exhibit craniofacial defects associated with perturbed Eph receptor crosstalk. Nature genetics *25*, 414-418.

Hall, A.C., Lucas, F.R., and Salinas, P.C. (2000). Axonal remodeling and synaptic differentiation in the cerebellum is regulated by WNT-7a signaling. Cell *100*, 525-535.

Harris, J., Honigberg, L., Robinson, N., and Kenyon, C. (1996). Neuronal cell migration in C. elegans: regulation of Hox gene expression and cell position. Development *122*, 3117-3131.

Harterink, M., Kim, D.H., Middelkoop, T.C., Doan, T.D., van Oudenaarden, A., and Korswagen, H.C. (2011). Neuroblast migration along the anteroposterior axis of C. elegans is controlled by opposing gradients of Wnts and a secreted Frizzled-related protein. Development *138*, 2915-2924.

Hashimoto, M., and Hamada, H. (2010). Translation of anterior-posterior polarity into left-right polarity in the mouse embryo. Current opinion in genetics & development *20*, 433-437.

Hedgecock, E.M., Culotti, J.G., Hall, D.H., and Stern, B.D. (1987). Genetics of cell and axon migrations in Caenorhabditis elegans. Development *100*, 365-382.

Heisenberg, C.P., Tada, M., Rauch, G.J., Saude, L., Concha, M.L., Geisler, R., Stemple, D.L., Smith, J.C., and Wilson, S.W. (2000). Silberblick/Wnt11 mediates convergent extension movements during zebrafish gastrulation. Nature *405*, 76-81.

Hikasa, H., Shibata, M., Hiratani, I., and Taira, M. (2002). The Xenopus receptor tyrosine kinase Xror2 modulates morphogenetic movements of the axial mesoderm and neuroectoderm via Wnt signaling. Development *129*, 5227-5239.

Ho, H.Y., Susman, M.W., Bikoff, J.B., Ryu, Y.K., Jonas, A.M., Hu, L., Kuruvilla, R., and Greenberg, M.E. (2012). Wnt5a-Ror-Dishevelled signaling constitutes a core developmental pathway that controls tissue morphogenesis. Proceedings of the National Academy of Sciences of the United States of America *109*, 4044-4051.

Houart, C., Caneparo, L., Heisenberg, C., Barth, K., Take-Uchi, M., and Wilson, S. (2002). Establishment of the telencephalon during gastrulation by local antagonism of Wnt signaling. Neuron *35*, 255-265.

Inoue, T., Oz, H.S., Wiland, D., Gharib, S., Deshpande, R., Hill, R.J., Katz, W.S., and Sternberg, P.W. (2004). C. elegans LIN-18 is a Ryk ortholog and functions in parallel to LIN-17/Frizzled in Wnt signaling. Cell *118*, 795-806.

Janda, C.Y., Waghray, D., Levin, A.M., Thomas, C., and Garcia, K.C. (2012). Structural basis of Wnt recognition by Frizzled. Science *337*, 59-64.

Jenny, A., Darken, R.S., Wilson, P.A., and Mlodzik, M. (2003). Prickle and Strabismus form a functional complex to generate a correct axis during planar cell polarity signaling. The EMBO journal *22*, 4409-4420.

Jessen, J.R., Topczewski, J., Bingham, S., Sepich, D.S., Marlow, F., Chandrasekhar, A., and Solnica-Krezel, L. (2002). Zebrafish trilobite identifies new roles for Strabismus in gastrulation and neuronal movements. Nature cell biology *4*, 610-615.

Jho, E.H., Zhang, T., Domon, C., Joo, C.K., Freund, J.N., and Costantini, F. (2002). Wnt/beta-catenin/Tcf signaling induces the transcription of Axin2, a negative regulator of the signaling pathway. Molecular and cellular biology *22*, 1172-1183.

Ji, N., Middelkoop, T.C., Mentink, R.A., Betist, M.C., Tonegawa, S., Mooijman, D., Korswagen, H.C., and van Oudenaarden, A. (2013). Feedback control of gene

expression variability in the Caenorhabditis elegans Wnt pathway. Cell *155*, 869-880.

Kamitori, K., Tanaka, M., Okuno-Hirasawa, T., and Kohsaka, S. (2005). Receptor related to tyrosine kinase RYK regulates cell migration during cortical development. Biochemical and biophysical research communications *330*, 446-453.

Kani, S., Oishi, I., Yamamoto, H., Yoda, A., Suzuki, H., Nomachi, A., Iozumi, K., Nishita, M., Kikuchi, A., Takumi, T., *et al.* (2004). The receptor tyrosine kinase Ror2 associates with and is activated by casein kinase Iepsilon. The Journal of biological chemistry *279*, 50102-50109.

Kazanskaya, O., Glinka, A., and Niehrs, C. (2000). The role of Xenopus dickkopf1 in prechordal plate specification and neural patterning. Development *127*, 4981-4992.

Keller, R., Davidson, L., Edlund, A., Elul, T., Ezin, M., Shook, D., and Skoglund, P. (2000). Mechanisms of convergence and extension by cell intercalation. Philosophical transactions of the Royal Society of London Series B, Biological sciences *355*, 897-922.

Kennerdell, J.R., Fetter, R.D., and Bargmann, C.I. (2009). Wnt-Ror signaling to SIA and SIB neurons directs anterior axon guidance and nerve ring placement in C. elegans. Development *136*, 3801-3810.

Kibar, Z., Capra, V., and Gros, P. (2007). Toward understanding the genetic basis of neural tube defects. Clinical genetics *71*, 295-310.

Kibar, Z., Vogan, K.J., Groulx, N., Justice, M.J., Underhill, D.A., and Gros, P. (2001). Ltap, a mammalian homolog of Drosophila Strabismus/Van Gogh, is altered in the mouse neural tube mutant Loop-tail. Nature genetics *28*, 251-255.

Kiecker, C., and Niehrs, C. (2001). A morphogen gradient of Wnt/beta-catenin signalling regulates anteroposterior neural patterning in Xenopus. Development *128*, 4189-4201.

Kikuchi, A., Yamamoto, H., and Sato, A. (2009). Selective activation mechanisms of Wnt signaling pathways. Trends in cell biology *19*, 119-129.

Kilian, B., Mansukoski, H., Barbosa, F.C., Ulrich, F., Tada, M., and Heisenberg, C.P. (2003). The role of Ppt/Wnt5 in regulating cell shape and movement during zebrafish gastrulation. Mechanisms of development *120*, 467-476.

Kim, C., and Forrester, W.C. (2003). Functional analysis of the domains of the C elegans Ror receptor tyrosine kinase CAM-1. Developmental biology *264*, 376-390.

Kim, C.H., Oda, T., Itoh, M., Jiang, D., Artinger, K.B., Chandrasekharappa, S.C., Driever, W., and Chitnis, A.B. (2000). Repressor activity of Headless/Tcf3 is essential for vertebrate head formation. Nature *407*, 913-916.

Kim, G.H., Her, J.H., and Han, J.K. (2008). Ryk cooperates with Frizzled 7 to promote Wnt11-mediated endocytosis and is essential for Xenopus laevis convergent extension movements. The Journal of cell biology *182*, 1073-1082.

Kirszenblat, L., Pattabiraman, D., and Hilliard, M.A. (2011). LIN-44/Wnt directs dendrite outgrowth through LIN-17/Frizzled in C. elegans Neurons. PLoS biology *9*, e1001157.

Korswagen, H.C. (2002). Canonical and non-canonical Wnt signaling pathways in Caenorhabditis elegans: variations on a common signaling theme. BioEssays : news and reviews in molecular, cellular and developmental biology *24*, 801-810.

Korswagen, H.C., Coudreuse, D.Y., Betist, M.C., van de Water, S., Zivkovic, D., and Clevers, H.C. (2002). The Axin-like protein PRY-1 is a negative regulator of a canonical Wnt pathway in C. elegans. Genes & development *16*, 1291-1302.

Korswagen, H.C., Herman, M.A., and Clevers, H.C. (2000). Distinct beta-catenins mediate adhesion and signalling functions in C. elegans. Nature *406*, 527-532.

Kuhl, M., Sheldahl, L.C., Malbon, C.C., and Moon, R.T. (2000). Ca(2+)/calmodulin-dependent protein kinase II is stimulated by Wnt and Frizzled homologs and promotes ventral cell fates in Xenopus. The Journal of biological chemistry *275*, 12701-12711.

Lai, S.S., Xue, B., Yang, Y., Zhao, L., Chu, C.S., Hao, J.Y., and Wen, C.J. (2012). Ror2-Src signaling in metastasis of mouse melanoma cells is inhibited by NRAGE. Cancer genetics *205*, 552-562.

Laird, D.J., Altshuler-Keylin, S., Kissner, M.D., Zhou, X., and Anderson, K.V. (2011). Ror2 enhances polarity and directional migration of primordial germ cells. PLoS genetics *7*, e1002428.

Lau, P.M., Zucker, R.S., and Bentley, D. (1999). Induction of filopodia by direct local elevation of intracellular calcium ion concentration. The Journal of cell biology *145*, 1265-1275.

Lei, Y.P., Zhang, T., Li, H., Wu, B.L., Jin, L., and Wang, H.Y. (2010). VANGL2 mutations in human cranial neural-tube defects. The New England journal of medicine *362*, 2232-2235.

Li, L., Hutchins, B.I., and Kalil, K. (2009). Wnt5a induces simultaneous cortical axon outgrowth and repulsive axon guidance through distinct signaling mechanisms. The Journal of neuroscience : the official journal of the Society for Neuroscience *29*, 5873-5883.

Li, V.S., Ng, S.S., Boersema, P.J., Low, T.Y., Karthaus, W.R., Gerlach, J.P., Mohammed, S., Heck, A.J., Maurice, M.M., Mahmoudi, T., *et al.* (2012). Wnt signaling through inhibition of beta-catenin degradation in an intact Axin1 complex. Cell *149*, 1245-1256.

Liu, C., Li, Y., Semenov, M., Han, C., Baeg, G.H., Tan, Y., Zhang, Z., Lin, X., and He, X. (2002). Control of beta-catenin phosphorylation/degradation by a dual-kinase mechanism. Cell *108*, 837-847.

Liu, Y., Rubin, B., Bodine, P.V., and Billiard, J. (2008). Wnt5a induces homodimerization and activation of Ror2 receptor tyrosine kinase. Journal of cellular biochemistry *105*, 497-502.

Liu, Y., Shi, J., Lu, C.C., Wang, Z.B., Lyuksyutova, A.I., Song, X.J., and Zou, Y. (2005). Ryk-mediated Wnt repulsion regulates posterior-directed growth of corticospinal tract. Nature neuroscience *8*, 1151-1159.

Logan, C.Y., and Nusse, R. (2004). The Wnt signaling pathway in development and disease. Annual review of cell and developmental biology *20*, 781-810.

Lu, W., Yamamoto, V., Ortega, B., and Baltimore, D. (2004). Mammalian Ryk is a Wnt coreceptor required for stimulation of neurite outgrowth. Cell *119*, 97-108.

Lyu, J., and Joo, C.K. (2005). Wnt-7a up-regulates matrix metalloproteinase-12 expression and promotes cell proliferation in corneal epithelial cells during wound healing. The Journal of biological chemistry *280*, 21653-21660.

Lyuksyutova, A.I., Lu, C.C., Milanesio, N., King, L.A., Guo, N., Wang, Y., Nathans, J., Tessier-Lavigne, M., and Zou,

Y. (2003). Anterior-posterior guidance of commissural axons by Wnt-frizzled signaling. Science *302*, 1984-1988.

Macheda, M.L., Sun, W.W., Kugathasan, K., Hogan, B.M., Bower, N.I., Halford, M.M., Zhang, Y.F., Jacques, B.E., Lieschke, G.J., Dabdoub, A., *et al.* (2012). The Wnt receptor Ryk plays a role in mammalian planar cell polarity signaling. The Journal of biological chemistry *287*, 29312-29323.

Maloof, J.N., Whangbo, J., Harris, J.M., Jongeward, G.D., and Kenyon, C. (1999). A Wnt signaling pathway controls hox gene expression and neuroblast migration in C. elegans. Development *126*, 37-49.

Maro, G.S., Klassen, M.P., and Shen, K. (2009). A beta-catenin-dependent Wnt pathway mediates anteroposterior axon guidance in C. elegans motor neurons. PloS one *4*, e4690.

Matthews, H.K., Broders-Bondon, F., Thiery, J.P., and Mayor, R. (2008). Wnt11r is required for cranial neural crest migration. Developmental dynamics : an official publication of the American Association of Anatomists *237*, 3404-3409.

McGrew, L.L., Hoppler, S., and Moon, R.T. (1997). Wnt and FGF pathways cooperatively pattern anteroposterior neural ectoderm in Xenopus. Mechanisms of development *69*, 105-114.

McGrew, L.L., Lai, C.J., and Moon, R.T. (1995). Specification of the anteroposterior neural axis through synergistic interaction of the Wnt signaling cascade with noggin and follistatin. Developmental biology *172*, 337-342.

McMahon, A.P., and Moon, R.T. (1989). Ectopic expression of the proto-oncogene int-1 in Xenopus embryos leads to duplication of the embryonic axis. Cell *58*, 1075-1084.

Mentink, R.A., Middelkoop, T.C., Rella, L., Ji, N., Chung, Y.T., Betist, M.C., van Oudenaarden, A., and Korswagen, H.C. (2014). Cell intrinsic modulation of Wnt signaling controls neuroblast migration in *C. elegans*. Developmental cell *in press*.

Middelkoop, T.C., Williams, L., Yang, P.T., Luchtenberg, J., Betist, M.C., Ji, N., van Oudenaarden, A., Kenyon, C., and Korswagen, H.C. (2012). The thrombospondin repeat containing protein MIG-21 controls a left-right asymmetric Wnt signaling response in migrating C. elegans neuroblasts. Developmental biology *361*, 338-348.

Mikels, A.J., and Nusse, R. (2006). Purified Wnt5a protein activates or inhibits beta-catenin-TCF signaling depending on receptor context. PLoS biology *4*, e115.

Modzelewska, K., Lauritzen, A., Hasenoeder, S., Brown, L., Georgiou, J., and Moghal, N. (2013). Neurons refine the Caenorhabditis elegans body plan by directing axial patterning by Wnts. PLoS biology *11*, e1001465.

Montcouquiol, M., Sans, N., Huss, D., Kach, J., Dickman, J.D., Forge, A., Rachel, R.A., Copeland, N.G., Jenkins, N.A., Bogani, D., *et al.* (2006). Asymmetric localization of Vangl2 and Fz3 indicate novel mechanisms for planar cell polarity in mammals. The Journal of neuroscience : the official journal of the Society for Neuroscience *26*, 5265-5275.

Mulligan, K.A., and Cheyette, B.N. (2012). Wnt signaling in vertebrate neural development and function. Journal of neuroimmune pharmacology : the official journal of the Society on NeuroImmune Pharmacology *7*, 774-787.

Niehrs, C. (2010). On growth and form: a Cartesian coordinate system of Wnt and BMP signaling specifies bilaterian body axes. Development *137*, 845-857.

Niehrs, C. (2012). The complex world of WNT receptor signalling. Nature reviews Molecular cell biology *13*, 767-779.

Nishita, M., Itsukushima, S., Nomachi, A., Endo, M., Wang, Z., Inaba, D., Qiao, S., Takada, S., Kikuchi, A., and Minami, Y. (2010). Ror2/Frizzled complex mediates Wnt5a-induced AP-1 activation by regulating Dishevelled polymerization. Molecular and cellular biology *30*, 3610-3619.

Nishita, M., Yoo, S.K., Nomachi, A., Kani, S., Sougawa, N., Ohta, Y., Takada, S., Kikuchi, A., and Minami, Y. (2006). Filopodia formation mediated by receptor tyrosine kinase Ror2 is required for Wnt5a-induced cell migration. The Journal of cell biology *175*, 555-562.

Nomachi, A., Nishita, M., Inaba, D., Enomoto, M., Hamasaki, M., and Minami, Y. (2008). Receptor tyrosine kinase Ror2 mediates Wnt5a-induced polarized cell migration by activating c-Jun N-terminal kinase via actin-binding protein filamin A. The Journal of biological chemistry *283*, 27973-27981.

Nusse, R., and Varmus, H.E. (1982). Many tumors induced by the mouse mammary tumor virus contain a provirus integrated in the same region of the host genome. Cell *31*, 99-109.

Nusslein-Volhard, C., and Wieschaus, E. (1980). Mutations affecting segment number and polarity in Drosophila. Nature *287*, 795-801.

O'Connell, M.P., Fiori, J.L., Xu, M., Carter, A.D., Frank, B.P., Camilli, T.C., French, A.D., Dissanayake, S.K., Indig, F.E., Bernier, M., *et al.* (2010). The orphan tyrosine kinase receptor, ROR2, mediates Wnt5A signaling in metastatic melanoma. Oncogene *29*, 34-44.

Ohkawara, B., and Niehrs, C. (2011). An ATF2-based luciferase reporter to monitor non-canonical Wnt signaling in Xenopus embryos. Developmental dynamics : an official publication of the American Association of Anatomists *240*, 188-194.

Oishi, I., Suzuki, H., Onishi, N., Takada, R., Kani, S., Ohkawara, B., Koshida, I., Suzuki, K., Yamada, G., Schwabe, G.C., *et al.* (2003). The receptor tyrosine kinase Ror2 is involved in non-canonical Wnt5a/JNK signalling pathway. Genes to cells : devoted to molecular & cellular mechanisms *8*, 645-654.

Pan, C.L., Howell, J.E., Clark, S.G., Hilliard, M., Cordes, S., Bargmann, C.I., and Garriga, G. (2006). Multiple Wnts and frizzled receptors regulate anteriorly directed cell and growth cone migrations in Caenorhabditis elegans. Developmental cell *10*, 367-377.

Park, M., and Moon, R.T. (2002). The planar cell-polarity gene stbm regulates cell behaviour and cell fate in vertebrate embryos. Nature cell biology *4*, 20-25.

Petersen, C.P., and Reddien, P.W. (2009). Wnt signaling and the polarity of the primary body axis. Cell *139*, 1056-1068.

Petrova, I.M., Malessy, M.J., Verhaagen, J., Fradkin, L.G., and Noordermeer, J.N. (2014). Wnt signaling through the Ror receptor in the nervous system. Molecular neurobiology *49*, 303-315.

Polakis, P. (2012). Wnt signaling in cancer. Cold Spring Harbor perspectives in biology *4*.

Prasad, B.C., and Clark, S.G. (2006). Wnt signaling establishes anteroposterior neuronal polarity and requires retromer in C. elegans. Development *133*, 1757-1766.

Qu, Y., Glasco, D.M., Zhou, L., Sawant, A., Ravni, A., Fritzsch, B., Damrau, C., Murdoch, J.N., Evans, S., Pfaff, S.L., *et al.* (2010). Atypical cadherins Celsr1-3 differentially regulate migration of facial branchiomotor neurons in mice. The Journal of neuroscience : the official journal of the Society for Neuroscience *30*, 9392-9401.

Raj, A., van den Bogaard, P., Rifkin, S.A., van Oudenaarden, A., and Tyagi, S. (2008). Imaging individual mRNA molecules using multiple singly labeled probes. Nature methods *5*, 877-879.

Rijsewijk, F., Schuermann, M., Wagenaar, E., Parren, P., Weigel, D., and Nusse, R. (1987). The Drosophila homolog of the mouse mammary oncogene int-1 is identical to the segment polarity gene wingless. Cell *50*, 649-657.

Roszko, I., Sawada, A., and Solnica-Krezel, L. (2009). Regulation of convergence and extension movements during vertebrate gastrulation by the Wnt/PCP pathway. Seminars in cell & developmental biology *20*, 986-997.

Salser, S.J., and Kenyon, C. (1992). Activation of a C. elegans Antennapedia homologue in migrating cells controls their direction of migration. Nature *355*, 255-258.

Sato, A., Yamamoto, H., Sakane, H., Koyama, H., and Kikuchi, A. (2010). Wnt5a regulates distinct signalling pathways by binding to Frizzled2. The EMBO journal *29*, 41-54.

Sawa, H., and Korswagen, H.C. (2013). Wnt signaling in *C. elegans*. WormBook : the online review of C elegans biology, 1-30.

Sawa, H., Lobel, L., and Horvitz, H.R. (1996). The Caenorhabditis elegans gene lin-17, which is required for certain asymmetric cell divisions, encodes a putative seven-transmembrane protein similar to the Drosophila frizzled protein. Genes & development *10*, 2189-2197.

Schambony, A., and Wedlich, D. (2007). Wnt-5A/Ror2 regulate expression of XPAPC through an alternative noncanonical signaling pathway. Developmental cell *12*, 779-792.

Schwarz-Romond, T., Merrifield, C., Nichols, B.J., and Bienz, M. (2005). The Wnt signalling effector Dishevelled forms dynamic protein assemblies rather than stable associations with cytoplasmic vesicles. Journal of cell science *118*, 5269-5277.

Shafer, B., Onishi, K., Lo, C., Colakoglu, G., and Zou, Y. (2011). Vangl2 promotes Wnt/planar cell polarity-like signaling by antagonizing Dvl1-mediated feedback inhibition in growth cone guidance. Developmental cell *20*, 177-191.

Sheldahl, L.C., Slusarski, D.C., Pandur, P., Miller, J.R., Kuhl, M., and Moon, R.T. (2003). Dishevelled activates Ca2+ flux, PKC, and CamKII in vertebrate embryos. The Journal of cell biology *161*, 769-777.

Shimizu, H., Julius, M.A., Giarre, M., Zheng, Z., Brown, A.M., and Kitajewski, J. (1997). Transformation by Wnt family proteins correlates with regulation of beta-catenin. Cell growth & differentiation : the molecular biology journal of the American Association for Cancer Research *8*, 1349-1358.

Silhankova, M., and Korswagen, H.C. (2007). Migration of neuronal cells along the anterior-posterior body axis of C. elegans: Wnts are in control. Current opinion in genetics & development *17*, 320-325.

Slusarski, D.C., Yang-Snyder, J., Busa, W.B., and Moon, R.T. (1997). Modulation of embryonic intracellular Ca2+ signaling by Wnt-5A. Developmental biology *182*, 114-120.

Smalley, M.J., Signoret, N., Robertson, D., Tilley, A., Hann, A., Ewan, K., Ding, Y., Paterson, H., and Dale, T.C. (2005). Dishevelled (Dvl-2) activates canonical Wnt signalling in the absence of cytoplasmic puncta. Journal of cell science *118*, 5279-5289.

Song, H., and Poo, M. (2001). The cell biology of neuronal navigation. Nature cell biology *3*, E81-88.

Song, S., Zhang, B., Sun, H., Li, X., Xiang, Y., Liu, Z., Huang, X., and Ding, M. (2010). A Wnt-Frz/Ror-Dsh pathway regulates neurite outgrowth in Caenorhabditis elegans. PLoS genetics *6*.

Strutt, D. (2003). Frizzled signalling and cell polarisation in Drosophila and vertebrates. Development *130*, 4501-4513.

Sugimura, R., and Li, L. (2010). Noncanonical Wnt signaling in vertebrate development, stem cells, and diseases. Birth defects research Part C, Embryo today : reviews *90*, 243-256.

Sulston, J.E., and Horvitz, H.R. (1977). Post-embryonic cell lineages of the nematode, Caenorhabditis elegans. Developmental biology *56*, 110-156.

Sulston, J.E., Schierenberg, E., White, J.G., and Thomson, J.N. (1983). The embryonic cell lineage of the nematode Caenorhabditis elegans. Developmental biology *100*, 64-119.

Sym, M., Robinson, N., and Kenyon, C. (1999). MIG-13 positions migrating cells along the anteroposterior body axis of C. elegans. Cell *98*, 25-36.

Tada, M., and Smith, J.C. (2000). Xwnt11 is a target of Xenopus Brachyury: regulation of gastrulation movements via Dishevelled, but not through the canonical Wnt pathway. Development *127*, 2227-2238.

Takeuchi, M., Nakabayashi, J., Sakaguchi, T., Yamamoto, T.S., Takahashi, H., Takeda, H., and Ueno, N. (2003). The prickle-related gene in vertebrates is essential for gastrulation cell movements. Current biology : CB *13*, 674-679.

Takeuchi, S., Takeda, K., Oishi, I., Nomi, M., Ikeya, M., Itoh, K., Tamura, S., Ueda, T., Hatta, T., Otani, H., *et al.* (2000). Mouse Ror2 receptor tyrosine kinase is required for the heart development and limb formation. Genes to cells : devoted to molecular & cellular mechanisms *5*, 71-78.

Tree, D.R., Ma, D., and Axelrod, J.D. (2002). A three-tiered mechanism for regulation of planar cell polarity. Seminars in cell & developmental biology *13*, 217-224.

Usui, T., Shima, Y., Shimada, Y., Hirano, S., Burgess, R.W., Schwarz, T.L., Takeichi, M., and Uemura, T. (1999). Flamingo, a seven-pass transmembrane cadherin, regulates planar cell polarity under the control of Frizzled. Cell *98*, 585-595.

van Amerongen, R., Mikels, A., and Nusse, R. (2008). Alternative wnt signaling is initiated by distinct receptors. Science signaling *1*, re9.

van Amerongen, R., and Nusse, R. (2009). Towards an integrated view of Wnt signaling in development. Development *136*, 3205-3214.

Veeman, M.T., Slusarski, D.C., Kaykas, A., Louie, S.H., and Moon, R.T. (2003). Zebrafish prickle, a modulator of noncanonical Wnt/Fz signaling, regulates gastrulation movements. Current biology : CB *13*, 680-685.

Vivancos, V., Chen, P., Spassky, N., Qian, D., Dabdoub, A., Kelley, M., Studer, M., and Guthrie, S. (2009). Wnt activity guides facial branchiomotor neuron migration, and involves the PCP pathway and JNK and ROCK kinases. Neural development *4*, 7.

Wada, H., Tanaka, H., Nakayama, S., Iwasaki, M., and Okamoto, H. (2006). Frizzled3a and Celsr2 function in the neuroepithelium to regulate migration of facial motor neurons in the developing zebrafish hindbrain. Development *133*, 4749-4759.

Wallingford, J.B., and Harland, R.M. (2002). Neural tube closure requires Dishevelled-dependent convergent extension of the midline. Development *129*, 5815-5825.

Wallingford, J.B., Rowning, B.A., Vogeli, K.M., Rothbacher, U., Fraser, S.E., and Harland, R.M. (2000). Dishevelled controls cell polarity during Xenopus gastrulation. Nature *405*, 81-85.

Wallingford, J.B., Vogeli, K.M., and Harland, R.M. (2001). Regulation of convergent extension in Xenopus by Wnt5a and Frizzled-8 is independent of the canonical Wnt pathway. The International journal of developmental biology *45*, 225-227.

Walsh, G.S., Grant, P.K., Morgan, J.A., and Moens, C.B. (2011). Planar polarity pathway and Nance-Horan syndrome-like 1b have essential cell-autonomous functions in neuronal migration. Development *138*, 3033-3042.

Wang, X., Zhou, F., Lv, S., Yi, P., Zhu, Z., Yang, Y., Feng, G., Li, W., and Ou, G. (2013). Transmembrane protein MIG-13 links the Wnt signaling and Hox genes to the cell polarity in neuronal migration. Proceedings of the National Academy of Sciences of the United States of America *110*, 11175-11180.

Wang, Y., Guo, N., and Nathans, J. (2006). The role of Frizzled3 and Frizzled6 in neural tube closure and in the planar polarity of inner-ear sensory hair cells. The Journal of neuroscience : the official journal of the Society for Neuroscience *26*, 2147-2156.

Wang, Y., Macke, J.P., Abella, B.S., Andreasson, K., Worley, P., Gilbert, D.J., Copeland, N.G., Jenkins, N.A., and Nathans, J. (1996). A large family of putative transmembrane receptors homologous to the product of the Drosophila tissue polarity gene frizzled. The Journal of biological chemistry *271*, 4468-4476.

Wend, P., Holland, J.D., Ziebold, U., and Birchmeier, W. (2010). Wnt signaling in stem and cancer stem cells. Seminars in cell & developmental biology *21*, 855-863.

Whangbo, J., and Kenyon, C. (1999). A Wnt signaling system that specifies two patterns of cell migration in C. elegans. Molecular cell *4*, 851-858.

White, J.G., Southgate, E., Thomson, J.N., and Brenner, S. (1986). The structure of the nervous system of the nematode Caenorhabditis elegans. Philosophical transactions of the Royal Society of London Series B, Biological sciences *314*, 1-340.

Witte, F., Bernatik, O., Kirchner, K., Masek, J., Mahl, A., Krejci, P., Mundlos, S., Schambony, A., Bryja, V., and Stricker, S. (2010). Negative regulation of Wnt signaling mediated by CK1-phosphorylated Dishevelled via Ror2. FASEB journal : official publication of the Federation of American Societies for Experimental Biology *24*, 2417-2426.

Wolf, A.M., Lyuksyutova, A.I., Fenstermaker, A.G., Shafer, B., Lo, C.G., and Zou, Y. (2008). Phosphatidylinositol-3-kinase-atypical protein kinase C signaling is required for Wnt attraction and anterior-posterior axon guidance. The Journal of neuroscience : the official journal of the Society for Neuroscience *28*, 3456-3467.

Wouda, R.R., Bansraj, M.R., de Jong, A.W., Noordermeer, J.N., and Fradkin, L.G. (2008). Src family kinases are required for WNT5 signaling through the Derailed/RYK receptor in the Drosophila embryonic central nervous system. Development *135*, 2277-2287.

Yamaguchi, T.P., Bradley, A., McMahon, A.P., and Jones, S. (1999). A Wnt5a pathway underlies outgrowth of multiple structures in the vertebrate embryo. Development *126*, 1211-1223.

Yamamoto, H., Yoo, S.K., Nishita, M., Kikuchi, A., and Minami, Y. (2007). Wnt5a modulates glycogen synthase kinase 3 to induce phosphorylation of receptor tyrosine kinase Ror2. Genes to cells : devoted to molecular & cellular mechanisms *12*, 1215-1223.

Yanagawa, S., Matsuda, Y., Lee, J.S., Matsubayashi, H., Sese, S., Kadowaki, T., and Ishimoto, A. (2002). Casein kinase I phosphorylates the Armadillo protein and induces its degradation in Drosophila. The EMBO journal *21*, 1733-1742.

Yang, L., Sym, M., and Kenyon, C. (2005). The roles of two C. elegans HOX co-factor orthologs in cell migration and vulva development. Development *132*, 1413-1428.

Yoshikawa, S., McKinnon, R.D., Kokel, M., and Thomas, J.B. (2003). Wnt-mediated axon guidance via the Drosophila Derailed receptor. Nature *422*, 583-588.

Zecca, M., Basler, K., and Struhl, G. (1996). Direct and long-range action of a wingless morphogen gradient. Cell *87*, 833-844.

Zhang, X., Abreu, J.G., Yokota, C., MacDonald, B.T., Singh, S., Coburn, K.L., Cheong, S.M., Zhang, M.M., Ye, Q.Z., Hang, H.C., *et al.* (2012). Tiki1 is required for head formation via Wnt cleavage-oxidation and inactivation. Cell *149*, 1565-1577.

Zhong, J., Kim, H.T., Lyu, J., Yoshikawa, K., Nakafuku, M., and Lu, W. (2011). The Wnt receptor Ryk controls specification of GABAergic neurons versus oligodendrocytes during telencephalon development. Development *138*, 409-419.

Zinovyeva, A.Y., and Forrester, W.C. (2005). The C. elegans Frizzled CFZ-2 is required for cell migration and interacts with multiple Wnt signaling pathways. Developmental biology *285*, 447-461.

Zinovyeva, A.Y., Yamamoto, Y., Sawa, H., and Forrester, W.C. (2008). Complex network of Wnt signaling regulates neuronal migrations during Caenorhabditis elegans development. Genetics *179*, 1357-1371.

Chapter 2

Cell intrinsic modulation of Wnt signaling controls neuroblast migration in *C. elegans*

Remco A. Mentink[1], Teije C. Middelkoop[1], Lorenzo Rella[1], Ni Ji[2, 3], Chung Yin Tang[1], Marco C. Betist[1], Alexander van Oudenaarden[1,2] and Hendrik C. Korswagen[1]

[1]Hubrecht Institute, Royal Netherlands Academy of Arts and Sciences and University Medical Center Utrecht, Utrecht, The Netherlands. [2]Department of Physics and department of Biology, [3]Department of Brain and Cognitive Sciences, Massachusetts Institute of Technology, Cambridge, Massachusetts, USA.

Adapted from Developmental Cell, in press

Abstract

Members of the Wnt family of secreted signaling proteins are key regulators of cell migration and axon guidance. In the nematode *C. elegans*, the migration of the QR neuroblast descendants requires multiple Wnt ligands and receptors. We found that the migration of the QR descendants is divided into three sequential phases that are each mediated by a distinct Wnt signaling mechanism. Importantly, the transition from the first to the second phase – which determines the final position of the QR descendants along the anteroposterior body axis – is mediated through a cell autonomous process, in which the time-dependent expression of a Wnt receptor turns on the canonical Wnt/ß-catenin signaling response that is required to terminate long-range anterior migration. Our results show that in addition to direct guidance of cell migration by Wnt morphogenic gradients, cell migration can also be controlled indirectly through cell intrinsic modulation of Wnt signaling responses.

Introduction

Morphogens such as Wnt proteins play a central role in embryonic patterning by providing positional information to cells in developing tissues (Zecca et al., 1996). In recent years, it has become clear that such morphogenic gradients also contribute to the guidance of migrating cells and axons in the developing nervous system (Zou and Lyuksyutova, 2007). In the mammalian spinal cord, for example, Wnt gradients control the migration of commissural axons (Liu et al., 2005; Lyuksyutova et al., 2003) and in *C. elegans*, a gradient of the Wnt protein EGL-20 acts as a repulsive guidance cue in the migration of the HSN neurons (Pan et al., 2006). In addition to acting as direct repulsive or attractive guidance signals, Wnt proteins can also function as permissive factors that enable cells to respond to other guidance cues (Whangbo and Kenyon, 1999; Witze et al., 2008). How migrating cells and growth cones interpret information from Wnt ligands to adopt a specific migratory response is, however, still largely unknown.

Wnt proteins can trigger different signaling cascades in responding cells (Angers and Moon, 2009). In canonical Wnt signaling, binding of Wnt to the receptors Frizzled and Lrp6 leads to stabilization of the cytoplasmic protein ß-catenin, which in turn interacts with members of the TCF family of transcription factors to co-activate the expression of specific sets of target genes (Clevers and Nusse, 2012). Wnt can also signal independently of ß-catenin through distinct non-canonical Wnt pathways, including a pathway that depends on the receptor tyrosine kinase Ror2 (Green et al., 2008b) and a pathway that requires the planar cell polarity (PCP) components Van Gogh (Vangl) and Prickle (Pk) (Wallingford, 2012).

Studies on the role of Wnt signaling in cell and axon migration have been hampered by the complexity of the vertebrate embryo and the multitude of Wnt ligands and receptors that are present in the vertebrate genome. The nematode *C. elegans* offers a more tractable system with only 5 Wnt ligands, 4 Frizzled receptors and single orthologs of Ror2, Vangl and Pk that control the migration and polarity of defined cells and axons (Eisenmann, 2005; Korswagen, 2002; Sanchez-Alvarez et al., 2011; Silhankova and Korswagen, 2007). Among the cells that migrate in response to Wnt signaling is the QR neuroblast and its descendants (Figure 1A). During the first stage of larval development, the QR lineage generates a specific set of descendants: an anterior daughter cell (QR.a) that divides once to generate an apoptotic cell and a cell (QR.ap) that differentiates into a chemosensory neuron, and a posterior daughter cell (QR.p) that divides twice to generate an apoptotic cell and two cells (QR.paa and QR.pap) that differentiate into a mechanosensory neuron and an interneuron, respectively (Sulston and Horvitz, 1977). Throughout this process, each QR neuroblast descendant migrates to a highly stereotypic position along the anteroposterior body axis. Previous studies have shown that the migration of QR.p and its descendants (abbreviated as QR descendants unless indicated otherwise) requires multiple Wnt ligands and receptors (Harterink et al., 2011; Kim and Forrester, 2003; Zinovyeva and Forrester, 2005; Zinovyeva et al., 2008). These observations raise the question how the QR descendants integrate this complex Wnt signaling information to migrate to their precisely defined final positions.

Here, we show that the migration of QR descendants can be divided into three sequential phases, each of which is controlled by a distinct Wnt signaling mechanism. First, anterior migration is mediated through parallel-acting MOM-5/Frizzled and CAM-1/Ror2 dependent non-canonical Wnt pathways. Second, once QR.pa reaches its final position, anterior migration is stopped by activation of canonical Wnt/ß-catenin signaling. Finally, the

migration of QR.paa and QR.pap to their specific dorsoventral positions requires the PCP pathway components VANG-1/Vangl and PRKL-1/Pk. Importantly, we found that Wnt ligands do not act instructively in this process. Instead, our results show that the final position of QR.pa along the anteroposterior body axis is determined through a cell intrinsic timing mechanism that turns on canonical Wnt/ß-catenin signaling by upregulating the expression of the Wnt receptor *mig-1*. Our results are consistent with a model in which time-dependent switching between Wnt signaling pathways rather than positional information from Wnt ligands controls the highly stereotypic migration of QR.p and its descendants.

Results

The Wnt ligands EGL-20 and CWN-1 do not provide positional information to the migrating QR.p descendants

Mutations in different Wnt ligand and receptor genes have been shown to interfere with the anterior migration of the QR descendants (Harris et al., 1996; Whangbo and Kenyon, 1999; Zinovyeva and Forrester, 2005; Zinovyeva et al., 2008). Using the final anterior position of QR.paa and QR.pap (abbreviated as QR.pax) as a measure of total migration distance, we confirmed that the QR.pax localize at more posterior positions in *egl-20* and *cwn-1* Wnt null mutants (Figure 1B). This defect was strongly enhanced in *cwn-1*; *egl-20* double mutants, indicating that the two Wnt ligands act in parallel to control anterior migration of the QR descendants (Zinovyeva et al., 2008). Mutation of the Wnt gene *cwn-2* did not affect QR.pax localization, but enhanced the undermigration phenotype of *egl-20* and weakly of *cwn-1*, consistent with a minor role of *cwn-2* in the migration process (Figure S1A).

egl-20 is expressed by a group of cells in the tail region and forms a posterior to anterior concentration gradient that acts instructively in guiding the migration of the HSN neurons (Coudreuse et al., 2006; Pan et al., 2006; Whangbo and Kenyon, 1999). Previous studies have indicated that this gradient does not function as a directional guidance signal in QR descendant migration (Whangbo and Kenyon, 1999). Consistently, we found that reversal of the EGL-20 concentration gradient by *ceh-22* promoter directed expression of *egl-20* in the pharynx (Okkema and Fire, 1994; Yamamoto et al., 2011) significantly rescues the QR.pax undermigration phenotype of *egl-20* mutants (Figure 1B). However, when *egl-20* is ubiquitously overexpressed using a heat inducible promoter, the QR.pax migrate beyond their wild type positions (Figure 1B) (Whangbo and Kenyon, 1999), indicating that EGL-20 can promote the migration of the QR descendants when present at elevated levels.

cwn-1 is also expressed in the posterior, but in a broader region than *egl-20* (Harterink et al., 2011; Pan et al., 2006). To investigate whether CWN-1 functions as an instructive guidance signal, we investigated whether uniform expression of *cwn-1* restores the normal anterior migration of the QR descendants in a *cwn-1* null mutant background. As shown in Figure 1B, heat-shock promoter directed expression of *cwn-1* rescued the undermigration phenotype of *cwn-1(ok546)*. Furthermore, expression of *cwn-1* in the pharynx also significantly rescued QR.pax migration in the *cwn-1* null mutant background. However, in contrast to EGL-20, overexpression of CWN-1 did not induce overmigration of the QR.pax. These results support the notion that morphogenic gradients of EGL-20 and CWN-1 do not provide positional information to the migrating QR descendants. There is, however, a difference in the ability of EGL-20 and CWN-1 to promote the migration of the QR descendants when these Wnt ligands are overexpressed.

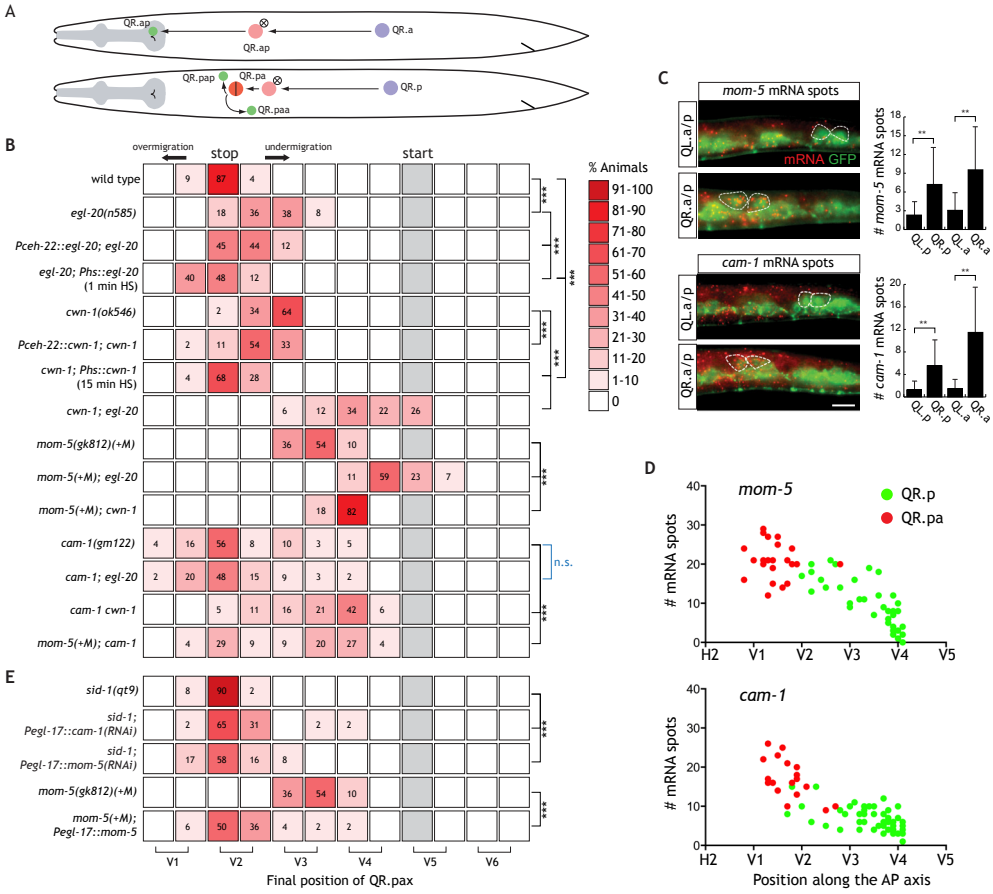

Figure 1. *mom-5/Frizzled* and *cam-1/Ror2* act in parallel genetic pathways to control the anterior migration of the QR descendants. (**A**) Schematic overview of the anterior migration of QR.a and QR.p and their descendants. Apoptotic cells are indicated as white cells with a cross, while the final QR descendants are indicated in green. The final position of QR.pa division is indicated in red. (**B, E**) Average position of the QR descendants QR.pap and QR.paa with respect to the seam cells V1.a to V6.p (lower brackets indicate Vn.a (left) and Vn.p (right) daughters of Vn cells). Values listed are percentiles of total cells scored, n>50 for all genotypes. A color (red) coded heat map represents the range of percentile values. The *hsp16.2* heat-shock promoter was used to drive ubiquitous expression of *egl-20* and *cwn-1* and time of heat-shock (HS) is indicated. The *ceh-22* promoter was used to drive anterior expression of *egl-20* and *cwn-1* in the pharynx (Okkema and Fire, 1994; Yamamoto et al., 2011). Q lineage specific RNAi was performed by expressing *cam-1* or *mom-5* dsRNA using the *egl-17* promoter (Burdine et al., 1998) in the RNAi spreading defective mutant *sid-1(qt9)* (Winston et al., 2002). Statistical significance was calculated using Fisher's exact test (*** p<0.0001). (**C**) Single molecule mRNA FISH of *cam-1* and *mom-5* mRNA (red). The Q neuroblasts (outlined with dotted line) and seam cells are labeled with GFP (*hels63*). Quantification of mRNA spots is indicated as mean ± SD (n>30). Statistical significance was calculated using an unpaired t-test (** p<0.001). (**D**) *cam-1* and *mom-5* transcription dynamics in single QR.p (green) and QR.pa (red) neuroblast daughter cells as measured in wild type animals (n>60 for both mRNA species). The number of mRNA spots per cell is plotted against the cell position with respect to the seam cells H2 to V5. See also Figure S1.

The Wnt receptors MOM-5/Frizzled and CAM-1/Ror2 act in parallel genetic pathways to promote anterior migration of the QR descendants

Analysis of Wnt receptor mutants showed that the QR.pax are posteriorly displaced in mutants of the Frizzled *mom-5* and the Ror2 ortholog *cam-1* (Figure 1B) (Kim and Forrester, 2003; Zinovyeva et al., 2008). *mom-5* has an essential function in early embryogenesis (Thorpe et al., 1997), but homozygous null mutant offspring of heterozygous mothers (*mom-5* +M) is viable. Despite this maternal contribution, *mom-5* (+M) mutants exhibit a highly penetrant QR.pax undermigration phenotype. To investigate whether *mom-5* acts cell autonomously in QR descendant migration, we first examined whether *mom-5* is expressed in the QR lineage. Using a quantitative single molecule mRNA fluorescent *in situ* hybridization (smFISH) method (Middelkoop et al., 2012; Raj et al., 2008), we found that *mom-5* is expressed in the Q neuroblasts and their descendants (Figure 1C). Quantification of *mom-5* mRNA spots revealed that *mom-5* is expressed at a significantly higher level in the QR descendants than in the lineally equivalent QL descendants, which is consistent with the observation that *mom-5* mutants are defective in QR, but not QL descendent migration (Zinovyeva et al., 2008). Furthermore, we found that the expression of *mom-5* gradually increases in the QR lineage (average of 2.9 ± 2.2 transcripts in QR, 7.8 ± 6.2 in QR.p and 21 ± 4.6 in QR.pa, n>20) (Figures 1D and S1D).

To investigate whether *mom-5* is required in the QR descendants, we used the *egl-17* promoter to specifically express wild type *mom-5* in the Q lineage of *mom-5* (+M) mutants (Burdine et al., 1998; Ou and Vale, 2009). As shown in Figure 1E, this significantly restored QR.pax migration in *mom-5(gk812)* (+M) mutants. Furthermore, we found that Q lineage specific knock down of *mom-5* by *egl-17* promoter directed expression of *mom-5* double stranded RNA (dsRNA) resulted in a weak but significant undermigration of the QR.pax (Figure 1E). We conclude that *mom-5* functions cell autonomously in QR descendant migration.

Mutation of the Ror2 ortholog *cam-1* also induced significant undermigration of the QR.pax (Figure 1B) (Kim and Forrester, 2003; Zinovyeva et al., 2008). The penetrance of this phenotype was however lower than in *mom-5* (+M) mutants, and the QR.pax also localized in a broader region along the anteroposterior axis. Examination of endogenous *cam-1* expression showed that *cam-1* is expressed in the Q neuroblast lineage (Figure 1C). Similar to *mom-5*, *cam-1* was expressed at a significantly higher level in the QR descendants than in the QL descendants, which is in agreement with the requirement of *cam-1* for QR, but not QL descendant migration (Zinovyeva et al., 2008). Furthermore, we found that the expression of *cam-1* also gradually increases during QR lineage progression (average of 5.3 ± 3.3 mRNA spots in QR, 5.5 ± 4.8 in QR.p and 17 ± 5.2 in QR.pa, n>20) (Figures 1D and S1D). To investigate whether *cam-1* is required in the QR descendants, we knocked down *cam-1* by Q lineage specific expression of *cam-1* dsRNA. As shown in Figure 1E, this resulted in weak but significant QR.pax undermigration, consistent with a cell autonomous function of *cam-1* in QR descendant migration.

To examine whether *mom-5* and *cam-1* are part of a common signaling mechanism or of parallel pathways, we examined *mom-5* (+M); *cam-1* double mutants (Figure 1B). We found that the final position of the QR.pax was shifted towards the posterior, indicating that loss of both receptors enhances the defect in QR descendant migration. In addition, the more widespread distribution of the QR.pax observed in *cam-1* single mutants was retained in the double mutant. We conclude that *mom-5* and *cam-1* act in parallel to control QR descendant migration.

Next, we investigated the genetic relationship between the two receptors and the different Wnt ligands involved in QR descendant migration. We found that the undermigration phenotype of *mom-5* (+M) was strongly enhanced by mutation of *egl-20*, indicating that *mom-5* and *egl-20* act in parallel genetic pathways (Figure 1B). In contrast, there was only weak (but statistically significant) enhancement in double mutants with *cwn-1*. A similar analysis showed that the undermigration phenotype of *cam-1* was strongly enhanced by mutation of *cwn-1*, while the *cam-1*; *egl-20* double mutant was not significantly different from *cam-1* single mutants (p=0.45, Fisher's exact test). Mutation of *cwn-2* weakly enhanced the *cam-1* induced undermigration phenotype, but had no effect in a *mom-5* (+M) mutant background (p=0.61, Fisher's exact test) (Figure S1A). Based on these results, we conclude that *egl-20* predominantly acts through the *cam-1* pathway, while *cwn-1* (and possibly *cwn-2*) mainly acts through the *mom-5* pathway.

The cytoplasmic protein Disheveled (Dvl) is a common component of both canonical and non-canonical Wnt signaling pathways (Angers and Moon, 2009). To investigate whether the parallel *cam-1* and *mom-5* pathways act through distinct Dvl isoforms, we assayed QR descendant migration in null mutants of the three Dvl orthologs *dsh-1*, *dsh-2* and *mig-5* (Figure S1C). We found that the QR.pax localized at more posterior positions in *dsh-2* (+M) single mutants. Furthermore, double mutant combinations of the different Wnt and Dvl mutants showed that *dsh-2* and *mig-5* enhanced the undermigration phenotype of *egl-20* as well as *cwn-1* and *cwn-2*, indicating that they act in both of the parallel pathways. This is consistent with the multifunctional nature of Dvl proteins in Wnt signal transduction (Gao and Chen, 2010).

MOM-5/Frizzled and CAM-1/Ror2 control distinct dynamic aspects of the long-range migration of QR.p

The migration of QR.p and its descendants can be divided into a long-range migration phase in which QR.p and QR.pa cover a total distance of about 38 µm along the anteroposterior body axis (29.2 ± 5.5 µm for QR.p and 8.9 ± 2.5 µm for QR.pa, n>70) and a short-range migration phase in which QR.paa and QR.pap localize to their final anteroposterior and dorsoventral positions (Figure 1A). We found that the distance of QR.p migration was strongly reduced in *egl-20*, *cwn-1*, *cam-1*, *mom-5* (+M) and *dsh-2* (+M) mutants (Figure S2B), indicating that the CAM-1/Ror2 and MOM-5/Frizzled dependent Wnt pathways are required for the long-range anterior migration of QR.p.

To examine dynamic aspects of QR.p migration, we performed static and time-lapse spinning-disc confocal imaging on animals in which the plasma membrane and nucleus of the Q neuroblasts and seam cells are marked with green fluorescent protein (GFP) (Middelkoop et al., 2012; Wildwater et al., 2011). Expression of these markers (a pleckstrin homology domain containing GFP and a fusion of histone 2B with GFP) did not influence the migration of the QR descendants (Middelkoop et al., 2012). We found that QR.p and its sister cell QR.a polarize along the anteroposterior axis during their migration. At the anterior side a leading edge is visible at which small filopodia like protrusions are formed, while the nucleus is positioned in the posterior half of the cell (Figure 2A and Movies 1A and 1B). Furthermore, we found that the F-actin binding protein COR-1/coronin, which marks the leading edge of migrating cells (Cai et al., 2007; Wang et al., 2013), is enriched at the anterior side of QR.p and QR.a (Figure S2A). To quantify QR.p polarity, we took the ratio of the distance of the nucleus to the most posterior (P) and the most anterior (A) side of the cell (Figure 2K). In

wild type animals, QR.p was predominantly polarized towards the anterior (ratio<1).

We found that this anterior polarization is lost in *cam-1* mutants (Figure 2D). Time-lapse imaging showed that QR.p and QR.a fail to maintain an anterior protrusion. Instead, the cells flip back and forth between anterior and posterior polarization (Movie 2), a behavior that is captured in the quantification of static images as a large spread in QR.p polarity

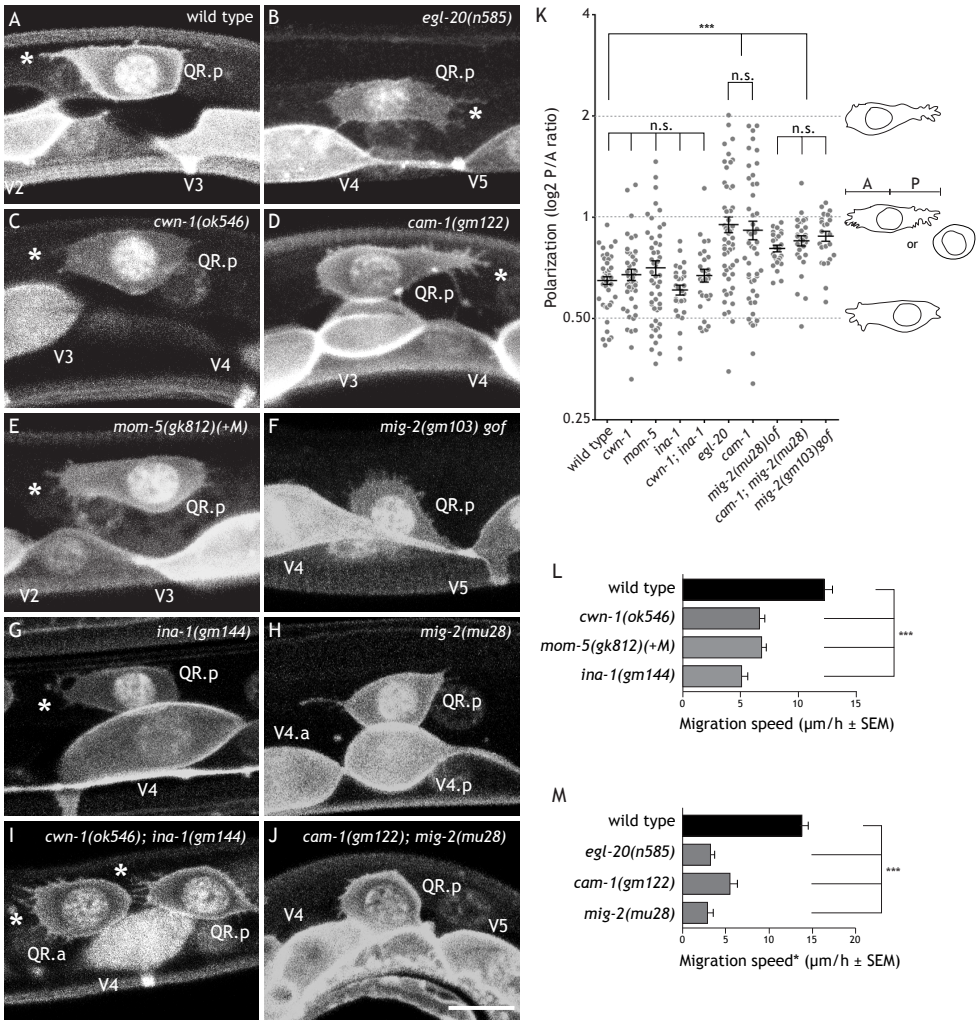

Figure 2. *egl-20/Wnt* and *cam-1/Ror2* are required for persistent polarization of QR.p. (**A-J**) Representative images of migrating QR.p cells in wild type and mutant animals in which QR.p and the seam cells express plasma membrane and nuclear localized GFP (*hels63*). Anterior is left. Asterisk (white) indicates the main protruding front (if any). Scale bar is 5 µm. (**K**) Quantification of QR.p polarity as the ratio of the distance of the nucleus to the posterior (P) and the anterior side (A) of the cell. Black lines indicate mean ± SEM. Statistical significance was calculated using an unpaired t-test (*** p<0.0001). The mean polarity of *cwn-1*, *mom-5*, *ina-1* and *cwn-1; ina-1* double mutants was not statistically different from wild type. (**L, M**) The speed of QR.p migration was calculated from the average anterior distance that QR.p covers in 1 hour (*or 2 hours in panel M) after the start of migration. Statistical significance was calculated using an unpaired t-test (*** p<0.0001). See also Figure S2.

ratios (Figure 2K) and loss of the asymmetric localization of COR-1 (Figure S2A). Consistent with our observation that *egl-20* and *cam-1* are part of the same genetic pathway, we found that the polarization and migration of QR.p was similarly affected in *egl-20* mutants (Figure 2B, K, M and Movie 3). We conclude that *egl-20* and *cam-1* are required for the persistent anterior polarization of QR.p.

In contrast, measurements of QR.p polarity in *cwn-1*, *cwn-2* and *mom-5* (+M) mutants showed that the average polarization direction is not significantly different from wild type (although it should be noted that polarization was more variable in *cwn-2* and *mom-5* mutants, $p<0.001$, Levene's test) (Figures 2C, 2E, 2K and S2C) and that COR-1 is normally localized at the anterior side of the cell (Figure S2A). Furthermore, time-lapse imaging revealed that QR.p and QR.a remain correctly polarized towards the anterior in *mom-5* (+M) mutants (Movie 4). The overall speed of migration was however significantly reduced (Figure 2L). The absence of a polarity phenotype in *cwn-1*, *cwn-2* and *mom-5* (+M) mutants is in agreement with the notion that these genes function in a common pathway that is functionally distinct from the *egl-20* and *cam-1* dependent pathway. This conclusion is further supported by the observation that loss of *cwn-1* does not significantly change the QR.p polarity phenotype of *egl-20* mutants (Figure S2C).

It has previously been shown that a gain of function mutation of the Rac family member *mig-2* affects the persistent polarization of the QL descendant QL.ap, while mutation of the integrin α-subunit gene *ina-1* affects the speed of QL.ap migration independently of polarity (Ou and Vale, 2009). It was therefore proposed that *mig-2* and *ina-1* function in distinct pathways that separately control the polarity and speed of QL.ap. Based on the similarity of the *cam-1* mutant phenotype to *mig-2*(gof) and *mom-5* to *ina-1*, we hypothesized that the *cam-1* pathway may localize the activity of Rac proteins such as *mig-2*, while the *mom-5* pathway may regulate migration speed by controlling integrin dynamics. Consistent with the study of Ou and colleagues, we found that loss of *ina-1* reduced QR.p migration speed without affecting QR.p polarity (Figures 2G, 2K and 2L and Movie 5). Because *mom-5; ina-1* double mutants were not viable, we examined QR.p polarity in *cwn-1; ina-1* double mutants. We found that the double mutant had a similar average QR.p polarity ratio as observed in the *cwn-1* and *ina-1* single mutants (Figures 2I and 2K). The final position of QR.p was however shifted posteriorly (Figure S2B), indicating that the defect in QR.p migration is enhanced in the double mutant. The lack of a polarity phenotype in the *cwn-1; ina-1* double mutant shows that both genes are dispensable for QR.p polarization. The enhanced defect in QR.p migration suggests, however, that the CWN-1 and MOM-5 dependent Wnt pathway and INA-1 control QR.p migration independently.

We found that QR.p did not form a clear leading edge and was mostly unpolarized in *mig-2(mu28)* loss of function and *mig-2(gm103)* gain of function mutants (Figures 2F, 2H and 2K and Movies 6 and 7). Furthermore, QR.p was mostly unpolarized in the *cam-1; mig-2(mu28)* double mutant, a phenotype that was quantitatively similar to the *mig-2(mu28)* single mutant (Figures 2J and 2K). The suppression of the random polarization phenotype of *cam-1* indicates that *mig-2* functions downstream of *cam-1*. This suppression could be related to a general requirement of *mig-2* for protrusion formation, but is also in agreement with our model that the CAM-1 pathway may control the persistent polarization of QR.p by regulating the activity of MIG-2. However, we found that the QR.p migration defect of the *cam-1*; *mig-2(mu28)* double mutants was enhanced compared to the single mutants (Figure S2B), indicating that in addition to this potentially shared function in QR.p polarization,

CAM-1 and MIG-2 also have separate functions in QR.p migration.

Taken together, these results support our conclusion that the Wnt receptors CAM-1/Ror2 and MOM-5/Frizzled function in parallel to control the long-range anterior migration of QR.p. Furthermore, our results demonstrate that CAM-1 and MOM-5 mediate distinct dynamic aspects of the migration, with the CAM-1 pathway regulating the persistent polarization of QR.p and the MOM-5 pathway controlling migration independently of polarity.

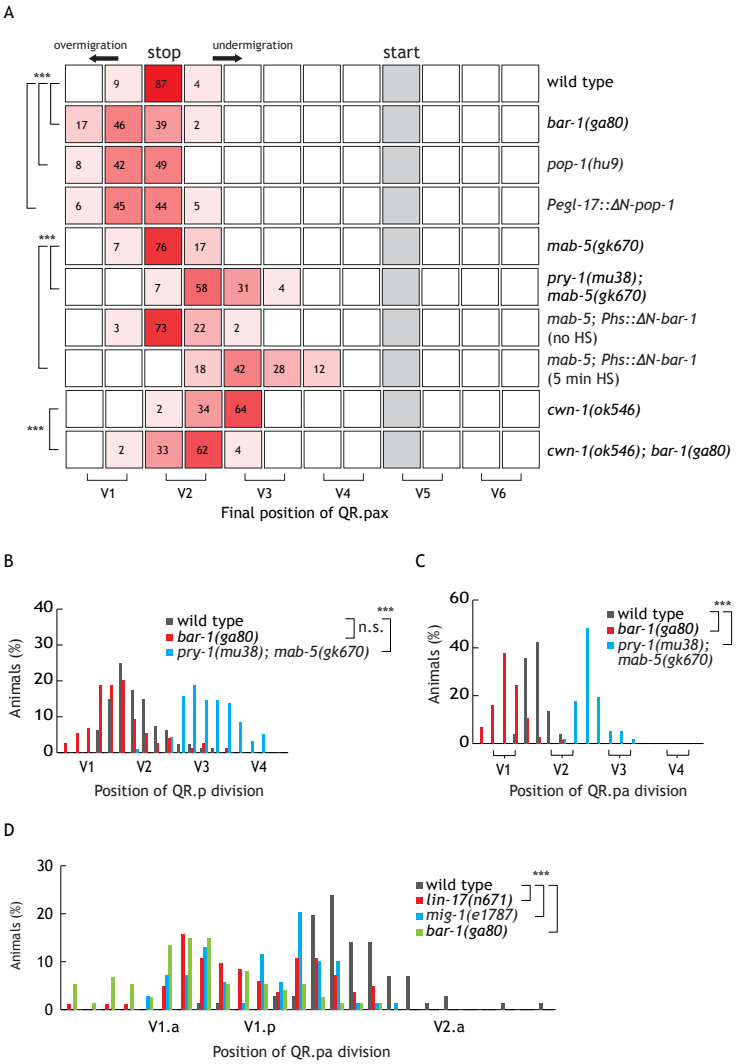

Figure 3. Canonical Wnt/ß-catenin signaling acts cell autonomously to terminate migration of QR.pa. (**A**) Average position of the QR descendants QR.pap and QR.paa with respect to the seam cells V1.a to V6.p (lower brackets indicate Vn.a (left) and Vn.p (right) daughters of Vn cells). Values listed are percentiles of total cells scored, n>50 for all genotypes. The time of heat-shock (HS) to induce expression of N-terminally truncated BAR-1 is indicated. (**B**) Position of QR.p division with respect to the seam cells V1-V4 (n>75 for all genotypes). (**C**) Position of QR.pa division with respect to the seam cells V1-V4 (n>70 for all genotypes). (**D**) Position of QR.pa division with respect to the seam cells V1.p to V2.a (n>70 for all genotypes). In all cases, statistical significance was calculated using Fisher's exact test (*** p<0.0001). See also Figure S3.

Termination of QR.pa migration requires activation of canonical Wnt/ß-catenin signaling

The long-range anterior migration of the QR descendants ends when QR.pa divides at a position between the seam cells V1.p and V2.a (Figure 1A). To investigate how QR.pa is instructed to stop at this specific position, we examined mutants in which the QR descendants migrate beyond their wild type positions. Again using the final position of QR.paa and QR.pap as a proxy for total migration distance, we found that the QR.pax overmigrate in mutants of the canonical ß-catenin gene *bar-1* (Figure 3A), as has been observed previously (Whangbo and Kenyon, 1999). ß-catenin is a central component of the canonical Wnt/ß-catenin pathway that binds to members of the TCF family of transcription factors to co-activate the expression of Wnt target genes (Clevers and Nusse, 2012). We found that mutation of the single *C. elegans* TCF ortholog *pop-1* induces a similar overmigration phenotype as *bar-1*. Furthermore, specific expression of dominant negative N-terminally truncated POP-1 (Korswagen et al., 2000) in the Q cell lineage induced significant overmigration as well (Figure 3A), demonstrating that *pop-1* functions cell autonomously in QR descendant migration.

The overmigration observed in *bar-1* and *pop-1* mutants indicates that activation of canonical Wnt/ß-catenin signaling may be required to stop migration of the QR descendants. To test this possibility, we expressed constitutively active N-terminally truncated BAR-1 using a heat-shock inducible promotor (Gleason et al., 2002) and asked whether early activation of Wnt/ß-catenin signaling prematurely terminates QR descendant migration. To prevent activation of the posterior migration pathway that is induced by Wnt/ß-catenin signaling in the QL lineage, we performed these experiments in animals carrying a null mutation in the Wnt target gene *mab-5* (Figure 3A) (Korswagen et al., 2000; Maloof et al., 1999; Salser and Kenyon, 1992). Consistent with our hypothesis, we found that a brief heat-shock at the beginning of the migration process leads to significant undermigration of the QR.pax (Figure 3A). A similar result was obtained when we constitutively activated Wnt/ß-catenin signaling by introducing a mutation in the negative regulator *pry-1*/Axin (Korswagen et al., 2002).

To directly examine the effect of canonical Wnt/ß-catenin signaling on the long-range migration of QR.p and QR.pa, we determined the position at which these cells end their migration in wild type and Wnt/ß-catenin pathway mutants. In *bar-1* mutants, the position at which QR.p terminates its migration and divides was similar to wild type (Figure 3B) (p=0.1, Fisher's exact test). In contrast, there was significant overmigration of QR.pa, with the majority of cells dividing at a more anterior position than in wild type animals (Figures 3C and 3D). The opposite phenotype was observed when Wnt/ß-catenin signaling was constitutively activated by mutation of *pry-1*, with both QR.p and QR.pa terminating their migration at a more posterior position than in wild type animals (Figures 3B and 3C). The short-range anteroposterior migration of QR.paa and QR.pap was not affected in *bar-1* mutants (Figure S3). Based on these results, we conclude that canonical Wnt/ß-catenin signaling is necessary and sufficient to inhibit the long-range anterior migration of the QR descendants.

The specific effect of *bar-1* on QR.pa migration indicates that canonical Wnt/ß-catenin signaling is activated at the end of the long-range migration phase to terminate QR.pa migration. To test this model, we determined QR.p migration speed and the final localization of the QR.pax in double mutants between *bar-1* and the QR.p migration mutant *cwn-1*. We found that the speed of QR.p migration was similar as in the *cwn-1* single mutant (Fig. 5C).

The final position of the QR.pax was however intermediate to the overmigration induced by *bar-1* and the undermigration induced by *cwn-1* (Fig. 3A). We conclude that long-range anterior migration (non-canonical Wnt signaling) and termination of anterior migration (canonical Wnt/ß-catenin signaling) are separate and sequentially acting processes.

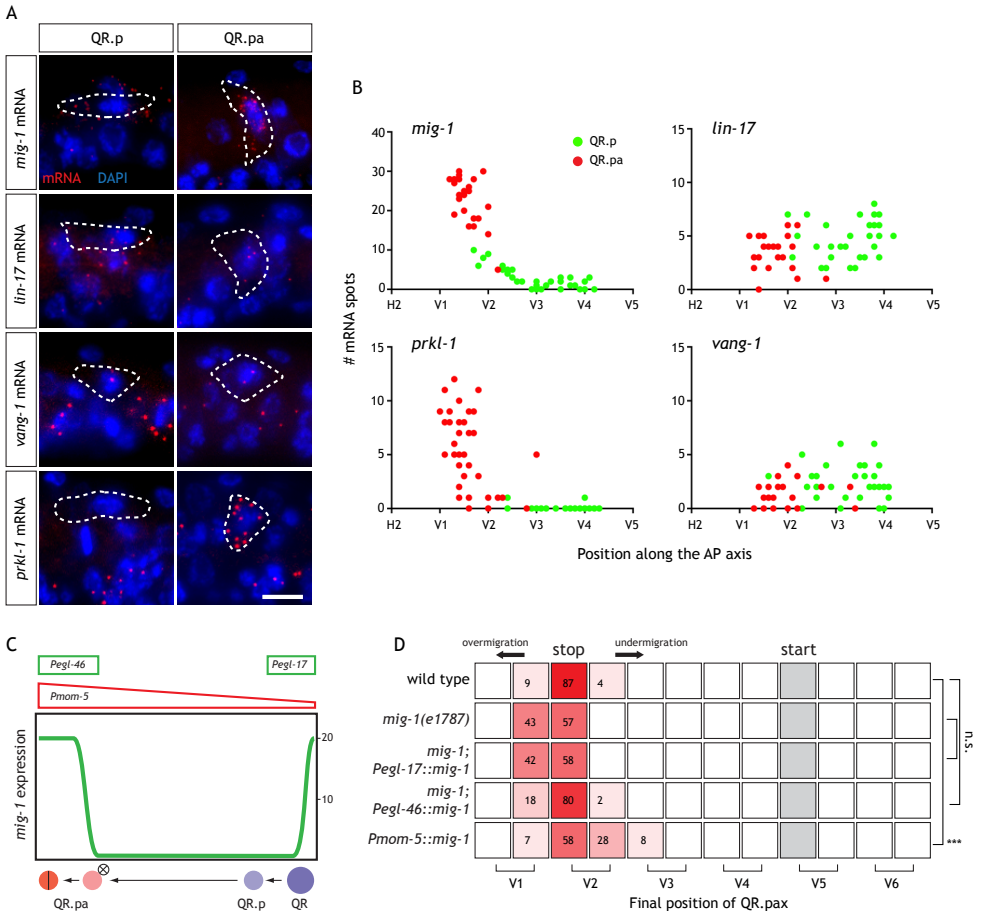

Figure 4. Upregulation of mig-1/Frizzled expression in QR.pa is necessary and sufficient to terminate QR.pa migration. (**A**) smFISH analysis of endogenous *mig-1*, *lin-17*, *vang-1* and *prkl-1* mRNA in QR.p and QR.pa. Images of QR.p and QR.pa were taken in synchronized populations grown for 5-6 and 7-8 hours after hatching, respectively. Nuclei are visualized with DAPI staining. Scale bar is 5 µm. (**B**) *mig-1*, *lin-17*, *vang-1* and *prkl-1* transcription dynamics in single QR.p (green) and QR.pa (red) neuroblast daughter cells as measured in wild type animals (n>55 for each mRNA species). The number of mRNA spots per cell is plotted against the cell position with respect to the seam cells H2 to V5. (**C**) Schematic overview of *mig-1* transcription dynamics in QR and its descendants during their migration in wild type animals. Expression is initially high in QR and then drops quickly during initial migration. In QR.p expression is low and rises sharply again in QR.pa. On top of the graph the transcription dynamics of *egl-17*, *egl-46* and *mom-5* are indicated. (**D**) Average position of the QR descendants QR.pap and QR.paa with respect to the seam cells V1.a to V6.p (lower brackets indicate Vn.a (left) and Vn.p (right) daughters of Vn cells). Values listed are percentiles of total cells scored, n>50 for all genotypes. Statistical significance was calculated using Fisher's exact test (*** p<0.0001).

MIG-1/Frizzled is necessary and sufficient for termination of QR.pa migration and is strongly upregulated at the end of the long-range migration phase

To investigate how QR.pa migration is regulated at the Wnt receptor level, we determined the position at which QR.pa divides in Frizzled mutants. We found that there was extensive overmigration of QR.pa in *mig-1* and *lin-17* mutants (Figure 3D). As in *bar-1* mutants, QR.p migration was not significantly affected (Figure S2B), indicating that *mig-1* and *lin-17* are specifically required for the canonical Wnt/ß-catenin pathway dependent termination of QR.pa migration. This is in agreement with the role of MIG-1 and LIN-17 in activation of canonical Wnt/ß-catenin signaling in the QL neuroblast lineage (Harris et al., 1996; Ji et al., 2013; Maloof et al., 1999).

Consistent with a cell autonomous function of *mig-1* and *lin-17* in migration termination, we found that both receptors are expressed in the QR.pa neuroblast (Figure 4A). However, quantification of *mig-1* and *lin-17* smFISH spots revealed that there are important differences in the temporal expression of the two receptors during QR lineage progression. We found that the expression of *lin-17* is relatively constant (average of 9.3 ± 4.7 transcripts in QR, 4.5 ± 1.6 transcripts in QR.p and 4.0 ± 1.6 transcripts in QR.pa, n>20) (Figures 4B and S1D). The expression of *mig-1*, on the other hand, is highly dynamic, with an initial expression of 19 ± 8.1 transcripts in QR, an almost complete loss of expression (1.2 ± 0.4) in QR.p and a striking eighteen-fold upregulation of expression (21 ± 1.2) in QR.pa (n>25) (Figures 4B and S1D).

The upregulation of *mig-1* at the end of the long-range anterior migration phase suggests that *mig-1* may act as a switch that turns on Wnt/ß-catenin signaling to stop anterior migration. To test this model, we asked which of the two phases of *mig-1* expression is required for the correct positioning of the QR.pax. We found that expression of *mig-1* using the *egl-17* promoter, which recapitulates the early expression of *mig-1* in QR (Figures 4C and S1D), did not rescue the overmigration phenotype of *mig-1(e1787)* (Figure 4D). In contrast, the overmigration phenotype was fully rescued when *mig-1* was specifically expressed in QR.pa using the *egl-46* promoter (Wu et al., 2001). Next, we examined whether expression of *mig-1* is sufficient to stop anterior migration. To test this, we used the *mom-5* promoter to express *mig-1* during QR.p migration. Consistent with our model, we found that such premature expression of *mig-1* resulted in significant undermigration of the QR.pax. We conclude that the upregulation of *mig-1* expression is necessary and sufficient to stop the anterior migration of QR.pa.

mig-1 expression is activated through a Q lineage intrinsic timing mechanism

Next, we investigated how the expression of *mig-1* is induced in QR.pa. One possibility is that positional cues – provided by localized or graded signals – induce *mig-1* expression at a specific position along the anteroposterior axis. An alternative possibility is that *mig-1* expression is regulated through a Q lineage intrinsic mechanism that turns on *mig-1* expression at a specific time in the migration process. To distinguish between these two possibilities, we first asked whether posterior displacement of QR.p and QR.pa interferes with *mig-1* expression. In gain of function mutants of the small GTPase *mig-2*, the anterior migration of QR.p is reduced (Ou and Vale, 2009) and the final position of QR.p and QR.pa is shifted about two seam cell positions to the posterior. We found that despite this difference in position along the anteroposterior axis, *mig-1* expression is still activated at wild type levels in QR.pa (Figure 5A). Next, we investigated whether anterior displacement of the

QR descendants influences *mig-1* expression. QR.p and QR.pa migrate beyond their normal positions when EGL-20 is overexpressed using a heat-inducible promoter (Figures 5A and 5B) (Whangbo and Kenyon, 1999). We found that when QR.p and QR.pa are shifted towards the anterior, *mig-1* is also expressed more anteriorly (Figure 5A). Taken together, these results

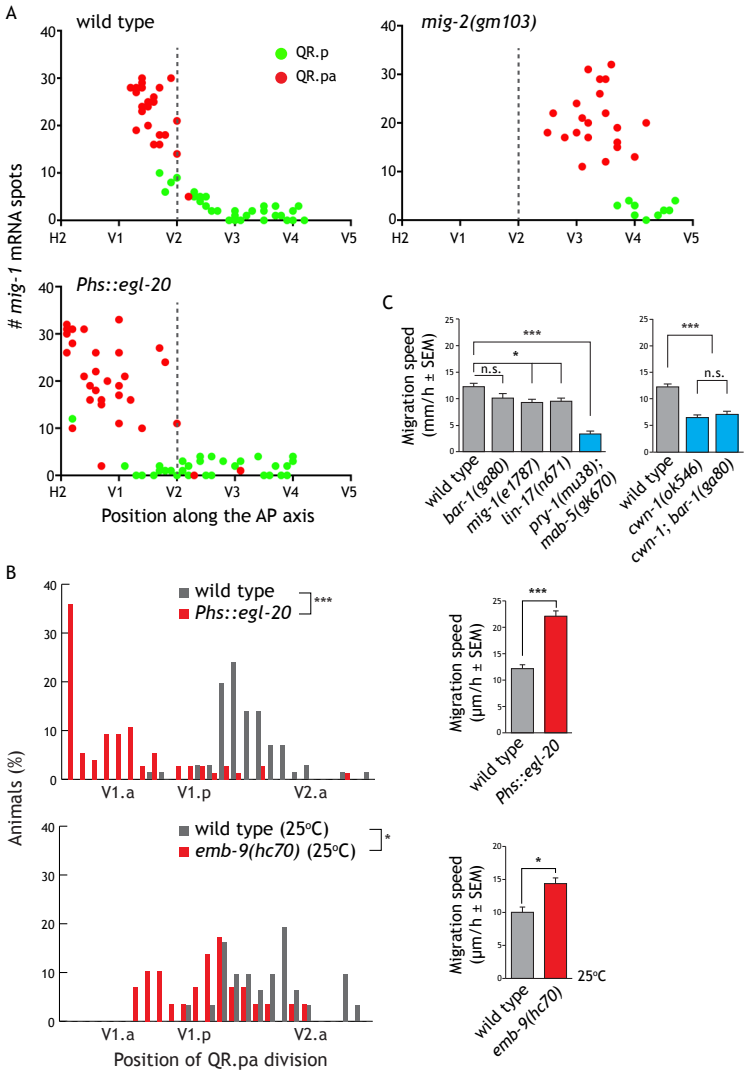

Figure 5. A QR lineage intrinsic mechanism controls the termination of QR.pa migration. (**A**) *mig-1* transcription dynamics in single QR.p (green) and QR.pa (red) neuroblast daughter cells as measured in wild type, *mig-2* (gof) mutants and *Phs::egl-20* transgenic animals (heat-shocked for 1 min) (n>30 for all genotypes). The number of mRNA spots per cell is plotted against the cell position with respect to the seam cells H2 to V5. Dashed line indicates the position of seam cell V2. (**B**) Left: Position of QR.pa division with respect to the seam cells V1.p to V2.a (n>30 for all genotypes). Statistical significance was calculated using Fisher's exact test (* p<0.01; *** p<0.0001). Right: The speed of QR.p migration was calculated from the average distance that QR.p covers in 1 hour after the start of migration. Statistical significance was calculated using an unpaired t-test (*** p<0.0001). EGL-20 expression was induced using a 1 min heat-shock. *emb-9* mutants were shifted to the non-permissive temperature of 25˚C 9-10 hours prior to analysis. (**C**) Speed of QR.p migration in wild type and mutant animals (* p<0.01; *** p<0.0001).

demonstrate that the upregulation of *mig-1* expression in QR.pa is not induced by positional cues.

The second possibility is that *mig-1* expression is regulated through a Q lineage intrinsic mechanism. We hypothesized that *mig-1* expression is induced by a timing mechanism that either counts total migration time or is coupled to the cell cycle of QR.p and QR.pa. In such a model, the position at which *mig-1* expression is induced and QR.pa migration is terminated will depend on the overall speed of migration: when migration speed is reduced, *mig-1* will be expressed more posteriorly and when speed is increased, *mig-1* will be expressed more anteriorly. This model is supported by the observation that in *mig-2* gain of function mutants, which express *mig-1* at a more posterior position than in wild type (Figure 5A), the speed of migration is strongly reduced (Ou and Vale, 2009). Furthermore, we found that overexpression of EGL-20, which leads to overmigration of QR.pa and more anterior *mig-1* expression, induces a significant increase in migration speed (Figure 5B). A similar correlation between migration speed and QR.pa overmigration was observed in the collagen mutant *emb-9* (Figure 5B), which may facilitate migration by providing a less dense extracellular matrix (C. Kenyon, personal communication).

The speed of QR.p migration was not increased in *mig-1*, *lin-17* and *bar-1* mutants (Figure 5C), which is consistent with our model that canonical Wnt/ß-catenin signaling is required for termination of QR.pa migration and not for the anterior migration process itself. Based on these results, we conclude that the end point of QR.pa migration is defined by the combined regulation of migration speed and the timing of *mig-1* expression and canonical Wnt/ß-catenin pathway activation.

The final short-range migration of QR.pap and QR.paa is dependent on the planar cell polarity components VANG-1/Vangl and PRKL-1/Pk

The last phase of QR descendant migration involves the short-range migration of the QR.pa daughter cells QR.pap and QR.paa (Figure 1A). Measurements of the final position of QR.pap and QR.paa showed that QR.pap localizes slightly anterior to the position of QR.pa division, while QR.paa migrates a short distance towards the posterior (Figures 6A, 6A' and 6A''). In addition, QR.pap moves to a specific dorsal position, where it differentiates into the neuron SDQR, while QR.paa migrates ventrally and differentiates into the neuron AVM (Figure 6C) (Hedgecock et al., 1987; Sulston and Horvitz, 1977).

In a small-scale screen of non-canonical Wnt pathway components (data not shown), we found that the average position of QR.paa and QR.pap was shifted towards the anterior in mutants of the planar cell polarity pathway components *vang-1*/Vangl and *prkl-1*/Pk (Figure S4A). Both genes likely function in the same pathway, as the QR.pax were similarly localized in the *vang-1; prkl-1* double mutant. Detailed analysis of the final localization of the individual QR descendants in *vang-1* and *prkl-1* mutants showed that the position of QR.pa division was not significantly different from wild type (p=0.97 and 0.10, Fisher's exact test, respectively) (Figure 6B), indicating that *vang-1* and *prkl-1* do not affect the canonical Wnt/ß-catenin pathway dependent termination of QR.pa migration. Instead, we found that *vang-1* and *prkl-1* are required for the final positioning of QR.paa and (to a lesser extent) of QR.pap (Figure 6B). Thus, in *vang-1* and *prkl-1* mutants, the short-range posterior migration of QR.paa was absent, with QR.paa either remaining at its starting position or moving slightly anterior. In the case of QR.pap, there was a slight but significant anterior shift in the final position.

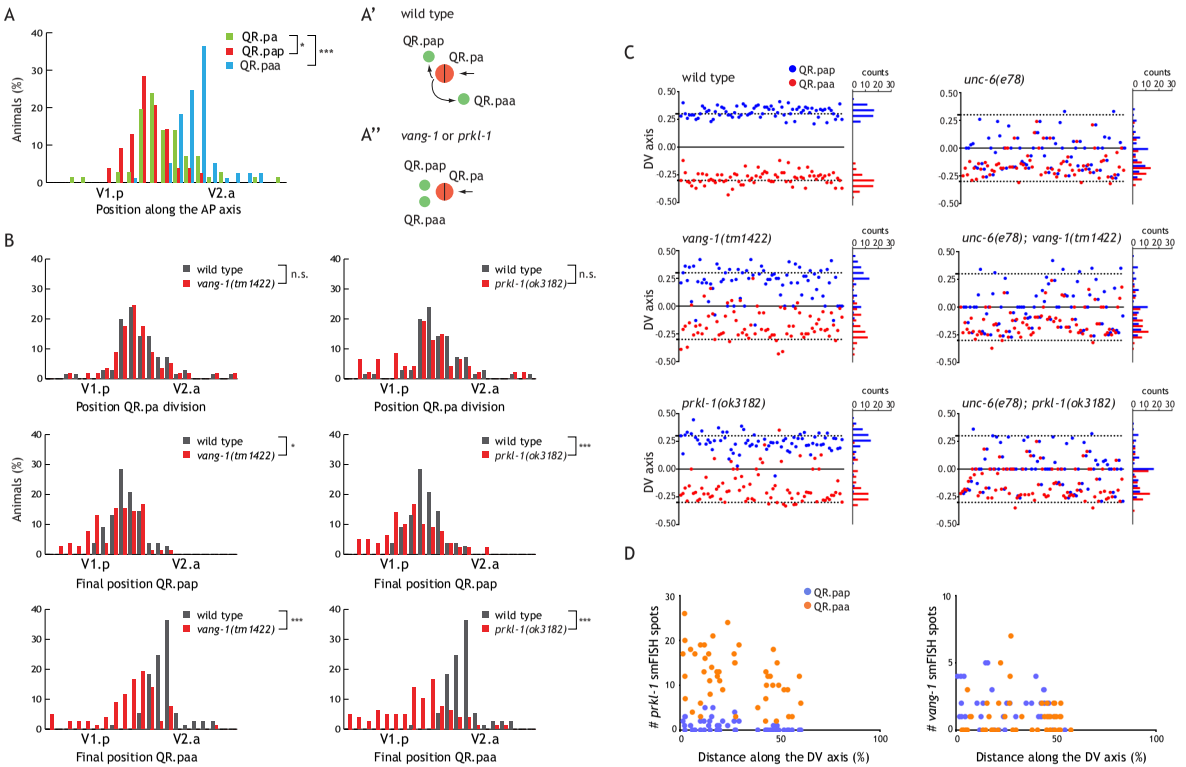

Figure 6. The planar cell polarity pathway components vang-1/Vangl and prkl-1/Pk control the final short-range migration of QR.pap and QR.paa. (**A**) Position of QR.pa, QR.pap and QR.paa relative to the seam cells V1.p to V2.a in wild type animals (n>70 for all cell types). Statistical significance was calculated using Fisher's exact test (* p<0.01; *** p<0.0001). (**A', A"**) Schematic representation of the short-range anteroposterior and dorsoventral migration of QR.paa and QR.pap in wild type and *vang-1* and *prkl-1* mutants. (**B**) Position of QR.pa, QR.pap and QR.paa relative to the seam cells V1.p to V2.a in wild type and mutant animals (n>70 for all genotypes). Statistical significance was calculated using Fisher's exact test (* p<0.01; *** p<0.0001). (**C**) Position of QR.pap and QR.paa on the dorsoventral axis (n>70 for all genotypes). Midline is set at 0 and dashed lines indicate the average position of QR.pap and QR.paa in wild type. The histogram on the right displays percentile counts along the dorsoventral axis. (**D**) *prkl-1* and *vang-1* transcription dynamics in single QR.pap (blue) and QR.paa (yellow) neuroblast daughter cells as measured in wild type animals (n>45 for both cell types). The number of mRNA spots per cell is plotted against the relative distance between the two QR.pax cells with respect to the total width of the dorsoventral axis, with a longer distance correlating to more advanced stages of dorsoventral migration. See also Figure S4.

We found that *vang-1* and *prkl-1* are also required for the dorsoventral positioning of QR.pap and QR.paa, with both cells showing either reduced or even reversed migration along the dorsoventral axis (Figure 6C). It has previously been shown that the dorsoventral position of QR.pap is regulated by UNC-6/netrin and the receptors UNC-5 and UNC-40/DCC (Kim et al., 1999). We confirmed the requirement of *unc-6* for the dorsal migration of QR.pap, but found that the ventral migration of QR.paa was also significantly affected in *unc-6*(*e78)* hypomorphic and *unc-6(ev400)* null mutants. In double mutants between *unc-6(ev400)* and *prkl-1*, QR.pap and QR.paa showed a similar dorsoventral distribution as in *unc-6* single mutants (p=0.58 and 0.13, unpaired, two tailed t-test, respectively) (Figures 6C and S4C). Comparable results were obtained with *unc-6*; *vang-1* double mutants. The absence of an enhanced dorsoventral migration phenotype in double mutants of *prkl-1* and *vang-1* with *unc-6* suggests that these genes may be part of a common genetic pathway. This conclusion is supported by our observation that the expression of the UNC-6 receptor *unc-40* is not influenced by loss of *prkl-1* (Figure S4D).

To determine in which cells *vang-1* and *prkl-1* are expressed during Q neuroblast migration, we performed smFISH analysis in L1 larvae (Figure S4B). We found that *vang-1* is expressed in both the QL and QR neuroblast lineages. In addition, *vang-1* mRNA was detected in hypodermal seam cells, the M mesoblast cell and in ventral nerve cord neurons. To investigate whether *vang-1* is required in the migrating QR descendants, we tested whether Q cell lineage specific expression of *vang-1* rescues QR.paa and QR.pap migration in a *vang-1* null mutant background. Consistent with a cell autonomous function of *vang-1*, we found that expression of *vang-1* in the Q cell lineage was sufficient to rescue QR.pax migration ($p<0.0001$, Fisher's exact test) (Figure S4A).

prkl-1 expression was observed in the Q neuroblast descendants, the M mesoblast cell and at low levels in ventral nerve cord neurons and unidentified cells in the head region (Figure S4B). Consistent with the more prominent role of *prkl-1* in QR.paa migration, we found that *prkl-1* is expressed at a significantly higher level in QR.paa than QR.pap (Figure 6D). Interestingly, smFISH analysis revealed that the expression of *prkl-1* is dynamically regulated during QR descendant migration. Thus, whereas *vang-1* transcription remained relatively constant throughout QR lineage progression, the expression of *prkl-1* was strongly upregulated at the end of the long-range migration phase (Figure 4B). These results indicate that – similar to the role of *mig-1* in QR.pa migration termination – upregulation of *prkl-1* expression may mediate the transition to the final short-range migration phase. In support of this model, we found that early expression of *prkl-1* in the QR lineage using the *egl-17* promoter did not rescue QR.pap and QR.paa migration in *prkl-1* null mutants (p=0.11, Fisher's exact test), while expression using the *egl-46* promoter, which is expressed late in the QR lineage, fully rescued the migration phenotype ($p<0.0001$, Fisher's exact test) (Figure S4A).

Discussion

Wnt proteins play an evolutionarily conserved role in guiding migrating cells and axons along the anteroposterior axis of the developing nervous system. In *C. elegans*, the anterior migration of the QR neuroblast descendants requires the activity of multiple Wnt ligands and receptors (Harterink et al., 2011; Kim and Forrester, 2003; Zinovyeva and Forrester, 2005; Zinovyeva et al., 2008). Here, we have investigated how the QR descendants integrate this

complex information to migrate to their precisely defined final positions. We found that the migration is divided in three sequential steps that are each mediated by a distinct Wnt signaling mechanism. Importantly, our results show that the QR descendants switch between these signaling mechanisms by temporally regulating the expression of the Frizzled receptor *mig-1* during the migration process. We conclude that cell intrinsic changes in the response to Wnt – rather than positional information from Wnt morphogenic gradients – control the highly stereotypic migration of QR descendants.

The long-range anterior migration of the QR descendants is dependent on the Wnt ligands EGL-20 and CWN-1. Both are expressed in the posterior body region and are expected to form posterior to anterior morphogenic concentration gradients (Coudreuse et al., 2006; Harterink et al., 2011; Pan et al., 2006; Whangbo and Kenyon, 1999). However, neither of these Wnt ligands appears to provide positional information to the migrating QR descendants, as uniform expression or even reversal of the EGL-20 and CWN-1 gradients is sufficient to restore normal QR.pax positioning in their respective mutant backgrounds. The permissive role of EGL-20 and CWN-1 indicates that other guidance signals may specify the direction of QR descendant migration. Previous studies have shown that anterior migration of the QR descendants requires the transmembrane protein MIG-13 (Masuda et al., 2012; Sym et al., 1999). Recent evidence suggests that MIG-13 acts cell autonomously in the QR descendants to promote anterior migration (Wang et al., 2013). Based on these observations and the results presented in this study, we propose that the QR descendants use MIG-13 to respond to an anterior guidance signal, but require Wnt signaling for motility (including regulation of migration speed by EGL-20), to terminate anterior migration and to switch to the final dorsoventral migration phase.

The first phase in the migration process is the MOM-5/Frizzled and CAM-1/Ror2 dependent long-range anterior migration of QR.p and QR.pa. Analysis of mutant combinations showed that CAM-1 and MOM-5 act in parallel pathways that control distinct aspects of the migration process. Using live cell time-lapse confocal imaging, we found that QR.p fails to persistently polarize in *cam-1* mutants, while in *mom-5* mutants, QR.p remains correctly polarized, but migrates at a strongly reduced speed. Interestingly, the phenotype of *cam-1* is remarkably similar to the defect in QL.ap polarity observed in gain of function mutants of the Rac-like small GTPase *mig-2*, while *mom-5* resembles mutants of the integrin alpha-subunit *ina-1* (Ou and Vale, 2009). Analysis of double mutants revealed that the *mom-5* pathway and *ina-1* likely function in parallel to control QR.p migration speed. The ectopic protrusion phenotype of *cam-1* was however suppressed by loss of *mig-2*, indicating that CAM-1 may control QR.p polarity by regulating the activity of MIG-2. In vertebrates, Ror2 has been shown to regulate filopodia formation (Schambony and Wedlich, 2007) and to control the polarity of migrating cells through reorientation of the microtubule organizing center (Nishita et al., 2010; Nomachi et al., 2008), but a direct link with Rac family GTPases has not been made. The CAM-1 dependent polarization of QR.a and QR.p therefore provides a valuable single cell assay to investigate how Ror2 signaling controls cell polarity and filopodia formation.

Previous studies have shown that CAM-1 has both cell autonomous and non-autonomous functions (Green et al., 2008b). CAM-1 has been proposed to act as a negative regulator of Wnt signaling by binding and sequestering Wnt proteins, a function that is required for the correct migration of the CAN and HSN neurons (Forrester et al., 1999; Kim and Forrester, 2003; Pan et al., 2006) and for modulating Wnt gradients during vulva development (Green et al., 2008a; Modzelewska et al., 2013). These functions are dependent on the

extracellular Wnt binding domain, but appear to be independent of the intracellular kinase domain. There is also evidence that CAM-1 acts as a Wnt receptor. Thus, kinase activity is required for the function of CAM-1 in orienting the division of vulva precursor cells (Green et al., 2008a), the guidance of the SIA and SIB axons that mediate nerve ring placement (Kennerdell et al., 2009) and for the outgrowth of the RME neurites (Song et al., 2010). Using *cam-1* alleles that mutate (*xd13*) or delete (*ks52*) the kinase domain, we could confirm that the kinase domain is also required for QR.p descendant migration (Figure S1B) (Kim and Forrester, 2003). The undermigration phenotype of these kinase domain mutants is however more subtle than observed in *cam-1* null mutants, indicating that CAM-1 has both kinase dependent and independent functions in QR descendant migration. This is consistent with the observation that the cytoplasmic domain of mammalian Ror2 also functions in the recruitment of effector proteins such as the actin regulator Filamin A (Nomachi et al., 2008). Interestingly, we found that in a low percentage of *cam-1* null mutants, the QR.pax migrate beyond their wild type positions. This phenotype was not observed in *cam-1* kinase mutants or when *cam-1* was specifically knocked down in the Q neuroblast lineage (Figures 1E and S1B), indicating that this represents a cell non-autonomous function. Overmigration of the QR.pax is also observed in mutants of the secreted Frizzled related protein *sfrp-1*, which acts as a general inhibitor of Wnt signaling (Harterink et al., 2011). Given this similarity in phenotype, we propose that in addition to a cell autonomous function in QR.p, *cam-1* also functions outside of the QR lineage to dampen Wnt signaling. Loss of this negative regulatory function may explain why – despite the similar defect in QR.p polarization and migration – *cam-1* null mutants show a more widespread distribution of the QR.pax than *egl-20* mutants.

The second step in QR descendant migration is termination of the MOM-5 and CAM-1 dependent long-range anterior migration phase. We found that this requires activation of canonical Wnt/ß-catenin signaling in QR.pa. Canonical Wnt/ß-catenin signaling may terminate migration by directly inhibiting the CAM-1 and MOM-5 dependent migration pathways, but may also stop migration by promoting division of QR.pa. Measurements of migration speed in *pry-1*/Axin mutants showed that constitutive activation of Wnt/ß-catenin signaling induces a significant reduction in QR.p migration speed (Figure 5C). This is in agreement with a direct role of Wnt/ß-catenin signaling in migration inhibition. Interestingly, QR.p was normally polarized in *pry-1* mutants (Figure S2C), indicating that canonical Wnt/ß-catenin signaling reduces migration speed independently of QR.p polarization.

The Frizzled *mig-1* plays a pivotal role in defining the end point of QR.pa migration. Quantification of *mig-1* expression showed that it is sharply upregulated in QR.pa and transgenic rescue experiments revealed that this induction of *mig-1* expression is necessary and sufficient for termination of migration. Importantly, we found that the expression of *mig-1* is not induced by positional cues from the extracellular environment. Instead, we found that *mig-1* expression is activated through a cell intrinsic timing mechanism. Consistent with this mechanism, we found that the position along the anteroposterior axis at which QR.pa expresses *mig-1* is correlated with the speed of migration. An interesting question is how *mig-1* expression is activated at such a specific time point in the migration process. One possibility is that the temporal regulation of *mig-1* expression is coupled to the QR.p lineage, with division of QR.p triggering the expression of *mig-1* in QR.pa, but a lineage independent time-keeping mechanism may be involved as well.

The final phase in the migration process is the short-range migration of QR.paa and

QR.pap. We found that this anteroposterior and dorsoventral migration is dependent on the PCP pathway components VANG-1/Vangl and PRKL-1/Pk. Similar to *mig-1*, we found that the expression of *prkl-1* is temporally regulated, indicating that the transition to this PCP related pathway may also be mediated through a cell intrinsic timing mechanism. Analysis of dorsoventral migration in double mutant combinations of *vang-1* and *prkl-1* with *unc-6*/Netrin showed that *vang-1* and *prkl-1* function in a common genetic pathway with the *unc-6* guidance signal. How PCP and UNC-6 Netrin signaling are coordinated to control the final dorsoventral positioning of QR.paa and QR.pap remains to be established.

Transcriptional regulation of guidance receptors and intracellular signaling components is an important mechanism in specifying the complex trajectories of migrating cells and axons (Derijck et al., 2010; Polleux et al., 2007; Su et al., 2000). The expression of such guidance components can be induced by extracellular signals, but our results show that cells can also utilize cell intrinsic mechanisms to express distinct Wnt pathway components at specific time points in the migration process. Such cell intrinsic regulation of migration also appears to be important in vertebrate nervous system development. During brain development, retinal ganglion cell (RGC) axons migrate towards the optic tectum. At a specific stage in their migration, the RGC axons induce the expression of neuropilin-1, which enables them to respond to semaphorin guidance cues (Derijck et al., 2010). The time-dependent induction of neuropilin-1 expression also occurs when RGC cells are grown *in vitro*, indicating that the temporal regulation of neuropilin-1 expression is a cell autonomous process (Campbell et al., 2001). How neuropilin-1 is upregulated at such a specific time point in RGC development is still unknown. Our observation that QR descendant migration is controlled through temporal regulation of Wnt responsiveness provides a powerful paradigm to study cell intrinsic timing mechanisms in a highly reproducible single cell migration system.

Experimental procedures

C. elegans strains and culture

Unless noted otherwise, *C. elegans* strains were cultured at 20°C using standard conditions (Lewis and Fleming, 1995). Bristol N2 was used as the wild type control. Mutant alleles and transgenes used in this study were: LGI: *mig-1(e1787)*, *lin-17(n671, rh75)*, *pop-1(hu9)*, *mom-5(gk812, ne12, or57)/hT2[bli-4(e937) let-?(q782) qIs48]*, *pry-1(mu38)*; LGII: *cwn-1(ok546)*, *dsh-2(ok2162)/mInI[mIs14 dpy-10(e128)]*, *dsh-1(ok1445)*, *mig-5(rh147)*, *cam-1(gm122, ks52)*; LGIII: *mab-5(gk670)*, *ina-1(gm144)*, *emb-9(hc70)*, *syIs90[Pegl-17::yfp;unc-119(+)]*; LGIV: *prkl-1(ok3182)*, *sfrp-1(gk554)*, *egl-20(hu105, n585)*, *cwn-2(ok895)*; LGV: *sid-1(qt9)*, *ayIs9[Pegl-17::gfp; dpy-20(+)]*, *heIs63[Pwrt-2::gfp-PH ;Pwrt-2::h2b-gfp; Plin-48::mTomato]* (Wildwater et al., 2011), *muIs53[hsp16::egl-20; unc-22(dn)]* (Whangbo and Kenyon, 1999); LGX: *vang-1(tm1422)*, *unc-6(e78, ev400)*, *bar-1(ga80)*, *mig-2(gm103, mu28)* and unassigned: *casIs49[Pegl-17::myristoylated-mCherry; Pegl-17::COR-1::gfp; Pegl-17::mCherry::TEV-S::his-24]* (Wang et al., 2013), *huIs4[hsp16::ΔN-POP-1; rol-6(su1006)]* (Korswagen et al., 2000), *huIs14[hsp16::ΔN-BAR-1; Pmec-7::gfp]*, *huIs149*, *huIs151[hsp16::cwn-1; Pmyo-2::mTomato]*. Extra-chromosomal transgenes used are: *huEx278[Pegl-17::ΔN-POP-1; Pmyo-2::mTomato]*; *huEx279*, *huEx280*, *huEx281[Pegl-17::vang-1-gfp; Pmyo-2::mTomato]*, *huEx523*, *huEx524[Pegl-17::cam-1(RNAi); Pmyo-2::mCherry]*, *huEx535*, *huEx537[Pegl-17::mom-5(RNAi); Pmyo-2::mCherry]*, *huEx621*, *huEx622*, *huEx623[Pegl-17::mig-1; Pmyo-2::gfp]*, *huEx624*, *huEx644[Pegl-17::mom-5; Plin-*

48::mTomato], huEx625, huEx626[Pegl-17::cam-1-gfp; Pmyo-2::gfp], huEx634, huEx635, huEx636[Pegl-46::mig-1; Pmyo-2::gfp], huEx640, huEx641, huEx642[Pmom-5::mig-1; Pmyo-2::gfp] , huEx662, huEx663, huEx664[Pegl-17::prkl-1; Pmyo-2::gfp], huEx667, huEx668, huEx669[Pegl-46::prkl-1; Pmyo-2::gfp], huEx506, huEx682[Pceh-22::egl-20::SL2::mCherry; Plin-48::mTomato], huEx679, huEx680[Pceh-22::cwn-1::SL2::mCherry; Plin-48::mTomato].

Molecular biology

The coding sequences of the *vang-1a* and *prkl-1a* isoforms, *cwn-1*, *egl-20*, *mom-5*, *mig-1* and *cam-1* were PCR amplified from total cDNA using primers containing attB1 and attB2 gateway recombination sites. ΔN-POP-1 cDNA was PCR amplified from a *hsp16::ΔN-POP-1* expression vector (Korswagen et al., 2000). The cDNA fragments were subsequently recombined with pDNR221 to generate gateway compatible entry clones. Promoter sequences of *ceh-22*, *egl-17*, *egl-46* and *mom-5* were cloned by PCR amplifying respectively 2.8 kb, 4.6 kb, 3.1 kb or 3.7 kb of upstream sequence from genomic DNA using primers containing attB4 and attB1R gateway recombination sites. Promoter sequences were then recombined with pDNRP4-P1R to generate entry clones. To confirm the *Pceh-22* driven anterior expression pattern for *egl-20* and *cwn-1*, both were recombined at the 3' end with a pDNRP2R-P3 entry clone containing an SL2 sequence – derived from the *gpd-2 gpd-3* polycistron intergenic region (Huang et al., 2001) – fused to mCherry. In each case, the 3' UTR used was derived from the *unc-54* gene. Expression constructs were generated by combining appropriate entry clones into the pCFJ150 expression vector. The *hsp16::cwn-1* construct was generated by recombining PCR amplified *cwn-1* cDNA using NcoI and SacI restriction sites into the pPD49.78 plasmid. Final constructs were injected at 10-50 ng/µl with 5-10 ng/µl co-injection marker and supplemented with pBluescriptII to 150 ng/µl. Tissue specific RNAi was performed as previously described (Esposito et al., 2007). *cam-1* and *mom-5* coding sequence was PCR amplified from total cDNA and cloned into pDNR221. The 4.6 kb *egl-17* promoter was PCR amplified from plasmid pKN115 and PCR fused to a 1 kb sense and antisense fragment of *cam-1* (contained within exon 7), or a 0.5 kb fragment of *mom-5* (exon 1). Sense and antisense PCR fusion products were gel purified and injected together at 3 ng/µl, using 5 ng/µl *Pmyo-2::mCherry* as injection marker.

Analysis of QR descendant migration

The final position of the QR descendants QR.paa and QR.pap was determined using DIC microscopy in late L1 larvae as described (Coudreuse et al., 2006). The position of QR.paa and QR.pap was determined with respect to the seam cell daughters V1.a to V6.p. To provide a more detailed measure of QR.paa and QR.pap migration distance, the position was determined with respect to the V1.p and V2.a seam cell nuclei. The relative position of QR.paa and QR.pap on the dorsoventral axis was determined by dividing the distance between QR.paa or QR.pap and the midline (defined as the middle of the V1.p nucleus) over the total dorsoventral distance at this position. The position of QR.pa was determined in transgenic animals expressing GFP in the Q cell lineage (transgenes *ayIs9* or *syIs90*). The relative position of QR.pa with respect to the V1.p and V2.a seam cell nuclei was determined by dividing the distance between V1.p and QR.pa over the total distance between V1.p and V2.a. The position of QR.p division was determined relative to the seam cells V1 to V4. The speed of QR.p migration was measured in synchronized larvae by determining the average distance of migration during the first hour after QR division. A 2 hour timeframe was chosen

for *egl-20*, *cam-1* and *mig-2(mu28)* mutants to reliably score anterior migration distance.

Imaging

For static imaging, animals were mounted on 2% agarose pads containing 10 mM sodium azide. Confocal images were obtained using a Leica TCS SPE confocal microscope. For imaging of QR.p polarity using the *heIs63* marker, settings were: 63x objective, 3x zoom, 15% 488 nm (gfp) laser power. For imaging of the plasma membrane and actin localization in QR.p using the *casIs49* marker, settings were: 63x objective, 3x zoom, 20% 488 nm (gfp) laser power, 20% 532 nm (mCherry) laser power. Z-stacks were made using a 0.5 µm step size. Image acquisition was performed using LASAF software. A maximum projection was made of all slices in which the Q cell was detected. DIC and epifluorescence images were obtained using a Zeiss Axioscope microscope equipped with a Zeiss Axiocam digital camera. Images were analyzed using ImageJ v1.43u software. For time lapse imaging, larvae synchronized at 5-6 hours after hatching were mounted in 0.5 µl of 0.1 µm diameter polystyrene microspheres in aqueous suspension (Polysciences 00876 2.5% w/v aqueous suspension) onto a 10% agarose pad (Kim et al., 2013). Animals were imaged using a PerkinElmer Ultraview Vox spinning disk confocal microscope (63x objective, 1x zoom, 4% 488 nm laser power). Z-stacks (0.5 µm) were made every 2 minutes for a 2-hour duration. Image acquisition was performed using Velocity software. Images were processed and movies were created using Velocity and ImageJ software, respectively.

Heat shock experiments

Heat shock experiments were performed as previously described (Middelkoop et al., 2012) with the following changes: L1 larvae synchronized at 0-1 hour after hatching were incubated at 33°C in a volume of 50 µl for the indicated length of time.

Single molecule fluorescence in situ hybridization

The smFISH protocol was performed as described elsewhere (Ji and van Oudenaarden, 2012; Middelkoop et al., 2012; Raj et al., 2008). In brief, synchronized L1 larvae were fixed using 4% paraformaldehyde and suspended in 70% ethanol. Hybridization was done overnight at 37°C in the dark. Short oligonucleotide probes were designed using a specially designed algorithm (www.singlemoleculefish.com) and chemically coupled to fluorescent dyes Alexa 594 (*mig-1* and *cfz-2* probe), TMR (*lin-17* probe) or Cy5 (all other probes). Animals were suspended in buffer containing DAPI for nuclear counterstaining before mounting. Z-stacks with a slice thickness of 0.5 µm were obtained with a Leica DM6000 microscope, equipped with a Leica DFC360FX camera, 100x oil objective and Y5 (Cy5), A4 (DAPI) and GFP filter cubes. Images were acquired with 1024 x 1024 resolution and subjected to a 2 x 2 binning. Quantification of mRNA was performed manually using the z-stacks. Only mRNA spots visible in at least two independent focal plains were counted. The Q cell boundary was marked by the *heIs63* transgene for measurements in QR, QR.p and QR.pa, while *ayIs9* or *syIs90* were used for measurements in QR.paa and QR.pap. Analysis was performed using ImageJ v1.43u software.

Statistical analysis

Statistical analysis of QR descendant position was performed using Fisher's exact test. A Monte Carlo approximation, iterated 10.000 times using SPSS version 20, was used to

estimate significance. Analysis of differences in QR.p polarity variability was performed using Levene's test for equal variance. In all other cases, statistical analysis was examined using unpaired, two-tailed Student's t-tests. Results were deemed significant if $p<0.05$.

Acknowledgements

We thank Erik Jorgensen, Jeroen Pasterkamp and Martin Harterink for critically reading the manuscript, Sander van den Heuvel, Wayne Forrester, Hitoshi Sawa, Guangshuo Ou and the *Caenorhabditis* Genetics Center (University of Minnesota, Minneapolis) for strains and the Hubrecht Imaging Center (HIC) for assistance with microscopy. This work was funded by a grant from the Dutch Cancer Society (HUBR 2008-4114) (HCK) and the NIH/NCI Physical Sciences Oncology Center at MIT (U54CA143874), a NIH Pioneer award (DP1CA174420) and an ERC Advanced grant (2011-294325_GeneNoiseControl) (AvO).

References

Angers, S., and Moon, R.T. (2009). Proximal events in Wnt signal transduction. Nature Rev Mol Cell Biol *10*, 468-477.

Burdine, R.D., Branda, C.S., and Stern, M.J. (1998). EGL-17(FGF) expression coordinates the attraction of the migrating sex myoblasts with vulval induction in *C. elegans*. Development *125*, 1083-1093.

Cai, L., Makhov, A.M., and Bear, J.E. (2007). F-actin binding is essential for coronin 1B function in vivo. J Cell Sci *120*, 1779-1790.

Campbell, D.S., Regan, A.G., Lopez, J.S., Tannahill, D., Harris, W.A., and Holt, C.E. (2001). Semaphorin 3A elicits stage-dependent collapse, turning, and branching in *Xenopus* retinal growth cones. J Neurosci *21*, 8538-8547.

Clevers, H., and Nusse, R. (2012). Wnt/ß-catenin signaling and disease. Cell *149*, 1192-1205.

Coudreuse, D.Y., Roel, G., Betist, M.C., Destree, O., and Korswagen, H.C. (2006). Wnt gradient formation requires retromer function in Wnt-producing cells. Science *312*, 921-924.

Derijck, A.A., Van Erp, S., and Pasterkamp, R.J. (2010). Semaphorin signaling: molecular switches at the midline. Trends Cell Biol *20*, 568-576.

Eisenmann, D.M. (2005). Wnt signaling. WormBook, 1-17.

Esposito, G., Di Schiavi, E., Bergamasco, C., and Bazzicalupo, P. (2007). Efficient and cell specific knock-down of gene function in targeted *C. elegans* neurons. Gene *395*, 170-176.

Forrester, W.C., Dell, M., Perens, E., and Garriga, G. (1999). A *C. elegans* Ror receptor tyrosine kinase regulates cell motility and asymmetric cell division. Nature *400*, 881-885.

Gao, C., and Chen, Y.G. (2010). Dishevelled: The hub of Wnt signaling. Cell Signal *22*, 717-727.

Gleason, J.E., Korswagen, H.C., and Eisenmann, D.M. (2002). Activation of Wnt signaling bypasses the requirement for RTK/Ras signaling during *C. elegans* vulval induction. Genes Dev *16*, 1281-1290.

Green, J.L., Inoue, T., and Sternberg, P.W. (2008a). Opposing Wnt pathways orient cell polarity during organogenesis. Cell *134*, 646-656.

Green, J.L., Kuntz, S.G., and Sternberg, P.W. (2008b). Ror receptor tyrosine kinases: orphans no more. Trends Cell Biol *18*, 536-544.

Harris, J., Honigberg, L., Robinson, N., and Kenyon, C. (1996). Neuronal cell migration in *C. elegans*: regulation of Hox gene expression and cell position. Development *122*, 3117-3131.

Harterink, M., Kim, D.H., Middelkoop, T.C., Doan, T.D., van Oudenaarden, A., and Korswagen, H.C. (2011). Neuroblast migration along the anteroposterior axis of *C. elegans* is controlled by opposing gradients of Wnts and a secreted Frizzled-related protein. Development *138*, 2915-2924.

Hedgecock, E.M., Culotti, J.G., Hall, D.H., and Stern, B.D. (1987). Genetics of cell and axon migrations in *Caenorhabditis elegans*. Development *100*, 365-382.

Huang, T., Kuersten, S., Deshpande, A.M., Spieth, J., MacMorris, M., and Blumenthal, T. (2001). Intercistronic region required for polycistronic pre-mRNA processing in *Caenorhabditis elegans*. Mol Cell Biol *21*, 1111-1120.

Ji, N., Middelkoop, T.C., Mentink, R.A., Betist, M.C., Tonegawa, S., Mooijman, D., Korswagen, H.C., and van Oudenaarden, A. (2013). Feedback control of gene expression variability in the *Caenorhabditis elegans* Wnt pathway. Cell *155*, 869-880.

Ji, N., and van Oudenaarden, A. (2012). Single molecule fluorescent in *situ hybridization* (smFISH) of *C. elegans* worms and embryos. WormBook, 1-16.

Kennerdell, J.R., Fetter, R.D., and Bargmann, C.I. (2009). Wnt-Ror signaling to SIA and SIB neurons directs anterior axon guidance and nerve ring placement in *C. elegans*. Development *136*, 3801-3810.

Kim, C., and Forrester, W.C. (2003). Functional analysis of the domains of the *C elegans* Ror receptor tyrosine kinase CAM-1. Dev Biol *264*, 376-390.

Kim, E., Sun, L., Gabel, C.V., and Fang-Yen, C. (2013). Long-term imaging of *Caenorhabditis elegans* using nanoparticle-mediated immobilization. PloS One *8*, e53419.

Kim, S., Ren, X.C., Fox, E., and Wadsworth, W.G. (1999). SDQR migrations in *Caenorhabditis elegans* are controlled by multiple guidance cues and changing responses to netrin UNC-6. Development *126*, 3881-3890.

Korswagen, H.C. (2002). Canonical and non-canonical Wnt signaling pathways in *Caenorhabditis elegans*: variations on a common signaling theme. Bioessays *24*, 801-810.

Korswagen, H.C., Coudreuse, D.Y., Betist, M.C., van de Water, S., Zivkovic, D., and Clevers, H.C. (2002). The Axin-like protein PRY-1 is a negative regulator of a canonical Wnt pathway in C. elegans. Genes Dev *16*, 1291-1302.

Korswagen, H.C., Herman, M.A., and Clevers, H.C. (2000). Distinct ß-catenins mediate adhesion and signalling functions in *C. elegans*. Nature *406*, 527-532.

Lewis, J.A., and Fleming, J.T. (1995). Basic culture methods. Methods Cell Biol *48*, 3-29.

Liu, Y., Shi, J., Lu, C.C., Wang, Z.B., Lyuksyutova, A.I., Song, X.J., and Zou, Y. (2005). Ryk-mediated Wnt repulsion regulates posterior-directed growth of corticospinal tract. Nat Neurosci *8*, 1151-1159.

Lyuksyutova, A.I., Lu, C.C., Milanesio, N., King, L.A., Guo, N., Wang, Y., Nathans, J., Tessier-Lavigne, M., and Zou, Y. (2003). Anterior-posterior guidance of commissural axons by Wnt-Frizzled signaling. Science *302*, 1984-1988.

Maloof, J.N., Whangbo, J., Harris, J.M., Jongeward, G.D., and Kenyon, C. (1999). A Wnt signaling pathway controls Hox gene expression and neuroblast migration in *C. elegans*. Development *126*, 37-49.

Masuda, H., Nakamura, K., Takata, N., Itoh, B., Hirose, T., Moribe, H., Mekada, E., and Okada, M. (2012). MIG-13 controls anteroposterior cell migration by interacting with UNC-71/ADM-1 and SRC-1 in *Caenorhabditis elegans*. FEBS Lett *586*, 740-746.

Middelkoop, T.C., Williams, L., Yang, P.T., Luchtenberg, J., Betist, M.C., Ji, N., van Oudenaarden, A., Kenyon, C., and Korswagen, H.C. (2012). The thrombospondin repeat containing protein MIG-21 controls a left-right asymmetric Wnt signaling response in migrating *C. elegans* neuroblasts. Dev Biol *361*, 338-348.

Modzelewska, K., Lauritzen, A., Hasenoeder, S., Brown, L., Georgiou, J., and Moghal, N. (2013). Neurons refine the *Caenorhabditis elegans* body plan by directing axial patterning by Wnts. PLoS Biol *11*, e1001465.

Nishita, M., Enomoto, M., Yamagata, K., and Minami, Y. (2010). Cell/tissue-tropic functions of Wnt5a signaling in normal and cancer cells. Trends Cell Biol *20*, 346-354.

Nomachi, A., Nishita, M., Inaba, D., Enomoto, M., Hamasaki, M., and Minami, Y. (2008). Receptor tyrosine kinase Ror2 mediates Wnt5a-induced polarized cell migration by activating c-Jun N-terminal kinase via actin-binding protein filamin A. J Biol Chem *283*, 27973-27981.

Okkema, P.G., and Fire, A. (1994). The *Caenorhabditis elegans* NK-2 class homeoprotein CEH-22 is involved in combinatorial activation of gene expression in pharyngeal muscle. Development *120*, 2175-2186.

Ou, G., and Vale, R.D. (2009). Molecular signatures of cell migration in *C. elegans* Q neuroblasts. J Cell Biol *185*, 77-85.

Pan, C.L., Howell, J.E., Clark, S.G., Hilliard, M., Cordes, S., Bargmann, C.I., and Garriga, G. (2006). Multiple Wnts and Frizzled receptors regulate anteriorly directed cell and growth cone migrations in *Caenorhabditis elegans*. Dev Cell *10*, 367-377.

Polleux, F., Ince-Dunn, G., and Ghosh, A. (2007). Transcriptional regulation of vertebrate axon guidance and synapse formation. Nature Rev Neurosci *8*, 331-340.

Raj, A., van den Bogaard, P., Rifkin, S.A., van Oudenaarden, A., and Tyagi, S. (2008). Imaging individual mRNA molecules using multiple singly labeled probes. Nature Methods *5*, 877-879.

Salser, S.J., and Kenyon, C. (1992). Activation of a *C. elegans* Antennapedia homologue in migrating cells controls their direction of migration. Nature *355*, 255-258.

Sanchez-Alvarez, L., Visanuvimol, J., McEwan, A., Su, A., Imai, J.H., and Colavita, A. (2011). VANG-1 and PRKL-1 cooperate to negatively regulate neurite formation in *Caenorhabditis elegans*. PLoS Genet *7*, e1002257.

Schambony, A., and Wedlich, D. (2007). Wnt-5A/Ror2 regulate expression of XPAPC through an alternative noncanonical signaling pathway. Dev Cell *12*, 779-792.

Silhankova, M., and Korswagen, H.C. (2007). Migration of neuronal cells along the anterior-posterior body axis of *C. elegans*: Wnts are in control. Curr Opin Genet Dev *17*, 320-325.

Song, S., Zhang, B., Sun, H., Li, X., Xiang, Y., Liu, Z., Huang, X., and Ding, M. (2010). A Wnt-Frz/Ror-Dsh pathway regulates neurite outgrowth in Caenorhabditis elegans. PLoS Genet *6*, e1001056.

Su, M., Merz, D.C., Killeen, M.T., Zhou, Y., Zheng, H., Kramer, J.M., Hedgecock, E.M., and Culotti, J.G. (2000). Regulation of the UNC-5 netrin receptor initiates the first reorientation of migrating distal tip cells in *Caenorhabditis elegans*. Development *127*, 585-594.

Sulston, J.E., and Horvitz, H.R. (1977). Post-embryonic cell lineages of the nematode, *Caenorhabditis elegans*. Dev Biol *56*, 110-156.

Sym, M., Robinson, N., and Kenyon, C. (1999). MIG-13 positions migrating cells along the anteroposterior body axis of *C. elegans*. Cell *98*, 25-36.

Thorpe, C.J., Schlesinger, A., Carter, J.C., and Bowerman, B. (1997). Wnt signaling polarizes an early *C. elegans* blastomere to distinguish endoderm from mesoderm. Cell *90*, 695-705.

Wallingford, J.B. (2012). Planar cell polarity and the developmental control of cell behavior in vertebrate embryos. Annu Rev Cell Dev Biol *28*, 627-653.

Wang, X., Zhou, F., Lv, S., Yi, P., Zhu, Z., Yang, Y., Feng, G., Li, W., and Ou, G. (2013). Transmembrane protein MIG-13 links the Wnt signaling and Hox genes to the cell polarity in neuronal migration. Proc Natl Acad Sci USA *110*, 11175-11180.

Whangbo, J., and Kenyon, C. (1999). A Wnt signaling system that specifies two patterns of cell migration in *C. elegans*. Mol Cell *4*, 851-858.

Wildwater, M., Sander, N., de Vreede, G., and van den Heuvel, S. (2011). Cell shape and Wnt signaling redundantly control the division axis of *C. elegans* epithelial stem cells. Development *138*, 4375-4385.

Winston, W.M., Molodowitch, C., and Hunter, C.P. (2002). Systemic RNAi in *C. elegans* requires the putative transmembrane protein SID-1. Science *295*, 2456-2459.

Witze, E.S., Litman, E.S., Argast, G.M., Moon, R.T., and Ahn, N.G. (2008). Wnt5a control of cell polarity and directional movement by polarized redistribution of adhesion receptors. Science *320*, 365-369.

Wu, J., Duggan, A., and Chalfie, M. (2001). Inhibition of touch cell fate by *egl-44* and *egl-46* in *C. elegans*. Genes Dev *15*, 789-802.

Yamamoto, Y., Takeshita, H., and Sawa, H. (2011). Multiple Wnts redundantly control polarity orientation in *Caenorhabditis elegans* epithelial stem cells. PLoS Genet *7*, e1002308.

Zecca, M., Basler, K., and Struhl, G. (1996). Direct and long-range action of a wingless morphogen gradient. Cell *87*, 833-844.

Zinovyeva, A.Y., and Forrester, W.C. (2005). The *C. elegans* Frizzled CFZ-2 is required for cell migration and interacts with multiple Wnt signaling pathways. Dev Biol *285*, 447-461.

Zinovyeva, A.Y., Yamamoto, Y., Sawa, H., and Forrester, W.C. (2008). Complex network of Wnt signaling regulates neuronal migrations during *Caenorhabditis elegans* development. Genetics *179*, 1357-1371.

Zou, Y., and Lyuksyutova, A.I. (2007). Morphogens as conserved axon guidance cues. Curr Opin Neurobiol *17*, 22-28.

Supplementary Figures

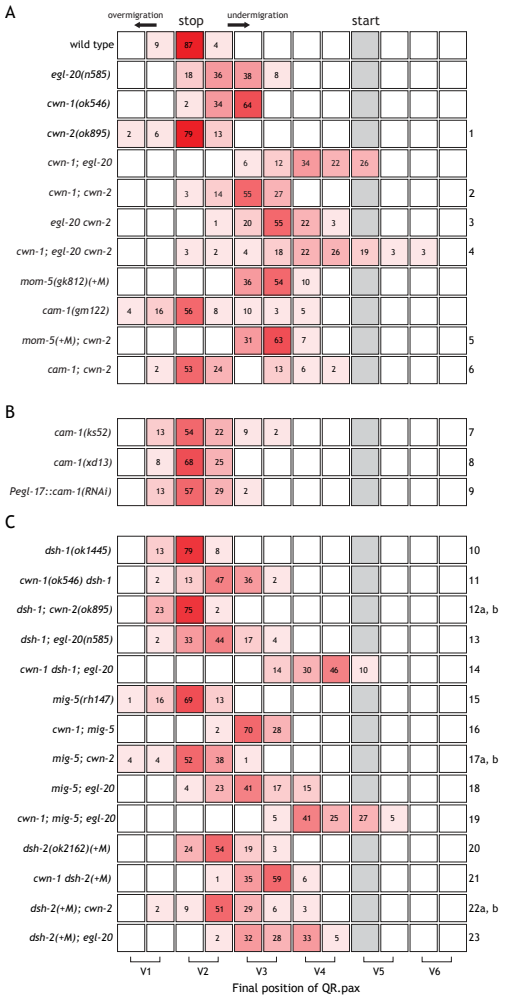

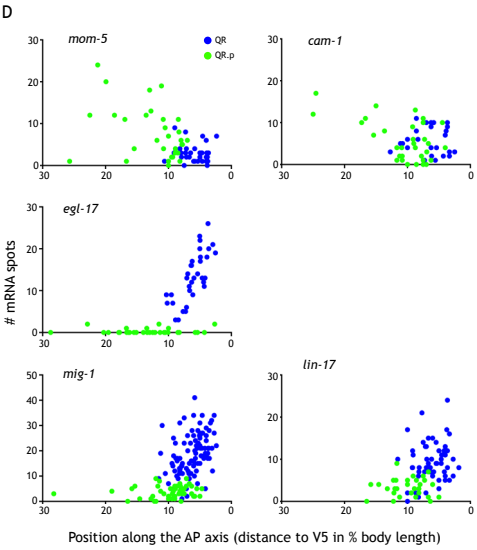

	Statistical analysis (Fisher's exact test)
1	wild type vs. *cwn-2(ok895)* p=0.11
2	*cwn-1(ok546)* vs. *cwn-1; cwn-2* p<0.0001
3	*egl-20(n585)* vs. *egl-20 cwn-2* p<0.0001
4	*cwn-1; egl-20* vs. *cwn-1;egl-20 cwn-2* p=0.53
5	*mom-5(gk812)(+M)* vs. *mom-5(+M); cwn-2* p=0.61
6	*cam-1(gm122)* vs. *cam-1; cwn-2* p<0.0001
7	wild type vs. *cam-1(ks52)* p<0.0001
8	wild type vs. *cam-1(xd13)* p<0.0001
9	wild type vs. *Pegl-17::cam-1(RNAi)* p<0.0001
10	wild type vs. *dsh-1(ok1445)* p=0.31
11	*cwn-1(ok546)* vs. *cwn-1 dsh-1* p=0.001
12a	*cwn-2(ok895)* vs. *dsh-1; cwn-2* p=0.01
12b	*dsh-1(ok1445)* vs. *dsh-1; cwn-2* p=0.13
13	*egl-20(n585)* vs. *dsh-1; egl-20* p=0.03
14	*cwn-1; egl-20* vs. *cwn-1 dsh-1; egl-20* p=0.02
15	wild type vs. *mig-5(rh147)* p=0.32
16	*cwn-1(ok546)* vs. *cwn-1 mig-5* p<0.0001
17a	*cwn-2(ok895)* vs. *mig-5; cwn-2* p=0.001
17b	*mig-5(rh147)* vs. *mig-5; cwn-2* p<0.0001
18	*egl-20(n585)* vs. *mig-5; egl-20* p=0.001
19	*cwn-1; egl-20* vs. *cwn-1 mig-5; egl-20* p=0.16
20	wild type vs. *dsh-2(ok2162)(+M)* p<0.0001
21	*cwn-1(ok546)* vs. *cwn-1 dsh-2(+M)* p<0.0001
22a	*cwn-2(ok895)* vs. *dsh-2(+M); cwn-2* p=0.001
22b	*dsh-2(ok2162)(+M)* vs. *dsh-2(+M); cwn-2* p=0.04
23	*egl-20(n585)* vs. *dsh-2(+M); egl-20* p<0.0001

Figure S1. Multiple Wnt ligands and receptors regulate the anterior migration of the QR descendants. (**A-C**) Average position of the QR descendants QR.pap and QR.paa with respect to the seam cells V1.a to V6.p (lower brackets indicate Vn.a (left) and Vn.p (right) daughters of Vn cells). Values listed are percentiles of total cells scored, n>50 for all genotypes. Numbers to the right of the graph refer to individual Fisher's exact tests performed to estimate significance of migration defects, which are indicated in the table to the right. (**B**) Q lineage specific knock down of *cam-1* phenocopies the *cam-1* intracellular domain mutants *ks52* and *xd13*. (**C**) The Dishevelled orthologs *mig-5* and *dsh-2* are required for QR.px migration. (**D**) Graphs indicate *mom-5*, *cam-1*, *egl-17*, *mig-1* and *lin-17* transcription dynamics during initial migration in single QR (blue) and QR.p (green) neuroblast daughter cells as measured in wild type animals (n>60 for all genotypes). The number of mRNA spots per cell is plotted against the total migratory distance of the cell in percentile body length (Ji et al., 2013).

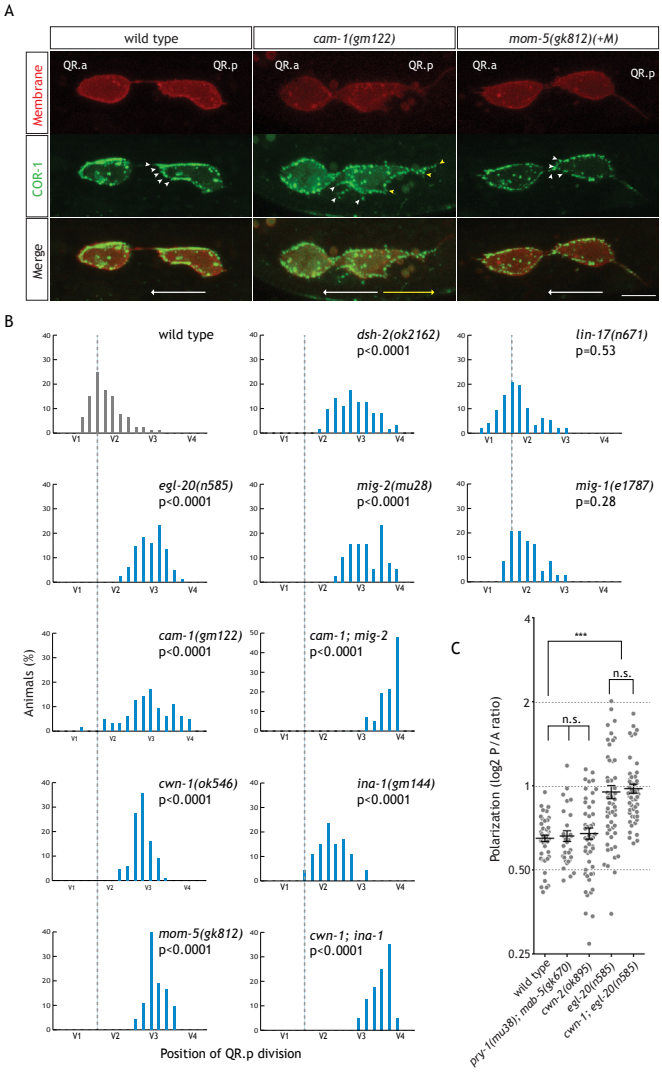

Figure S2. (**A**) Representative images of migrating QR.p and QR.a neuroblasts expressing the leading edge marker COR-1::GFP (F-actin) and myristoylated mCherry (plasma membrane) (*casIs49*) (Wang et al., 2013) in wild type and *cam-1* and *mom-5* mutants. Anterior is left. Arrowheads indicate localization of COR-1::GFP to cellular protrusions in the front (white) or back (yellow) of QR.p. Arrows indicate the direction of QR.p protrusion formation to the anterior (white) or posterior (yellow). In *mom-5* mutants, localization of COR-1::GFP is predominantly in the anterior protrusion, as in wild type. In *cam-1* mutants, COR-1::GFP localizes to the posteriorly formed protrusions as well. Scale bar is 5 µm. (**B**) Position of QR.p division in Wnt ligand and receptor mutants. Position of QR.p division with respect to the seam cells V1-V4 (n>65 for all genotypes). Statistical significance was calculated using a Fisher's exact test. A Fisher's exact test comparing *egl-20* to *cam-1* mutants returns a value of p=0.14, indicating they are statistically identical. (**C**) Quantification of QR.p polarity as the ratio of the distance of the nucleus to the posterior (P) and the anterior side (A) of the cell. Lines indicate mean ± SEM. Statistical significance was calculated using an unpaired t-test (*** p<0.0001). The mean polarity of *cwn-2* and *pry-1; mab-5* double mutants is not statistically different from wild type (p=0.46 and p=0.71), while *cwn-1; egl-20* double mutants are statistically identical to *egl-20* mutants (p=0.67).

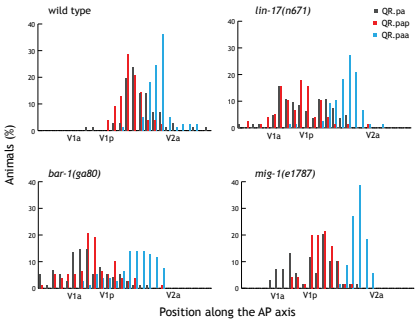

Figure S3. Canonical Wnt/ß-catenin signaling does not influence the short-range anteroposterior migration of QR.pap and QR.paa. Position of QR.pa, QR.pap and QR.paa relative to the seam cells V1.a to V2. a (n>70 for all genotypes). Note that the relative position of QR.pap and QR.paa with respect to QR.pa in Wnt/ß-catenin pathway mutants is similar as in wild type animals.

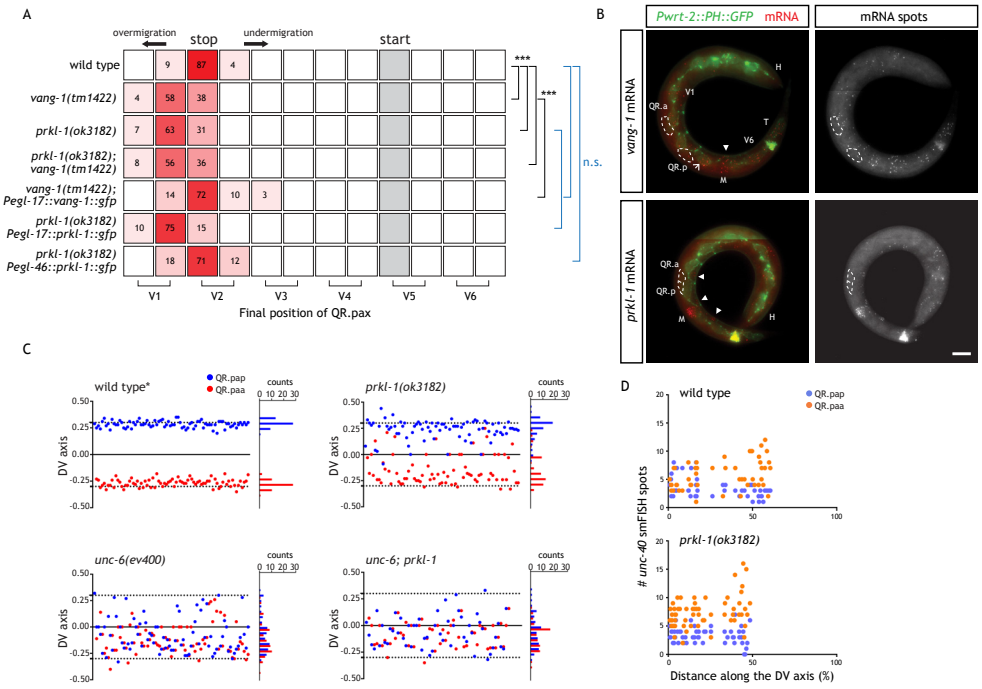

Figure S4. The PCP pathway components vang-1 and prkl-1 act cell autonomously in QR.px migration. (**A**) Average position of the QR descendants QR.pap and QR.paa with respect to the seam cells V1.a to V6.p (lower brackets indicate Vn.a (left) and Vn.p (right) daughters of Vn cells). Values listed are percentiles of total cells scored, n>50 for all genotypes. Statistical significance was calculated using a Fisher's exact test (*** p=<0.0001). (**B**) Staining of endogenous mRNA (red) of *vang-1* and *prkl-1* in L1 stage larvae in which the QR descendants and the seam cells are labeled with GFP (*heIs63*). Expression in the seam cells V1, V6 and T, the mesoblast cell M and ventral nerve cord neurons (arrow heads) is indicated. H, anterior head region. Scale bar is 5 µm. (**C**) Position of QR.pap and QR.paa on the dorsoventral axis (n>70 for all genotypes). Midline is set at 0 and dashed lines indicate the average position of QR.pap and QR.paa in wild type. The histogram on the right displays percentile counts along the dorsoventral axis. *Data shown in this panel were obtained from animals carrying a *Pmec-7::gfp* (*muls32*) transgene to mark the AVM cell for comparison. (**D**) *unc-40* transcription dynamics in single QR.pap (blue) and QR.paa (yellow) neuroblast daughter cells as measured in wild type (top) and *prkl-1* mutant (bottom) animals (n>50 for both cell types). The number of mRNA spots per cell is plotted against the relative distance between the two QR.pax cells with respect to the total width of the dorsoventral axis, with a longer distance correlating to more advanced stages of dorsoventral migration. Notice the smaller average final distance between the QR.pax in *prkl-1* mutants, corresponding to their dorsoventral migration phenotype.

Chapter 3

The planar cell polarity protein VANG-1/Vangl negatively regulates β-catenin dependent Wnt signaling in *C. elegans*

Remco A. Mentink, Marco C. Betist and Hendrik C. Korswagen

Hubrecht Institute, Royal Netherlands Academy of Arts and Sciences and University Medical Center Utrecht, The Netherlands.

Manuscript submitted

Abstract

Vangl2 and Pk are core components of the non-canonical Wnt planar cell polarity pathway that controls epithelial polarity and cell migration. Studies in vertebrate model systems have suggested that Vangl2 and Pk may also inhibit signaling through the canonical Wnt/ß-catenin pathway, but the functional significance of this potential cross-talk between non-canonical and canonical Wnt pathways remained unclear. Here, we show that the *C. elegans* Vangl2 ortholog VANG-1 promotes non-canonical Wnt signaling in migrating Q neuroblasts by enhancing the threshold for canonical Wnt pathway activation. This modulation of canonical Wnt signaling depends on the interaction of VANG-1 with the Dishevelled MIG-5, but is independent of the Pk ortholog PRKL-1. We conclude that cross-talk between VANG-1 and the canonical Wnt pathway is an evolutionarily conserved mechanism that ensures robust specification of Wnt signaling responses.

Introduction

Wnt proteins are members of an evolutionarily conserved family of secreted signaling molecules that play a central role in development, adult tissue homeostasis and disease (Clevers and Nusse, 2012; Polakis, 2012). Wnt proteins can trigger a variety of responses in target cells - including cell fate specification, cell polarization and migration - that are mediated through distinct canonical and non-canonical Wnt signal transduction pathways (Angers and Moon, 2009).

The pathway that has been studied in most detail is the canonical Wnt pathway, which controls target gene expression through the effector protein ß-catenin (Angers and Moon, 2009; Clevers and Nusse, 2012). In the absence of Wnt signaling, ß-catenin is targeted for proteasomal degradation by a destruction complex that consists of the scaffold protein Axin, the tumor suppressor gene product APC and the protein kinases CK1 and GSK3ß. Binding of Wnt to the receptors Frizzled and LRP6 leads to inhibition of ß-catenin degradation through a mechanism that involves the cytoplasmic protein Dishevelled and recruitment of Axin to LRP6 at the plasma membrane. This enables the stabilized ß-catenin to translocate to the nucleus, where it interacts with TCF/Lef1 transcription factors to co-activate target gene transcription.

Non-canonical Wnt signaling occurs independently of ß-catenin and comprises several different pathways that directly influence cytoskeletal dynamics to control cell polarity or migration (Angers and Moon, 2009). One of these non-canonical Wnt pathways is known as the planar cell polarity (PCP) pathway, which is required in *Drosophila* and vertebrates for the correct polarization of epithelial cells along the plane of the epithelial tissue (Gray et al., 2011). The core components of this pathway are the trans-membrane proteins Frizzled and Van Gogh-like (Vangl) and the cytoplasmic proteins Dishevelled (Dvl) and Prickle (Pk), which drive planar polarization by asymmetrically localizing to the proximal (Vangl and Pk) and distal side (Frizzled and Dvl) of epithelial cells. How this asymmetric localization of PCP pathway components is established and which role Wnt ligands play in this process is still poorly understood.

In addition to planar cell polarity, Vangl2 and Pk also have other functions. Both are required for cell migration during vertebrate development. Examples are the convergence and extension cell movements during gastrulation in zebrafish and Xenopus (Jessen et al., 2002; Takeuchi et al., 2003; Wallingford et al., 2000), cell movements during neurulation and neural tube formation (Kibar et al., 2007; Lei et al., 2010) and the migration of motoneurons during brain development (Glasco et al., 2012; Jessen et al., 2002). Furthermore, there may be an antagonistic relationship between Vangl2 and Pk and the canonical Wnt/ß-catenin signaling pathway. Overexpression of Vangl2 or Pk has been shown to reduce canonical Wnt signaling activity in reporter gene assays (Park and Moon, 2002; Veeman et al., 2003) and under specific conditions *in vivo*, loss of Vangl2 has been shown to induce phenotypes that are indicative of increased Wnt signaling activity in zebrafish (Angonin and Van Raay, 2013; Li et al., 2011).

To further study this potential cross-talk between Vangl2 and Pk and the canonical Wnt pathway, we turned to the nematode *C. elegans*, which offers a more simplified Wnt signaling system with only 5 Wnt ligands, 4 Frizzled receptors and single orthologs of Vang and Pk that control the migration and polarity of defined cells and axons (Green et al., 2008; Hoffmann et al., 2010; Korswagen, 2002; Sanchez-Alvarez et al., 2011; Sawa and Korswagen, 2013;

Silhankova and Korswagen, 2007; Zinovyeva et al., 2008). Among the cells that respond to Wnt ligands are the two Q neuroblasts and their descendants (Silhankova and Korswagen, 2007). QL and QR are born at similar positions on the left and right lateral side of the animal, but migrate in opposite directions: QL and its descendants migrate posteriorly, while QR and its descendants migrate towards the anterior (Sulston and Horvitz, 1977). The difference in migration direction is specified by distinct responses of QL and QR to the Wnt ligand EGL-20 (Whangbo and Kenyon, 1999). EGL-20 activates a canonical Wnt/ß-catenin pathway in QL that leads to the expression of the homeotic gene *mab-5* (Figure 4A) (Ji et al., 2013; Korswagen et al., 2002; Korswagen et al., 2000; Maloof et al., 1999), which in turn directs the migrating QL descendants (QL.px) towards the posterior (Harris et al., 1996; Salser and Kenyon, 1992). QR also responds to EGL-20, but activates a non-canonical Wnt signaling mechanism that induces migration of the QR descendants (QR.px) towards the anterior (Figure 1A) (Mentink et al., 2014; Zinovyeva et al., 2008, see also **Chapter 2**). Importantly, both QL and QR can activate canonical Wnt signaling, but a difference in response threshold ensures that under normal conditions only QL activates *mab-5* expression (Whangbo and Kenyon, 1999). When EGL-20 is overexpressed or when negative regulators such as the Axin ortholog *pry-1* are mutated, both QL and QR activate canonical Wnt signaling and *mab-5* expression, and as a consequence, both the QL.px and QR.px migrate towards the posterior (Figure 1A). Conversely, in mutants that disrupt canonical Wnt signaling, *mab-5* fails to be expressed in QL and the QL.px localize to similar anterior positions as the QR.px (Figure 4A). The final position of the Q neuroblast descendants therefore provides a sensitive assay to study the interplay between canonical and non-canonical Wnt signaling mechanisms.

We have previously shown that the *C. elegans* orthologs of Vangl2 and Pk, VANG-1 and PRKL-1, are part of a non-canonical Wnt signaling pathway that controls the short-range migration of the final QR descendants QR.paa and QR.pap (Mentink et al., 2014, see also **Chapter 2**). Here, we show that in addition to this direct role in cell migration, VANG-1 also functions as a negative regulator of the canonical Wnt pathway dependent expression of *mab-5* in the Q neuroblast lineage. Mechanistically, we show that VANG-1 acts independently of PRKL-1 to restrict the activity of MIG-5/Dvl. Our results provide the first conclusive genetic evidence for an evolutionarily conserved function of Vangl as a negative regulator of canonical Wnt signaling.

Results

Simultaneous loss of vang-1 and sfrp-1 leads to ectopic activation of canonical Wnt/ß-catenin signaling and mab-5 expression in the QR lineage

A first indication of a role for *vang-1* in canonical Wnt/ß-catenin signaling came from our analysis of double mutants between *vang-1* and *sfrp-1* (Figures 1A and 1B). *sfrp-1* encodes a secreted Frizzled-related protein that functions as a negative regulator of Wnt signaling by binding and sequestering Wnt ligands (Harterink et al., 2011). Loss of *sfrp-1* results in a global increase in Wnt signaling, but is insufficient to trigger canonical Wnt signaling and *mab-5* expression in QR. However, when we combined *sfrp-1* with a *vang-1* mutation, over 60% of the double mutants showed posterior localization of the QR.px. Examination of *mab-5*; *sfrp-1*; *vang-1* triple mutants revealed that in the absence of *mab-5* the QR.px failed to localize in the posterior, indicating that *vang-1* and *sfrp-1* act genetically upstream of *mab-5*.

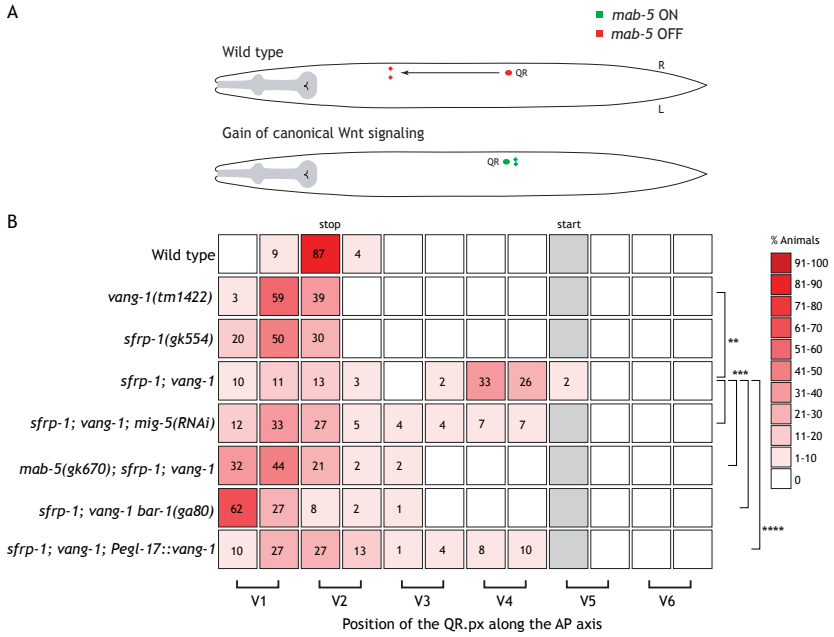

Figure 1. Loss of *vang-1* and *sfrp-1* leads to ectopic activation of canonical Wnt/ß-catenin signaling in the QR descendants. (**A**) Schematic representation of QR.px migration. In the wild type animals, *mab-5* is not expressed in QR (red) and the QR.px migrate anteriorly. A gain of canonical Wnt/ß-catenin signaling leads to expression of *mab-5* (green) and posterior localization of the QR.px. (**B**) Final positions of the QR.px with respect to the seam cells V1.a to V6.p (lower brackets indicate Vn.a (left) and Vn.p (right) daughters of Vn cells). Values listed are the cumulative percentiles of the total number of cells scored in 3 independent experiments, n>30 for each experiment. A color (red) coded heat map represents the range of percentile values. Statistical significance was calculated using a Student's t-test (** p<0.01, *** p<0.001, **** p<0.0001). For details on statistics see experimental procedures section.

To investigate whether *mab-5* is ectopically expressed in *sfrp-1*; *vang-1* double mutants, we quantitatively measured *mab-5* expression in the QR lineage using a single molecule mRNA fluorescent in situ hybridization (smFISH) approach (Raj et al., 2008). In wild type animals and *vang-1* or *sfrp-1* single mutants, less than five *mab-5* transcripts were detected in QR (Figures 2A and 2C). This number decreased in QR.p and no *mab-5* transcripts could be detected in QR.pa (Figures 2B and 2C). In *sfrp-1*; *vang-1* double mutants, on the other hand, there was a clear increase in *mab-5* transcript number in the QR lineage, with some animals showing over 20 *mab-5* transcripts in QR.p or QR.pa. Consistent with the role of *mab-5* in promoting posterior localization of the Q neuroblast descendants (Salser and Kenyon, 1992), high *mab-5* expression was only observed in QR.p or QR.pa cells positioned in the posterior (Figure 2C). Furthermore, time-lapse live cell imaging showed that such posteriorly localized QR.p cells remain at this position because they fail to migrate anteriorly (Movies S1 and S2).

In the QL lineage, the expression of *mab-5* is triggered by canonical Wnt/ß-catenin signaling (Harris et al., 1996; Ji et al., 2013; Korswagen et al., 2002; Maloof et al., 1999). To test whether the ectopic expression of *mab-5* in the QR lineage of *sfrp-1*; *vang-1* double mutants is also dependent on canonical Wnt/ß-catenin signaling, we examined QR.px position in triple mutants of *sfrp-1*, *vang-1* and the canonical ß-catenin gene *bar-1*. As shown in Figure 1B, the QR.px localized anteriorly in *sfrp-1*; *vang-1 bar-1* mutants. A similar result

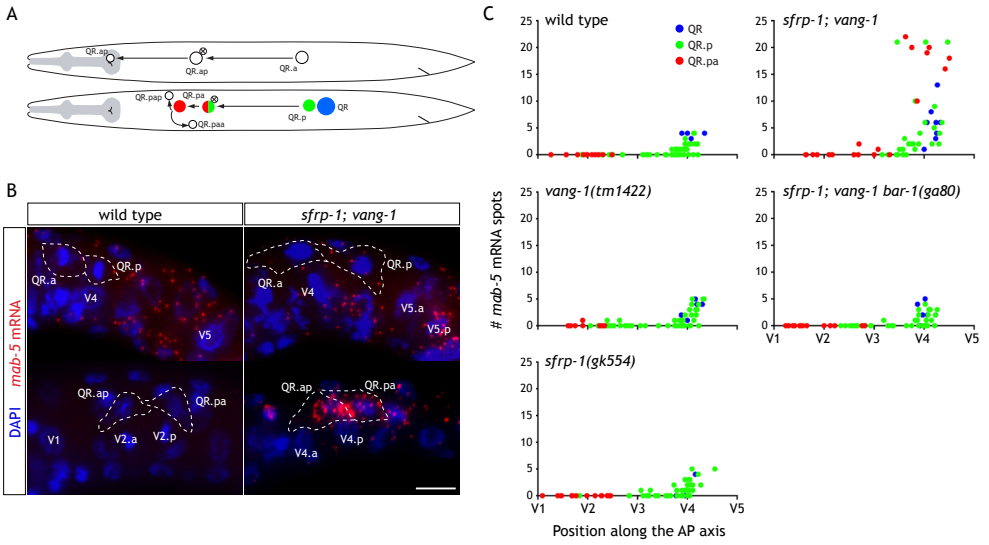

Figure 2. *mab-5* mRNA is ectopically expressed upon simultaneous loss of *vang-1* and *sfrp-1*. (**A**) Schematic overview of the anterior migration of the QR neuroblast and its descendants QR.a and QR.p. Apoptotic cells are represented as white cells with a cross. Expression of *mab-5* mRNA was quantified in QR (blue), QR.p (green) and QR.pa (red). Colors correspond to those used in the graphs depicting *mab-5* transcription dynamics in panel 2C. (**B**) Single molecule mRNA FISH of *mab-5* mRNA (red) in wild type and *sfrp-1; vang-1* double mutants. A high number of *mab-5* mRNA spots can be observed in the QR.pa and QR.ap cells of *sfrp-1; vang-1* mutant animals. Q neuroblasts were identified by GFP labeling using the *heIs63* transgene. Nuclei are visualized with DAPI staining (blue). Scale bar is 5 µm. (**C**) Transcription dynamics of *mab-5* in wild type and mutant animals as quantified in QR (blue), QR.p (green) and QR.pa (red) neuroblasts, n>60 for all genotypes. The number of mRNA spots per cell is plotted against the position of the cell with respect to the seam cells V1 to V5.

was obtained when we knocked down the Dvl ortholog *mig-5* (Figure 1B). Furthermore, there was no increase in *mab-5* expression in the *sfrp-1*; *vang-1 bar-1* triple mutant (Figure 2C). Indeed, the overall expression dynamics of *mab-5* in the QR lineage was comparable to the *sfrp-1* and *vang-1* single mutants. We conclude that the combined loss of *sfrp-1* and *vang-1* leads to activation of canonical Wnt/ß-catenin signaling and *mab-5* expression in the QR lineage.

vang-1 mutants display a lower threshold for EGL-20 induced canonical Wnt/ß-catenin pathway activation

Even though canonical Wnt/ß-catenin signaling and *mab-5* expression is normally not induced in QR, the QR neuroblast can activate the pathway when the Wnt ligand EGL-20 is overexpressed (Whangbo and Kenyon, 1999). As loss of *sfrp-1* has been shown to increase EGL-20 Wnt ligand activity (Harterink et al., 2011), we hypothesized that loss of *vang-1* may activate *mab-5* expression in the *sfrp-1* mutant background by lowering the threshold for EGL-20 induced canonical Wnt/ß-catenin pathway activation. To test this model, we inducibly expressed *egl-20* using a heat shock promoter in an *egl-20* mutant background and compared the response of wild type and *vang-1* mutant animals to increasing doses of EGL-20 (Figure 3). As expected, there was a clear correlation between the duration of heat shock and the percentage of animals with posteriorly displaced QR.px. Consistent with our hypothesis, we found that under each of these conditions, the percentage of posteriorly

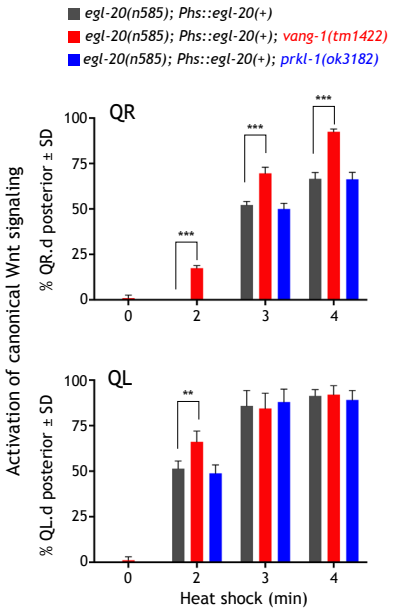

Figure 3. Loss of *vang-1* lowers the threshold for EGL-20 dependent activation of canonical Wnt/ß-catenin signaling in the QL and QR neuroblast lineages. Activation of canonical Wnt/ß-catenin signaling in *egl-20* (grey), *egl-20; vang-1* (red) and *egl-20 prkl-1* (blue) mutants ectopically expressing *egl-20* from a heat shock promoter. The percentage of QR.px cells (top graph) and QL.px cells (lower graph) localized in the posterior is plotted against the heat shock duration. Quantification of posteriorly localized Q.px cells is indicated as mean ± SD and represents the results of experiments performed in triplicate. Statistics were calculated using a Student's t-test (** p<0.01, *** p<0.001).

displaced QR.px was significantly higher in the *vang-1* mutant background (p<0.0001, Student's t-test). We conclude that loss of *vang-1* increases the sensitivity of QR for EGL-20 induced canonical Wnt/ß-catenin pathway activation.

vang-1 negatively regulates canonical Wnt/ß-catenin signaling in the QL lineage

To investigate whether *vang-1* also influences canonical Wnt/ß-catenin signaling in the QL lineage, we asked whether loss of *vang-1* influences QL.px migration in mutants in which canonical Wnt/ß-catenin signaling is partially disrupted. The Frizzled receptors *mig-1* and *lin-17* are part of interlocked positive and negative feedback loops that ensure robust activation of *mab-5* expression in QL (Ji et al., 2013) (see **Chapter 4**). In *mig-1* mutants, *mab-5* expression is strongly reduced and as a consequence, the QL.px frequently migrate anteriorly (Figures 4A and 4B) (Harris et al., 1996). A similar, but more subtle phenotype is observed in *lin-17* mutants. When we combined the *mig-1* mutant with *vang-1*, there was significant rescue of posterior QL.px localization, a trend that was also observed in the *lin-17*; *vang-1* double mutant. The restoration of posterior QL.px positioning suggests that loss of *vang-1* compensates for reduced Wnt/ß-catenin signaling activity and is consistent with a general negative regulatory role of *vang-1* in the Q neuroblast lineage. This conclusion is further supported by our finding that in *vang-1* mutants, QL showed an enhanced canonical Wnt/ß-catenin signaling response to ectopically expressed *egl-20* (Figure 3).

Mutation of *vang-1* did not restore posterior QL.px localization in *bar-1* and *pop-1*/TCF mutants, indicating that *vang-1* acts upstream of *bar-1*/ß-catenin (Figure S1A). This is in agreement with the observation that *mab-5* expression is lost in the QL lineage of *sfrp-1*; *vang-1 bar-1* triple mutants (Figure S2). Loss of *vang-1* also had no significant effect on QL.px localization in *egl-20* mutants or mutants of the Wnt secretion factor *mig-14* (Yang et al., 2008) (Figure 4B), indicating that loss of *vang-1* does not activate canonical Wnt/ß-catenin signaling in the absence of Wnt ligand stimulation.

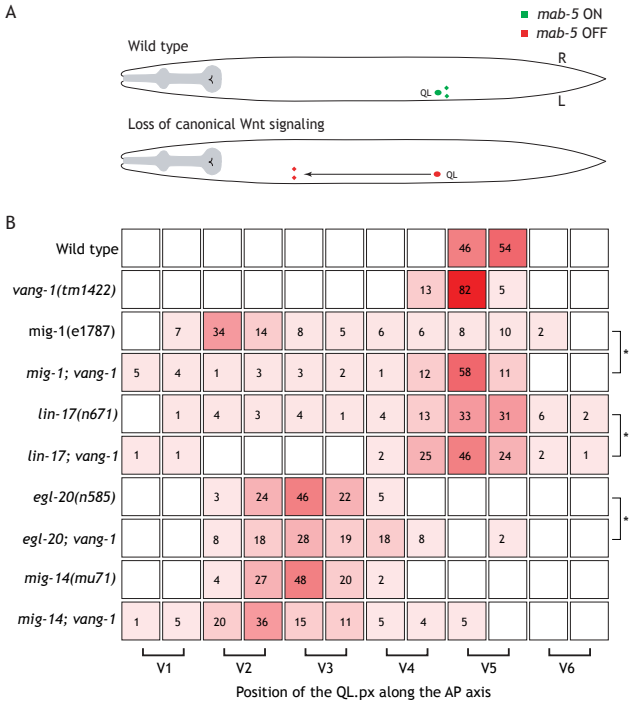

Figure 4. Loss of *vang-1* restores posterior localization of the QL.px cells in *mig-1* and *lin-17* Frizzled mutants. (**A**) Schematic representation of QL.px migration. In wild type animals, *mab-5* is expressed in QL (green) and the QL.px localize in the posterior. When canonical Wnt/ß-catenin signaling is abrogated, *mab-5* is not expressed (red) and the QL.px cells migrate anteriorly. (**B**) Final positions of the QR.px with respect to the seam cells V1.a to V6.p (lower brackets indicate Vn.a (left) and Vn.p (right) daughters of Vn cells). Values listed are the cumulative percentiles of the total number of cells scored in at least 3 independent experiments, n>30 for each experiment. Statistical significance was calculated using a Student's t-test (* p<0.05).

vang-1 functions cell autonomously in the Q neuroblast lineage

We have previously shown that *vang-1* is expressed in the QR descendants QR.p and QR.pa (Mentink et al., 2014, see also **Chapter 2**). Here, we have extended this analysis and show that *vang-1* transcripts can be detected in both the QL and QR neuroblasts at the onset of larval development (Figure 5). During the initial polarization and migration of the Q neuroblasts that precedes their response to Wnt ligands (Honigberg and Kenyon, 2000; Middelkoop et al., 2012), there is a clear increase in *vang-1* expression in both neuroblasts to an average of 4 ± 1.5 transcripts. After division, there is a significant decrease in *vang-*

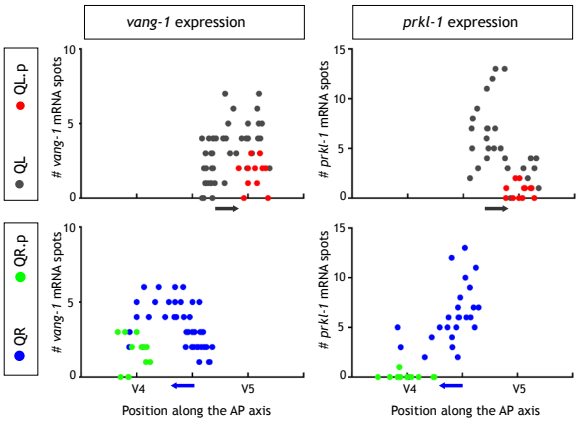

Figure 5. *vang-1* and *prkl-1* are expressed in both the QL and QR lineage and show opposite expression dynamics during initial polarization and migration. Transcription dynamics of *vang-1* (left panels) and *prkl-1* (right panels) as quantified in QL (grey), QL.p (red), QR (blue) and QR.p (green), n>35 for both genes. The number of mRNA spots per cell is plotted against the cell position with respect to the seam cells V4 and V5. The direction of the initial polarization and migration of QL and QR is indicated by an arrow.

1 expression in QL.p (1.5 ± 1 transcripts) and QR.p (1.5 ± 1 transcripts), but expression remains relatively constant during QR.p and QR.pa migration (Mentink et al., 2014, see also **Chapter 2**). To investigate whether *vang-1* is required within the Q neuroblast lineage, we expressed wild type *vang-1* in *sfrp-1*; *vang-1* double mutants using the Q neuroblast specific *egl-17* promoter (Ou and Vale, 2009). We found that the percentage of animals with posteriorly displaced QR.px cells was significantly lower as in the non-transgenic siblings (Figure 1B). We conclude that *vang-1* functions cell autonomously to negatively regulate canonical Wnt/ß-catenin signaling in the Q neuroblast lineage.

Interaction of VANG-1 with Dishevelled is required for modulation of canonical Wnt/ß-catenin signaling

Consistent with a negative regulatory role of *vang-1* in canonical Wnt/ß-catenin signaling, we found that overexpression of *vang-1* using a heat inducible promoter induced anterior migration of the QL.px (Figure 6). To further refine the epistatic relationship between *vang-1* and the canonical Wnt/ß-catenin pathway, we overexpressed *vang-1* in a *pry-1*/Axin mutant background. Loss of *pry-1*, a component of the ß-catenin destruction complex, induces constitutive canonical Wnt signaling activity (Korswagen et al., 2002). We found that overexpression of *vang-1* in *pry-1* mutants had no effect on QL.px localization, placing *vang-1* upstream of *pry-1*. Together with the double mutant analysis, these results indicate that *vang-1* acts at a level between the Frizzled receptors and the cytoplasmic signaling protein Dvl.

It has previously been shown that the carboxy-terminus of Van Gogh binds to the PDZ domain of Dvl (Park and Moon, 2002; Torban et al., 2004). To investigate whether this interaction is required for the activity of VANG-1 in canonical Wnt signaling, we tested whether overexpression of a *vang-1* mutant that lacks the Dvl binding domain inhibits canonical Wnt/ß-catenin signaling in the QL lineage. As shown in Figure 6, overexpression

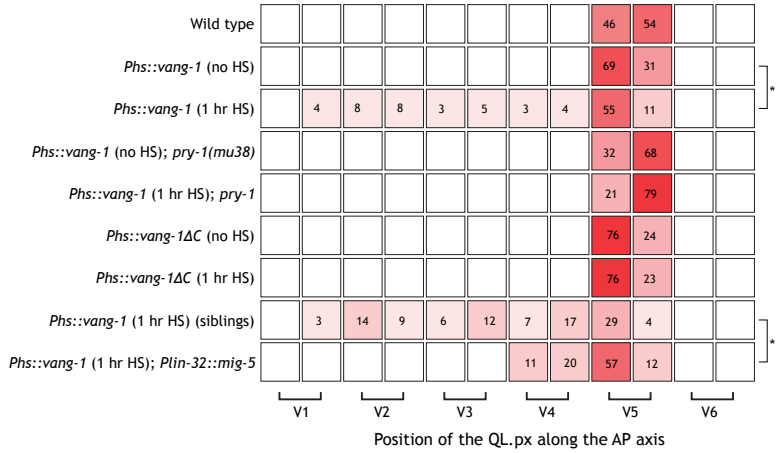

Figure 6. *vang-1* negatively regulates canonical Wnt/ß-catenin signaling through interaction with *mig-5*/Dvl. Final positions of the QL.px with respect to the seam cells V1.a to V6.p (lower brackets indicate Vn.a (left) and Vn.p (right) daughters of Vn cells). Values listed are the cumulative percentiles of the total number of cells scored in at least 3 independent experiments, n>30 for each experiment. A *Phsp16::gfp* construct was used as an expression control in the animals carrying the *Phsp16::vang-1ΔC* extrachromosomal transgene. Statistical significance was calculated using a Student's t-test (* p<0.05).

of *vang-1ΔC* had no effect on QL.px localization, indicating that Dvl binding is indeed key to the function of *vang-1* in canonical Wnt signaling.

Dvl is a highly versatile protein that is a common component of both canonical and non-canonical Wnt signaling pathways (Gao and Chen, 2010). We hypothesized that VANG-1 may modulate canonical Wnt/ß-catenin signaling by restricting the availability of Dvl. In such a scenario, overexpression of *vang-1* will sequester Dvl away from the canonical Wnt pathway, while loss of *vang-1* will increase the availability of Dvl. To test this model, we asked whether overexpression of *mig-5*/Dvl neutralizes the effect of *vang-1* overexpression. Consistent with our hypothesis, we found that overexpression of *mig-5* in the Q neuroblast lineage using the *lin-32* promoter restored posterior QL.px localization in animals that overexpress *vang-1* (Figure 6). We conclude that VANG-1 regulates the availability of Dvl for canonical Wnt/ß-catenin signaling.

prkl-1/Pk does not modulate canonical Wnt/ß-catenin signaling in the Q neuroblast lineage

In contrast to *vang-1*, loss of *prkl-1*/Pk did not induce posterior displacement of the QR.px in the *sfrp-1* mutant background (Figure S1C). Furthermore, *prkl-1* did not influence the sensitivity of QL and QR to ectopically expressed *egl-20* (Figure 3) nor did it suppress the Wnt signaling defect of *mig-1* and *lin-17* Frizzled mutants (Figure S1B). Despite having no apparent role in canonical Wnt/ß-catenin signaling, smFISH analysis revealed that *prkl-1* is expressed in the Q neuroblasts (Figure 5). With a gradual decrease in transcript number during the initial, Wnt independent polarization and short-range migration of QL and QR, the expression dynamics of *prkl-1* are however opposite to *vang-1*. We conclude that *vang-1* functions independently of *prkl-1* in modulating Wnt/ß-catenin signaling.

Discussion

Vangl2 and Pk are core components of the planar cell polarity pathway (Gray et al., 2011). In addition to their role in epithelial polarity and cell migration, studies in vertebrate model systems have suggested that there may be an antagonistic relationship between Vangl2 and Pk and the canonical Wnt/ß-catenin pathway (Angonin and Van Raay, 2013; Li et al., 2011; Park and Moon, 2002; Veeman et al., 2003). To study this potential cross-talk, we performed a comprehensive mutant analysis in *C. elegans*. Here, we show that the Vangl2 ortholog VANG-1 negatively regulates canonical Wnt/ß-catenin signaling in migrating Q neuroblasts. This negative regulatory function depends on the interaction of VANG-1 with Dvl, but is independent of the Pk ortholog PRKL-1. We conclude that Vangl2 has an evolutionarily conserved function in dampening canonical Wnt/ß-catenin signaling.

The Q neuroblasts QL and QR have different response thresholds for canonical Wnt/ß-catenin pathway activation (Whangbo and Kenyon, 1999). At physiological levels of the Wnt ligand EGL-20, QL activates canonical Wnt signaling and expression of the target gene *mab-5*, while QR adopts a non-canonical Wnt signaling response that enables the QR descendants to migrate anteriorly. We found that this response threshold is lowered in *vang-1* mutants, leading to ectopic canonical Wnt pathway activation and *mab-5* expression in QR when EGL-20 signaling activity is increased by removal of the global Wnt inhibitor *sfrp-1* or ectopic expression of EGL-20. Loss of *vang-1* also lowers the threshold for canonical Wnt/ß-catenin signaling in QL, indicating that *vang-1* is not responsible for the difference in signaling

response between the two Q neuroblasts. Consistently, smFISH analysis showed that *vang-1* displays similar expression dynamics and transcript numbers in QL and QR.

Even though loss of *vang-1* reduces the threshold for canonical Wnt/ß-catenin signaling, we did not observe ectopic activation of canonical Wnt signaling at physiological levels of the EGL-20 ligand. This indicates that VANG-1 primarily functions as a buffer that prevents erroneous canonical Wnt pathway activation at elevated Wnt ligand levels. Observations in zebrafish suggest that Vangl2 may have a similar function in vertebrates. Thus, while mutation of Vangl2 does not induce ectopic canonical Wnt/ß-catenin pathway activation (Jessen et al., 2002), loss of Vangl2 has been shown to enhance the response to ectopic expression of the canonical Wnt ligand Wnt8a (Angonin and Van Raay, 2013).

Our results indicate that the cross-talk between VANG-1 and the canonical Wnt/ß-catenin pathway is mediated through the cytoplasmic signaling protein Dvl. We found that *vang-1* acts genetically upstream of the Dvl ortholog *mig-5* and that deletion of a conserved Dvl interaction domain of VANG-1 eliminates the inhibitory effect of *vang-1* overexpression. Based on these results, we propose that VANG-1 negatively regulates canonical Wnt/ß-catenin signaling by restricting the availability of MIG-5. Consistently, we found that overexpression of MIG-5 neutralizes the inhibitory effect of VANG-1 overexpression.

Studies in vertebrate model systems suggest that Pk may also negatively regulate canonical Wnt/ß-catenin signaling. Pk has been shown to bind and destabilize Dvl, possibly by promoting its degradation (Carreira-Barbosa et al., 2003; Chan et al., 2006). Furthermore, overexpression of Pk was found to inhibit canonical Wnt signaling in reporter gene assays (Chan et al., 2006; Veeman et al., 2003). However, our genetic analysis did not reveal a role for *prkl-1* in canonical Wnt/ß-catenin signaling. Even though *prkl-1* is expressed in the Q neuroblasts, loss of *prkl-1* did not influence the response to EGL-20. Our results therefore support the conclusion that in *C. elegans*, PRKL-1 is not part of the cross-talk between VANG-1 and the canonical Wnt/ß-catenin pathway.

Deregulation of canonical Wnt/ß-catenin signaling is one of the primary causes of colon cancer (Clevers and Nusse, 2012). Recent clinical studies have demonstrated that Vangl2 is frequently silenced by promoter hypermethylation in colon cancer cell lines and tumor samples (Piazzi et al., 2013). Our results on the inhibitory effect of VANG-1 on canonical Wnt/ß-catenin signaling provide a mechanistic explanation for the role of Vangl2 as a tumor suppressor gene.

Experimental procedures

C. elegans strains and culture

Unless noted otherwise, *C. elegans* strains were cultured at 20°C using standard conditions. As wild type, the Bristol N2 strains was used. Mutant alleles and transgenes used in this study are LGI: *mig-1(e1787)*, *lin-17(n671)*, *pop-1(hu9)*, *pry-1(mu38)*; LGII: *mig-14(mu71)*; LGIII: *mab-5(gk670)*; LGIV: *unc-5(e53)*, *sfrp-1(gk554)*, *prkl-1(ok3182)*, *egl-20(n585)*, *dpy-20(e1362)*; LGV: *hels63 [Pwrt-2::gfp-ph; Pwrt-2::h2b-gfp; Plin-48::mTomato]* (Wildwater et al., 2011), *muIs53 [Phsp16::egl-20; unc-22(dn)]* (Whangbo and Kenyon, 1999); LGX: *vang-1(tm1422)*, *bar-1(ga80)* and unassigned, *huIs143 [Phsp16::vang-1; Pmyo-2::mTomato]* and the extra-chromosomal transgenes *huEx279*, *huEx280*, *huEx281 [Pegl-17::vang-1-gfp; Pmyo-2::mTomato]*, *huEx654*, *huEx655 [Phsp16::vang-1ΔC; Phsp16::gfp; Plin-48::mTomato]*, *huEx673 [Plin-32::mig-5::gfp; Plin-48::mTomato]*. To construct the *sfrp-1(gk554) prkl-*

1(ok3182) double mutant, first an *unc-5(e53) prkl-1(ok3182) dpy-20(e1362)* triple mutant was constructed. Triple mutants were crossed to wild type males and the resulting heterozygous males were in turn crossed to *sfrp-1(gk554)* hermaphrodites. The F2 generation was screened for Dpy non-Unc animals homozygous for *prkl-1(ok3182)* and heterozygous for *sfrp-1(gk554)*. The *dpy-20(e1362)* allele was subsequently removed by outcrossing.

Molecular biology
Total RNA was isolated from mixed stage animals and reversed transcribed to obtain cDNA. Individual cDNA clones encoding the *vang-1a* isoform and *mig-5* were PCR amplified from mixed stage cDNA using primers containing attB1 and attB2 Gateway recombination sites. cDNA fragments were subsequently recombined with pDNR221 to generate Gateway compatible entry clones. Promoter sequences of *egl-17* and *lin-32* (4.6 kb or 3.0 kb of upstream sequence, respectively) were cloned by PCR amplifying from genomic DNA using primers containing attB4 and attB1R Gateway recombination sites and recombined with pDNRP4-P1R to generate entry clones. Expression constructs were generated by combining appropriate entry clones in the pCFJ150 expression vector. Expression constructs were injected at 20-50 ng/µl with 5-10 ng/µl co-injection marker and supplemented with pBluescriptII to 150 ng/µl. The Phsp16::vang-1 construct was made by PCR amplifying *vang-1a* from the Gateway donor vector and cloning the PCR product into the pPD49.87 heat shock vector using NheI and BamHI restriction sites. The Phsp16::vang-1ΔC construct was made by deleting the C-terminal Dvl interaction domain of *vang-1a* (Park and Moon, 2002) by using primers 5'-GGGGACAAGTTTGTACAAAAAAGCAGGCTatgtcgtatcaagat-aacag-3' and 5'-GGGGACCACTTTGTACAAGAAAGCTGGGTtcactcgaggagcacaa-cagaga-3'.

Phenotypic analysis and microscopy
The positions of the final QR and QL descendants were scored with DIC microscopy in late L1 stage larvae as previously described (Middelkoop et al., 2012). Animals were mounted on 2% agarose pads containing 10 mM sodium azide for immobilization.

Time lapse live cell imaging
To follow Q cell migration in time, synchronized animals (4-5 hours after hatching) carrying the *heIs63 [Pwrt-2::gfp-ph;Pwrt-2::h2b-gfp;Plin-48::mTomato]* transgene were mounted in 0.5 µl of 0.1 µm diameter polystyrene beads in aqueous solution (Polysciences 00876 2.5% w/v aqueous suspension) on 10% agarose pads (Kim et al. 2013). Images were acquired using a Leica TCS SPE confocal microscope (63x objective, zoom 1.0x, 10% 488 nm laser power). Z-stacks of 0.5 µm per stack were made every 15 minutes for 7 hours. Images were acquired using LASAF software. Image processing and analysis were performed using ImageJ v1.43u and movie construction using Adobe Photoshop CS5.1 software.

Heat shock experiments
Heat shock experiments on animals carrying the *muIs53 [Phs::egl-20; unc-22(dn)]* transgene were performed as previously described (Middelkoop et al., 2012), except as follows: synchronized L1 larvae (aged 0-1 hours after hatching) were incubated at 33°C in a volume of 50 µl M9 buffer for 2, 3 or 4 minutes. Placing the tubes on ice for 10 seconds ended the heat shock treatment. Animals were cultured overnight on OP50 seeded NGM agar plates at 20°C and the positions of the Q cell descendants were scored the following morning. Heat

shock experiments on animals carrying the *huIs143 [Phsp16::vang-1; Pmyo-2::mTomato]* or *huEx654*, *huEx655 [Phsp16::vang-1ΔC; Phsp16::gfp; Plin-48::mTomato]* were performed similarly, excepting that the heat shock treatment was one hour and tubes were not chilled on ice.

Single molecule fluorescence in situ hybridization

The smFISH protocol was performed as described elsewhere (Raj et al., 2008). In brief, synchronized L1 larvae were fixed using 4% paraformaldehyde and suspended in 70% ethanol. Hybridization was done overnight at 33˚C in the dark. Short oligonucleotide probes were designed using a specially designed algorithm (www.singlemoleculefish.com) and chemically coupled to the fluorescent dye Cy5. Animals were suspended in buffer containing DAPI for nuclear counterstaining before mounting. Z-stacks with a slice thickness of 0.5 µm were obtained with a Leica DM6000 microscope, equipped with a Leica DFC360FX camera, 100x oil objective and Y5 (Cy5), A4 (DAPI) and GFP filter cubes. Images were acquired with 1024x1024 resolution and subjected to a 2x2 binning. Quantification of mRNA was performed manually on the obtained z-stacks. Only mRNA spots visible in at least two independent focal planes were counted. The Q cell boundary was marked by the *heIs63* transgene. Analysis was performed using ImageJ v1.43u software.

Statistical analysis

The final position of the Q.px cells was used as an assay to determine canonical Wnt/ß-catenin pathway activity: QL.px cells were scored as having activated canonical Wnt/ß-catenin signaling if located on V4.p or more posterior, QR.px cells if located on V3.p or more posterior. Each strain was scored in 3 independent experiments. Statistical comparisons were performed using unpaired, two tailed Student's t-tests. Results were deemed significant if $p<0.05$

Acknowledgments

We thank members of the Korswagen group for critically reading the manuscript, the *Caenorhabditis* Genetics Center (University of Minnesota, Minneapolis) and the National Bioresource Project for the Nematode (Tokyo, Japan) for strains and the Hubrecht Imaging Center (HIC) for assistance with microscopy.

References

Angers, S., and Moon, R.T. (2009). Proximal events in Wnt signal transduction. Nat Rev Mol Cell Biol *10*, 468-477.

Angonin, D., and Van Raay, T.J. (2013). Nkd1 functions as a passive antagonist of Wnt signaling. PloS One *8*, e74666.

Carreira-Barbosa, F., Concha, M.L., Takeuchi, M., Ueno, N., Wilson, S.W., and Tada, M. (2003). Prickle1 regulates cell movements during gastrulation and neuronal migration in zebrafish. Development *130*, 4037-4046.

Chan, D.W., Chan, C.Y., Yam, J.W., Ching, Y.P., and Ng, I.O. (2006). Prickle-1 negatively regulates Wnt/ß-catenin pathway by promoting Dishevelled ubiquitination/degradation in liver cancer. Gastroenterology *131*, 1218-1227.

Clevers, H., and Nusse, R. (2012). Wnt/ß-catenin signaling and disease. Cell *149*, 1192-1205.

Gao, C., and Chen, Y.G. (2010). Dishevelled: The hub of Wnt signaling. Cell Signal *22*, 717-727.

Glasco, D.M., Sittaramane, V., Bryant, W., Fritzsch, B., Sawant, A., Paudyal, A., Stewart, M., Andre, P., Cadete Vilhais-Neto, G., Yang, Y., *et al.* (2012). The mouse Wnt/PCP protein Vangl2 is necessary for migration of facial branchiomotor neurons, and functions independently of Dishevelled. Dev Biol *369*, 211-222.

Gray, R.S., Roszko, I., and Solnica-Krezel, L. (2011). Planar cell polarity: coordinating morphogenetic cell behaviors with embryonic polarity. Dev Cell *21*, 120-133.

Green, J.L., Inoue, T., and Sternberg, P.W. (2008). Opposing Wnt pathways orient cell polarity during organogenesis. Cell *134*, 646-656.

Harris, J., Honigberg, L., Robinson, N., and Kenyon, C. (1996). Neuronal cell migration in *C. elegans*: regulation of Hox gene expression and cell position. Development *122*, 3117-3131.

Harterink, M., Kim, D.H., Middelkoop, T.C., Doan, T.D., van Oudenaarden, A., and Korswagen, H.C. (2011). Neuroblast migration along the anteroposterior axis of *C. elegans* is controlled by opposing gradients of Wnts and a secreted Frizzled-related protein. Development *138*, 2915-2924.

Hoffmann, M., Segbert, C., Helbig, G., and Bossinger, O. (2010). Intestinal tube formation in *Caenorhabditis elegans* requires *vang-1* and *egl-15* signaling. Dev Biol *339*, 268-279.

Honigberg, L., and Kenyon, C. (2000). Establishment of left/right asymmetry in neuroblast migration by UNC-40/DCC, UNC-73/Trio and DPY-19 proteins in *C. elegans*. Development *127*, 4655-4668.

Jessen, J.R., Topczewski, J., Bingham, S., Sepich, D.S., Marlow, F., Chandrasekhar, A., and Solnica-Krezel, L. (2002). Zebrafish trilobite identifies new roles for Strabismus in gastrulation and neuronal movements. Nat Cell Biol *4*, 610-615.

Ji, N., Middelkoop, T.C., Mentink, R.A., Betist, M.C., Tonegawa, S., Mooijman, D., Korswagen, H.C., and van Oudenaarden, A. (2013). Feedback control of gene expression variability in the *Caenorhabditis elegans* Wnt pathway. Cell *155*, 869-880.

Kibar, Z., Capra, V., and Gros, P. (2007). Toward understanding the genetic basis of neural tube defects. Clinical Genet *71*, 295-310.

Korswagen, H.C. (2002). Canonical and non-canonical Wnt signaling pathways in *Caenorhabditis elegans*: variations on a common signaling theme. BioEssays *24*, 801-810.

Korswagen, H.C., Coudreuse, D.Y., Betist, M.C., van de Water, S., Zivkovic, D., and Clevers, H.C. (2002). The Axin-like protein PRY-1 is a negative regulator of a canonical Wnt pathway in *C. elegans*. Genes Dev *16*, 1291-1302.

Korswagen, H.C., Herman, M.A., and Clevers, H.C. (2000). Distinct ß-catenins mediate adhesion and signalling functions in *C. elegans*. Nature *406*, 527-532.

Lei, Y.P., Zhang, T., Li, H., Wu, B.L., Jin, L., and Wang, H.Y. (2010). VANGL2 mutations in human cranial neural-tube defects. New Engl J Med *362*, 2232-2235.

Li, S., Esterberg, R., Lachance, V., Ren, D., Radde-Gallwitz, K., Chi, F., Parent, J.L., Fritz, A., and Chen, P. (2011). Rack1 is required for Vangl2 membrane localization and planar cell polarity signaling while attenuating canonical Wnt activity. Proc Natl Acad Sci USA *108*, 2264-2269.

Maloof, J.N., Whangbo, J., Harris, J.M., Jongeward, G.D., and Kenyon, C. (1999). A Wnt signaling pathway controls hox gene expression and neuroblast migration in *C. elegans*. Development *126*, 37-49.

Mentink, R.A., Middelkoop, T.C., Rella, L., Ji, N., Chung, Y.T., Betist, M.C., van Oudenaarden, A., and Korswagen, H.C. (2014). Cell intrinsic modulation of Wnt signaling controls neuroblast migration in *C. elegans*. Developmental cell *in press*.

Middelkoop, T.C., Williams, L., Yang, P.T., Luchtenberg, J., Betist, M.C., Ji, N., van Oudenaarden, A., Kenyon, C., and Korswagen, H.C. (2012). The thrombospondin repeat containing protein MIG-21 controls a left-right asymmetric Wnt signaling response in migrating *C. elegans* neuroblasts. Dev Biol *361*, 338-348.

Ou, G., and Vale, R.D. (2009). Molecular signatures of cell migration in *C. elegans* Q neuroblasts. J Cell Biol *185*, 77-85.

Park, M., and Moon, R.T. (2002). The planar cell-polarity gene *stbm* regulates cell behaviour and cell fate in vertebrate embryos. Nat Cell Biol *4*, 20-25.

Piazzi, G., Selgrad, M., Garcia, M., Ceccarelli, C., Fini, L., Bianchi, P., Laghi, L., D'Angelo, L., Paterini, P., Malfertheiner, P., *et al.* (2013). Van-Gogh-like2 antagonises the canonical Wnt pathway and is methylated in colorectal cancers. British J Cancer *108*, 1750-1756.

Polakis, P. (2012). Wnt signaling in cancer. Cold Spring Harbor Pers Biol *4*.

Raj, A., van den Bogaard, P., Rifkin, S.A., van Oudenaarden, A., and Tyagi, S. (2008). Imaging individual mRNA molecules using multiple singly labeled probes. nat Meth *5*, 877-879.

Salser, S.J., and Kenyon, C. (1992). Activation of a *C. elegans* Antennapedia homologue in migrating cells controls their direction of migration. Nature *355*, 255-258.

Sanchez-Alvarez, L., Visanuvimol, J., McEwan, A., Su, A., Imai, J.H., and Colavita, A. (2011). VANG-1 and PRKL-1 cooperate to negatively regulate neurite formation in Caenorhabditis elegans. PLoS Genet *7*, e1002257.

Sawa, H., and Korswagen, H.C. (2013). Wnt signaling in C. elegans. Wormbook, doi/10.1895/wormbook.1.7.2

Silhankova, M., and Korswagen, H.C. (2007). Migration of neuronal cells along the anterior-posterior body axis of *C. elegans*: Wnts are in control. Curr Opin Genet Dev *17*, 320-325.

Sulston, J.E., and Horvitz, H.R. (1977). Post-embryonic cell lineages of the nematode, *Caenorhabditis elegans*. Dev Biol *56*, 110-156.

Takeuchi, M., Nakabayashi, J., Sakaguchi, T., Yamamoto, T.S., Takahashi, H., Takeda, H., and Ueno, N. (2003). The prickle-related gene in vertebrates is essential for gastrulation cell movements. Curr Biol *13*, 674-679.

Torban, E., Wang, H.J., Groulx, N., and Gros, P. (2004). Independent mutations in mouse Vangl2 that cause neural tube defects in looptail mice impair interaction with members of the Dishevelled family. J Biol Chem *279*, 52703-52713.

Veeman, M.T., Slusarski, D.C., Kaykas, A., Louie, S.H., and Moon, R.T. (2003). Zebrafish prickle, a modulator of noncanonical Wnt/Fz signaling, regulates gastrulation movements. Curr Biol *13*, 680-685.

Wallingford, J.B., Rowning, B.A., Vogeli, K.M., Rothbacher, U., Fraser, S.E., and Harland, R.M. (2000). Dishevelled controls cell polarity during *Xenopus* gastrulation. Nature *405*, 81-85.

Whangbo, J., and Kenyon, C. (1999). A Wnt signaling system that specifies two patterns of cell migration in *C. elegans*. Mol Cell *4*, 851-858.

Wildwater, M., Sander, N., de Vreede, G., and van den Heuvel, S. (2011). Cell shape and Wnt signaling redundantly control the division axis of *C. elegans* epithelial stem cells. Development *138*, 4375-4385.

Yang, P.T., Lorenowicz, M.J., Silhankova, M., Coudreuse, D.Y., Betist, M.C., and Korswagen, H.C. (2008). Wnt signaling requires retromer-dependent recycling of MIG-14/Wntless in Wnt-producing cells. Dev Cell *14*, 140-147.

Zinovyeva, A.Y., Yamamoto, Y., Sawa, H., and Forrester, W.C. (2008). Complex network of Wnt signaling regulates neuronal migrations during *Caenorhabditis elegans* development. Genetics *179*, 1357-1371.

Supplemental figures

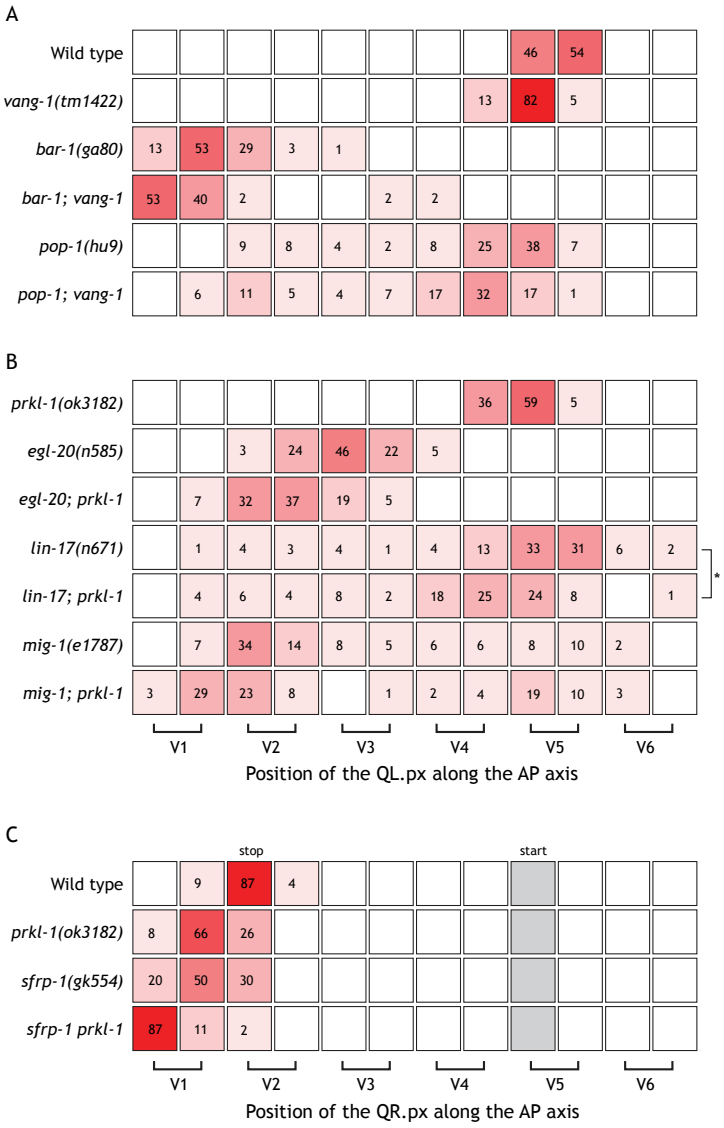

Figure S1. *vang-1* acts upstream of *bar-1* and *pop-1*, while loss of *prkl-1* does not affect canonical Wnt signaling. (**A-C**) Final positions of the QL.px (**A, B**) and the QR.px (**C**) with respect to the seam cells V1.a to V6.p (lower brackets indicate Vn.a (left) and Vn.p (right) daughters of Vn cells). Values listed are the cumulative percentiles of the total number of cells scored in at least 3 independent experiments, n>30 for each experiment. Statistical significance was calculated using a Student's t-test (* p<0.05).

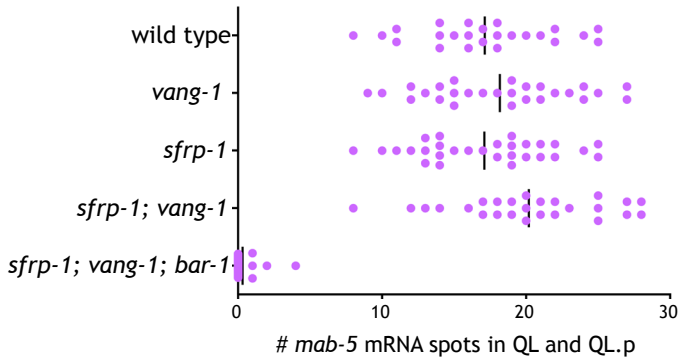

Figure S2. Expression of *mab-5* mRNA is lost in the QL lineage in *sfrp-1; vang-1; bar-1* triple mutants. Displayed are the *mab-5* mRNA counts in QL and QL.p cells that have completed initial migration.

Chapter 4

Feedback control of gene expression variability in the *C. elegans* Wnt pathway

Ni Ji[1,5], Teije C. Middelkoop[3,5], Remco A. Mentink[3], Marco C. Betist[3], Satto Tonegawa[4], Dylan Mooijman[3], Hendrik C. Korswagen[3], Alexander van Oudenaarden[2,3]

[1]Department of Brain and Cognitive Sciences, Massachusetts Institute of Technology, Cambridge, MA, USA, [2]Department of Physics and Department of Biology, Massachusetts Institute of Technology, Cambridge, MA, USA, [3]Hubrecht Institute, Royal Netherlands Academy of Arts and Sciences and University Medical Center Utrecht, The Netherlands, [4]Milton Academy, Milton, MA, USA

[5]These authors contributed equally to this work.

Adapted from Cell. (2013) 155, 869-80.

Abstract

Variability in gene expression contributes to phenotypic heterogeneity even in isogenic populations. Here, we used the stereotyped, Wnt signaling-dependent development of the Caenorhabditis elegans Q neuroblast to probe endogenous mechanisms that control gene expression variability. We found that the key Hox gene that orients Q neuroblast migration exhibits increased gene expression variability in mutants in which Wnt pathway activity has been perturbed. Distinct features of the gene expression distributions prompted us on a systematic search for regulatory interactions, revealing a network of interlocked positive and negative feedback loops. Interestingly, positive feedback appeared to cooperate with negative feedback to reduce variability while keeping the Hox gene expression at elevated levels. A minimal model correctly predicts the increased gene expression variability across mutants. Our results highlight the influence of gene network architecture on expression variability and implicate feedback regulation as an effective mechanism to ensure developmental robustness.

Introduction

Gene expression is inherently variable, even among isogenic cells situated in identical environments (Raj and van Oudenaarden, 2008; Raj et al., 2008; Eldar and Elowitz, 2010; Bala´ zsi et al., 2011; Li and Xie, 2011). On the one hand, variability in gene expression may confer beneficial phenotypic diversity. For example, it may serve as a ''bet-hedging'' strategy for isogenic microbial populations to ensure survival in fluctuating environments (Thattai and van Oudenaarden, 2004; Kussell and Leibler, 2005; Wolf et al., 2005; Acar et al., 2008; Beaumont et al., 2009; Eldar et al., 2009) or as a ''symmetry-breaking'' mechanism to induce multiple cell fates from a single progenitor cell type (Wernet et al., 2006; Chang et al., 2008; Kalmar et al., 2009). On the other hand, excessive variability in gene expression could disrupt normal development and tissue maintenance, leading to aberrant phenotypes (Aranda-Anzaldo and Dent, 2003; Chung and Levens, 2005; Henrichsen et al., 2009; Raj et al., 2010). The remarkable robustness of numerous physiological events implies that endogenous mechanisms must exist to effectively control variability in gene expression (Nijhout, 2002; Fe´ lix and Wagner, 2008; Boettiger and Levine, 2013). In a simple model of constitutive gene expression, the equilibrium level of messenger RNA (mRNA) transcripts is expected to follow a Poisson probability distribution. A distinct feature of the Poisson distribution is that the ratio between the variance and the mean, termed the Fano factor, equals exactly one, regardless of the detailed parameters. For genes under transcriptional regulation, substantial deviations from the Poisson behavior have been theoretically proposed (Kepler and Elston, 2001; Friedman et al., 2006; Shahrezaei and Swain, 2008) and experimentally observed in a series of studies (Golding et al., 2005; Cai et al., 2006; Raj et al., 2006; Zenklusen et al., 2008). Such deviation has often been attributed to transcriptional bursting, where the promoter transitions stochastically between its active and inactive states. In addition, fluctuation in the abundance of the upstream regulators can also propagate to increase the variability of the target gene expression (Hooshangi et al., 2005; Pedraza and van Oudenaarden, 2005; Rosenfeld et al., 2005; Dunlop et al., 2008).

Pioneering theoretical and synthetic biology studies have highlighted the potential of regulatory networks in controlling gene expression variability. Negative feedback, a common mode of regulation, has been shown to suppress variability in synthetic gene expression systems (Becskei and Serrano, 2000; Austin et al., 2006). Positive feedback has been extensively studied for its ability to induce multimodal or ''switch-like'' behavior in both synthetic and endogenous systems (Becskei et al., 2001; Xiong and Ferrell, 2003; Ozbudak et al., 2004; Acar et al., 2005; Weinberger et al., 2005; To and Maheshri, 2010). In contrast to the simplicity of synthetic circuits, endogenous genes are embedded in densely connected networks with mixed feedback loops and multilayered cascades (Milo et al., 2002; Davidson, 2010; Hirsch et al., 2010). Whether and how regulatory networks regulate gene expression variability endogenously remain to be explored.

Caenorhabditis elegans provides an excellent model for studying the endogenous control of gene expression variability. Its highly stereotyped development (Sulston and Horvitz, 1977) implicates underlying mechanisms that robustly control transcriptional variability. Here, we study specifically the stereotyped migratory decision of the C. elegans Q neuroblast. Two Q neuroblasts, QL and QR, are born at bilaterally symmetrical positions in the C. elegans embryo but migrate oppositely along the anterior-posterior axis upon hatching (Figure 1A). In the left Q neuroblast (QL), expression of the Hox gene *mab-5*/Antennapedia is

necessary and sufficient to ensure the posterior migration of the QL descendants. In the right Qneuroblast (QR), however, the absence of *mab-5* expression drives the cell to migrate toward the anterior (Salser and Kenyon, 1992; Harris et al., 1996). In wild type animals, *mab-5* expression in QL is dependent on the canonical Wnt signal transduced through the posteriorly produced Wnt ligand, EGL-20 (Figures 1A and 1B) Whangbo and Kenyon, 1999; Coudreuse et al., 2006). Two out of the four *C. elegans* Frizzled type Wnt receptors, MIG-1 and LIN-17, are required for *mab-5* expression in QL (Harris et al., 1996). The other Frizzled homologs, *mom-5* and *cfz-2*, have also been implicated in the regulation of the migration of QL descendants (Zinovyeva et al., 2008). Interestingly, Frizzled mutants exhibit varying degrees of partially penetrant migratory defects, where a fraction of QL descendants reverse to migrate anteriorly (Zinovyeva et al., 2008) (Figures 1C and S1A). Whether this phenotypic heterogeneity originates at or downstream from *mab-5* expression is unclear.

By combining single-cell transcript counting with genetic manipulation, we identified a strong link between the variability in *mab-5* expression and the penetrance of the migratory phenotype. We observed a complex relationship between the variability and the mean levels of *mab-5* expression, implicating feedback regulation. A systematic search for regulatory interactions revealed a network of positive and negative feedback loops between the Frizzled receptors and the Wnt signaling pathway. A minimal network model captures the variability in *mab-5* expression across mutants and provides mechanistic insights on how the wild type network achieves robustness. Our results demonstrate, in a developmentally relevant context, the contribution of a regulatory network to controlling gene expression variability.

Results

Wnt signaling activates mab-5 expression to a stable range in wild type QL

To explore the putative relation between *mab-5* expression and the phenotypic heterogeneity in the Wnt pathway mutants, it is necessary to quantitatively compare *mab-5* expression between wild type and mutants. We started by characterizing *mab-5* expression in the wild type QL neuroblasts (Figures 1D and 1E). Using single molecule fluorescent in situ hybridization (smFISH, Raj et al., 2008), we counted *mab-5* transcripts at various stages of QL migration (Figure 1D). The total migratory distance (MD) of QL and QR (Figure 1E, top, and Figure S1B) was used as an indicator of migratory stage. Data from many single QL cells were combined to obtain a population profile of *mab-5* expression dynamics (Figure 1E, bottom).

Before the onset of migration, *mab-5* transcripts were present at low levels in QL (Figures 1D and 1E, MD = 0–2). Thereafter, QL began to polarize, and *mab-5* transcripts started to appear in the cytoplasm. Concurrently, nascent transcripts began to cumulate in the nucleus as bright transcription centers (TCs, Figures 1D and S1C). The frequent appearance of paired TCs likely indicates heightened transcriptional activity on both alleles (Raj et al., 2006). After a period of initial variability, *mab-5* expression converged to around 50–60 transcripts per cell (MD ≥ 8, Figure 1E). The variability in *mab-5* expression stabilized to a Fano factor of 2.4. This value is greater than the average measurement of 1.6 in *Escherichia coli* (Taniguchi et al., 2010) yet is over 10-fold lower than those reported for mammalian mRNAs (Raj et al., 2006).

Although Wnt signaling has been suggested as the main activator of *mab-5* transcription

(Korswagen, 2002), whether it acts directly within QL remains uncertain. We probed the cell autonomous role of Wnt signaling by blocking it either globally or Q cell specifically using a dominant-negative form of POP-1/TCF (*DN-pop-1*) (Korswagen et al., 2000). In both

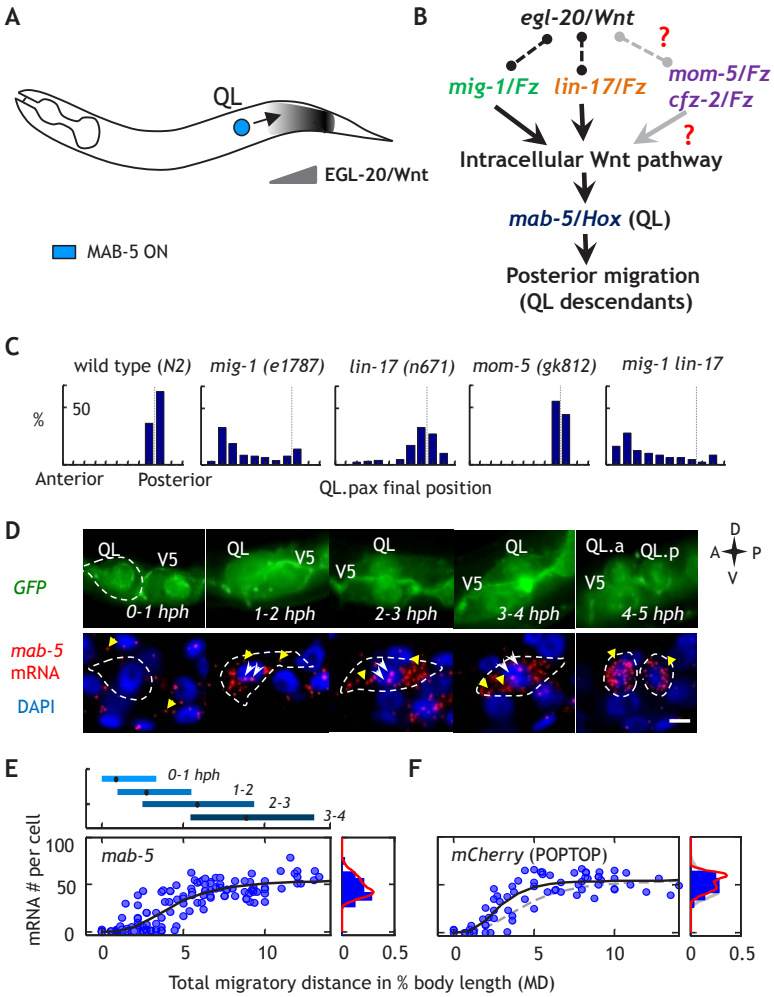

Figure 1. Using single-cell transcript counting to study the control of *mab-5* expression. (**A**) Schematic representation of the activation of MAB-5 expression in QL in response to the posterior- to-anterior gradient of EGL-20/Wnt. (**B**) Model of Wnt signaling based on published studies. Question marks and gray edges indicate lack of definitive evidence. (**C**) Final position of QL descendants in wild type and various Frizzled loss-of-function mutants. Unless otherwise noted, compound mutants carry the same alleles as single mutants. (**D**) Detection of *mab-5* transcripts using smFISH over the course of QL migration. Upper: QL at different stages of its migration. V5 is a stationary cell used as spatial reference. Lower: smFISH staining of *mab-5* transcripts in the same cells as shown above. Yellow arrowheads: single *mab-5* transcripts; white arrowheads: transcription centers in the nucleus. Scale bar represents 2.5 mm. (**E**) *mab-5* transcription dynamics in single QL neuroblasts in wild type animals. Upper: normalized total MD for worms collected at different time-points after hatching. Black dots mark the mean, and blue bars span 2.5–97.5 percentiles. Lower: number of *mab-5* transcripts per cell plotted against MD. The histogram to the right is generated using data points to the left with MD > 8. Black lines are generated by fitting to a sigmoidal function. Red curves are generated by fitting with two Gaussian distributions. (**F**) mCherry transcription dynamics in the POPTOP strain. See also Figure S1.

mutants, we observed a more than 95% reduction in *mab-5* transcripts in QL (Figure S1D), confirming a cell-autonomous role of Wnt signaling in activating *mab-5* expression.

The above finding suggests that *mab-5* expression may serve as an endogenous readout of Wnt pathway activity in QL. To confirm this possibility, we first compared the transcription dynamics of *mab-5* to that of a *mCherry* transgene driven by a *pes-10* minimal promoter with seven POP-1 binding sites (POP-1 and TCF Optimal Promoter [POPTOP]; Green et al., 2008). The dynamics of *mCherry* transcripts closely resembled that of *mab-5* (Figures 1E and 1F). Furthermore, mutation of a conserved TCF binding motif in the *mab-5* promoter (K. Cadigan, personal communication) led to a significant reduction in reporter transgene expression (Figures S1E and S1F). Taken together, these observations motivate the use of *mab-5* transcript level as an endogenous readout of Wnt signaling in QL.

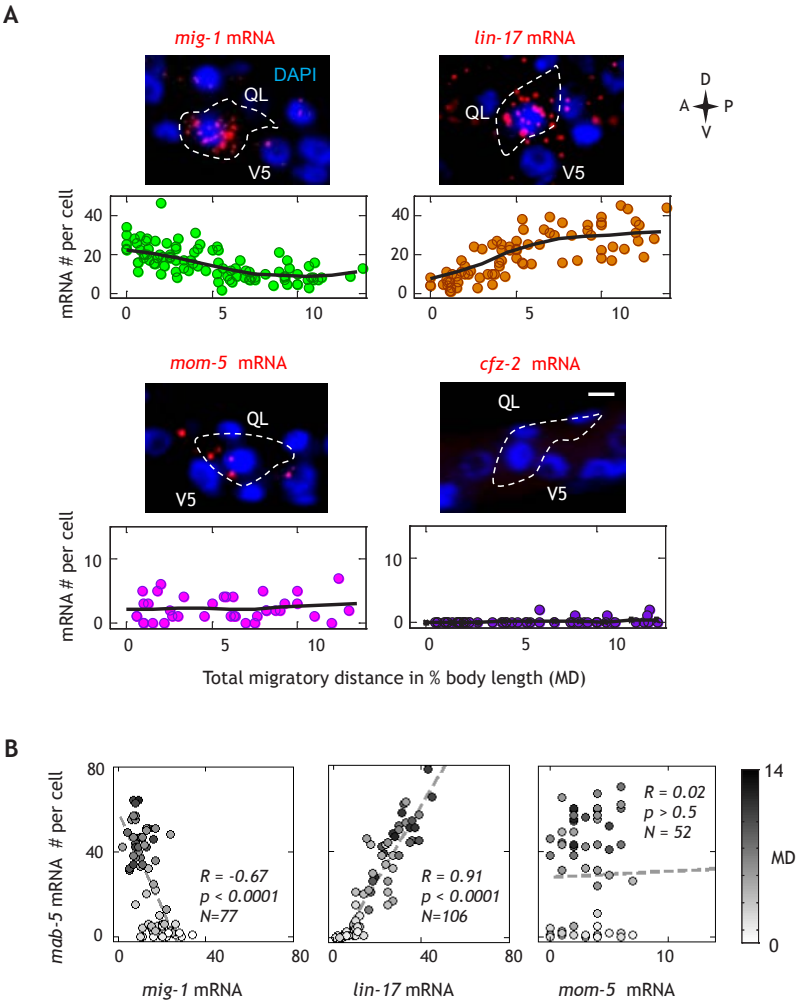

Figure 2. Three Frizzled paralogs are dynamically transcribed in QL. (**A**) smFISH staining and single-cell transcript counts for the four *C. elegans* Frizzled paralogs over the course of QL migration. (**B**) Single-cell correlation between Frizzled and *mab-5* transcript counts. Shades of dots indicate corresponding MD value. See also Figure S2.

Three Frizzled receptors are expressed in QL and exhibit distinct expression dynamics
Because mutation of different Frizzled paralogs leads to different penetrance in migratory phenotype (Figures 1C and S1A), we speculated that, apart from their difference in functional efficacy, individual Frizzled paralogs may be expressed at different levels in QL. To test this, we used paralog-specific smFISH to quantify the expression of the four Frizzled receptors in QL. QL-specific expression was detected for *mig-1*, *lin-17*, and *mom-5*, but not for *cfz-2* (Figures 2A and S2A). In addition to difference in average abundance, these paralogs also differed in their temporal patterns of expression. *mig-1* transcripts decreased from an average of 27 copies per cell to less than 10 over the course of migration. *lin-17*, on the opposite, rose from less than 10 copies per cell to an average of 34. *mom-5* was expressed at less than 10 copies per cell throughout QL migration (Figure S2A). Outside QL, the four Frizzleds also exhibited distinct global expression patterns (Figure S2B).

Intuitively, a positive correlation may be expected between the expression of a receptor and that of its signaling target. A negative correlation was, however, observed between the abundance of *mig-1* transcripts and that of *mab-5* (Figure 2B, Pearson's $R = -0.67$, $p < 0.001$). Compared to *mig-1*, mutation of *lin-17* leads to a weaker migratory defect (Figure 1C). However, a strong positive correlation was observed between *lin-17* and *mab-5* transcripts at the single-cell level (Pearson's $R = 0.91$, $p < 0.001$). No significant correlation was observed between *mom-5* and *mab-5* (Pearson's $R = 0.02$, $p > 0.5$). Together, the distinct transcriptional and correlation profiles suggest that divergent transcriptional regulatory programs exist upstream of the Frizzled receptors.

Frizzled mutants exhibit different degrees of variability in mab-5 expression
Having assessed *mab-5* and Frizzled expression in the wild type, we next asked how *mab-5* expression is affected by mutations in the Frizzled receptor genes. Previously, reduction in MAB-5 antibody staining has been reported in *mig-1* and *lin-17* single mutants (Harris et al., 1996). In agreement, we observed a strong reduction in *mab-5* transcripts in QL in most of *mig-1(e1787)* single mutants (Figure 3A). A small fraction of QLs, however, retained significant levels of *mab-5* expression (20 transcripts per cell or higher). Cell-to-cell heterogeneity was also evident in the *lin-17(n671)* single mutant. Individual QLs exhibited between very low to a near-wild type amount of *mab-5* transcripts. The *mom-5(gk812)* mutant, unlike the wildtype, exhibited high variability in *mab-5* expression beyond the initial phase of QL migration (MD > 5, note cells with <25 copies of *mab-5*). In comparison, *mab-5* levels in the *cfz-2(ok1201)* mutant were indistinguishable from the wild type.

Homozygous mutation in two or more of the three Frizzled receptors (*mig-1*, *lin-17*, and *mom-5*) resulted in nearly complete loss of *mab-5* expression in QL (Figure 3A). In contrast, heterozygotes of these mutants exhibited similar average *mab-5* levels as the wild type. Interestingly, heterozygotes of the Frizzled triple mutant (triple het) showed increased variability in *mab-5* expression, where a small fraction of late-stage QLs contained less than 20 *mab-5* transcripts (Figure 3A). This observation, together with those from the single mutants, indicates that partial reduction of Frizzled receptor function could disrupt the reliable activation of *mab-5* transcription in QL.

Motivated by the recent discovery that variability in gene expression underlies partial penetrance (Raj et al., 2010), we questioned whether variability in *mab-5* transcript level is predictive of the phenotypic penetrance of different mutants. We hypothesized that *mab-5* expression must exceed a certain threshold to prevent the QL descendants from migrating

anteriorly. Under this hypothesis, we searched (Figure S3C) and found threshold values of around 25 transcripts per cell (Figure 3C) to yield accurate predictions of the phenotypic penetrance. *mom-5* single and compound mutants were not included in this analysis due to the *mab-5*-independent requirement of *mom-5* for anterior migration (Zinovyeva et al., 2008). Thus, upregulating *mab-5* expression above a certain threshold may be critical in driving robust migratory decisions of the QL descendants.

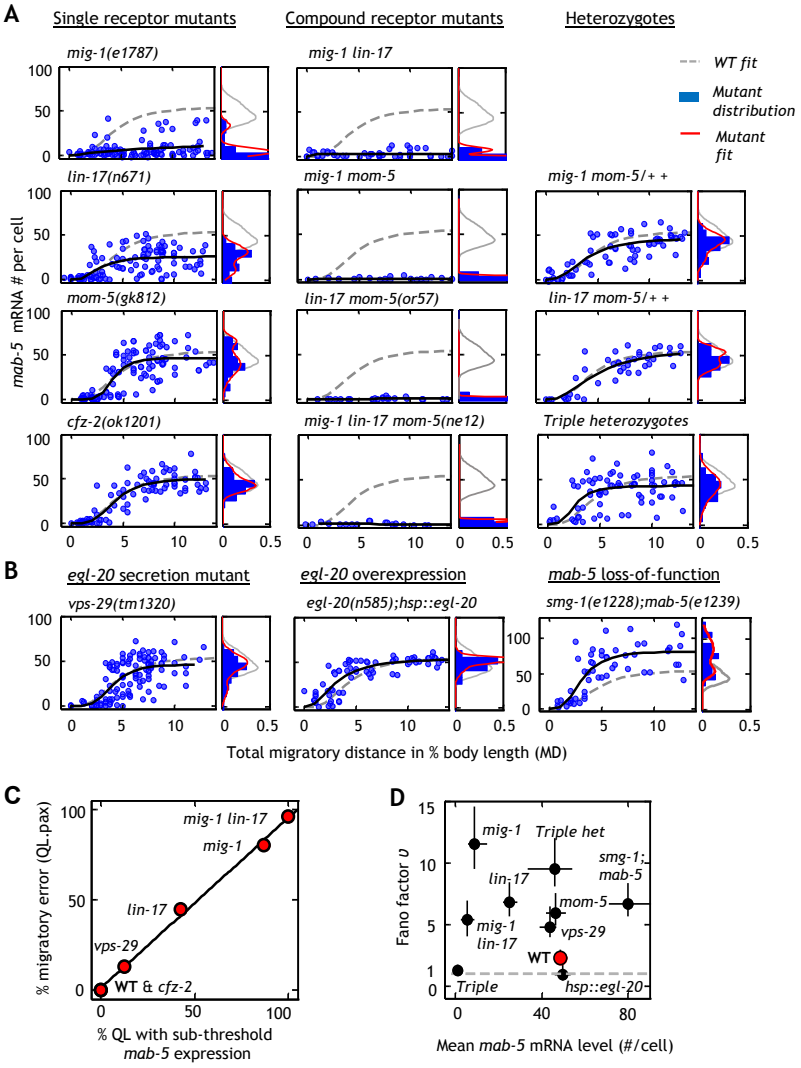

Figure 3. Wnt signaling mutants exhibit different variability in *mab-5* expression. (**A**) Dynamic and steady-state *mab-5* expression in Frizzled single and compound mutants. (**B**) Dynamic and steady-state *mab-5* expression in mutants with altered EGL-20/Wnt gradient or loss of MAB-5 function. (**C**) Correlation between *mab-5* transcript levels and the migratory phenotype of QL descendants in various Wnt pathway mutants. Same mutant alleles as listed in (**A**) and (**B**). (**D**) Fano factor versus the steady-state mean of *mab-5*. Wild type is marked in red. Gray broken line: Fano factor = 1. Error bars are 95% confidence intervals (CI). See also Figure S3.

Perturbing EGL-20 and MAB-5 function increases variability in mab-5 expression
To test whether the increase in *mab-5* variability is unique to the Frizzled mutants, we next perturbed the input to the Wnt pathway, the EGL-20/Wnt gradient. We used the *vps-29(tm1320)* mutant in which destabilization of the retromer complex leads to a shortened and reduced EGL-20 gradient (Coudreuse et al., 2006). In these mutants, *mab-5* expression was reduced to below 25 transcripts per cell in around 10% of QLs (Figure 3B). The variability in *mab-5* expression was again predictive of the phenotypic penetrance: about 13% of the QL descendants were misplaced anteriorly (Figure 3C).

Conversely, we tested the effect of EGL-20 overexpression by expressing an EGL-20 transgene under the control of a heat shock promoter (Whangbo and Kenyon, 1999). The increased EGL-20 concentration (Figure S3B), however, did not significantly increase the average level of *mab-5* expression (Figure 3B, Mann-Whitney test, $p > 0.1$). Rather, *mab-5* expression in late stage QLs appeared less variable (F test $p < 0.05$) than the wild type. Although increased variability is frequently accompanied by reduced expression levels, this was not the case in the *smg-1(e1228); mab-5*(e1239) mutant (see Supplemental Information for motivations to use the smg-1(e1228) background). Instead, an increase in average *mab-5* level coincided with an increase in cell-cell variability (F test $p < 0.001$) (Figure 3B).

A complex relationship exists between mab-5 variability and average expression level
To quantitatively compare the variability in *mab-5* expression, we next calculated the Fano factor of *mab-5* transcript levels for both wild type and mutants.

In most strains, Fano factors were initially high and decreased to stable values over the course of migration (Figure S3D). Plotting the steady-state Fano factor against the average transcript level revealed several interesting features (Figure 3D). First, Fano factor varied greatly across strains (range: 0.95–11.5). Thus, constitutive transcription with Poisson dynamics is insufficient to explain our observations. Alternatively, a model of bursty transcription would predict Fano factor to increase (if burst size is modulated) or decrease (if burst frequency is modulated) monotonically with the mean (Raser and O'Shea, 2004). However, the observed relation could not be summarized in a simple monotonic function (Figure 3D). Furthermore, whereas mutant QLs with reduced *mab-5* expression exhibited variable numbers of TCs (between 0 and 2) per nucleus, suggestive of bursty transcription (Figure S3E), the *smg-1;mab-5* mutant, which consistently exhibited two TCs per nucleus and high *mab-5* synthesis rate (Figures S3F and S3G), nonetheless showed increased variability in *mab-5* levels. As common models could not fully explain the complex relationship between *mab-5* variability and average expression level, other mechanisms, likely upstream of *mab-5* transcription, may play a role to influence *mab-5* expression variability.

All three Frizzleds are transcriptional targets of the Wnt pathway
As *mab-5* expression consisted of distinct high and low subpopulations in a number of mutants (e.g., the *mig-1* single mutant and the triple heterozygotes), a feature attainable in systems with positive feedback (Becskei et al., 2001), we wondered whether feedback regulation exists within the Wnt pathway in QL. Although Wnt signaling is conventionally viewed as a feedforward cascade, evidence from nonnematode species suggests that feedback regulation exists and may play a role in Wnt pathway regulation (Cadigan et al., 1998; Sato et al., 1999; Willert et al., 2002).

To test whether Frizzled receptors are transcriptional targets of the Wnt pathway, we

blocked Wnt signaling both globally and Q cell specifically. In both cases, we observed a more than 2-fold difference in the transcript levels of all three Frizzled genes (Figure 4A). In addition, the temporal dynamics of *mig-1* and *lin-17* transcription were lost in the mutants. Together, these observations indicate a role of feedback regulation in determining the levels and temporal dynamics of Frizzled expression (Figure 2A).

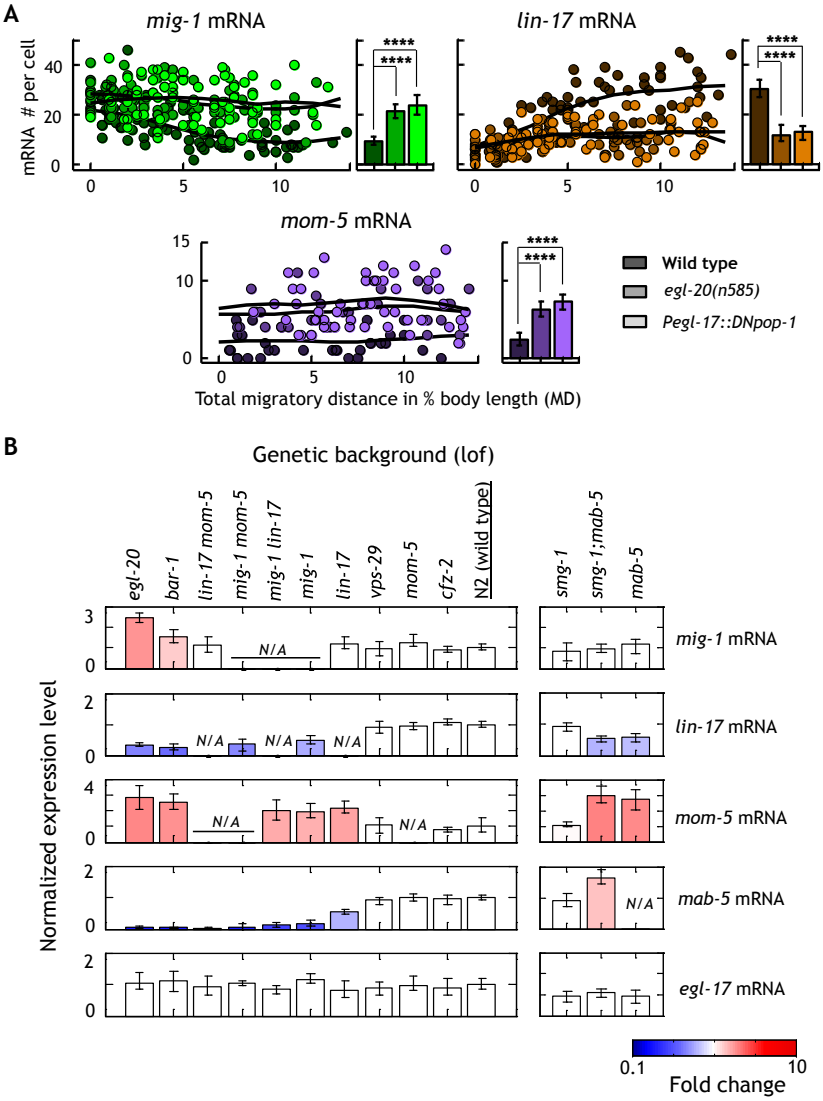

Figure 4. Frizzled paralogs, *mig-1*, *lin-17*, and *mom-5*, are transcriptional targets of the Wnt pathway. (**A**) Dynamic and steady-state (MD > 8) Frizzled transcript levels in mutants with global or QL-specific blockade of EGL-20-dependent Wnt signaling. Same wild type data as in Figure 2A. ****p < 0.0001. (**B**) Normalized expression levels of Frizzleds and *mab-5* in various genetic backgrounds. Only values significantly different from the wild type (FDR corrected p < 0.05) were colored. Genotypes are indicated atop the bar graph with same mutant alleles as indicated previously. Error bars are 95% CI of the mean.

By ranking various Wnt signaling mutants by their average *mab-5* levels, we established a mutant series in which Wnt signaling level in QL varied in a graded manner (Figure 4B, left). In the majority of the strains, low levels of *mab-5* expression were consistently accompanied by low levels of *lin-17* and high levels of *mig-1* and *mom-5* and vice versa. These observations are again consistent with the notion of Frizzled receptors as transcriptional targets of Wnt signaling.

An exception to the above trend was found in the *smg-1; mab-5* mutants in which an increase in *mab-5* levels was observed with a concurrent decrease in *lin-17* and an increase in *mom-5* (Figure 4B, right). This exception suggests that functional MAB-5 is required for the feedback regulation of *lin-17* and *mom-5*. Meanwhile, the fact that *mig-1* expression remains unaltered in *mab-5* mutants suggests that the transcriptional feedback on *mig-1* is likely *mab-5* independent. Thus, both *mab-5*-dependent feedback and *mab-5*-independent feedback appear to exist in the Wnt signaling pathway in QL.

Interlocked positive and negative feedback loops exist within the Wnt pathway

We next sought to incorporate the feedback interactions into a network model of the Wnt pathway. With feedback, perturbation to a single gene can propagate to affect many genes in the network, making it difficult to deduce the immediate targets of the perturbed gene. We tackled this general challenge in network inference by employing Modular Response Analysis (MRA, Bruggeman et al., 2002; Kholodenko et al., 2002) (Figure 5A). This algorithm is robust to unknown network components and reports only interactions between ''closest neighbors'' to avoid redundant reference to the same network structure.

Applying MRA to the average transcription profiles, we obtained a complex network of interlocked feedback loops (Figures 5B, 5C, and S4A–S4C). At the receptor level, positive feedback targeting *lin-17* and negative feedback targeting *mig-1* and *mom-5* are coupled by their shared dependence on Wnt signaling. Downstream of the Wnt pathway, *mab-5* not only mediates feedback to the Frizzleds but also negatively regulates its own transcription.

As Hox genes are master regulators with many transcriptional targets, we wondered whether *mab-5*, an *Antennapedia*-like Hox gene, regulates the expression of the Frizzled receptors and of itself by directly binding to the *cis*-regulatory regions of the respective genes. Previous chromatin immunoprecipitation sequencing (ChIP-seq) analysis (Niu et al., 2011) on L3 stage larvae has identified MAB-5 binding regions in the promoters and sometimes intronic regions of the above genes. To assess whether the same regions are also bound by MAB-5 during the time of Q neuroblast migration, we performed ChIP-qPCR on synchronized L1 animals, pulling down the GFP tag on the MAB-5::GFP fusion protein. Among the sequences tested, enrichment of MAB-5::GFP binding was specifically observed in the third intron of *mab-5* (Figure 5D). To confirm this, we built transgenic strains expressing *mCherry* under the control of both *mab-5* promoter and intronic sequences (Figure 5E, Supplemental Information). Interestingly, elimination of the MAB-5 binding regions specifically in the third intron induced a strong increase in mCherry expression both within (Figures 5E and S5E) and outside (Figure S4E) QL. Thus, the results from both approaches support a direct role of *mab-5* in repressing its own transcription. We additionally built reporter strains to test putative MAB-5 binding motifs in the regulatory regions of *lin-17* and *mom-5* (Figure S4F). However, no significant difference in transgene expression was found upon mutation of the selected motifs.

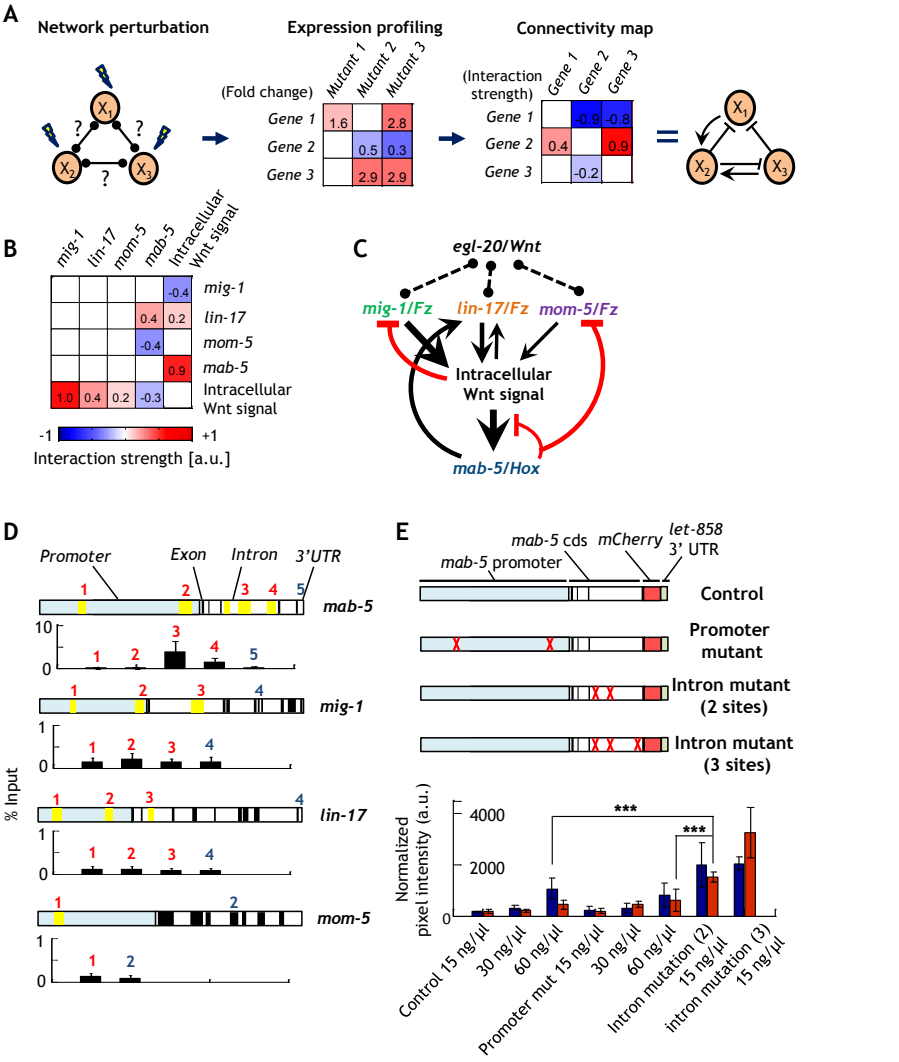

Figure 5. Inferring the regulatory network within the Wnt pathway using the MRA algorithm. (**A**) Schematic of the work flow for implementing the MRA algorithm. (**B**) Inferred connectivity matrix. Network components listed on top of the matrix represent putative regulators, and those listed on the right represent putative regulatory targets. Only significant (p value with Bonferroni correction < 0.05) interactions are colored based on the inferred interaction strengths. (**C**) Revised Wnt pathway model based on the inference results. (**D**) ChIP-qPCR reveals MAB-5::GFP binding to the intronic regions of the *mab-5* gene. Light blue: the promoter regions, where exons and introns are marked in black and white, respectively. Yellow: sequences enriched for MAB binding in the L3 stage (Niu et al., 2011). Numbers in red: locations of qPCR primers that target putative MAB-5 binding sites. Numbers in blue: locations of primers that target putative negative control regions (i.e., exonic or 30 untranslated regions). n = 3 for all putative MAB-5 binding sites, and n = 2 for all negative control regions. (**E**) Upper: schematic of the control and mutated reporter constructs carrying regulatory and coding sequences from the *mab-5* gene. Red crosses: sites of deletion. Lower: quantification of mCherry smFISH signal in QL neuroblasts in strains carrying reporters of *mab-5* regulatory sequence. Normalized pixel intensity is quantified as the sum of the top 20% pixel values in QL normalized by the average pixel intensity of single smFISH spots in the same image. Error bars are SDs of the mean. For each condition, two independent extrachromosomal lines (red and blue) were examined. n > 15 for each strain. See also Figure S4.

Positive and negative feedback cooperate to minimize variability

To probe whether and how network topology influences the variability in *mab-5* expression, we constructed an ordinary differential equation (ODE) model of the inferred network (Table S1 and Supplemental Information). We first obtained model parameters by fitting the full 5-component model to average gene expression profiles (Figure S5A, Table S2, and Supplemental Information). The full model was then reduced to a one-dimensional (1D) model by exploiting timescale differences (Figures 6A and S5B and Supplemental Information).

We then extended the deterministic model to a stochastic one and derived the expected Fano factor and mean level of the network output. To explore the general impact of network topology on the variability in its output, we modified the wild type network to explore four different classes of topologies: those with no feedback, with negative feedback only (NFB

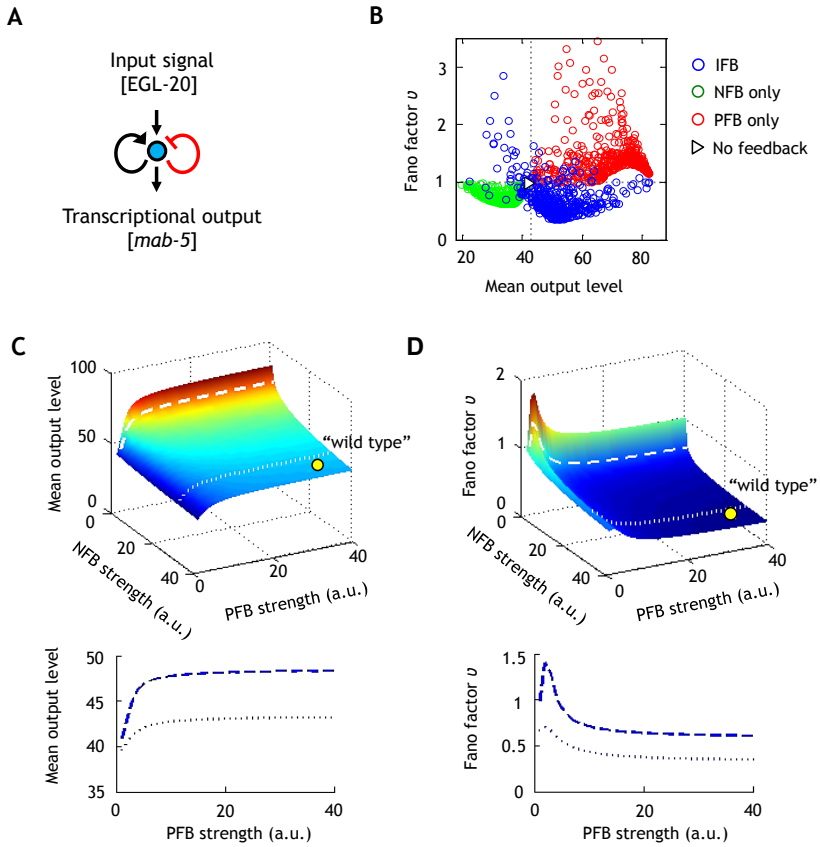

Figure 6. Modeling reveals synergistic contribution of positive and negative feedback in reducing output variability. (**A**) Schematic of the reduced 1D model. (**B**) Analytically derived Fano factor versus mean output values for networks with IFB, NFB only, PFB only, and no feedback. (**C**) Upper: mean output value of the interlocked feedback network as a function of feedback strengths. Lower: replotting of the broken and dotted lines in the upper panel. Note difference in mean expression level at high PFB strength. (**D**) Upper: Fano factor value of the interlocked feedback network as a function of feedback strengths. Lower: Replotting of the broken and dotted lines in the upper panel. Note the difference in Fano factor value at high PFB strength. See also Figure S5 and Tables S1 and S2.

only), with positive feedback only (PFB only), and with interlocked positive and negative feedback (IFB, Figure 6B). We then randomly varied the strengths (i.e., the half-activation threshold) and the amount of cooperativity of each feedback interaction between 0 to 10 times their wild type values while keeping other parameters fixed.

As illustrated in Figure 6B, different classes of networks occupied distinct domains of the Fano factor versus mean output space. Low output variability and low mean output levels were generally found in NFB-only networks, whereas the opposite was true for PFB-only networks. This variability versus mean trade-off was alleviated in networks with IFB. Many of the randomly sampled IFB networks occupied the lower right quadrant (i.e., low variability and high mean), a region hardly accessed by the other types of networks (see also Figure S5C).

We focused next on the IFB network and examined how output mean and variability depend on feedback strength. We found that output mean consistently decreased with strong negative feedback and increased with strong positive feedback. The effect of negative feedback was essentially compensated by positive feedback, resulting in intermediate mean values when both are strong (Figure 6C).

Meanwhile, output variability consistently decreased with strong negative feedback (Figure 6D; see also Figure S5E), which is consistent with results from synthetic circuits (Becskei and Serrano, 2000; Austin et al., 2006). With a fixed level of negative feedback, the extent to which variability was dampened, however, depends strongly on the strength of the positive feedback. While the Fano factor decreased to around 0.6 at low positive feedback strength, it rapidly dropped to less than 0.5 at high positive feedback strength (Figure 6D, dotted line). As a result, the lowest Fano factor values were found when both positive and negative feedback were strong. Thus, positive feedback indirectly promotes low variability by increasing the mean expression level (Figure S5D).

We additionally explored the dependence of output variability on the timescales at which the two types of feedback operate. Consistent with previous theoretical (Hornung and Barkai, 2008) and experimental studies (Austin et al., 2006), we found that Fano factor generally increased with fast positive feedback and with slow negative feedback (Figure S5F).

Model predicts mab-5 variability in the mutants

Because our network model was inferred and parameterized using average expression levels, we wondered whether it could predict the observed variability in *mab-5* expression. The observed variability likely originates from both intrinsic and extrinsic sources. To account for the latter, we included a parameter (D) to describe the effect of extrinsic fluctuations and determined its magnitude by fitting to the wild type *mab-5* distribution (Supplemental Information). Remarkably, the revised model not only captured the distribution of *mab-5* levels in the wild type but also predicted the changes in *mab-5* variability in various Wnt pathway mutants (Figures 7A, 7B, and S6A). Thus, alterations in network topology likely underlie the changes in *mab-5* variability across the mutants. Conversely, the wild type network may contribute strongly to the observed low variability in *mab-5* expression.

Together, our results support a model in which variability in gene expression is controlled through a network of interlocked positive and negative feedback within the Wnt signaling pathway. The signal-amplifying effect of the positive feedback appears to be co-opted to ensure a strong negative feedback, one that is needed to effectively dampen fluctuations in gene expression (Figure 7C). Increasing evidence of feedback regulation challenges the

conventional notion of signaling pathways as linear, unidirectional cascades. It is likely the rule rather than the exception that feedback regulation is widely exploited in development and homeostasis to ensure robust control of gene expression.

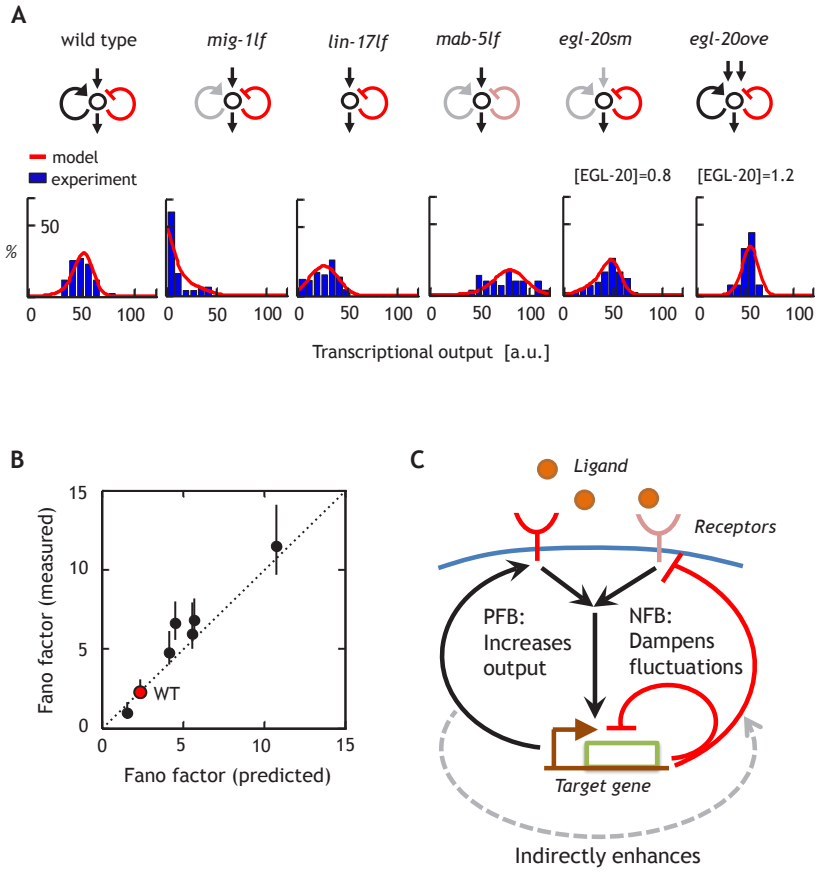

Figure 7. Model predicts variability in various strains. (**A**) Model prediction of the distribution of *mab-5* transcript levels in wild type and various Wnt signaling mutants. Network diagrams indicate the speculated changes in network topology. Gray arrows indicate weakened interactions, and double arrows symbolize an increase in EGL-20 concentration. *egl-20sm*: *egl-20* secretion mutant; *egl-20ove*: *egl-20* overexpression mutant. (**B**) Theoretically predicted versus the experimentally measured Fano factor values for the strains shown in (**A**). Error bars are 95% CI of the mean. (**C**) Conceptual model of the interplay between the positive and the negative feedback in reducing variability. See also Figure S6.

Discussion

Regulatory network as an endogenous mechanism to control variability

Theoretical and synthetic studies over the past decade have provided "proof-of-principle" evidence that a regulatory network can be exploited to limit, tolerate, or amplify gene expression variability. Two common regulatory modules, positive feedback and negative feedback, have each been examined in detail. The joint action of the two, however, appears more complex (Acar et al., 2005; Brandman et al., 2005). Interlocked positive and negative feedback has been found to play a critical role in oscillatory systems (Ferrell et al., 2011).

Our findings suggest that the same motif can be adapted to ensure stable gene expression at high levels. The versatility of the interlocked feedback motif exemplifies the rich potential of regulatory networks in implementing robust gene expression control.

Extrinsic versus intrinsic mechanisms in controlling gene expression variability

As regulatory networks often act upstream of the transcriptional machinery, they serve as ''extrinsic'' mechanisms in modulating transcriptional variability. In contrast, mechanisms that directly affect the assembly and release of the transcription machinery, such as promoter architecture (Boeger et al., 2008), chromatin organization (Weinberger et al., 2012), and the pausing of RNA polymerase II (Levine, 2011; Lagha et al., 2012), would serve as ''intrinsic'' mechanisms. Although both types of mechanisms have been extensively studied, how the two interact to influence gene expression variability is only beginning to be explored.

The results of this study implicate that extrinsic mechanisms may act through intrinsic mechanisms to modulate gene expression variability. Among the Wnt mutants we examined, a partial reduction in *mab-5* expression was often accompanied by a reduced and heterogeneous presence of transcription centers (Figure S3E). Thus, *mab-5* transcription may be inherently bursty, where the burst frequency and the burst size may be subject to modulation by extrinsic factors such as the Wnt signal. By promoting a strong Wnt signal, the regulatory network may efficiently reduce the burstiness and thereby dampen the variability in *mab-5* transcription. Mechanistically, a strong Wnt signal may allow BAR-1/ß-catenin to reliably bind to POP-1/TCF, thus promoting robust release of polymerase II from the *mab-5* promoter region.

Cell-to-cell variability carries signatures of network topology

An emerging view in the study of stochastic gene expression argues that variability, or noise, can inform about the underlying mechanism of regulation (Ca_gatay et al., 2009; Chalancon et al., 2012; Munsky et al., 2012). In this study, we used average gene expression to infer network topology and found a surprising link between network topology and the variability in gene expression. In retrospect, signatures of network topology may already be found in the variability in *mab-5* expression.

For example, low variability in the wild type and the inability to increase *mab-5* level via EGL-20/Wnt overexpression suggest the existence of a negative feedback loop (Figures 3B and 3D). An experiment that eliminates the putative negative feedback was thus carried out to test this possibility (Figure 3B). Similarly, the distinct subpopulations of *mab-5* ON and OFF cells in strains such as the *mig-1* single mutant implicate the existence of positive feedback. Furthermore, we observed at the single-cell level a strong positive correlation between *lin-17* and *mab-5* levels in both the wild type and multiple mutants in which both genes are intact (data not shown). This strong single-cell correlation may be attributed to a common upstream regulator (Dunlop et al., 2008) or a feedback loop. Both mechanisms turned out to exist in the inferred network (Figure 5C). Thus, cell-to-cell variability in gene expression may carry distinct signatures of the underlying network and serve as a useful guide to network identification.

Experimental procedures

C. elegans strains and culture
C. elegans strains were grown at 20°C using standard culture conditions. A full list of mutant alleles and transgenes are described in the Supplemental Information.

Scoring QL descendant migration
The precise positions of the Q descendants QL.pap/QL.paa were scored by DIC microscopy in late L1 stage larvae as described (Coudreuse et al., 2006).

Single-molecule Fluorescence In Situ Hybridization
SmFISH was performed as described (Raj et al., 2008). Manual segmentation of GFP-marked QL periphery was performed, followed by automated spot counting in MATLAB-based custom-written software. Total MD was assayed by manually marking the nuclear position of QL and QR, tracing the A-P axis of the worm, and automatically computing the distance between QL and QR along the A-P axis. All smFISH probe sequences are listed in Table S3.

Heat shock activation of *hsp::egl-20*
Heat shock experiments were performed on *egl-20(n585)* animals carrying *muIs53* [*hsp::egl-20; unc-22(dn)*] as described (Whangbo and Kenyon, 1999). Briefly, heat shock treatment was given to 0–0.5 hr synchronized L1 larvae in a total volume of 50 µl at 33°C for a desired length of time. Heat shock was terminated by chilling tubes on ice for 10 s, and worms were then grown on fresh plates at 20°C for an additional 2–2.5 hr.

ChIP-qPCR
Synchronized animals aged 3–5 hr posthatching were fixed in fresh 1%PFA for 30 min (Mukhopadhyay et al., 2008). Fixed samples were incubated with 400 µg/ml pronase in 0.1% SDS at 37°C for 15 min, followed by sonication and subsequent immunoprecipitation using the EpiTectChIP One-Day Kit (SABiosciences). Upon DNA elution, qPCR was performed immediately using the Phusion Master Mix (NEB). All ChIP-qPCR signals were normalized to total input DNA. qPCR primer sequences are listed in Table S4.

Cloning
mab-5 and Frizzled regulatory sequences were PCR amplified from N2 genomic DNA. To mutate putative MAB-5 binding motifs (11 bps) by base pair substitution, we used site-directed mutagenesis followed by gateway cloning to obtain transcriptional *mCherry* fusion constructs. To delete stretches of MAB-5 binding regions (<700 bp), we used yeast-mediated homologous recombination to clone genomic sequences and the *mCherry* coding sequence into the pNP30 vector (kind gift of N. Paquin). *Pegl-17::DN-pop-1* was made by cloning *DN-pop-1* from the *Phs::DN-pop-1* construct (Korswagen et al., 2000). Where feasible, transgenes were integrated into the genome as single copies using Mos1-mediated transgenesis as previously described (Frøkjaer-Jensen et al., 2008). See also the Extended Experimental Procedures.

Network inference
Gene expression data from a defined window of QL migration (MD > 8) were used for network inference. All transcript counts were normalized to the wild type mean, and the MRA algorithm (Kholodenko et al., 2002) was iteratively applied to bootstrap samples of the normalized data. The resulting distributions of interaction strengths were used to determine the significance of each putative interaction. See also the Extended Experimental Procedures.

Modeling
An ODE model was constructed based on the inferred network. Genetic interactions were described in Hill function form. Model parameters were obtained through nonlinear least square fitting to the gene expression data. The deterministic ODE model was extended to a Langevin-type stochastic model, from which Fano factors were analytically derived and numerically evaluated. See also the Extended Experimental Procedures for more details.

Statistical Analysis
The Mann-Whitney test was used to compare mean expression levels, and the F test was used to test equal variance between the wild type and mutants. Nonparametric bootstrap was used to derive confidence intervals on average transcript counts and Fano factors values. The Benjamini-Hochberg procedure was used to achieve a false discovery rate (FDR) of less than 0.04 for comparison of transcript abundance; the Bonferroni correction with n = 20 was applied to the bootstrap p values of the inferred network interactions. Corrected p value of less than 0.05 was considered significant.

Acknowledgments

This project was supported by the NIH/NCI Physical Sciences Oncology Center at MIT (U54CA143874), a NIH Pioneer award (DP1CA174420), an ERC Advanced grant (2011-294325_GeneNoiseControl) (A.v.O.), and a grant from the Dutch Cancer Society (HUBR 2008-4114) (H.C.K.). We thank N. Paquin for MosSCI cloning vector, N. Bhatla and Y. Zheng for help with strain construction, D. Grun for identifying enriched MAB-5 binding motifs, K. Cadigan for information on putative TCF binding sites, J. Goncalves and Y. Yuan for discussion on network inference, C. Kenyon, K. Shen, H. Sawa, H.R. Horvitz, and the Caenorhabditis Genetics Center (University of Minnesota, Minneapolis) for strains and transgenes, and we also thank H.R. Horvitz, J. Slotine, E. Nedivi, E. Sontag, D. Del Vecchio, G. Neuert, S. Itzkovitz, M. Bienko, and T. Okubo for critical discussion on the project.

References

Acar, M., Becskei, A., and van Oudenaarden, A. (2005). Enhancement of cellular memory by reducing stochastic transitions. Nature *435*, 228–232.

Acar, M., Mettetal, J.T., and van Oudenaarden, A. (2008). Stochastic switching as a survival strategy in fluctuating environments. Nat. Genet. *40*, 471–475.

Aranda-Anzaldo, A., and Dent, M. a. R. (2003). Developmental noise, ageing and cancer. Mech. Ageing Dev. *124*, 711–720.

Austin, D.W., Allen, M.S., McCollum, J.M., Dar, R.D., Wilgus, J.R., Sayler, G.S., Samatova, N.F., Cox, C.D., and Simpson, M.L. (2006). Gene network shaping of inherent noise spectra. Nature *439*, 608–611.

Balázsi, G., van Oudenaarden, A., and Collins, J.J. (2011). Cellular decision making and biological noise: from microbes to mammals. Cell *144*, 910–925.

Beaumont, H., Gallie, J., Kost, C., Ferguson, G., and Rainey, P. (2009). Experimental evolution of bet hedging. Nature *462*, 90–93.

Becskei, a, and Serrano, L. (2000). Engineering stability in gene networks by autoregulation. Nature *405*, 590–593.

Becskei, a, Séraphin, B., and Serrano, L. (2001). Positive feedback in eukaryotic gene networks: cell differentiation by graded to binary response conversion. EMBO J. *20*, 2528–2535.

Boeger, H., Griesenbeck, J., and Kornberg, R.D. (2008). Nucleosome retention and the stochastic nature of promoter chromatin remodeling for transcription. Cell *133*, 716–726.

Boettiger, A.N., and Levine, M. (2013). Rapid transcription fosters coordinate snail expression in the Drosophila embryo. Cell Rep. *3*, 8–15.

Brandman, O., Ferrell, J.E., Li, R., and Meyer, T. (2005). Interlinked fast and slow positive feedback loops drive reliable cell decisions. Science *310*, 496–498.

Bruggeman, F.J., Westerhoff, H. V, Hoek, J.B., and Kholodenko, B.N. (2002). Modular Response Analysis of Cellular Regulatory Networks. J. Theor. Biol. *218*, 507–520.

Cadigan, K.M., Fish, M.P., Rulifson, E.J., and Nusse, R. (1998). Wingless repression of Drosophila frizzled 2 expression shapes the Wingless morphogen gradient in the wing. Cell *93*, 767–777.

Cağatay, T., Turcotte, M., Elowitz, M.B., Garcia-Ojalvo, J., and Süel, G.M. (2009). Architecture-dependent noise discriminates functionally analogous differentiation circuits. Cell *139*, 512–522.

Cai, L., Friedman, N., and Xie, X.S. (2006). Stochastic protein expression in individual cells at the single molecule level. Nature *440*, 358–362.

Chalancon, G., Ravarani, C.N.J., Balaji, S., Martinez-Arias, A., Aravind, L., Jothi, R., and Babu, M.M. (2012). Interplay between gene expression noise and regulatory network architecture. Trends Genet. *28*, 221–232.

Chang, H.H., Hemberg, M., Barahona, M., Ingber, D.E., and Huang, S. (2008). Transcriptome-wide noise controls lineage choice in mammalian progenitor cells. Nature *453*, 544–547.

Chung, H., and Levens, D. (2005). Minireview Molecules and c-myc Expression : Keep the Noise Down ! *20*, 157–166.

Coudreuse, D.Y.M., Roël, G., Betist, M.C., Destrée, O., and Korswagen, H.C. (2006). Wnt gradient formation requires retromer function in Wnt-producing cells. Science *312*, 921–924.

Davidson, E.H. (2010). Emerging properties of animal gene regulatory networks. Nature *468*, 911–920.

Dunlop, M.J., Cox, R.S., Levine, J.H., Murray, R.M., and Elowitz, M.B. (2008). Regulatory activity revealed by dynamic correlations in gene expression noise. Nat. Genet. *40*, 1493–1498.

Eldar, A., and Elowitz, M.B. (2010). Functional roles for noise in genetic circuits. Nature *467*, 167–173.

Eldar, A., Chary, V.K., Xenopoulos, P., Fontes, M.E., Losón, O.C., Dworkin, J., Piggot, P.J., and Elowitz, M.B. (2009). Partial penetrance facilitates developmental evolution in bacteria. Nature *460*, 510–514.

Félix, M., and Wagner, a (2008). Robustness and evolution: concepts, insights and challenges from a developmental model system. Heredity (Edinb). *100*, 132–140.

Ferrell, J.E., Tsai, T.Y.-C., and Yang, Q. (2011). Modeling the cell cycle: why do certain circuits oscillate? Cell *144*, 874–885.

Friedman, N., Cai, L., and Xie, X. (2006). Linking Stochastic Dynamics to Population Distribution: An Analytical Framework of Gene Expression. Phys. Rev. Lett. *97*, 1–4.

Frøkjaer-Jensen, C., Davis, M.W., Hopkins, C.E., Newman, B.J., Thummel, J.M., Olesen, S.-P., Grunnet, M., and Jorgensen, E.M. (2008). Single-copy insertion of transgenes in Caenorhabditis elegans. Nat. Genet. *40*, 1375–1383.

Golding, I., Paulsson, J., Zawilski, S.M., and Cox, E.C. (2005). Real-time kinetics of gene activity in individual bacteria. Cell *123*, 1025–1036.

Green, J., Inoue, T., and Sternberg, P.W. (2008). Opposing Wnt pathways orient cell polarity during organogenesis. Cell *134*, 646–656.

Harris, J., Honigberg, L., Robinson, N., and Kenyon, C. (1996). Neuronal cell migration in C. elegans: regulation of Hox gene expression and cell position. Development *122*, 3117–3131.

Henrichsen, C.N., Chaignat, E., and Reymond, A. (2009). Copy number variants, diseases and gene expression. Hum. Mol. Genet. *18*, R1–8.

Hirsch, H. a, Iliopoulos, D., Joshi, A., Zhang, Y., Jaeger, S. a, Bulyk, M., Tsichlis, P.N., Shirley Liu, X., and Struhl, K. (2010). A transcriptional signature and common gene networks link cancer with lipid metabolism and diverse human diseases. Cancer Cell *17*, 348–361.

Hooshangi, S., Thiberge, S., and Weiss, R. (2005). Ultrasensitivity and noise propagation in a synthetic transcriptional cascade. Proc. Natl. Acad. Sci. U. S. A. *102*, 3581–3586.

Hornung, G., and Barkai, N. (2008). Noise propagation and signaling sensitivity in biological networks: a role for positive feedback. PLoS Comput. Biol. *4*, e8.

Kalmar, T., Lim, C., Hayward, P., Muñoz-Descalzo, S., Nichols, J., Garcia-Ojalvo, J., and Martinez Arias, A. (2009). Regulated fluctuations in nanog expression mediate cell fate decisions in embryonic stem cells. PLoS Biol. *7*, e1000149.

Kepler, T.B., and Elston, T.C. (2001). Stochasticity in transcriptional regulation: origins, consequences, and mathematical representations. Biophys. J. *81*, 3116–3136.

Kholodenko, B.N., Kiyatkin, A., Bruggeman, F.J., Sontag, E., Westerhoff, H. V, and Hoek, J.B. (2002). Untangling the wires: a strategy to trace functional interactions in signaling and gene networks. Proc. Natl. Acad. Sci. U. S. A. *99*, 12841–12846.

Korswagen, H.C. (2002). Canonical and non-canonical Wnt signaling pathways in Caenorhabditis elegans: variations on a common signaling theme. Bioessays *24*, 801–810.

Korswagen, H.C., Herman, M. a, and Clevers, H.C. (2000). Distinct beta-catenins mediate adhesion and signalling functions in C. elegans. Nature *406*, 527–532.

Kussell, E., and Leibler, S. (2005). Phenotypic diversity, population growth, and information in fluctuating environments. Science *309*, 2075–2078.

Lagha, M., Bothma, J.P., and Levine, M. (2012). Mechanisms of transcriptional precision in animal development. Trends Genet. *28*, 409–416.

Levine, M. (2011). Paused RNA polymerase II as a developmental checkpoint. Cell *145*, 502–511.

Li, G.-W., and Xie, X.S. (2011). Central dogma at the single-molecule level in living cells. Nature *475*, 308–315.

Milo, R., Shen-Orr, S., Itzkovitz, S., Kashtan, N., Chklovskii, D., and Alon, U. (2002). Network motifs: simple building blocks of complex networks. Science *298*, 824–827.

Mukhopadhyay, A., Deplancke, B., Walhout, A.J.M., and Tissenbaum, H. a (2008). Chromatin immunoprecipitation (ChIP) coupled to detection by quantitative real-time PCR to study transcription factor binding to DNA in Caenorhabditis elegans. Nat. Protoc. *3*, 698–709.

Munsky, B., Neuert, G., and van Oudenaarden, A. (2012). Using gene expression noise to understand gene regulation. Science *336*, 183–187.

Nijhout, H.F. (2002). The nature of robustness in development. Bioessays *24*, 553–563.

Niu, W., Lu, Z.J., Zhong, M., Sarov, M., Murray, J.I., Brdlik, C.M., Janette, J., Chen, C., Alves, P., Preston, E., et al. (2011). Diverse transcription factor binding features revealed by genome-wide ChIP-seq in C. elegans. Genome Res. *21*, 245–254.

Ozbudak, E.M., Thattai, M., Lim, H.N., Shraiman, B.I., and Van Oudenaarden, A. (2004). Multistability in the lactose utilization network of Escherichia coli. Nature *427*, 737–740.

Pedraza, J.M., and van Oudenaarden, A. (2005). Noise propagation in gene networks. Science *307*, 1965–1969.

Raj, A., and van Oudenaarden, A. (2008). Nature, nurture, or chance: stochastic gene expression and its consequences. Cell *135*, 216–226.

Raj, A., Peskin, C.S., Tranchina, D., Vargas, D.Y., and Tyagi, S. (2006). Stochastic mRNA synthesis in mammalian cells. PLoS Biol. *4*, e309.

Raj, A., Bogaard, P. Van Den, Rifkin, S.A., Oudenaarden, A. Van, and Tyagi, S. (2008). Imaging individual mRNA molecules using multiple singly labeled probes. Nat. Methods *5*, 877–879.

Raj, A., Rifkin, S.A., Andersen, E., and Oudenaarden, A. Van (2010). Variability in gene expression underlies incomplete penetrance. Nature *463*, 913–918.

Raser, J.M., and O'Shea, E.K. (2004). Control of stochasticity in eukaryotic gene expression. Science *304*, 1811–1814.

Rosenfeld, N., Young, J.W., Alon, U., Swain, P.S., and Elowitz, M.B. (2005). Gene regulation at the single-cell level. Science *307*, 1962–1965.

Salser, S.J., and Kenyon, C. (1992). Activation of a C. elegans Antennapedia homologue in migrating cells controls their direction of migration. Nature *355*, 255–258.

Sato, A., Kojima, T., Ui-Tei, K., Miyata, Y., and Saigo, K. (1999). Dfrizzled-3, a new Drosophila Wnt receptor, acting as an attenuator of Wingless signaling in wingless hypomorphic mutants. Development *126*, 4421–4430.

Shahrezaei, V., and Swain, P.S. (2008). The stochastic nature of biochemical networks. Curr. Opin. Biotechnol. *19*, 369–374.

Sulston, J.E., and Horvitz, H.R. (1977). Post-embryonic cell lineages of the nematode, Caenorhabditis elegans. Dev. Biol. *56*, 110–156.

Taniguchi, Y., Choi, P.J., Li, G.-W., Chen, H., Babu, M., Hearn, J., Emili, A., and Xie, X.S. (2010). Quantifying E. coli proteome and transcriptome with single-molecule sensitivity in single cells. Science *329*, 533–538.

Thattai, M., and van Oudenaarden, A. (2004). Stochastic gene expression in fluctuating environments. Genetics *167*, 523–530.

To, T.-L., and Maheshri, N. (2010). Noise can induce bimodality in positive transcriptional feedback loops without bistability. Science *327*, 1142–1145.

Weinberger, L., Voichek, Y., Tirosh, I., Hornung, G., Amit, I., and Barkai, N. (2012). Expression Noise and Acetylation Profiles Distinguish HDAC Functions. Mol. Cell *47*, 193–202.

Weinberger, L.S., Burnett, J.C., Toettcher, J.E., Arkin, A.P., and Schaffer, D. V (2005). Stochastic gene expression in a lentiviral positive-feedback loop: HIV-

1 Tat fluctuations drive phenotypic diversity. Cell *122*, 169–182.

Wernet, M.F., Mazzoni, E.O., Celik, A., Duncan, D.M., Duncan, I., and Desplan, C. (2006). Stochastic spineless expression creates the retinal mosaic for colour vision. Nature *440*, 174–180.

Whangbo, J., and Kenyon, C. (1999). A Wnt signaling system that specifies two patterns of cell migration in C. elegans. Mol. Cell *4*, 851–858.

Willert, J., Epping, M., Pollack, J.R., Brown, P.O., and Nusse, R. (2002). A transcriptional response to Wnt protein in human embryonic carcinoma cells. BMC Dev. Biol. *2*, 8.

Wolf, D.M., Vazirani, V., and Arkin, A.P. (2005). Diversity in times of adversity: probabilistic strategies in microbial survival games. J. Theor. Biol. *234*, 227–253.

Xiong, W., and Ferrell Jr, J.E. (2003). A positive-feedback-based bistable " memory module " that governs a cell fate decision. Nature *426*, 460–465.

Zenklusen, D., Larson, D.R., and Singer, R.H. (2008). Single-RNA counting reveals alternative modes of gene expression in yeast. Nat. Struct. Mol. Biol. *15*, 1263–1271.

Zinovyeva, A.Y., Yamamoto, Y., Sawa, H., and Forrester, W.C. (2008). Complex network of Wnt signaling regulates neuronal migrations during Caenorhabditis elegans development. Genetics *179*, 1357–1371.

Supplemental figures

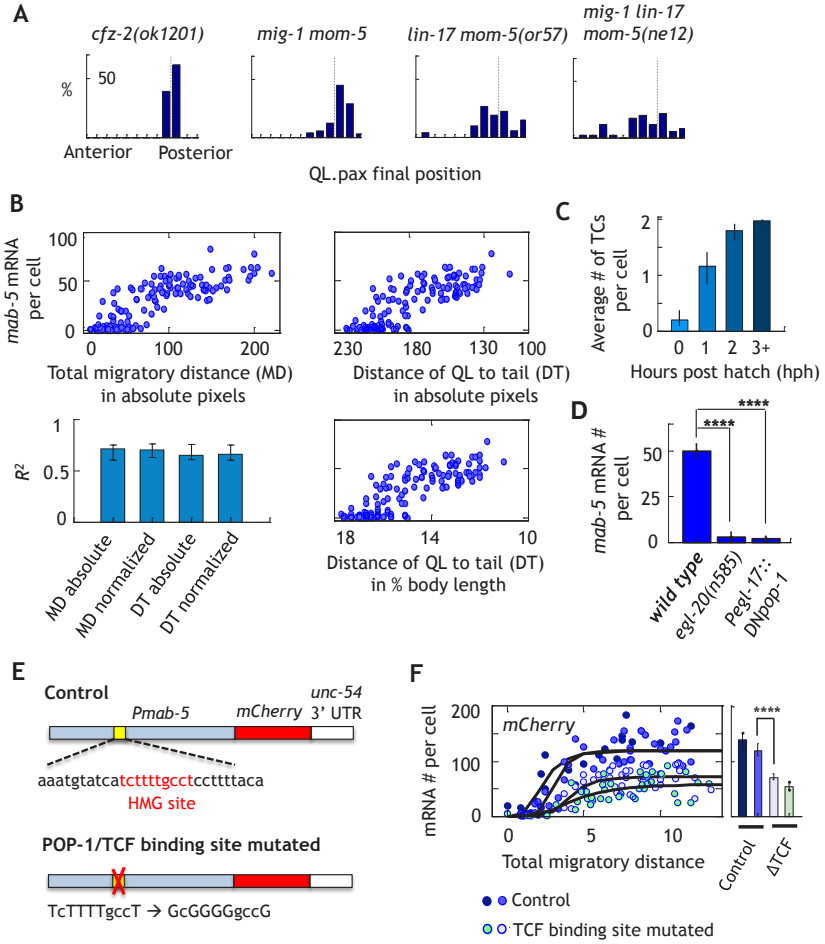

Figure S1 associated with Figure 1. Additional mutant phenotypes, alternative measures of migratory distance, and validation of *mab-5* as a transcriptional readout of Wnt signaling in QL. (**A**) Final position of QL.ds in additional Frizzled mutants. (**B**) Upper left clockwise to lower right: *mab-5* transcript counts plotted against other parameters associated with Q cell migration. Lower left: Squared correlation coefficients between *mab-5* transcript count and various migration-related parameters. (**C**) Mean number of transcription centers (TCs) per cell over time. Error bars are 95% CI of the mean. (**D**) Final (MD>8) *mab-5* transcript counts in wild type compared to mutants with global or QL-specific blockade of EGL-20 dependent Wnt signaling. N>40 for each data set. Error bars are 95% CI of the mean. (**E**) Schematic of the reporter transgenes designed to test the putative TCF binding motif in the *mab-5* promoter region. (**F**) *mCherry* transcription dynamics in single QLs in strains carrying the transgenes described in **E**. (**E**) Results from two independent lines of each genotype are presented. Error bars are 95% CI of the mean.

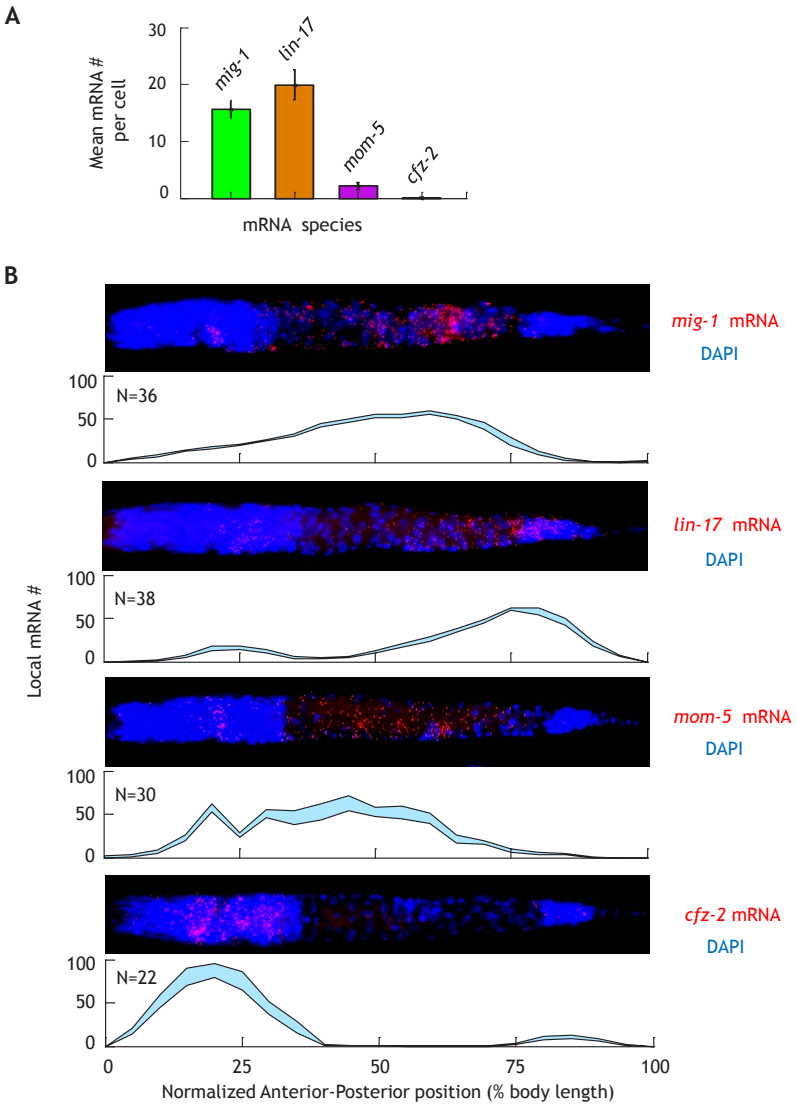

Figure S2 associated with Figure 2. Mean transcript levels of Frizzled genes within QL and across the animal body. (**A**) Average transcript abundance over the course of migration for the four Frizzled paralogs. Error bars are 95% CI of the mean. N>40 for each data set. (**B**) smFISH staining and quantification of transcript abundance along the anterior-posterior axes for the four Frizzled genes. Light blue patches represent 95% CI of the mean.

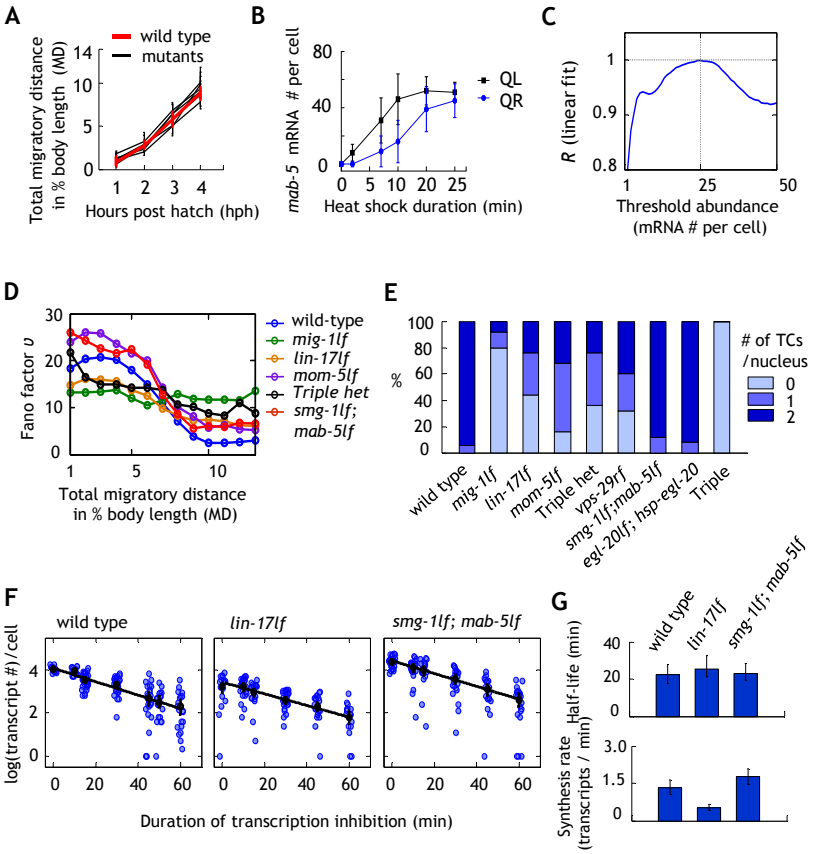

Figure S3 associated with Figure 3. Control experiments for the quantification of *mab-5* variability in wild type and mutant strains. (**A**) Total migratory distance (MD) plotted against worm age (hours post hatching) in wild type (red) and all mutants (black) listed in Figure 3. Error bars mark 2.5-97.5 percentiles. (**B**) *mab-5* transcript levels in the *egl-20 (n585); hs::egl-20* strain in response to various durations of 33˚C heat shock. Note QR in the wild type does not express *mab-5*. Extended heat shock activated *mab-5* expression to wild-type levels in both QL and QR. Error bars are standard deviations of the mean. (**C**) Correlation coefficients for the analysis in Figure 3C calculated for a full range of hypothetical thresholds in transcript abundance. (**D**) Evolution of Fano factor values over the course of QL migration for wild type and various mutant strains. X axis marks the center of the moving window (width=3) within which the Fano factor is calculated. (**E**) Quantification of the number of transcription sites in late-stage QLs in wild type and various Wnt signaling mutants. N>30 for each genetic background. (**F**) *mab-5* transcript counts in QL after ActD application in *lin-17lf* and *smg-1lf;mab-5gf* strains. Errorbars are 95% CI of the mean. (**G**) Top: *mab-5* mRNA half-life derived from data in F). Bottom: *mab-5* mRNA synthesis rates calculated from data in **F** and steady state average *mab-5* transcript levels in the respective strains. Errorbars are 95% CI of the mean.

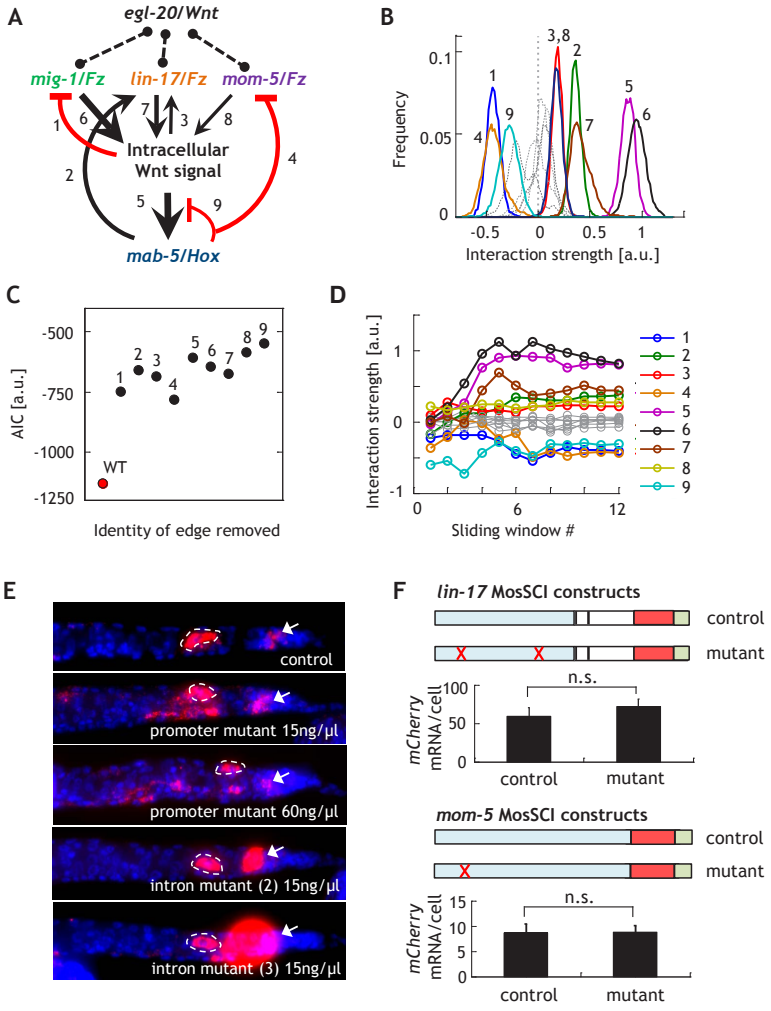

Figure S4 associated with Figure 5. Computational analysis on the dependence of inference results on data variability, averaging window and model complexity; mutation of putative MAB-5 binding sites alter the expression of *mab-5*, but not *lin-17* or *mom-5* transcriptional reporters. (**A**) The inferred network interactions are labeled 1-9 to correspond to the references in (**B-D**). (**B**) Bootstrap distributions of inferred connectivity strengths. (**C**) Akaike Information Criterion (AIC) values for the inferred network (red) and alternative topologies (black). Numbers on the data points indicate the network interactions that were forced to be zero. (**D**) Network interaction strengths inferred using data from different ranges of MD values (sliding window # 1-12, see Supplemental Methods). Colors correspond to individual network interactions as listed to the right. (**E**) Representative images of *mCherry* transcript distribution in control and mutant reporter strains. Broken white lines demarcate the boundary of QL. White arrows point to *mCherry* expression in the tail. Note the expanded and elevated *mCherry* expression in the tail region of the intronic mutants. Intron mutant (2): mutant where 2 putative MAB-5 binding sites in the 3rd intron of *mab-5* have been deleted. Intron mutant (3): mutant where 3 putative binding sites in the 3rd intron have been deleted. (**F**) Genetic manipulation of putative MAB-5 binding motifs in *lin-17* and *mom-5 cis*-regulatory regions. Top: Schematic of the *lin-17* reporter transgenes and *mCherry* transcript levels in QL in strains carrying MosSCI integrated versions of the respective transgenes. Red crosses indicate locations where putative MAB-5 binding motifs have been mutated. Bottom: Schematic of the *mom-5* reporter transgenes and *mCherry* transcript levels in QL in strains carrying MosSCI integrated versions of the respective transgenes. N>20 for each strain. Errorbars are 95% CI.

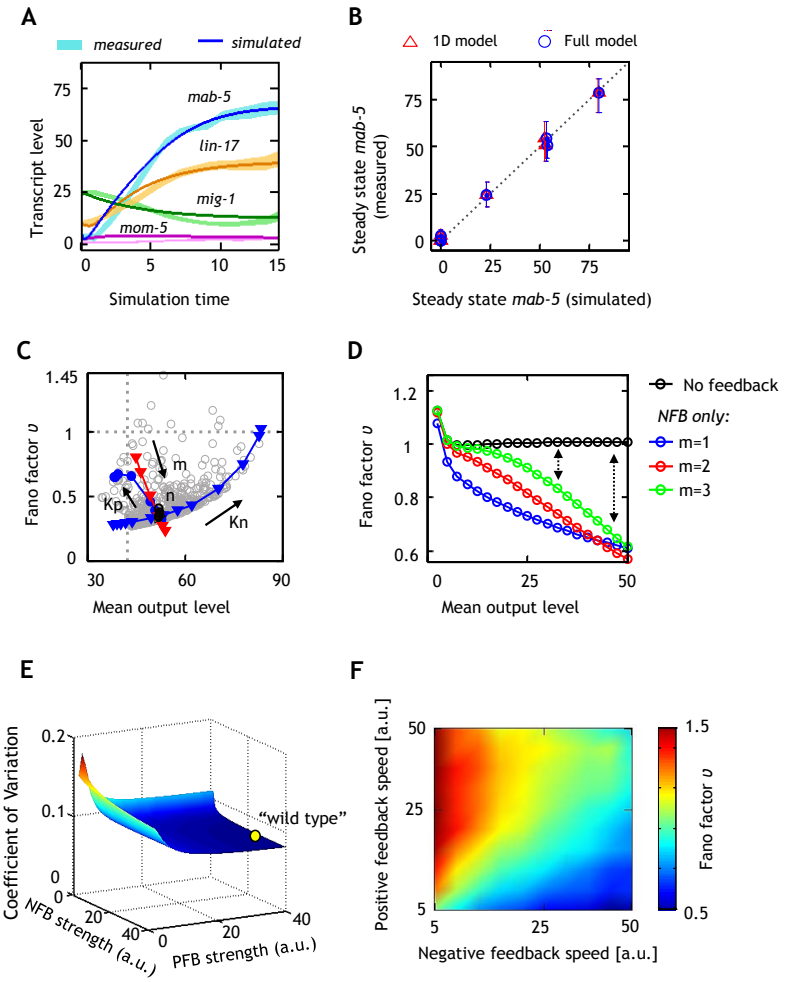

Figure S5 associated with Figure 6. Parameterization, dimension reduction, sensitivity analysis of the network model. (**A**) Simulation of gene expression dynamics with the fitted 5-component model (full model). Colored patches represent experimentally measured gene expression levels whose boundaries indicate 95% CI of the mean. (**B**) Simulation with the 1D model (red triangles) and the full model (blue circles) produced identical steady state *mab-5* expression values. Error bars are 95% CI of the mean. (**C**) Dependence of the Fano factor value on the feedback activation thresholds and Hill coefficient values. Kp: activation threshold of the positive feedback (blue circles), Kn: activation threshold of the negative feedback (blue triangles), n: Hill coefficient of the positive feedback (black circles, clustered around the intersection), m: Hill coefficient of the negative feedback (red triangles). (**D**) Dependence of the Fano factor value on average gene expression level in a network with negative feedback. In comparison to a network with no feedback (black), negative feedback always reduces the Fano factor value, and does so more dramatically when the average gene expression level is high. (**E**) Dependence of the coefficient of variation (standard deviation/mean) on the feedback strength. Same analysis as in Figure 6C&D. (**F**) Systematic variation of feedback speed (i.e. timescale) reveals a requirement for fast negative feedback and slow positive feedback to minimize output variability.

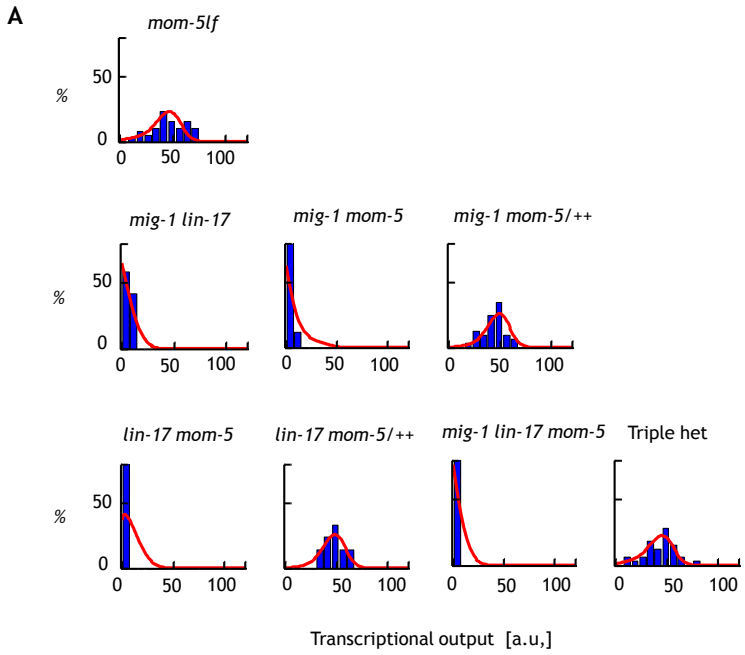

Figure S6 associated with Figure 7. Measured and predicted distributions of *mab-5* transcript levels in additional Wnt signaling mutants. (**A**) Comparison of the theoretical (red curves) and measured (blue histograms) steady state *mab-5* distribution in mutants not listed in Figure 7A. Note for the heterozygote mutants, functional *mig-1* and *mom-5* transcripts were assumed to be 70% of their wild-type levels, and functional lin-17 transcript was modeled to be at 80% of its wild-type level. The exact amounts of these transcripts could not be measured due to the presence of residual transcripts from the mutant allele.

Supplemental tables

Table S1 associated with Figure 6. Summary of modeling procedures.

	Motivation	Approach	Notes
Step 1	Infer network topology.	Modular Response Analysis (MRA).	Perform nonparametric bootstrap to obtain confidence intervals; use AIC to account for model complexity.
Step 2	Construct realistic (nonlinear) network model.	Incorporate Michaelis-Menten kinetics and cooperativity in the model .	Obtain model parameters by fitting to average gene expression profiles.
Step 3	Model reduction.	Time scale separation.	
Step 4	Extend to stochastic model.	Rewrite model in master equation form and apply second-order approximation.	To probe the dependence of variability on network parameters, we varied feedback strength by changing the half maximum value (K_m) of the corresponding Hill function.
Step 5	Test predictive power of stochastic model.	Fit stochastic model to wild type *mab-5* distribution; then modify network topology to predict distributions in mutants.	An additional parameter describing the magnitude of extrinsic fluctuations was included to allow fitting to the wild type distribution; all other parameters remain the same as obtained from Step 2.

Table S2 associated with Figure 6. Model parameters obtained through fitting to average gene expression profiles. Note that parameters V1 through n4 were fit using steady state gene expression data using the NonLinearModel.fit routine in MATLAB. The degradation rates were fit using time series gene expression data using the lsqnonlin function in MATLAB.

Parameter	Estimated value	Standard Error	p-Value	RMSE
V_1	11.1	0.9	$6.4*10^{-26}$	2.8
K_1	0.2	0.2	0.043	
β_1	9.8	0.4	$2.58*10^{-57}$	
n_1	1.0	-	-	
V_2	34.0	1.4	$1.30*10^{-56}$	1.6
c	7.9	1.9	$6.00*10^{-05}$	
K_2	58.4	12.0	$2.50*10^{-06}$	
n_2	3.0	-	-	
V_3	6.1	0.3	$9.80*10^{-53}$	1.1
K_3	42.8	7.9	$1.80*10^{-07}$	
n_3	1.0	-	-	
V_w	3.6	0.2	$5.62*10^{-21}$	17.7
s_1	0.4	0.1	$8.90*10^{-09}$	
s_2	0.27	0.1	0.015	
s_3	0.0014	0.0003	$2.60*10^{-05}$	
s_4	0.13	0.02	$3.80*10^{-05}$	
K_w	62.1	8.9	$8.80*10^{-17}$	
n_4	6.0	-	-	
γ_1	0.4	-	-	7.5
γ_2	1.1	-	-	
γ_3	10.0	-	-	
γ_w	0.06	-	-	
γ_t	5.7	-	-	

Table S3 associated with Experimental Procedures. smFISH probe sequences used in this study. smFISH probes for *mab-5*, *mCherry* and all four Frizzled are designed against the cDNA sequences only. Probes for *egl-17* were designed against both the cDNA and the 5' UTR and the 3' UTR to obtain a sufficiently large probe set.

***mig-1* (48 probes):**			
gaggtaaccacgaaatggtc	ggccctttcatgcacatttt	aataaccgatgtcgcacaaa	cagacgaaagagcaatggag
atcacaaagagcaacaggag	atcttgaattgctccttgct	gcacgagatttggaactgat	attgacatcctgctcatcag
gttgcacatctcatgatcca	ttctttcgctgcaaactttg	aacatggaacatgggaaagc	atagactgccgcaatgactc
gctcgttaagttatacggca	tactcgatcattaccgtcgt	gtaaatcagtgaggccactg	gcatgtagaatagtccagca
cgtctttccatgattcctcg	ctcatcctgtgggcattttc	ccagagacgtgagcaagttg	gtggcatcgttcacaaatga
aggaagaatttgagctgctc	cacacactttgaggatcgat	cacgacacacagatcaagag	ctgtcaagtgagagaaacgg
tagtttctcgttgcacatcg	caaccttctgtgggttcgag	cgatgtccttgtcgccttat	atcaaacgagaacttggtcg
aaagacacaatggacggcat	gaaacaacaagagtcgggtg	ggttctggagtcgtccaata	aaataagacaaaacgcgcac
ggaagacacttttcctggac	agtattacagagctcagcga	attcccaggatgagcatgat	ctagtcagcttgaacagcaa
gaaaccgaaactttccagca	agacgtgataagccgactat	tgctccgatgaagcagagtc	gccggttgatatccttcttt
atcacaacgaatcacatcgg	cagtttccgtaagtgagtgg	gaagttgaagatccagtcgg	taggtgttcgatcgtacact
gattgttctccaacgggaac	gagatgcacgagaagaacat	gaggaatagaatgagctccc	attagttcgaaacgtcgacg
***lin-17* (48 probes):**			
cattttggagaaggagccag	gccgaaaatcctccagttat	aacattaaccaccaaagggc	aattgtcattcgggtccatt
gaatgatgcccaaagaatgc	atgagctcgagccttttgta	caccgctcaaatacagtgta	tgcacctgactgttgttta
gaaaattgatcctgtggcga	gatccacatcgacaaggtca	catgcttcgataccttctgg	catgtaaatttcagcctgcg
atcggaatgcatttcccttt	gaatgcacaatgcgacttgg	caggcaacaaaatgcacata	gtggcgagactggaaattac
caggtctttgcatagctcaa	aaacatcacattcgactggc	atgagcacaataatcgtggc	ccacatcagacacgagaatc
tttcatcaacggcttgaagt	ggcaaaccaaattgaccatg	cgaattcaaattcccaacgg	agcacattccacagaagatg
gcaaaaacggagcaaatgaa	cgaacgtcaagaaggagaaa	aatcacaaaccagagcaacg	tcgattgggtttttaaccgg
cattccaatcgggcacattg	aaacggaatcgctttcggtc	caatgcaaatagttcgggga	cgagcaatggacgtgttgat
aaacggatttgcagcttgtc	aggtagaagacgcatctctc	gccccttgttctgaaactaa	atttgcatgtataccggtgg
aatatcgagaagcaatccgc	gatcggagcatcgatgaaga	tctccaatttcgatgtgtct	ctgggtctccatgaattctg
ggaattgtgcacaattcagc	aaatgttccgattgacaggt	ataaagcacagaagaagccc	aaaaatctcgctcagacgacatca
gtaggcttcatgcaaagctc	ccgctgtactgaagaagtag	gacagacaagttcgatgacg	tcggttttgtcatggg
***mom-5* (48 probes):**			
gatcagctgataagcatccg	agaaaggacaacttcgttgg	ctccttgcgtaacaagtgtt	ggcaccgattctcaacatta
ttcgagttgttgagaatcca	tgagatccgcttgttgtatg	gaacaacagcaagagcacta	agcattcattgcagttggta
ccagatttttgcacattgga	cactgagaagaggcaatgaa	cgcacaacttgacatgaaga	caggcatatttactgcctga
ccagcttcagattgtgttgt	aatgaacattcaggaaggcg	ctagacacagtacaagccac	tgatgaagccatccttcaag
gattgaattgcgcaattgct	acttgattgtcagcttcaca	acagagcagcaattgattca	cgatcttgaagtcgaacaca
agacaggtgcatagacagta	gtcgaacacgtccatcaaac	cacattgcgtggaagtatgg	ctggatacgtgaaaccgaat
tctcgacatggttgaattgg	gctgtccagattcgaagaat	tccatcgacagaatttgtca	ggatccatcggacaatcatc
ctcgcatccatttttgcag	agtgaataaagagcacacga	ccaactgaacagattccagt	aacaataatctccggagctg
aatccaattgatctggccat	acgcgaatcgtgataaatca	caacgatacaacgatcggag	tgaagagacaacccaaatgg
ggaattcttgccaacacaca	tacaaaatcggtcgaactgg	aaacgagtaaaactgctccg	ccaggtaagccttgtgataa
ttttagagttgctcgactcg	ttgctagataacagaacgcg	cgaatacggatcattgacca	cagtaggtgacctcgaagag
tgttgaaacaccgaatgtga	atacgttccacaagcgaatc	catcggcgtgttgaagttta	aacctgatcaacatgagcag

***cfz-2* (48 probes):**			
gagccaagcaataggaacag	atctgatccgacatctttgg	gcccacgaaatatcgaatca	ctctccagtgaaggatgttg
gacgttttccaaaaagagcc	gcttctttggtgtatctggt	taatcctcatcgagtcgcat	caactgcgtgattttatggg
ggaattgtgatttgctcaca	ttatgatgatgccccttgtg	tccagagttatcatcagccc	gagcaatgagaaaatcccga
ttgtagccaataccttgca	gggccatctggactatagtt	ggaaaacgacgaagcacaag	cgatgattctgctcgtagaa
aactattcgggaacgatgtc	cgatcttggaaattccgact	gccattccgaagaaataggt	ctgcgattgctcccataatg
cggcttcttcctgtttttca	ggaccggctattacttcatt	caggttagcgaaaggatcac	cgatagtttgctttggcgag
tccaccagcggataaaattg	gttacaagtgcactgacact	aatgagaacgaggaaatcgc	tgcacatacagcaagttttg
gagatgttggaaacaaccga	tttggacttttcagatgcca	agttatcggatcaccatcga	ccacgacgatagagttttgg
gtagttttcctggcagatcg	agtaggcgcaatttgttaca	cagtatttcccacgtagcag	aggaacccaaacagcaaata
cacacaaagttccatgcacg	tcggtctcgataaggaatgt	agcacaaagattcgttggaa	tatgtctgccggttggtatt
attattggactgcacttgct	caacatgaagatcggacgtt	agaacaaaactccaacgatg	tgacatgtcagatttagcgt
gccatctgaatccgtacttg	caaccatgagctgacagaat	tccacaaattgcagaatccg	cctccgtaaagatggttgtg
***mab-5* (27 probes):**			
catccaggatacatgctcat	gttcatgtaggtgtgattgt	cgcccatcttcatccatgga	tttacttgtctttcagtcaa
ccagtacgaatcgtcgcctg	cagcaagcatatgtttcata	tttgattctccacctttttgc	acgacgattttggaaccaga
aagaagccgttgtgccggcg	gatgaattatccatccaacc	tgaatatgtctgacgagtgc	ttgcctctttttttgtgtttc
gtgccggatgatgcggattg	tgggttataggcgaatggat	ctaattccaatgtttgactt	ttcattgcttccaccttctc
actagacgatgctgaagcag	aatttgcagatgttgcttga	ttgtgataatgaaattccttt	cttgatttgattcttcatct
tggcagcagcagcagcggca	attgaagttctagtttcacc	ccgacgtttcctagtcaagt	gaatgttgttcattttgctc
agttcgtaggttttcaaatt	tactggttgcgagattgctg	gcaatgtttctgaaatttct	
***mCherry* (36 probes):**			
caacaacagcggaatcagac	gcattgatctggatgacatt	ggccttctttggcttggcag	ctcatgcccattgacagatc
acctttggctcgacagcggc	cttgagagcctgacggagat	ttgaccttcttatctccggt	ctcatatggtcggccttctc
cttggcggccttagcctttg	cttgaacaagggccttgctg	aaccttctttgggctcttgg	cctttagttttgcggtttgt
caactttggttggcttggcg	gtccgttggctccggatccg	ccttcttggcagctggcttg	ccgcctttagttacctgaaa
gcgactggagccttggcctt	gccttctctggcacacggaa	cttcttggctggagacttgg	gtcccaggcgaatggtaatg
ctccttgatcatgttgatgt	ttggctgctgctggcttctt	cttggcgatcttctttggag	ccatacatgaactgtggaga
ggtccttgagctgcttgatg	ctggtttcttggctgctgct	ctggcttggcggccttcttg	atctggtatatctgccggat
atgaacttgaggattgcctg	ctccagtggctttcttggcg	cttcacccttgagaccatg	ctccgggaatgaaagtttca
ctccgagcttgtagttttgg	gctggcttctttgccttctt	gcaccttgaaacgcataaac	gagtcttgcgtcactgtaac
***egl-17* (27 probes):**			
cgggcaccttggaattttat	gttcagggagcctagaaatg	gagaaaacccattatcccga	actgcatgatggacaaatga
ggactttgagcatagctcac	aatgtttgtccggatatccc	ggtttccatgaagaccgtaa	aaactatcatgtgtggcaga
agtttgtcgacaacatcagg	accacattccaatcggttag	cgttgaagcctaaataaagt	ttctggatttcattgtacga
ttgaaatcgtgcgcatgtat	gttgtaaccgaaactttcca	ggattttgaaatctaccacg	ctggaacaatgatatattca
ccgagataatgaacgtttgg	aaaaactttctcgactgtgc	agcttgatccagtcaaaaca	gtacatatacaaacattcgg
gaatagttgccaatgggtct	ccttgctcttttgttaaagc	ggattctgcaacataacgga	tttgacggtttacatattct
taacatgccttggctgcatt	ataaatgtgcatttggcgtc	gagttgagcagacgcttttc	

Table S4 associated with Experimental Procedures. qPCR primers used in ChIP-qPCR.

	Forward primer	Reverse primer
mab-5	gtcccatcctctctccgtgtg	tggcggtaaaaaggcaaaggatgc
	cccagtcttttcatgctcctccc	gcggccgactggtcg
	cgcaagaggggaggtcctag	ttccgtccttttcccgccg
	gctttctcgatcattacgccatcgttg	cctatccc cccctg acg c
	acctcgtttccggtcgcttttcattg	caaagacccgtcgaaagggcg
mig-1	cccgccttgcacacacac	ggcgggggacgatgg
	cgccagccatctcccaac	cacaccagtggcagcacc
	gagcaccacaaaacgcccc	gccaccaccacaccacc
	cgaccgcctcaacggaaaatgc	gggtggcggattcacggtc
lin-17	gacaccaccagcagcagc	cccgggtggagcagagtac
	acctcaacctcctccgtctcc	ggaggaggagggtgggc
	acacggtaagccccccttcacc	accagcgtcagtcggttccc
	gccatcaacacgtccattgctcg	tgggatgaaatgggcgcgg
mom-5	cgt gaatgcaagaaaacgaagcacc	gccatttgccgcaatatccagg
	cctggttcctggcggc	cccagcacattgcgtggaag

Supplemental Methods

***C. elegans* strains**

The Bristol N2 strain was used as wild type. Mutant alleles and transgenes used in the study are: Linkage Group I (LGI*): mig-1(e1787), lin-17(n671), smg-1(e1228), mom-5(gk812), mom-5(or57), mom-5(ne12);* LGII: *huSi15 [Pmab-5::mCherry; unc-119(+)], huSi16 [Pmab-5::mCherry; unc-119(+)], huSi17 [Pmom-5 Δ mab-5::mCherry; unc-119(+)], huSi18 [Plin-17::mCherry; unc-119(+)], huSi19 [Pmom-5::mCherry; unc-119(+)], huSi20 [Pmab-5 Δ TCF::mCherry; unc-119(+)], huSi22 [Pmab-5 Δ TCF::mCherry; unc-119(+)], huSi23 [Plin-17 Δ mab-5::mCherry; unc-119(+)]* LGIII: *mab-5(e1239), vps-29(tm1320); unc-119(ed9);* LGIV: *egl-20(n585);* LGV: *heIs63[Pwrt-2::gfp-ph; Pwrt-2::h2b-gfp; Plin-48::tomato]* (Wildwater et al., 2011), *muIs53[hs::egl-20; unc-22(dn)]* (Whangbo and Kenyon, 1999); LG unknown: *syIs187[POPTOP]* (Green et al., 2008). Extrachromosomal arrays: *huEx278 [Pegl-17::DN-pop-1; Pmyo-2::mTomato]; huEx579 [Pmab-5::mab-5g::mCherry;Pmyo-2::h2b-gfp]; huEx580 [Pmab-5ΔMAB-5::mab-5g::mCherry;Pmyo-2:: h2b-gfp]; huEx581[Pmab-5::mab-5g ΔMAB-5x2::mCherry;Pmyo-2:: h2b-gfp]; huEx583[Pmab-5::mab-5g ΔMAB-5x3::mCherry;Pmyo-2:: h2b-gfp].* Notes on the *smg-1(e1228); mab-5(e1239)* strain: The *smg-1 (e1228)* background was used to allow visualization of *mab-5* transcripts in the *mab-5(e1239)* mutants. Normally, transcripts from nonsense mutant alleles (as in the case of *mab-5(e1239)*) are subject to nonsense-mediated RNA decay (Pulak and Anderson, 1993), which abolishes the majority of the mutant transcripts. We circumvented this problem using the *smg-1(e1228)* mutation which compromises the nonsense mediated decay pathway (Denning et al., 2001; Grimson et al., 2004).

Gateway cloning

First, *mab-5*, *lin-17* and *mom-5* promoter regions were PCR amplified from N2 genomic DNA. Using these PCR products entry clones were made using the pDONRP4-P1R vector. *Pmab-5:* 10 kb of sequence upstream of the *mab-5* ATG was used. To mutate the putative POP-1 binding motif , site directed mutagenesis was performed using a 5'-ctggtagtaaatgtatcaGcGGGGgccGccttttacagccataacacac-3' and 5'-gtgtgttatggctgtaaaaggCggcCCCCgCtgatacatttactaccag-3' primer pair. *Plin-17:* a genomic region spanning 5.5 kb upstream of the *lin-17* ATG to 2269 bp into the *lin-17* gene (including exon 1, exon 2, intron 1 and a large part of intron 2) was used.

To obtain the mutant construct, two putative MAB-5 binding motifs in the upstream regulatory region were mutated by site directed mutagenesis using 5'-gtctccatctctccctctgtcTCGGTATATATcattcgccacgatttatagc-3' / 5'-gctataaatcgtggcgaatgATATATACCGAgacagagggagagatggagac-3' and 5'-ctctatgtcataaatctcttaaattTCGTGATTTGTcctcctcctccgacatcatcg-3' / 5'-cgatgatgtcggaggaggaggACAAATCACGAaatttaagagatttatgacatagag-3' primers pairs. *Pmom-5:* 3.7 kb of sequence upstream of the *mom-5* ATG was used.

To mutate putative MAB-5 binding motifs, site directed mutagenesis was performed using a 5'-gttcttcttcttcttcgttgttTAGCTTTATTTcctattttccctcttctttttc-3' and 5'-gaaaaagaagagggaaaataggAAATAAAGCTAaacaacgaagaagaagaagaac-3' primer pair. The *mCherry* coding sequence and the *unc-54* 3' UTR were cloned into pDONR221 and pDONRP2R-P3 respectively. Transcriptional fusion constructs were made by Gateway recombining the promoter element, *mCherry* and the *unc-54* 3' UTR entry clones into the

pCFJ150 destination vector, which is compatible with Mos1 mediated transgenesis (see Section III.3 below).

To obtain *Pegl-17::DN-pop-1* first *DN-pop-1* was PCR amplified from the *Phs::DN-pop-1* construct made previously (Korswagen et al., 2000) and recombined into pDONR221 using Gateway technology. Then *Pegl-17::DN-pop-1* was made by gateway recombining entry clones containing *Pegl-17* (Middelkoop et al., 2012), *DN-pop-1* and the *unc-54 3'UTR* into the pCFJ150 destination vector.

Yeast-mediated homologous recombination (for deletion of putative MAB-5 binding regions)

mab-5 promoter and intronic sequences, *lin-17* and *mom-5* promoter sequences and *mCherry* coding sequence were PCR-amplified into less than 4 kb long fragments, each with >10 bp homologous overhangs on both ends. Each set of PCR amplicons were then recombined with pNP30 (kind gift of Nick Paquin), a MosSCI compatible vector carrying the yeast URA3 gene, using the protocol outlined in (Andersen, 2011).

Pmab-5: a genomic region spanning 6.3 kb upstream of the *mab-5* ATG to 32 bp into the 4th exon of the *mab-5* gene was PCR-amplified in three consecutive fragments. For the mutant construct, the following regulatory sequences were excluded:

Promoter mutation (*Pmab-5ΔMAB-5::mab-5g::mCherry*):
Deletion 1: 5'- CTTTCGTCTTGTCCACTATA - (70 bps) - GATGTTATGCCGACTCTCGC - 3'
Deletion 2: 5'- TTTTCATGCTCCTCCCAATT - (378 bps) - TCATGATTATCAAATAATGA - 3'

Intron 3 mutation (2 sites) (*Pmab-5::mab-5g ΔMAB-5x2::mCherry*):
Deletion 1: 5'- GAAAACCCACGAATTCGAGC - (504 bps) - CAAAGTCAAAAAATATACAT - 3'
Deletion 2: 5'- TGTTAATTTATTAATTGTTT - (256 bps) - TAACCATGTAATCTTGAGAC - 3'

Intron 3 mutation (3 sites) (*Pmab-5::mab-5g ΔMAB-5x3::mCherry*):
Deletions 1 & 2: same as Intron 3 mutation (2 sites);
Deletion 3: 5'- ATTTCCATTTTCACTATTTG - (254 bps) - GATCCTTTTTCTCTAAATCG - 3'

The *mCherry* coding sequence along with the *let-585* 3' UTR were amplified together from the POPTOP vector (Green et al., 2008).

Generation of single copy transgenes

Transgenes were integrated into the genome as single copies using Mos1 mediated transgenesis as previously described (Frøkjaer-Jensen et al., 2008). We used the ttTi5605 MosSCI insertion site. Injection mixes contained pCFJ90 (*Pmyo-2::mCherry*, 2.5 ng/µl), pJORG1912 (*Prab-3::mCherry*, 10 ng/µl), pCFJ104 (*Pmyo-3::mCherry*, 5 ng/µl), pJL43.1 (*Pglh-2::Mos1* transposase, 50 ng/µl) and the respective expression construct (50 ng/µl).

Determination of steady state gene expression window

To quantify the mean and variability of *mab-5* expression at steady state (Figure 1 and 3), a sliding window of size 4 was moved along the axis of total migratory distance (MD) and the mean and Fano factor for *mab-5* transcripts counts within the window were calculated. A steady state was defined when both the mean and the Fano factor varied by less than 10%

or within ±1 of their final value (corresponding to MD=10-14).

Measurement of mab-5 mRNA half-life and synthesis rates

Synchronized animals aged between 2.5-3 hours post hatching were continuously incubated in 100 µg/ml Actinomycin D (Sigma) for desired amount of times (Kauffman et al., 2010; Klass et al., 1982). Animals were immediately fixed in 4% paraformaldehyde at the end of the incubation. Measured *mab-5* mRNA levels ($y(t)$) were used to derive mRNA half-life and synthesis rates by fitting to the following model:

$$log(y(t)) = -\gamma * t + c$$

where γ is the mRNA degradation rate and c accounts for initial transcript dynamics before complete transcription inhibition is established. mRNA synthesis rate (β) is calculated as:

$$\beta = A * \gamma$$

where A is the steady state *mab-5* level in a given strain.

Implementation of the MRA algorithm

Following procedures outlined in Kholodenko et al. 2002, the raw transcript count for a given gene in a given strain is transformed into the central fraction difference (CFD) value using the following formula:

$$\Delta ln\, x_j = 2 * \frac{(x_j^{(1)} - x_j^{(0)})}{x_j^{(1)} + x_j^{(0)}}$$

where $x_j^{(0)}$ denotes the transcript count of gene j in the wild type, and $x_j^{(1)}$ the transcript count in the strain of interest (e.g. all wild type measurements would yield a CFD value of 0). Based on the transformed CFD value, a 5x5 matrix was assembled by bootstrap sampling for each gene in each mutant background. This "gene expression matrix" was then substituted into the following inference algorithm (van Kampen, 2007):

$$r = -[diag(R^{-1})]^{-1} * R^{-1}$$

where *r* stands for the connectivity matrix, *R* represents the gene expression matrix, and "*diag*" denotes the matrix diagonal. Bootstrapping followed by the inference routine was repeated 10,000 times and the resulting connectivity matrices were pooled to obtain the probability distribution and FDR adjusted p-value for each connectivity strength.

In implementing the above algorithm, we have assumed that the real network can be largely approximated by a linear model (i.e. the functions describing individual network interactions are operating within a quasi-linear regime). Another implicit assumption is that all errors in the measured mean expression levels are normally distributed. Under this assumption, the inferred network is essentially the maximum likelihood estimation of the real network.

Computational validation of the inferred topology

To control for network complexity, we compared the Akaike Information Criterion (AIC) value (Akaike, 1974) of the wild-type network to a series of 9 alternative networks using the following equation (Burnham and Anderson, 2002):

$$AIC = n\,ln(RSS / n) + 2k + C$$

Where *RSS* is the residual sum of squares from model fitting, *n* denotes the size of the data set used for model fitting, *k* denotes the number of model parameters, and *C* is a constant independent of the model (which we set to zero for simplicity). Given a set of candidate models for the data, the preferred model is the one with the minimum AIC value. The alternative networks were constructed by eliminating one at a time of the inferred network interactions. Specifically, this was done by forcing the corresponding model parameter to be zero and proceed with least-squares parameter fitting. The AIC value allows for a fair comparison between models with different number of parameters (model complexity). As shown in Figure S4C, the inferred model yielded a much lower AIC value than all the alternative models tested, which validates the inferred model as the most likely model given the gene expression data set.

We next tested the sensitivity of inferred topology to the definition window of steady state gene expression. Briefly, a sliding window that spans MD=X-1 to MD=X+3, where X varied from 1 to 12, were used to selected data points for network inference. Following the same data transformation as outlined in Methods, the MRA algorithm was applied and the resulting average interaction strengths were reported in Figure S4D. The inferred values varied greatly for X=1 to 6, but stabilized for X>6. The initial fluctuation in interaction strengths reflected the initial variation in transcript abundance, and the stabilization of inferred interaction strengths validate the use of MD>8 as a window for steady state gene expression.

Modeling

Model construction

Based on the inferred network topology (Figure 5C), we constructed the following ordinary differential equation (ODE) model. As listed below, the variables *R1-3*, *W* and *T* denote the per-cell abundance of each of the five network components.

R1: *mig-1*

$$\dot{R}1 = \gamma 1 * (V1 * (\frac{K1^{n1}}{K1^{n1} + W^{n1}}) + \beta 1 - R1) \quad (1)$$

R2: *lin-17*

$$\dot{R}2 = \gamma 2 * (V2 * (\frac{c * T^{n2} + W^{n2}}{K2^{n2} + c * T^{n2} + W^{n2}}) - R2) \quad (2)$$

R3: *mom-5*

$$\dot{R}3 = \gamma 3 * (V3 * (\frac{K3^{n3}}{K3^{n3} + T^{n3}}) - R3) \quad (3)$$

W: Intracellular Wnt signal

$$\dot{W} = \gamma w * (Vw * L * (\frac{R1 + s1 * R2 + s2 * R3}{+s3 * R1 * R2 + s4 * R1 * R3}) * (\frac{K_w^{n4}}{K_w^{n4} + T^{n4}}) - W) \quad (4)$$

T: *mab-5*

$$\dot{T} = \gamma t * (W - T) \quad (5)$$

Note 1: *L* denotes the amount of EGL-20 ligand available. Since *egl-20* was expressed at similar levels across strains (data not shown), we assumed the local EGL-20 level to be unaltered in all strains except for mutants directly affecting the function or the secretion of EGL-20 (i.e. *egl-20 (n585)* and *vps-29 (tm1320)*). The value of *L* denotes the local concentration of *L* relative to the wild type. To minimize the number of free parameters, we assumed *L* to stay constant in all genetic backgrounds and assigned *L* with an arbitrary value of 1. Potential interactions between the Frizzleds and the Wnt ligand, while not explored in the current study, can be incorporated into the model by modeling *L* as a function of the *R1~3* (i.e. *L=L(Ri)*).
Note 2: To model the non-additive relation between Frizzled single mutants and compound mutants (e.g. the reduction in *mab-5* in the *lin-17 mom-5* double mutant is much greater than the summed loss in the two single mutants (Figure 3A)), it was necessary to include the interaction terms (i.e. $s*Ri*Rj$) in (4). This way the near complete loss of mab-5 expression in Frizzled compound mutants can be recapitulated by the model.
Note 3: In this model, we have let all regulatory interactions to act by modulating the transcript synthesis (as opposed to degradation) rates of the target genes. This decision was based on that the measured *mab-5* half-life remains relatively constant between wild type and multiple mutants, whereas the transcript synthesis rates vary greatly across the strains (Figure S3G).

Parameter estimation
We next fitted the above model to the gene expression profile of wild-type and mutant strains. To constrain the number of parameters and facilitate fitting, we manually tested Hill coefficient values of 1, 3, 6 and 9. We only accepted higher Hill coefficients when the increase in Hill coefficient led to considerable decrease in the mean squared error (MSE) without a compromise in the *p*-values. We used similar criteria to determine whether to include the basal transcription rates (βi) in a given equation. In general, keeping the minimal number of parameters yielded close approximation of the experimental data. The parameter estimates were obtained from the least squares fitting routines in MATLAB (MathWorks, Natick, MA) and listed in Table S2.

Model reduction
With the fit parameters, the model exhibits temporal dynamics that approximates the wild-type expression profile (Fig S5A). Next, by observing that *yw* is much smaller than the other time scales (*y1-3,* and *yt*), we reduce the model down to a deterministically equivalent 1D model by setting equations (1)-(3) and (5) to zero and substituting the resulting equalities into equation (4):

$$\dot{W} = \gamma w * (Vw * L * Rtot * (\frac{K_w^{n4}}{K_w^{n4} + T^{n4}}) - W) \quad (6)$$

where $Rtot = R1 + s1*R2 + s2*R3 + s3*R1*R2 + s4*R1*R3$ with *R1-3* defined as in (1)-(3).

Analytical calculation of the Fano factor

To obtain the theoretical Fano factor values, we first rewrite the 1D model in the following format:

$$\dot{x} = f(x) - g(x) \tag{7}$$

where $f(x) = \gamma w * Vw * L * Rtot * (\frac{K_w^{n4}}{K_w^{n4} + W^{n4}})$, $g(x) = \gamma w * W$, and $Rtot$ defined the same as in (6).

To model the effect of stochastic fluctuations, we construct the following Langevin model:

$$\dot{x} = f(x) - g(x) + \sqrt{f + g + D} * \Gamma \tag{8}$$

where the magnitude of the intrinsic and extrinsic fluctuations are defined by their autocorrelation functions:

Intrinsic fluctuation εi: $< \varepsilon i(t) \varepsilon i(t') >= 2 * (f + g) * \delta(t - t')$

Extrinsic fluctuation εe: $< \varepsilon e(t) \varepsilon e(t') >= 2 * D * \delta(t - t')$

Here we assume the intrinsic and the extrinsic fluctuations are uncorrelated. The stationary probability distribution of x can then be analytically calculated using the Fokker-Planck formalism. The drift ($A(x)$) and diffusion ($B(x)$) terms in a corresponding Fokker-Planck model can thus be represented as (van Kampen, 2007):

$$A(x) = f - g \quad \text{and} \quad B(x) = f + g + D$$

The value of D was set to 0 for the computational analysis on the effect of network topology on output variability (Figure 6 and S5) and determined by fitting to the wild-type *mab-5* distribution to allow the prediction of *mab-5* variability in the Wnt signaling mutants (Figure 7 and S6). It follows that the probability density of the stochastic model is:

$$p(x) = \frac{const}{B(x)} * exp[2 * \int_0^x \frac{A(x')}{B(x')} dx'] \tag{9}$$

The mean and variance then follow from the probability density, with the ratio of the two leading to the expression of the Fano factor ν:

$$\nu = \frac{\int_0^{+\infty} [x^2 * p(x)] dx - (\int_0^{+\infty} [x * p(x)] dx)^2}{\int_0^{+\infty} [x * p(x)] dx}$$

Note that by reducing the model to a 1D system, we are implicitly assuming that the molecules that mediate the feedback (e.g. the protein products of *mab-5* and the Frizzleds) are produced instantaneously. In this reduced, idealistic system, it is in principle possible for the Fano factor to reach very low levels (i.e. $\nu << 1$). In a more realistic multidimensional model, however, there would be fundamental limits on the noise-suppression ability of the feedback network (Lestas et al., 2010).

Predicting mab-5 variability in the mutants

Following the derivation of the probability density function, the distribution of *mab-5* expression can be directly calculated for different network topologies. As the exact level of the extrinsic fluctuations (*D*) is unknown, we first fit the wild-type *mab-5* distribution,

D was varied incrementally from 0 up and a value of 450 was found to well approximate the wild-type distribution. The same value of D was then kept fixed while the topology of the model network was varied to mimic the altered network topology in the mutants. The probability density function was then derived and the Fano factor value calculated for each "mutant" network.

Supplemental References

Akaike, H.A.I. (1974). A New Look at the Statistical Model Identification. IEEE Trans. Automat. Contr. *AC-19*, 716–723.

Andersen, E.C. (2011). PCR-Directed In Vivo Plasmid Construction Using Homologous Recombination in Baker's Yeast. In Molecular Methods for Evolutionary Genetics, V. Orgogozo, and M. V. Rockman, eds. (Totowa, NJ: Humana Press), pp. 409–421.

Burnham, K.P., and Anderson, D.R. (2002). Model Selection and Multimodel Inference: A Practical Information-Theoretic Approach (New York: Springer-Verlag).

Denning, G., Jamieson, L., Maquat, L.E., Thompson, E. a, and Fields, a P. (2001). Cloning of a novel phosphatidylinositol kinase-related kinase: characterization of the human SMG-1 RNA surveillance protein. J. Biol. Chem. *276*, 22709–22714.

Frøkjaer-Jensen, C., Davis, M.W., Hopkins, C.E., Newman, B.J., Thummel, J.M., Olesen, S.-P., Grunnet, M., and Jorgensen, E.M. (2008). Single-copy insertion of transgenes in Caenorhabditis elegans. Nat. Genet. *40*, 1375–1383.

Green, J., Inoue, T., and Sternberg, P.W. (2008). Opposing Wnt pathways orient cell polarity during organogenesis. Cell *134*, 646–656.

Grimson, A., Connor, S.O., Newman, C.L., and Anderson, P. (2004). SMG-1 Is a Phosphatidylinositol Kinase-Related Protein Kinase Required for Nonsense-Mediated mRNA Decay in Caenorhabditis elegans. Mol. Cell. Biol. *24*, 7483–7490.

Van Kampen, N.G. (2007). Stochastic Processes in Physics and Chemistry (Amsterdam: Elsevier).

Kauffman, A.L., Ashraf, J.M., Corces-Zimmerman, M.R., Landis, J.N., and Murphy, C.T. (2010). Insulin signaling and dietary restriction differentially influence the decline of learning and memory with age. PLoS Biol. *8*, e1000372.

Klass, M., Dow, B., and Herndon, M. (1982). Cell-Specific Transcriptional Regulation of the Major Sperm Protein in Caenorhabditis elegans. Dev. Biol. *93*, 152–164.

Korswagen, H.C., Herman, M. a, and Clevers, H.C. (2000). Distinct beta-catenins mediate adhesion and signalling functions in C. elegans. Nature *406*, 527–532.

Lestas, I., Vinnicombe, G., and Paulsson, J. (2010). Fundamental limits on the suppression of molecular fluctuations. Nature *467*, 174–178.

Middelkoop, T.C., Williams, L., Yang, P.-T., Luchtenberg, J., Betist, M.C., Ji, N., van Oudenaarden, A., Kenyon, C., and Korswagen, H.C. (2012). The thrombospondin repeat containing protein MIG-21 controls a left-right asymmetric Wnt signaling response in migrating C. elegans neuroblasts. Dev. Biol. *361*, 338–348.

Pulak, R., and Anderson, P. (1993). mRNA surveillance by the Caenorhabditis elegans smg genes. Genes Dev. *7*, 1885–1897.

Whangbo, J., and Kenyon, C. (1999). A Wnt signaling system that specifies two patterns of cell migration in C. elegans. Mol. Cell *4*, 851–858.

Wildwater, M., Sander, N., de Vreede, G., and van den Heuvel, S. (2011). Cell shape and Wnt signaling redundantly control the division axis of C. elegans epithelial stem cells. Development *138*, 4375–4385.

Chapter 5

Migrating *C. elegans* neurons express specific combinations of Wnt receptors

Remco A. Mentink, Marco C. Betist and Hendrik C. Korswagen

Hubrecht Institute, Royal Netherlands Academy of Arts and Sciences and University Medical Center Utrecht, The Netherlands.

Manuscript in preparation

Abstract

During *C. elegans* embryogenesis, four bilateral pairs of neurons migrate to specific positions along the anteroposterior body axis. Previous studies have shown that these migrations are controlled by Wnt signaling. Here, we show that each of the migrating neurons expresses a unique combination of Wnt receptors, which act in parallel to guide the neurons to their precisely defined final positions. In addition, we found that receptors that are not expressed in the neurons influence their migration as well. We conclude that both cell autonomous and non-autonomous Wnt signaling mechanisms guide the migration of embryonic neurons.

Introduction

During development, the migration of neurons and axons sets up the complex wiring of the nervous system. These highly stereotypic migrations are controlled through various signaling molecules that act as attractive or repulsive guidance cues (Chilton, 2006; Marin et al., 2010). One family of secreted guidance molecules comprises the Wnt proteins (Salinas, 2012). Wnt proteins are predominantly expressed in the posterior of the embryo and control cell and axon migration along the anteroposterior body axis in organisms ranging from cnidarians to vertebrates (Harterink et al., 2011; Petersen and Reddien, 2009). Examples are the migration of commissural and corticospinal tract axons along the embryonic spinal cord in the mouse (Liu et al., 2005; Lyuksyutova et al., 2003) and the migration of neuroblasts along the anteroposterior axis in the nematode *C. elegans* (Pan et al., 2006). In the latter example, the Wnt protein EGL-20 has been shown to act instructively, functioning as a repulsive guidance cue that directs the HSN neuron away from its source of expression (Pan et al., 2006).

Wnt proteins can trigger several distinct downstream signaling pathways. These include a canonical Wnt pathway - which leads to stabilization of the effector protein ß-catenin and the activation of specific target genes - and a collection of less well-described non-canonical Wnt pathways, which directly modulate the cytoskeleton to control cell polarity and migration (Angers and Moon, 2009; Clevers and Nusse, 2012). Historically, Wnt proteins have been subdivided into canonical or non-canonical ligands based on their ability to induce Wnt/ß-catenin signaling (Du et al., 1995; Shimizu et al., 1997). Recently, it has become clear that a single Wnt ligand can activate more than one signaling pathway. For example, Wnt5a and Wnt11 are known to act during Xenopus axis formation, which is dependent on canonical Wnt signaling (Cha et al., 2008; Tao et al., 2005). However, both Wnts are also involved in regulating convergence and extension cell movements, which involves a non-canonical Wnt signaling response (Kim et al., 2008; Wallingford et al., 2001). *In vitro* studies have shown that the Wnt signaling response of a cell is determined by the Wnt receptors that it expresses (Mikels and Nusse, 2006). A striking example is the response of tissue-culture cells to Wnt5a: when the Wnt receptor Frizzled4 is expressed, the cells activate canonical Wnt signaling, while in the presence of the Ror2 receptor tyrosine kinase, canonical Wnt signaling is inhibited. *In vivo*, such mechanisms are likely to be more complex, as signaling responses will also be influenced by the developmental history and cell fate of the responding cell (van Amerongen et al., 2012a; van Amerongen et al., 2012b).

With only five Wnt ligands and six Wnt receptors, *C. elegans* offers a tractable system to study how Wnt ligands and receptors trigger distinct signaling responses in migrating neurons (Eisenmann, 2005; Korswagen, 2002). During embryogenesis, four bilateral pairs of neurons migrate along the developing anteroposterior body axis (Hedgecock et al., 1987; Sulston et al., 1983). Two neurons migrate posteriorly: the canal-associated neurons (CANs) migrate from the head towards the mid-body region, while the anterior lateral microtubule neurons (ALMs) migrate from a position close to the epidermal seam cell V1 to seam cell V3. The other two neurons migrate anteriorly: the BDU neurons, which are the sister cells of the ALMs, migrate a short distance towards the anterior and the hermaphrodite-specific neurons (HSNs) migrate from the tail to a position in the mid-body region, just posterior to where the CANs end their migration (Hedgecock et al., 1987; Sulston et al., 1983). It has previously been shown that each of these neuronal migrations is dependent on Wnt signaling (Forrester

et al., 1999; Pan et al., 2006; Zinovyeva and Forrester, 2005; Zinovyeva et al., 2008). An extensive genetic analysis conducted by Zinovyeva and colleagues has demonstrated that in each case multiple Wnt ligands and receptors are involved (Zinovyeva et al., 2008). We sought to expand upon these data and gain more insight into the Wnt signaling mechanisms that control the migration of the four neurons. Double mutants between Wnt ligands (*egl-20*, *cwn-1*, *cwn-2*) and receptors (*mig-1*, *lin-17*, *mom-5*, *cfz-2* and *cam-1*) were constructed in order to study Wnt-receptor interactions. Furthermore, mutants of the three Dishevelled orthologs were examined to determine to which extent these intracellular signaling hubs contribute to signaling specificity. Finally, we quantitatively examined Wnt receptor expression to determine the receptor repertoire of each of the neurons.

Our results show that the migrating HSN, ALM, CAN and BDU neurons each express a different combination of Wnt receptors. However, we found that in addition to this specific receptor repertoire, other receptors modulate the migration as well, indicating that non cell-autonomous Wnt signaling mechanisms also contribute to the correct positioning of the HSN, ALM, CAN and BDU neurons.

Results

The migrating HSN, ALM, CAN and BDU neurons each express a unique combination of Wnt receptors

We used a single molecule mRNA fluorescent in situ hybridization (smFISH) approach to quantitatively determine the expression of the four Frizzled Wnt receptors and the single Ror2 ortholog *cam-1* (Raj et al., 2008). The HSN, ALM, CAN and BDU neurons were visualized using specific GFP reporters and expression was quantified by counting smFISH spots in the

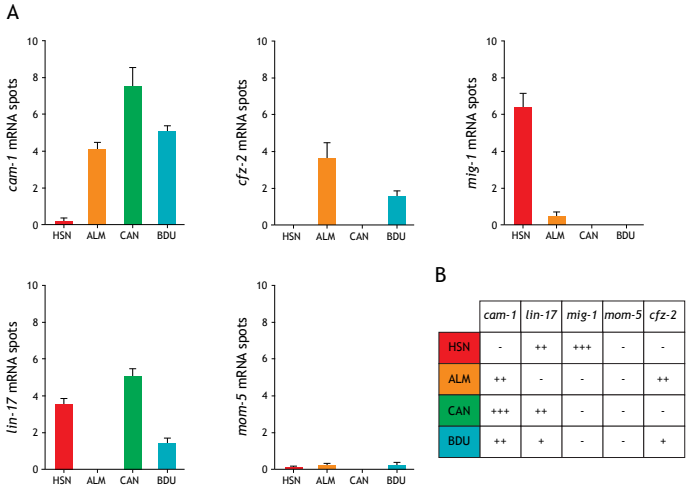

Figure 1. Each of the embryonically migrating HSN, ALM, CAN and BDU neurons expresses their specific set of Wnt receptors. (**A**) Quantification of single molecule mRNA FISH performed on *cam-1*, *cfz-2*, *mig-1*, *lin-17* and *mom-5* mRNA. Bar graphs display mRNA counts of each Wnt receptor in HSN (red), ALM (orange), CAN (green) and BDU (blue) and represent the mean ± S.D, n>10. The *kyIs179[Punc-86::GFP;lin-15(+)]* transgene was used to visualize HSN, ALM and BDU neurons, while the *kyIs4[Pceh-23::GFP; lin-15(+)]* served to visualize CAN neurons. (**B**) Table representing the average number of mRNA spots quantified (no mRNA or <1 counts (-), 1-3 counts (+), 3-5 counts (++), >6 counts (+++)) per neuron for each Wnt receptor.

GFP labeled neurons during or just after completion of migration in synchronized late stage embryos. We found that each of the neurons expresses a different subset of Wnt receptors (Figures 1A and 1B): the HSN neurons express *mig-1* and *lin-17*, the ALM neurons *cam-1* and *cfz-2*, the CAN neurons *cam-1* and *lin-17* and the BDU neurons *cam-1*, *lin-17* and *cfz-2*. Transcripts of *mom-5* were only occasionally detected, indicating that this receptor is not or only weakly expressed in the four neurons.

Analysis of the global expression patterns of *mig-1*, *lin-17*, *mom-5* and *cfz-2* has revealed that they are expressed in partially overlapping domains along the anteroposterior body axis (Ji et al., 2013). *lin-17* is mostly expressed in the posterior, *mig-1* and *mom-5* in the mid-body, while *cfz-2* is most abundant in the head region. This regional expression of the Wnt receptors appears to be maintained in HSN and ALM. The HSN neuron, which migrates form the tail to the mid-body region, expresses the posterior *lin-17* receptor, while ALM, which migrates from the head region to the mid-body region, expresses the anterior *cfz-2* receptor. This correlation is however absent in CAN and BDU. Thus, although CAN also migrates from the head to the mid-body region and the short-range migration of BDU is limited to the anterior body region, both express the posterior *lin-17* receptor. These results indicate that the expression of Wnt receptors in migrating neurons is only partially linked to their regionalized global expression patterns.

HSN migration is mediated through parallel acting MIG-1 and LIN-17 dependent Wnt pathways

The HSN neurons migrate anteriorly from the tail towards the midbody region (Figure 2A). Previous studies have shown their migration to be controlled by a complex Wnt signaling system (Pan et al., 2006; Zinovyeva et al., 2008). The main Wnt ligand required for HSN migration is EGL-20, which is expressed in the tail and acts as a repulsive guidance signal that directs the HSN neurons towards the anterior. In addition, there is a role for the Wnt ligands *cwn-1* and *cwn-2*, with significant undermigration in *cwn-1*; *cwn-2* double mutants (Figure 2C). At the receptor level, HSN migration is strongly affected in *mig-1* mutants (Figure 2B). Consistent with our smFISH expression analysis, *mig-1* has been shown to act cell autonomously in the HSN neurons (Pan et al., 2006). Interestingly, the undermigration induced by *mig-1* was suppressed by loss of *lin-17*, indicating that *mig-1* and *lin-17* have opposing functions and that other receptor(s) mediate HSN migration in the absence of MIG-1 and LIN-17. The slight posterior shift of the average HSN position in the *mig-1 lin-17 mom-5* triple mutant suggests that *mom-5* is one of these receptors (Figure 2B). However, our expression data shows that *mom-5* is either very lowly or not expressed in HSN (Figures 1A and 1B). Perhaps these low levels are sufficient to mediate the migratory response or, alternatively, *mom-5* contributes non-autonomously to HSN migration. A small degree of undermigration is observed in the *mom-5 lin-17* double mutant, indicating that *lin-17* may have multiple roles and also promote HSN migration in parallel to *mom-5* (Figure 2B).

To investigate the functional relationship between the different Wnt ligands and receptors, we performed a comprehensive double and triple mutant analysis with null alleles of the different Wnt pathway components (Figures 2B, 2C and 2D). At the Wnt ligand level, we found that *cwn-1* weakly enhances the undermigration phenotype of *egl-20*, whereas *cwn-2 egl-20* double mutants are identical to the *egl-20* single mutant. These results indicate that *cwn-1* and *egl-20* act in parallel genetic pathways, while *cwn-2* and *egl-20* may be part of the same pathway (Figure 2C). Combinations of Wnt ligand and receptor mutations showed

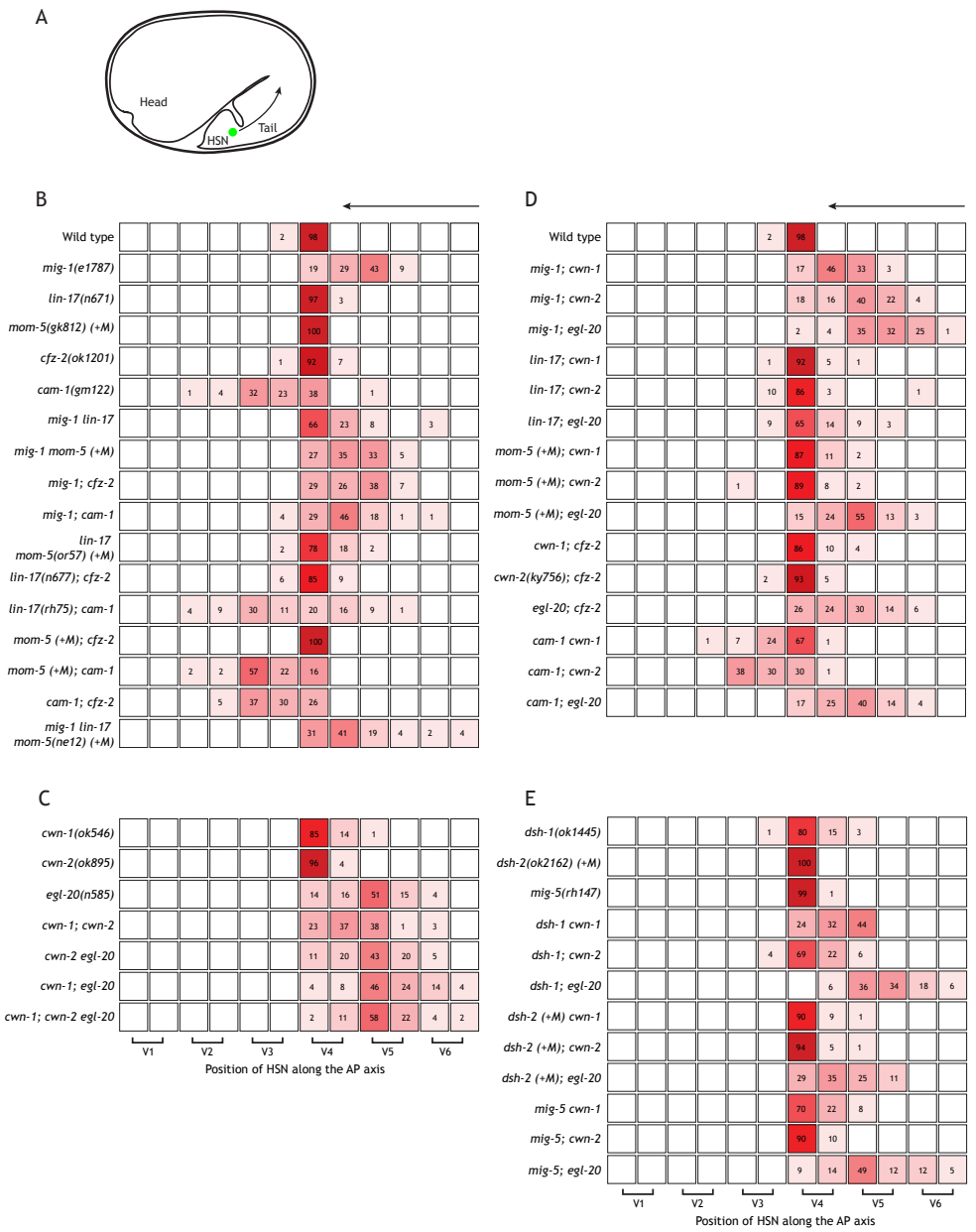

Figure 2. HSN migration is mediated through parallel acting MIG-1 and LIN-17 dependent Wnt pathways. (**A**) Schematic representation of the anterior migratory route of the HSN neuron (green) during embryogenesis. (**B-E**) Average position of the HSN neurons in Wnt receptor mutants (**B**), Wnt mutants (**C**), Wnt/Wnt receptor double mutants (**D**) and Wnt/Dsh double mutants (**E**) with respect to the seam cells V1.a to V6.p (lower brackets indicate Vn.a (left) and Vn.p (right) daughters of Vn cells). Values listed are percentiles of total cells scored, n>50 for all genotypes. A color (red) coded heat map represents the range of percentile values.

that the *mig-1*; *cwn-1* double mutant has a similar phenotype as the *mig-1* single mutant, indicating that they are part of the same pathway. The HSN migration defect of *mig-1* and *egl-20* was however strongly enhanced in the double mutant. Taken together with the phenotypes of the single mutants, these results suggest that in addition to signaling through MIG-1, EGL-20 also acts through other receptor(s), most likely the same receptor(s) that mediate anterior migration in the *mig-1*; *lin-17* double mutant. We have found that *mom-5* contributes slightly to migration in the absence of *mig-1* and *lin-17,* so EGL-20 could be signaling partly via this receptor (Figure 2B). This is consistent with removal of *mom-5* not enhancing the undermigration of the *egl-20* mutant, indicating that they are in the same pathway (Figure 2D). Finally, mutation of *cfz-2* did not significantly modulate the phenotype of any of the Wnt of receptor mutants tested and we have therefore not found any evidence for its involvement in HSN migration (Figures 2B and 2D).

In *cam-1* mutants, the HSN neurons migrate beyond their wild type positions. It has previously been shown that the CAN neurons act as a barrier for the migrating HSN neurons, most likely by functioning as a sink for the EGL-20 guidance signal (Forrester et al., 2004; Pan et al., 2006). As discussed below, loss of *cam-1* interferes with the posterior migration of the CAN neurons and may therefore indirectly influence the final positioning of the HSN neurons. Consistent with such a cell non-autonomous function, we found that *cam-1* is not expressed in the HSN neurons (Figures 1A and 1B). Furthermore, double mutants between *cam-1* and *mig-1* showed a migration phenotype that is identical to the *mig-1* single mutant (Figure 2B), demonstrating that the function of *mig-1* in HSN migration is independent of *cam-1*.

In addition to the Wnt ligands and receptors, we also examined the function of the three Dishevelled (Dvl) orthologs in HSN migration (Figure 2E). We found that HSN migration was mildly affected in *dsh-1* mutants, while no migration defects were observed in *dsh-2* or *mig-5* mutants. Furthermore, *dsh-1* enhanced the undermigration phenotype of *cwn-1* and *egl-20*, indicating that it functions in parallel to both Wnt ligands. As Dishevelled proteins act as multifunctional signaling hubs in Wnt signaling (Gao and Chen, 2010), such a complex genetic relationship is to be expected. Interestingly, *dsh-2* significantly suppressed the undermigration phenotype of *egl-20* mutants. This is similar to the antagonizing effect of *lin-17* and suggests that *dsh-2* may be part of the same pathway.

ALM migration is controlled by parallel acting CFZ-2 and CAM-1 dependent Wnt pathways

The ALM neurons migrate posteriorly from a position just behind the head to the midbody region (Figure 3A). Analysis of Wnt ligand and receptor mutants has shown that their migration is a Wnt dependent process (Zinovyeva et al., 2008). We found that the final position of ALM was shifted slightly posterior in *cwn-1* and *cwn-2* single mutants and that this effect was enhanced in double mutants between *cwn-1* and *egl-20* (Figure 3C). In *cwn-1*; *cwn-2* double mutants, on the other hand, the final position of ALM became highly variable, with animals showing either extensive under or overmigration of the ALM neurons.

At the receptor level, there was a slight posterior shift in ALM position in *mom-5* mutants, while the ALM neurons showed significant undermigration in *cfz-2* and *cam-1* mutants. This phenotype was strongly enhanced in the double mutant, indicating that *cfz-2* and *cam-1* act in parallel genetic pathways (Figure 3B). The requirement of *cfz-2* and *cam-1* for ALM migration is consistent with our expression analysis (Figures 1A and 1B) and suggests that

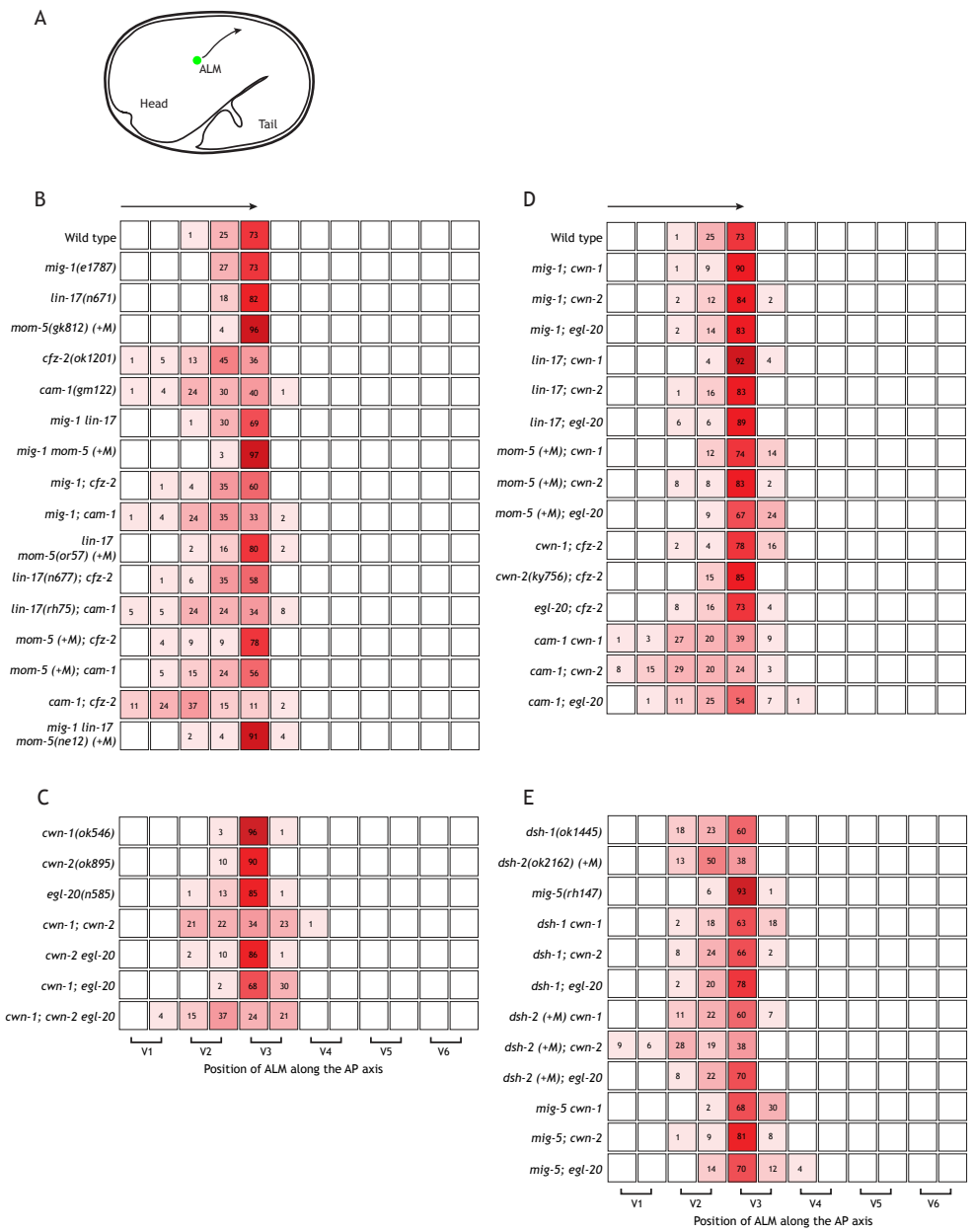

Figure 3. ALM migration is controlled by parallel acting CFZ-2 and CAM-1 dependent Wnt pathways. (**A**) Schematic representation of the posterior migratory route of the ALM neuron (green) during embryogenesis. (**B-E**) Average position of the ALM neurons in Wnt receptor mutants (**B**), Wnt mutants (**C**), Wnt/Wnt receptor double mutants (**D**) and Wnt/Dsh double mutants (**E**) with respect to the seam cells V1.a to V6.p (lower brackets indicate Vn.a (left) and Vn.p (right) daughters of Vn cells). Values listed are percentiles of total cells scored, n>50 for all genotypes. A color (red) coded heat map represents the range of percentile values.

these receptors function cell autonomously.

The overmigration observed in *mom-5* mutants indicates that it may counteract the *cfz-2* and *cam-1* dependent posterior migration of the ALM neurons. In agreement with previous observations, we found that *mom-5*, as well as *mig-1* and *lin-17*, suppress the undermigration of *cfz-2* (Figure 3B) (Zinovyeva et al., 2008). As *mom-5*, *mig-1* and *lin-17* are not expressed in the ALM neurons, they likely function cell non-autonomously in this process. *mom-5*, *mig-1* and *lin-17* did not affect ALM migration in a *cam-1* mutant background, further supporting our conclusion that *cam-1* and *cfz-2* are part of distinct genetic pathways (Figure 3B).

Examination of double mutants between Wnt ligands and receptors revealed complex genetic relationships. Loss of *cwn-1* did not affect ALM positioning in *cam-1* mutants, but *cwn-2* significantly enhanced the undermigration phenotype of *cam-1* (Figure 3D). This indicates that *cwn-1* and *cam-1* may be part of a common pathway, while *cwn-2* functions in parallel to *cam-1* to promote posterior migration. In combination with *cfz-2*, on the other hand, loss of *cwn-1*, *cwn-2* or *egl-20* resulted in a posterior shift in ALM position, an effect that was also observed in combination with *mom-5* (Figure 3D). These results suggest that the three Wnt ligands can both promote and inhibit posterior migration of the ALM neurons and are in agreement with the observation that ALM position becomes highly variable in *cwn-1*; *cwn-2* double mutants.

At the level of the three Dishevelled orthologs, there was significant undermigration in *dsh-1* and *dsh-2* mutants (Figure 3E). In combination with Wnt mutants, there was significant overmigration in *dsh-1 cwn-1* double mutants, while the undermigration of *dsh-2* was significantly enhanced by *cwn-2*. Loss of *mig-5* resulted in a slight posterior shift in ALM position (Figure 3E). Similar to *mom-5*, this overmigration was enhanced in combination with mutations in *cwn-1* or *egl-20*, indicating that *mom-5* and *mig-5* may be part of the same pathway.

CAN migration is dependent on CAM-1

The CAN neurons migrate posteriorly from within the head to the midbody region (Figure 4A). Analysis of single Wnt ligand mutants revealed that *cwn-2* is required for their posterior migration (Figure 4C) (Zinovyeva et al., 2008). *cwn-2* is however not the only Wnt required to promote migration. In c*wn1*; *cwn-2* and *cwn-2 egl-20* double mutants, the CAN neurons frequently migrate beyond their wild type positions, indicating that *cwn-2* acts redundantly with *cwn-1* and *egl-20* to both stimulate and antagonize migration (Figure 4C). At the receptor level, migration is mainly dependent on *cam-1* (Figure 4B) (Forrester et al., 1999; Zinovyeva et al., 2008). This is consistent with the expression of *cam-1* in the CAN neurons (Figures 1A and 1B) and suggests a cell autonomous function of *cam-1* in CAN migration. Mutation of the different Frizzleds only produced weak migration defects in double mutants of *lin-17*; *cfz-2* and *mom-5*; *cfz-2*. However, all four Frizzled mutants strongly enhanced *cam-1*, indicating that they mostly act in parallel (Figure 4B).

By combining *cam-1* with mutations in the different Wnt ligands, we found that *cwn-1* and *cwn-2* strongly enhance the *cam-1* phenotype (Figure 4D). *cam-1*; *egl-20* double mutants, on the other hand, showed a similar CAN cell distribution as *cam-1* single mutants (Figure 4D). These results indicate that *egl-20* and *cam-1* function in the same pathway, while *cwn-1* and *cwn-2* act in parallel to *cam-1*. Combining *cwn-1* or *egl-20* with any of the Frizzled mutants did not lead to strong migration defects. However, double mutants between *cwn-2* and the different Frizzleds resulted in enhancement of the undermigration phenotype as

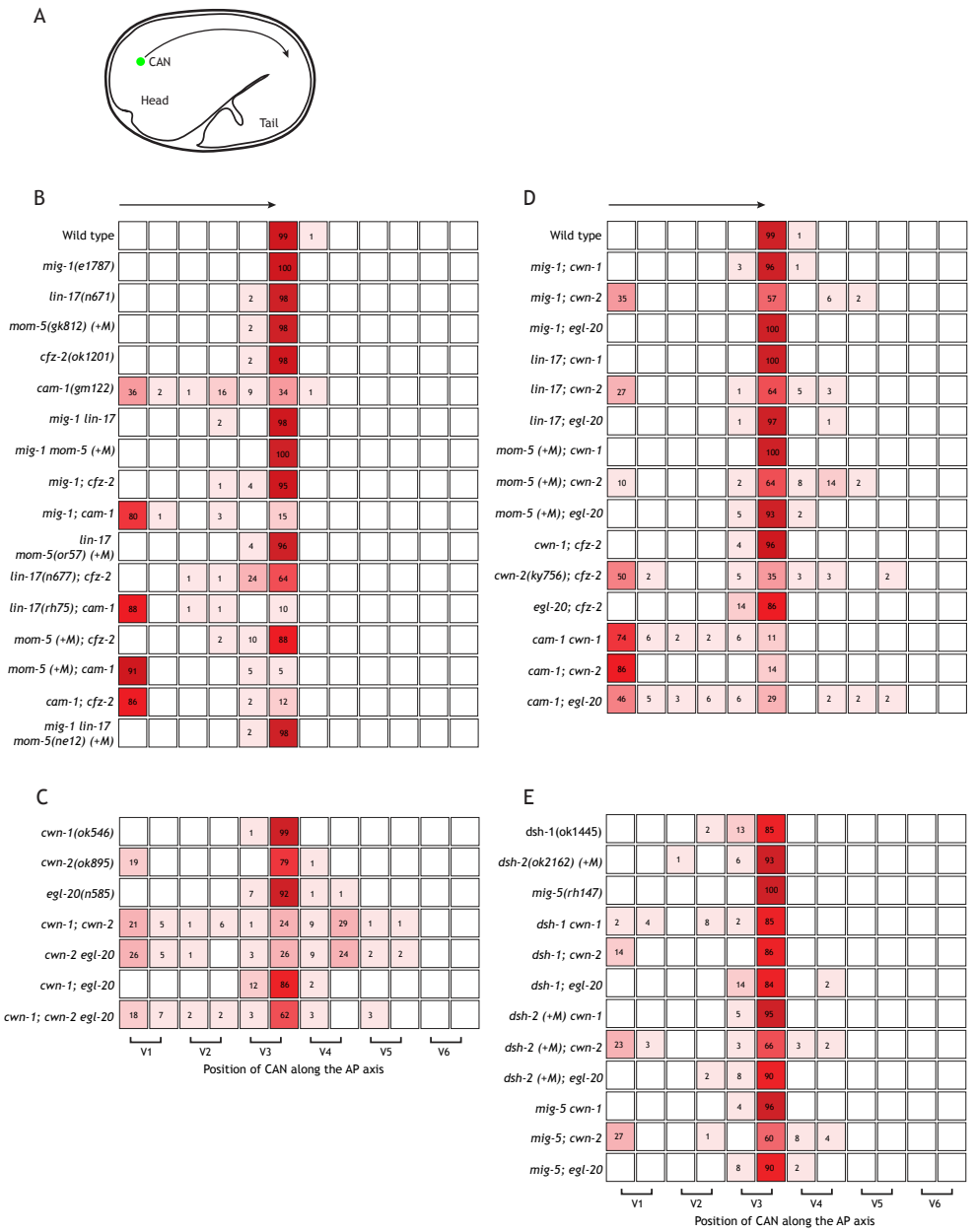

Figure 4. CAN migration is dependent on CAM-1. (**A**) Schematic representation of the posterior migratory route of the CAN neuron (green) during embryogenesis. (**B-E**) Average position of the CAN neurons in Wnt receptor mutants (**B**), Wnt mutants (**C**), Wnt/Wnt receptor double mutants (**D**) and Wnt/Dsh double mutants (**E**) with respect to the seam cells V1.a to V6.p (lower brackets indicate Vn.a (left) and Vn.p (right) daughters of Vn cells). Values listed are percentiles of total cells scored, n>50 for all genotypes. A color (red) coded heat map represents the range of percentile values.

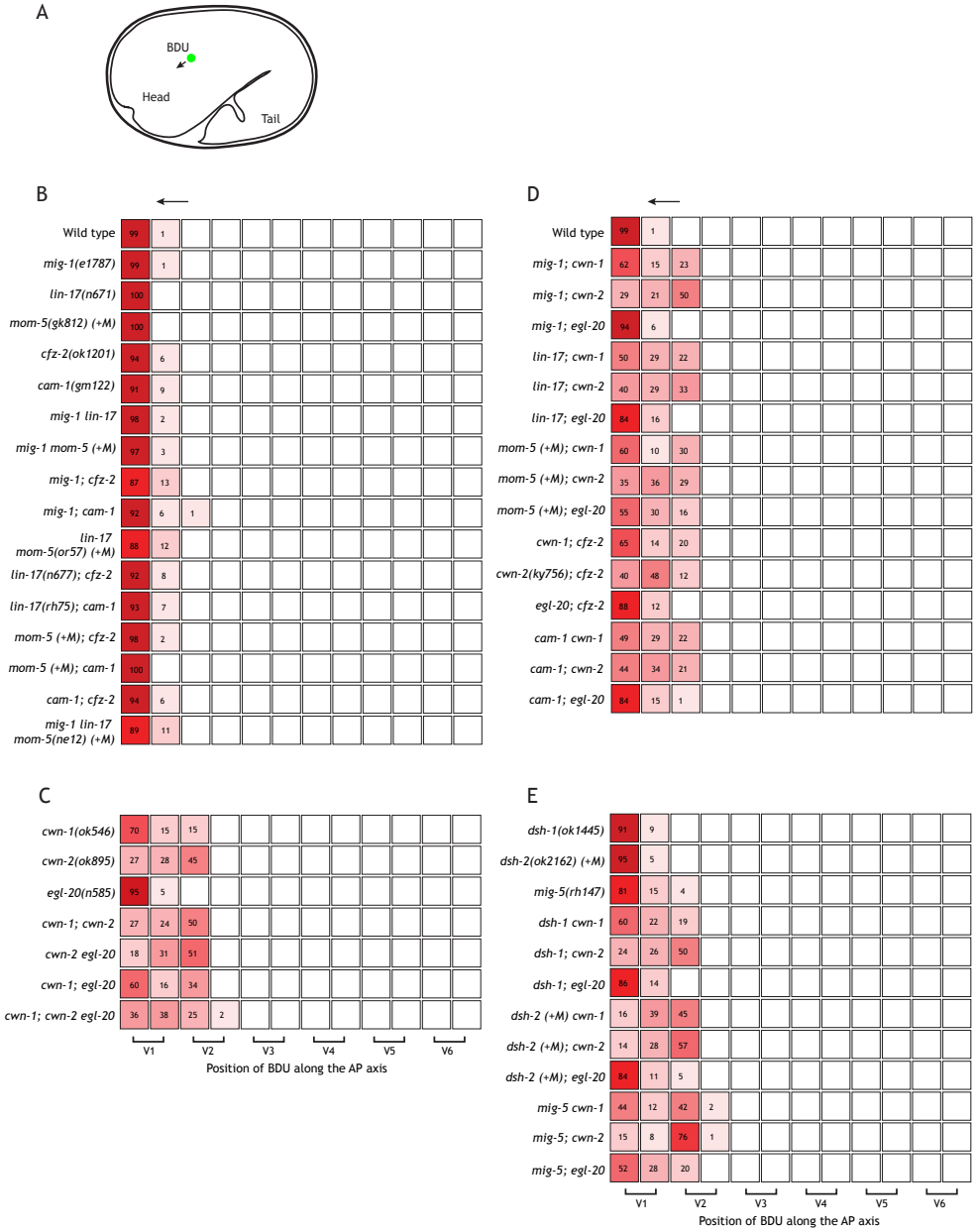

Figure 5. Multiple Wnt ligands and receptors redundantly regulate BDU migration. (**A**) Schematic representation of the anterior migratory route of the BDU neuron (green) during embryogenesis. (**B-E**) Average position of the BDU neurons in Wnt receptor mutants (**B**), Wnt mutants (**C**), Wnt/Wnt receptor double mutants (**D**) and Wnt/Dsh double mutants (**E**) with respect to the seam cells V1.a to V6.p (lower brackets indicate Vn.a (left) and Vn.p (right) daughters of Vn cells). Values listed are percentiles of total cells scored, n>50 for all genotypes. A color (red) coded heat map represents the range of percentile values.

well as varying degrees of CAN cell overmigration (Figure 4D). We conclude that *cam-1* is required for posterior migration of the CAN neurons, but that the correct positioning of the CAN neurons is dependent on a complex interplay between the different Wnt ligands and Frizzleds.

The three Dvl orthologs all appear to be required for CAN migration, but likely function redundantly, as only weak migration phenotypes were observed in single mutants or in combination with mutations in the different Wnt ligands (Figure 4E).

Multiple Wnt ligands and receptors redundantly regulate BDU migration

The BDU neurons migrate a very short distance anteriorly in a region just behind the head (Figure 5A). Their migration is mainly dependent on the Wnt ligands *cwn-1* and *cwn-2* (Figure 5C) (Zinovyeva et al., 2008), while *egl-20* has a minor role that becomes apparent in *cwn-1*; *egl-20* double mutants. Interestingly, mutations in none of the different receptors - either as single mutant or in mutant combinations - resulted in significant defects in BDU migration, indicating that there is a high degree of redundancy among the Wnt receptors (Figure 5B). Furthermore, most of the combinations of Wnt ligand and receptor mutants that we examined did not display a phenotype that significantly differed from the Wnt single mutants (Figure 5D). Exceptions were an undermigration phenotype in *mom-5*; *egl-20* double mutants and suppression of the *cwn-2* migration defect by loss of *cfz-2* or *cam-1* (Figure 5D). A role of *cfz-2* and *cam-1* is consistent with the expression of these receptors in BDU (Figures 1A and 1B). At the level of the Dvl orthologs, we found that *dsh-2* and *mig-5* are required for BDU migration (Figure 5E). *mig-5* mutation results in a mild defect in BDU migration and enhances the undermigration phenotype of each of the three Wnt ligand mutants, while *dsh-2* enhances the migration defect of *cwn-1*.

5

Discussion

During *C. elegans* embryogenesis, the bilateral pairs of HSN, ALM, CAN and BDU neurons migrate to specific positions along the anteroposterior axis. Previous studies have indicated that these migrations are controlled through complex Wnt dependent migration mechanisms (Zinovyeva et al., 2008). Here, we show that each of the migrating neurons expresses a unique combination of receptors. These receptors are essential for migration, but our results show that also receptors that are not expressed in the neurons influence their migration. We conclude that both cell autonomous and non-autonomous Wnt signaling mechanisms contribute to the correct positioning of the HSN, ALM, CAN and BDU neurons.

Expression analysis has revealed that the five Wnt genes of *C. elegans* are expressed in partially overlapping domains along the anteroposterior axis (Harterink et al., 2011). Of the Wnt ligands examined in this study, *egl-20* is expressed in the tail, *cwn-1* in the posterior mid-body region and *cwn-2* mostly in the head region. In agreement with this regionalized activity, we found that the migration of the HSN neurons from the tail to the mid-body is dependent on *egl-20*, while the migrations of CAN, ALM and BDU in the anterior body region all require *cwn-2*. However, Wnt ligands are secreted proteins and are therefore expected to diffuse over broader regions. Indeed, visualization of EGL-20 has shown that it forms a concentration gradient that ranges from the tail to the mid-body region (Coudreuse et al., 2006). Previous studies have shown that this gradient has a direct, instructive role in HSN migration by acting as a repulsive signal that guides the HSN neuron away from the source

of EGL-20 in the tail (Pan et al., 2006). Whether CWN-1 and CWN-2 also form gradients and act instructively in neuronal migration remains to be determined.

We found that the four migrating neurons express specific combinations of Wnt receptors. In each case, these receptors were required for migration, consistent with a cell autonomous function in the migration process. In addition, we found that other Wnt receptors influenced the migration of the embryonic neurons as well. Such cell non-autonomous functions can be explained through several mechanisms. First, loss of a Wnt receptor may influence the uptake and diffusion of its ligand and thereby change its range of activity. An example is the increase in intensity and range of the EGL-20 concentration gradient in *lin-17* Frizzled mutants (see **Addendum I**). Such modulation of Wnt ligand activity may explain some of the effects of the different Frizzled mutations on ALM and CAN cell migration. Second, a Wnt ligand or receptor may have a different site of action and influence migration indirectly. In *cam-1* mutants, for example, the CAN neuron is displaced anteriorly. As the CAN neuron acts as a barrier for HSN migration (Forrester et al., 2004; Pan et al., 2006), such an anterior shift in CAN position will result in a more anterior localization of the HSN neuron. Such an indirect effect may also explain the HSN undermigration observed in *cwn-1*; *cwn-2* and *cwn-2 egl-20* double mutants. We found that the CAN neurons migrate beyond their normal position in these double mutant combinations, and this posterior displacement may prevent the HSN neurons from migrating to their normal positions. Finally, Wnt ligands and receptors may act non-autonomously by influencing the expression of other guidance cues. With the exception of EGL-20, no other direct guidance signals for embryonic neuronal migrations have, however, been identified.

In each of the four neurons, we found that the expressed receptors act in parallel genetic pathways to control the migration process. Such parallel pathways may regulate different aspects of the migration, such as polarization, adhesion to the extracellular matrix or termination of migration once the cell reaches its final position. An example of such multilevel control of cell migration by Wnt signaling is the Wnt dependent migration of the QR.p descendants (Mentink et al., 2014, see also **Chapter 2**). The anterior migration of the QR.p descendants is dependent on CAM-1 and MOM-5, which control persistent polarization and migration speed, respectively, while MIG-1 is required to stop migration. Future studies will determine how in each of the four embryonic migrations different Wnt signaling pathways are utilized to guide the neurons to their precisely defined final position.

Experimental procedures

C. elegans strains and culture

General methods for *C. elegans* strain culture and maintenance were as previously described. Animals were cultured at 20°C using standard conditions (Lewis and Fleming, 1995). Bristol N2 was used as the wild type control. Mutant alleles and transgenes used in this study were: LGI: *mig-1(e1787)*, *lin-17(n671, n677, rh75)*, *mom-5(gk812, ne12, or57)/hT2 [bli-4(e937) let-?(q782) qIs48]*; LGII: *cwn-1(ok546)*, *dsh-2(ok2162)/mInI [mIs14 dpy-10(e128)]*, *dsh-1(ok1445)*, *mig-5(rh147)*, *cam-1(gm122, ks52)*; LGIV: *egl-20(n585)*, *cwn-2(ok895, ky756)*, *kyIs179 [Punc-86::GFP;lin-15(+)]*; LGV: *cfz-2(ok1201)*; LGX: *kyIs4 [Pceh-23::GFP; lin-15(+)]*.

Analysis of embryonic neuronal migrations

Final positions of ALM, HSN, CAN and BDU neurons were scored in late L1 larvae using

DIC microscopy. Neurons were identified based on nuclear morphology and positions were compared to stationary seam cells V1.a until V6.p.

Single molecule fluorescence in situ hybridization
The smFISH protocol to stain *C. elegans* embryo's was performed as described elsewhere (Ji and van Oudenaarden, 2012). Briefly, embryo's released from bleached gravid adults were grown 6 hours at 20°C and subsequently fixed using 4% paraformaldehyde, freeze cracked in liquid nitrogen and suspended in 70% ethanol. Embryo's were hybridized overnight at 37°C in the dark. Specific oligonucleotide probes were designed using a dedicated algorithm (www.singlemoleculefish.com) and coupled to fluorescent dyes Alexa 594 (*mig-1* and *cfz-2* probes), TMR (*lin-17* probe) or Cy5 (*mom-5* and *cam-1* probes). Embryo nuclei were counterstained using DAPI before mounting. Z-stacks with a slice thickness of 0.5 µm were obtained with a Leica DM6000 microscope, equipped with a Leica DFC360FX camera, 100x oil objective and TX2 (TMR), Y3 (Alexa 594), Y5 (Cy5), A4 (DAPI) and GFP filter cubes. Images were acquired with 1024 x 1024 resolution and subjected to a 2 x 2 binning. Manual quantification of mRNA was performed using the z-stacks. Only mRNA spots visible in at least two independent focal plains were counted. CAN neurons were visualized by a *Pceh-23::gfp* transgene, while ALM, HSN and BDU neurons could be identified using a *Punc-86::gfp* transgene. Analysis was performed using ImageJ v1.43u software.

Statistical analysis
Statistical analysis of ALM, HSN, CAN and BDU position was performed using Fisher's exact test. A Monte Carlo approximation, iterated 10.000 times using SPSS version 20, was used to estimate significance. Results were deemed significant if $p<0.05$.

Acknowledgements

We thank Cornelia Bargmann, Wayne Forrester, Hitoshi Sawa and the Caenorhabditis Genetics Center (University of Minnesota, Minneapolis) for strains and the Hubrecht Imaging Center (HIC) for assistance with microscopy. This work was funded by a grant from the Dutch Cancer Society (HUBR 2008-4114) (HCK).

References

Angers, S., and Moon, R.T. (2009). Proximal events in Wnt signal transduction. Nature reviews Molecular cell biology *10*, 468-477.

Cha, S.W., Tadjuidje, E., Tao, Q., Wylie, C., and Heasman, J. (2008). Wnt5a and Wnt11 interact in a maternal Dkk1-regulated fashion to activate both canonical and non-canonical signaling in Xenopus axis formation. Development *135*, 3719-3729.

Chilton, J.K. (2006). Molecular mechanisms of axon guidance. Developmental biology *292*, 13-24.

Clevers, H., and Nusse, R. (2012). Wnt/beta-catenin signaling and disease. Cell *149*, 1192-1205.

Coudreuse, D.Y., Roel, G., Betist, M.C., Destree, O., and Korswagen, H.C. (2006). Wnt gradient formation requires retromer function in Wnt-producing cells. Science *312*, 921-924.

Du, S.J., Purcell, S.M., Christian, J.L., McGrew, L.L., and Moon, R.T. (1995). Identification of distinct classes and functional domains of Wnts through expression of wild-type and chimeric proteins in Xenopus embryos. Molecular and cellular biology *15*, 2625-2634.

Eisenmann, D.M. (2005). Wnt signaling. Wormbook, 1-17.

Forrester, W.C., Dell, M., Perens, E., and Garriga, G. (1999). A C. elegans Ror receptor tyrosine kinase regulates cell motility and asymmetric cell division. Nature *400*, 881-885.

Forrester, W.C., Kim, C., and Garriga, G. (2004). The Caenorhabditis elegans Ror RTK CAM-1 inhibits EGL-20/Wnt signaling in cell migration. Genetics *168*, 1951-1962.

Gao, C., and Chen, Y.G. (2010). Dishevelled: The hub of Wnt signaling. Cellular signalling *22*, 717-727.

Harterink, M., Kim, D.H., Middelkoop, T.C., Doan, T.D., van Oudenaarden, A., and Korswagen, H.C. (2011). Neuroblast migration along the anteroposterior axis of C. elegans is controlled by opposing gradients of Wnts and a secreted Frizzled-related protein. Development *138*, 2915-2924.

Hedgecock, E.M., Culotti, J.G., Hall, D.H., and Stern, B.D. (1987). Genetics of cell and axon migrations in Caenorhabditis elegans. Development *100*, 365-382.

Ji, N., Middelkoop, T.C., Mentink, R.A., Betist, M.C., Tonegawa, S., Mooijman, D., Korswagen, H.C., and van Oudenaarden, A. (2013). Feedback control of gene expression variability in the Caenorhabditis elegans Wnt pathway. Cell *155*, 869-880.

Ji, N., and van Oudenaarden, A. (2012). Single molecule fluorescent in situ hybridization (smFISH) of C. elegans worms and embryos. Wormbook, 1-16.

Kim, G.H., Her, J.H., and Han, J.K. (2008). Ryk cooperates with Frizzled 7 to promote Wnt11-mediated endocytosis and is essential for Xenopus laevis convergent extension movements. The Journal of cell biology *182*, 1073-1082.

Korswagen, H.C. (2002). Canonical and non-canonical Wnt signaling pathways in Caenorhabditis elegans: variations on a common signaling theme. BioEssays : news and reviews in molecular, cellular and developmental biology *24*, 801-810.

Lewis, J.A., and Fleming, J.T. (1995). Basic culture methods. Methods in cell biology *48*, 3-29.

Liu, Y., Shi, J., Lu, C.C., Wang, Z.B., Lyuksyutova, A.I., Song, X.J., and Zou, Y. (2005). Ryk-mediated Wnt repulsion regulates posterior-directed growth of the corticospinal tract. Nature neuroscience *8*, 1151-1159.

Lyuksyutova, A.I., Lu, C.C., Milanesio, N., King, L.A., Guo, N., Wang, Y., Nathans, J., Tessier-Lavigne, M., and Zou, Y. (2003). Anterior-posterior guidance of commissural axons by Wnt-frizzled signaling. Science *302*, 1984-1988.

Marin, O., Valiente, M., Ge, X., and Tsai, L.H. (2010). Guiding neuronal cell migrations. Cold Spring Harbor perspectives in biology *2*, a001834.

Mentink, R.A., Middelkoop, T.C., Rella, L., Ji, N., Chung, Y.T., Betist, M.C., van Oudenaarden, A., and Korswagen, H.C. (2014). Cell intrinsic modulation of Wnt signaling controls neuroblast migration in C. elegans. Developmental cell *in press*.

Mikels, A.J., and Nusse, R. (2006). Purified Wnt5a protein activates or inhibits beta-catenin-TCF signaling depending on receptor context. PLoS biology *4*, e115.

Pan, C.L., Howell, J.E., Clark, S.G., Hilliard, M., Cordes, S., Bargmann, C.I., and Garriga, G. (2006). Multiple Wnts and frizzled receptors regulate anteriorly directed cell and growth cone migrations in Caenorhabditis elegans. Developmental cell *10*, 367-377.

Petersen, C.P., and Reddien, P.W. (2009). Wnt signaling and the polarity of the primary body axis. Cell *139*, 1056-1068.

Raj, A., van den Bogaard, P., Rifkin, S.A., van Oudenaarden, A., and Tyagi, S. (2008). Imaging individual mRNA molecules using multiple singly labeled probes. Nature methods *5*, 877-879.

Salinas, P.C. (2012). Wnt signaling in the vertebrate central nervous system: from axon guidance to synaptic function. Cold Spring Harbor perspectives in biology *4*.

Shimizu, H., Julius, M.A., Giarre, M., Zheng, Z., Brown, A.M., and Kitajewski, J. (1997). Transformation by Wnt family proteins correlates with regulation of beta-catenin. Cell growth & differentiation : the molecular biology journal of the American Association for Cancer Research *8*, 1349-1358.

Sulston, J.E., Schierenberg, E., White, J.G., and Thomson, J.N. (1983). The embryonic cell lineage of the nematode Caenorhabditis elegans. Developmental biology *100*, 64-119.

Tao, Q., Yokota, C., Puck, H., Kofron, M., Birsoy, B., Yan, D., Asashima, M., Wylie, C.C., Lin, X., and Heasman, J. (2005). Maternal wnt11 activates the canonical wnt signaling pathway required for axis formation in Xenopus embryos. Cell *120*, 857-871.

van Amerongen, R., Bowman, A.N., and Nusse, R. (2012a). Developmental stage and time dictate the fate of Wnt/beta-catenin-responsive stem cells in the mammary gland. Cell stem cell *11*, 387-400.

van Amerongen, R., Fuerer, C., Mizutani, M., and Nusse, R. (2012b). Wnt5a can both activate and repress Wnt/beta-catenin signaling during mouse embryonic development. Developmental biology *369*, 101-114.

Wallingford, J.B., Vogeli, K.M., and Harland, R.M. (2001). Regulation of convergent extension in Xenopus by Wnt5a and Frizzled-8 is independent of the canonical Wnt pathway. The International journal of developmental biology *45*, 225-227.

Zinovyeva, A.Y., and Forrester, W.C. (2005). The C. elegans Frizzled CFZ-2 is required for cell migration and interacts with multiple Wnt signaling pathways. Developmental biology *285*, 447-461.

Zinovyeva, A.Y., Yamamoto, Y., Sawa, H., and Forrester, W.C. (2008). Complex network of Wnt signaling regulates neuronal migrations during Caenorhabditis elegans development. Genetics *179*, 1357-1371.

Chapter 6

Quantitative single molecule mRNA fluorescent *in situ* hybridization in *C. elegans*

Remco A. Mentink[1,4], Ni Ji[2,3,4], Alexander van Oudenaarden[1,2] and Hendrik C. Korswagen[1]

[1]Hubrecht Institute, Royal Netherlands Academy of Arts and Sciences and University Medical Center Utrecht, Utrecht, The Netherlands. [2]Department of Physics and department of Biology, [3]Department of Brain and Cognitive Sciences, Massachusetts Institute of Technology, Cambridge, Massachusetts, USA.

[4]These authors contributed equally to this work.

Adapted from Neuromethods "In situ hybridization methods", in press

Abstract

One of the key steps in determining the biological function of a gene of interest is to examine its expression pattern. Traditionally, gene expression in *C. elegans* has mostly been studied through reporter transgenes in which upstream regulatory sequence is fused to marker genes such as Green Fluorescent Protein (GFP) or lacZ. In addition, expression can be determined through RNA *in situ* hybridization or antibody staining. An important downside of these different approaches is that gene expression is not measured quantitatively. Here, we describe a technique termed single molecule mRNA fluorescent *in situ* hybridization (smFISH) that visualizes endogenous mRNA transcripts of the gene of interest at single molecule resolution. These smFISH spots can be computationally counted to provide a highly quantitative measure of gene expression *in vivo*.

1. Introduction

The expression pattern of a gene – in which cells, at what developmental stages, and at what level it is expressed – provides important information on its biological function. Different techniques have been developed to study gene expression in *C. elegans*. The approach that is most frequently used is to fuse upstream promotor sequence of the gene of interest to reporter genes such as GFP or lacZ (Boulin et al., 2006). After generation of transgenic lines, expression of the reporter gene will reflect the expression pattern of the endogenous gene. A potential problem with this approach is that not all regulatory sequences may be included in the reporter transgene, resulting in incomplete or ectopic expression (Boulin et al., 2006). Furthermore, the read-out of GFP fluorescence or lacZ activity only provides an indication of expression levels and not a precise quantitative value. Other techniques include antibody staining and RNA *in situ* hybridization (ISH) (Shakes et al., 2012; Tabara et al., 1996), but these are notoriously difficult to perform in larval and adult stages and also provide only limited quantitative information on gene expression levels. Therefore, a novel mRNA ISH method (smFISH) was developed that – in addition to being much more robust than traditional ISH methods – allows the quantitative measurement of mRNA transcripts *in vivo* (Raj et al., 2008).

To perform smFISH, a library of 48 relatively short oligonucleotide probes is generated that covers the mRNA transcript of the gene of interest. As each of the oligonucleotides is labeled with a single fluorophore, binding of the probes to the target mRNA will yield a bright diffraction-limited speck of fluorescence that corresponds to a single mRNA molecule (Raj et al., 2008). In contrast to previously described attempts at high-resolution mRNA detection, this method generates uniform signals that can be computationally identified to yield accurate mRNA counts. Combined with the power of the *C. elegans* system, the smFISH techniques can be used to study many aspects of gene expression regulation in development and physiology. An example of an important discovery that was made with this technique is that incomplete penetrance of certain mutants in *C. elegans* can be explained by variability in gene expression (Raj et al., 2010). Another example of smFISH analysis is the quantification of Wnt gene expression along the anteroposterior axis of *C. elegans*, which revealed that Wnt genes are expressed in an evolutionarily conserved pattern (Harterink et al., 2011).

The smFISH method is performed in three steps. First, a set of oligonucleotide probes (typically 17-22 base pairs in length) is designed to target the mRNA of interest. Next, the oligonucleotides are pooled, coupled to a single fluorophore and purified to generate the probe mixture. Finally, the probe is added to fixed animals to stain the mRNA of interest.

2. Materials

Below we provide a list of all chemicals and materials required to perform each step of the smFISH procedure in *C. elegans*. Storage conditions are room temperature (RT) unless indicated otherwise. We provide coupling and purification protocols for the preparation of smFISH probes. Alternatively, labeled and purified smFISH probes can also be directly ordered from Biosearch Technologies (Novato, CA).

2.1 Probe coupling and purification

- DMSO (if coupling to TMR)
- 0.1 M Sodium Bicarbonate (in RNase free water, pH 8.0) (see **Note 1**)
- 1 M Sodium Bicarbonate (in RNase free water, pH 8.0) (see **Note 1**)
- Ethanol (>95% pure)
- 3 M Sodium Acetate, pH 5.2
- Fluorophore with succinimidyl ester group
- 0.1 M Triethylammonium acetate, pH 6.5, filtered and degassed (Buffer A)
- Acetonitrile for HPLC (Buffer B)
- HPLC with a dual wavelength detector to measure both DNA and fluorophore absorbtion
- C18 Column for HPLC, 218TP104
- Speedvac rated for acetonitrile

2.2 C. elegans fixation

- Bleaching solution (per 50 mL, store at 4°C)
  - 16.6 mL "thin bleach" (5% NaHOCl)
  - 2.50 mL 5M NaOH
  - 30.9 mL ultrapure water (e.g. Milli-Q, MQ)
- M9 buffer (per 1L) (with and without +0.05% Tween-20) (see **Note 2**)
  - 3.0 g KH_2PO_4
  - 6.0 g Na_2HPO_4
  - 5.0 g NaCl
  - Add MQ to 1 L
  - (Add 500 µL of Tween-20)
  - Autoclave
  - After cooling, add 1 mL of 1M $MgCl_2$
- 4% paraformaldehyde (PFA) solution in PBS (prepare PBS in RNAse free water)
- PBS in RNAse free water (with and without +0.05% Tween-20) (see **Note 2**)
- 70% ethanol in RNAse free water

2.3 Probe hybridization

- Hybridization buffer (per 10 mL, aliquot in 200 µL units and keep at -80°C for long-term storage)
  - 1.0 g Dextran sulfate (see **Note 3**)
  - 10 mg *E. coli* tRNA
  - 100 µL 200 mM vanadyl riobonucleoside complex (NEB)
  - 40 µL 50 mg/mL RNase free BSA (Ambion)
  - Formamide (deionized, Ambion) (see **Note 4**)
  - Add RNAse free water to a total volume of 10 mL
- Wash buffer (per 50 mL)
  - Formamide (deionized, Ambion): use the same concentration as in the hybridization buffer.
  - 5 mL 20x SSC in RNAse free water

250 µL of 10% Tween-20 in RNAse free water
Add RNAse free water to a total volume of 50 mL

- DAPI stain (prepare working stock of 25 ng/mL in RNAse free water)
- 2x SSC in DEPC water (prepare from 20x SSC)
- Antifade buffer (1 mL, prepare fresh each time)
  850 µL of RNAse free water
  100 µL of 20x SSC in RNAse free water
  40 µL of 10% glucose in RNAse free water
  10 µL of 1M Tris-Cl
- Glycosidase (Sigma-Aldrich) stock (dilute Glox in 50 mM sodium acetate to 3.7 mg/mL, adjust pH to 5.0. Aliquot in 100 µL units and store at -20°C)
- Catalase (Sigma-Aldrich, store at 4°C)

2.4 Image acquisition

- A standard wide-field fluorescence microscope (we use a Leica DM6000) (see **Note 5**).
- A strongly emitting light-source such as a mercury or metal-halide lamp. In general a brighter lamp will allow for better spot detection and shorter exposure times.
- Excitation, dichroic and emission filter sets compatible with the fluorophore that is used.
- A CCD camera that is optimized for imaging with low-level light.
- A high NA (>1.3) 100x DIC objective. Images can also be acquired using a 63x objective, but (automatic) spot detection will be more difficult.
- Standard microscopy software that allows for storage of sample positions and z-stack imaging.

3. Methods

3.1 Probe design

smFISH probes should be short (typically 17-22 bp) DNA oligos that target well separated regions (no less than 2 bp apart) in the RNA transcript. The optimal GC content is 45% while the total number of probes used is typically between 30-96 (as low as 20 has been found to work).

When designing probes, it is good practice to blast probe sequences against the genome of interest. Probes with high homology to ORFs outside the region of interest should be avoided. Web-based probe design software developed by Raj *et al*. (2008) is available free of charge through the Biosearch Technologies (Novato, CA) website: http://www.biosearchtech.com/stellarisdesigner/. Probe sequences designed through this web interface can then be directly submitted for probe synthesis.

3.2 Probe synthesis

Following probe design, smFISH probes can be synthesized *en masse* using 96-well DNA synthesizers. Biosearch Technologies (Novato, CA) offers a synthesizing service for custom-designed smFISH probes. Depending on experimental needs, researchers may either order

probes readily coupled to the desired fluorophores or obtain uncoupled probes and proceed with in-house coupling. If performing in-house coupling, the probes should be ordered with a 3' amine group to allow subsequent oligo-fluorophore conjugation. Additionally the oligos should be desalted and re-suspended in water as opposed to Tris EDTA.

Commonly used commercially available fluorophores are: Cy5 (GE Amersham), Alexa 594 (Molecular probes, Invitrogen) and tetramethylrhodamine (TMR) (Molecular Probes, Invitrogen). While choosing fluorophores, it is important to keep in mind that different fluorophores can vary in photostability and background autofluorescence level. For example, Cy5 bleaches easily and requires the use of fresh anti-bleaching agents (e.g. glycosidase and catalase) to prevent the decay of fluorescent signal. Furthermore, fluorophores with shorter emission wavelengths (such as Alexa 488) tend to lead to higher background fluorescence signals. It is also desirable to avoid using fluorophores with close excitation/emission wavelengths so as to minimize bleed-through of signal from one fluorescence channel to another.

3.3 Probe coupling and purification

Day 1:

1. From the uncoupled probe stock, combine 1 nmol (e.g. 10 µL from a 100 µM stock) of each probe into a single microcentrifuge tube.
2. Add 0.11 volumes 1 M sodium bicarbonate to give a final concentration of 0.1 M. If the total volume at this stage is < 0.3 mL, add additional 0.1 M sodium bicarbonate to bring the total volume to 0.3 mL.
3. Dissolve a small amount (roughly 0.2 mg) of dye into 50 µL of 0.1 M sodium bicarbonate (see **Note 6**).
4. Add the dissolved fluorophore to the oligos.
5. Cover the tube in foil to prevent photo bleaching and let the reaction proceed overnight at room temperature with gentle rocking.

Day 2:

6. In the morning, precipitate the oligos by adding 10% volume/volume of 3M sodium acetate and then adding 2.5 volumes of 100% EtOH. Store at –70°C for at least 1 hour (up to overnight).
7. Spin down the sample in a 4°C microcentrifuge for at least 15 minutes at maximum speed (~16.000 g).
8. After centrifugation, one should see a small colored pellet at the bottom of the tube. Aspirate away the fluorescent supernatant (containing uncoupled dye molecules) as completely as possible. If purification is not performed right away, the pellet is stable and can be stored at -20°C.

Day 2 (if continued immediately after coupling step 8):

9. Resuspend pellet in appropriate volume (0.1 to 0.5 mL nuclease free water, depending on the HPLC setup).

10. Inject the coupled probe onto the column and run a program in which the percentage of buffer B varies from 7% to 30% over the course of around 30 minutes with a flow rate of 1 mL/minute (see **Note 7**).
11. As the program proceeds, one will observe two broad peaks in the measured absorption wavelengths (Figure 1). The first contains uncoupled probes and will only show a peak in the 260 nm channel. The second contains pure coupled probes and will show peaks in both channels. The two peaks will typically be separated by a few minutes of time or longer, with TMR having narrowly separated peaks and Cy5 having broadly separated peaks. With a series of microcentrifuge tubes, collect the entire second peak as soon as the signal begins to rise and until it drops back to the baseline.

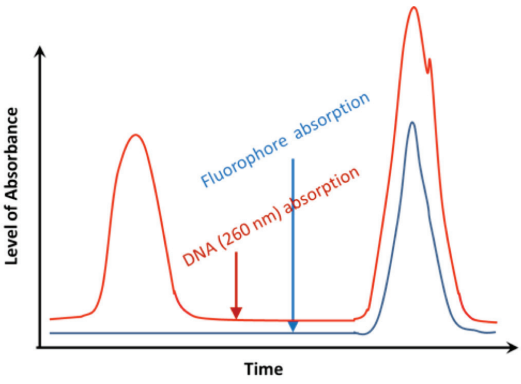

Figure 1. Schematic overview of a typical HPLC readout during probe purification. The first peak (in the DNA absorption channel only) corresponds to uncoupled probes. The second peak (in both the DNA and the fluorophore channels) corresponds to coupled probes. The onset of the second peak signifies the time to start collecting the output.

Day 3:

12. Dry the purified probes in a speedvac (~ 3-5 hours for 0.5 mL) (see **Note 8**).
13. Resuspend all tubes together in a total volume of 50-100 µL TE, pH 8.0 (equivalent to roughly 0.1-1 µM). This is the concentrated probe stock.
14. (Optional) Dilute this probe 1:10, 1:20, 1:50 and 1:100 in TE to make working stocks for testing probe concentration.
15. At this point, probe synthesis is complete. Probes can be stored in TE at -20°C for years.

3.4 C. elegans fixation

Animals of any age can be fixed for use in smFISH experiments. The fixation of embryo's requires a freeze-cracking step in order to break the impermeable eggshell.

Fixation for larvae and adults:

1. Grow animals on NGM plates seeded with OP50 bacteria (see **Note 9**).
2. Wash animals from plates using 5 ml M9 buffer and transfer to 15 mL conical centrifuge tube (see **Note 10**).
3. Spin down the animals at 1200 rpm for 1 min and aspirate solution.
4. Wash animals using 5 mL M9 buffer (see **Note 11**).
5. Spin down the animals and aspirate (see **Note 12**).
6. Add 1 mL fixation solution and rotate tube for 45 min at RT (see **Note 13**).

7. Wash using 1 mL of PBS + 0.05% Tween-20 (or, if an increased volume of fixation solution was used due to having a large amount of animals, use that same volume of PBS).
8. Wash using the same volume of PBS without added Tween-20.
9. Spin and resuspend the animals in 1 mL 70% ethanol (again considering the previously used volumes) and store at 4°C (animals can be kept at this temperature for 1 month).

Fixation for embryos:

1. Grow animals on NGM plates seeded with OP50 bacteria until many gravid adults or obtained (see **Note 14**).
2. Wash animals from plates using 5 ml M9 buffer and transfer to 15 mL conical centrifuge tube (see **Note 10**).
3. Spin down the animals at 1200 rpm for 1 min and aspirate solution. Add 5 mL of bleaching solution and incubate while regularly inverting the tube until the adult animals are completely dissolved (~5-8 mins) (see **Note 15**).
4. Add 10 mL of ice-cold M9 buffer + 0.05% Tween-20 to stop the bleaching process, spin down the embryos and aspirate.
5. Wash with 10 mL of ice-cold M9 buffer + 0.05% Tween-20.
6. Wash with 10 mL of M9 buffer without added Tween-20.
7. Spin down and resuspend embryos in 1 mL fixation solution, transfer to microcentrifuge tube and rotate for 15 mins at RT (see **Note 16**).
8. Vortex and submerge tube in liquid nitrogen for 1 min to freeze crack the eggshells.
9. Thaw in water at RT.
10. Vortex thawed tube and incubate on ice for 20 mins.
11. Wash twice using 1 mL PBS (Adding +0.05% Tween-20 on the first wash).
12. Spin and resuspend embryos in 1 mL 70% ethanol and store at 4°C (embryos can be kept at this temperature for 1 week).

3.5 Probe hybridization

Day 1:

1. Prepare hybridization solution: to 100 µL of hybridization buffer add 1 µL of each probe at the appropriate concentration and vortex (see **Note 17** and **18**).
2. Transfer fixed animals to a microcentrifuge tube and spin twice for 30 sec at 1600 rpm, once having the cap hinge facing up and once facing down. Aspirate away the ethanol, careful not to disturb the pellet (see **Note 19**).
3. Add 1 mL of wash buffer, which contains the same amount of formamide as the hybridization buffer used. Let stand for 2-5 minutes.
4. Spin twice for 30 sec at 1600 rpm and aspirate.
5. Add the hybridization solution, vortex and incubate in the dark overnight at 37°C.

Day 2:

6. The next morning, add 1 mL of wash buffer to the sample, vortex, spin twice and aspirate. Then add another 1 mL of wash buffer, vortex and incubate in the dark at

37°C for 1 hr.
7. Wash using 1 mL of wash buffer and incubate in the dark at 37°C for 1 hr.
8. Spin down and aspirate. Resuspend in 1 mL wash buffer.
9. Add 10 µL DAPI working stock for nuclear counterstain and incubate in the dark at 37°C for 15 mins.
10. Spin down and aspirate. Resuspend in 1 mL 2x SSC, vortex, spin down and aspirate.
11. If imaging without using antifade solution (possible for Alexa594 and TMR labeled probes) resuspend in 100 µL 2x SSC and proceed to imaging.
12. If imaging with antifade solution, add 1 µL glycosidase and 1 µL catalase to 100 µL antifade buffer in a separate microcentrifuge tube. Resuspend the animals in the leftover buffer (900 µL). Let stand for 1-2 mins, spin and resuspend in the 100 µL antifade solution with enzymes. Proceed to imaging (see **Note 20**).

3.6 Image acquisition

1. Pipette 24 µL of the sample on a 24 mm x 32 mm cover glass, using a yellow tip from which the extreme end was cut using a razor to prevent damaging the animals through suction.
2. Gently lower a microscope slide onto the drop of sample solution to adhere the cover glass to the slide.
3. Quickly flip the microscope slide to have the cover glass face up and gently remove excess sample solution from the rim using a tissue (see **Note 21** and **22**).
4. Mount the microscope slide on the microscope stage with the cover glass facing the objective. Proceed to finding individual larvae or embryos for imaging.

Images should be acquired as z-stacks with 0.5µm spacing between the single stacks. If the signal intensity of the smFISH spots is low in comparison to the background signal, 2x2 binning can be used during the acquisition.

3.7 Expected results

If successful, an smFISH experiment will yield bright fluorescent spots representing single mRNA molecules. The optical diffraction limit of these spots (200-500 nm) is below that of a typical widefield microscope (1 µm). Spots should have a distinct, round morphology and be readily identifiable by eye. Usually the signal intensity of different spots will be similar, but transcription centers can be detected that are much brighter in intensity. It is possible though that a (trans)gene is so highly expressed that different spots will overlap and form a so-called “fireball”. In this case reliable quantification is unfortunately not possible. Transgenic markers that are expressed in specific cells can be used to outline cells and count transcripts in these cells only. Figure 2 gives an example of a smFISH experiment in which the expression of *prkl-1* mRNA is probed in descendants of the QR neuroblast. *prkl-1* is the *C. elegans* homologue of the PCP gene PRICKLE and has previously been found to be involved in neurite outgrowth (Gubb et al., 1999; Huarcaya Najarro and Ackley, 2013; Sanchez-Alvarez et al., 2011). The expression of *prkl-1* mRNA changes in time and is found to be higher in the QR.pa cell than in the QR.p cell. A transgenic marker that expresses GFP to mark both the cell membrane and nucleus is used to identify the QR cell lineage.

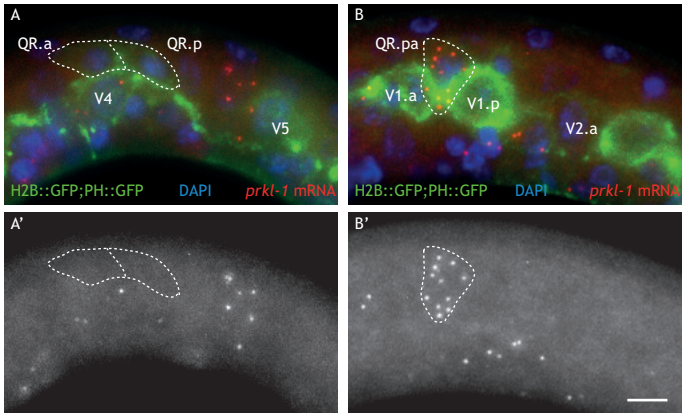

Figure 2. Staining of *prkl-1* mRNA in L1 larvae. (**A, B**) smFISH staining of *prkl-1* mRNA (red) in whole L1 larvae. Seam cells and QR descendants are marked with nuclear and membrane GFP (green). DAPI is used as nuclear counterstain (blue). Shown is a maximum projection of chosen stacks. (**A', B'**) Grayscale representation of the images displayed in **A** and **B**. Scale bar is 5 µm.

3.8 Data analysis

Because of its single-molecule resolution, smFISH is readily compatible with a variety of quantitative analyses. Computer-aided image analysis allows data processing and quantification to be carried out in a rapid, consistent, and semi-automated manner. Below we introduce common building blocks to a custom-written image analysis software and list common algorithms used to execute each computational step. The order of the following steps is not unique and should be tailored to fit different analysis needs.

3.8.1 Importing image data

Common graphical file formats, such as .tiff or .stk, cannot be directly analyzed by certain computing software (e.g. MATLAB). However, built-in functions often exist to convert raw images into data structures suitable for downstream processing. Each raw image is typically converted into a data structure containing the original pixel values. At this step, images from multiple stacks or channels can be concatenated into a single data structure or merged for ease of visual display.

3.8.2 Image segmentation and annotation

To assign an smFISH signal to a specific cell or tissue, the tissue or cell of interest must be demarcated from the rest of the image. Additionally, tracing and annotating also enables information such as cell position or tissue size to be extracted in parallel to the gene expression data. Oftentimes, visible tissue landmarks can be combined with patterns of DAPI staining, antibody staining, GFP reporter expression, as well as smFISH staining to guide the identification of the region of interest (ROI).

To perform supervised (manual or semiautomatic) segmentation, a user interface can be established where image data are displayed on the screen and the researcher allowed to draw, mark, or annotate onto particular regions of the graph (Figure 3). The traces drawn can be read into the computer as cursor positions and the annotations can be stored as either text strings or numbers (see Table 1 for related MATLAB functions).

While a greater challenge, fully automated image segmentation can be made possible

with the right type of tissue landmark and computational algorithm. The central idea of an automated segmentation algorithm is to identify regions in an image that enrich for specific markers (e.g. GFP, smFISH staining) or bear particular morphological features (e.g. shape or size). To ensure robust ROI identification, multiple rounds of image enhancement (see section 3.8.3 Image sharpening) followed by computational transformation (see Table 1 for related MATLAB functions) are often necessary.

After segmentation, the tracings and annotations can be saved as separate data files to be called later for region-specific spot counting and other analyses.

Table 1. MATLAB functions useful for semi-automated analysis of smFISH data.

	Function name	Description
Importing image data	*imread*	Reads image data from graphical files. Compatible with many common formats including .tiff, .jpeg, .png, .bmp.
	tiffread2	Available online at MATLAB Central: http://www.mathworks.com/matlabcentral/fileexchange/10298.
Image enhancement	*imadjust*	Adjust image intensity values by mapping a range of input values to a range of output values.
	deconvreg	Deblurs an image by deconvolving with its known or estimated point spread function (PSF).
	fspecial	Creates the correlation matrix of a pre-defined 2D filter (e.g. LoG filter) to be used in the function *imfilter*.
	imfilter	Filters multidimensional image with an custom-defined filter.
	convn	Convolves image data with an N-dimensional filter.
	edge	Detects edges in a grayscale image.
	imtophat	Smoothens uneven background illumination using top-hat transform.
Image segmentation	*roipoly*	Initiates interactive polygon tool to allow manual outline of the ROI.
	imcrop	Crops one or a set of images based on the mask.
	watershed	Useful for detecting objects that are partially overlapping.
	regionprops	Extract quantitative properties of an image object, including area, outline, center position, and max and min intensity value.
ROI based spot detection	*bwlabeln*	Label connected components in an image. Useful for detecting smFISH spots.
	imregionalmax	Finds local maxima for regions of custom-defined size; a single smFISH spot should contain one regional maxima, whereas multiple juxtaposed spots would contain multiple maxima.
	inpolygon	Detects whether a particular point is inside a 2D polygon.

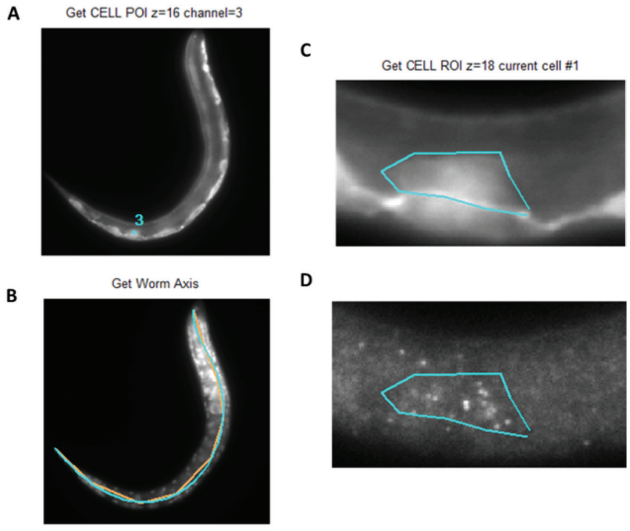

Figure 3. Segmentation and feature extraction performed on smFISH images. (**A**) Annotation of cell or tissue landmarks on a fluorescent image of an L1 larva. The annotation (cyan) as well as its coordinate information can be saved as data files for later analysis. Seam cells and the Q neuroblasts are marked with nuclear and membrane GFP (bright white). (**B**) Tracing and measurement for the tissue of interest. The body axis of the worm is manually traced out (light orange lines) based on the DAPI signal (bright white). The software then fits a spline (cyan curve) to the tracings and estimates the length of the animal based on the length of the fitted spline. (**C**) Cropping and segmenting the region of interest (ROI). The image in **A** is cropped to preserve only the cell of interest (the QL neuroblast). The boundary of the cell is manually traced (cyan) based on the membrane-bound GFP marker (bright white). (**D**) The segmented ROI can be subsequently used to quantify smFISH spots within the cell. Shown here is smFISH staining for *mab-5* mRNA.

3.8.3 Image enhancement

Even with an optimized probe design and hybridization protocol, factors such as tissue auto-fluorescence and out-of-focus light can obscure the smFISH signal, making automatic spot detection difficult. The image enhancement techniques outlined below can often effectively circumvent these issues.

Deblurring: The point spread function (PSF) describes how a single point light source is diffracted by the imaging set up and can thus explain a large portion of blurring in the image. If the PSF is known, one may deconvolve the raw image with the PSF to restore the "true" appearance of the specimen. Otherwise, the PSF can be determined by imaging fluorescent beads with sub-resolution sizes (e.g. 200 nm in diameter) and fitting the obtained image with a multi-dimensional Gaussian distribution.

Enhancing contrast: Global (image-wide) contrast enhancement can be achieved by rescaling the range pixel intensities of the image. Algorithmically, one may first assign an upper intensity value to be mapped to white (highest intensity on a greyscale), and a lower intensity value to black (lowest intensity). All intensity values in between the upper and lower bounds can then be proportionally mapped to new values on a greyscale.

Local contrast enhancement can be achieved by convolving each image file (i.e. a matrix consisting of individual pixel values) with two mathematical functions (kernels), a Gaussian followed by a Laplacian. In practice the two functions can be convolved first to form a computational filter called the Laplacian of Gaussian (LoG). In effect, the Gaussian filter smoothens the background to reduce small speckles that could be confused with real spots,

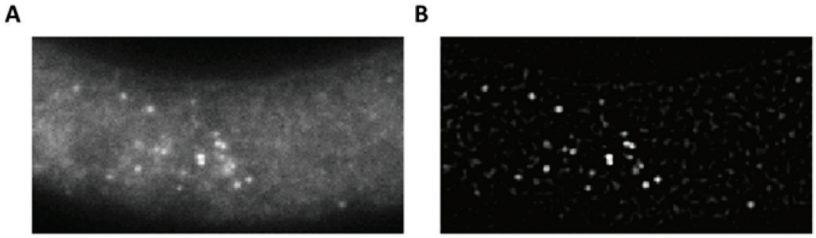

Figure 4. Effects of LoG filtering on an smFISH image. (**A**) smFISH staining of *mab-5* mRNA in an L1 larva (shown is a single image from a stack). (**B**) The same image after convolution by a LoG filter with parameters μ=12 and σ=1.2. Note the strong reduction in background and the amplification of the smFISH signal.

while the Laplacian filter performs edge detection by amplifying the contrast between adjacent dim and bright pixels (Figure 4). In principle, the Full Width at Half Maximum (FWHM, related to the standard deviation by a factor of $\sqrt{8\ln(2)}$) of the filter should equal the expected width of the signal (e.g. the width of the smFISH spot or the tissue landmark used for segmentation). Alternatively the optimal FWHM can be found by trial and error through visually comparing the filtered and original images. In addition to the LoG filter, the Sobel filter also effectively sharpens the edges of objects in an image. In practice, it is often more convenient to use the negative of the LoG or Sobel filtered image, as the filtered image would otherwise appear as a negative of the original image (see **Note 23**).

3.8.4 Spot detection

Since smFISH signals are often much brighter than the background, individual smFISH spots can be reliably detected by identifying connected regions in the image with pixel intensities above a certain threshold. This threshold can be determined by systematically screening threshold values in incremental steps from the minimum to the maximum pixel intensities. For a given threshold value, the software identifies filled regions, or "connected objects", wherein all pixel values are above threshold. Most often, each filled region corresponds to one smFISH spot, or one labeled mRNA transcript. However, due to optic blurring of the image, multiple closely juxtaposed spots may occasionally appear as one connected object. To ensure robust single spot identification, one strategy is to identify the number of local maxima within each connected object. A connected object corresponding to a single smFISH spot should have only one maximum, whereas a cluster of spots often exhibits multiple maxima (see **Note 24**). Ultimately, the total number of local maxima among all connected objects would constitute the total number of spots detected for a given threshold.

After spot detection and counting have been carried out for all thresholds, a plot can be generated showing total spot counts as a function of different threshold values. With high quality imaging data this curve is expected to start high, then drop rapidly to reach a plateau before it finally approaches zero (Figure 5). The size of the plateau depends on the amount of difference in intensity between the smFISH signal and the background auto-fluorescence. The total spot count is approximately constant in this range and corresponds reliably to the number of actual smFISH spots. The computationally detected spots can be plotted over the original image to ensure that no over- or under-counting has occurred.

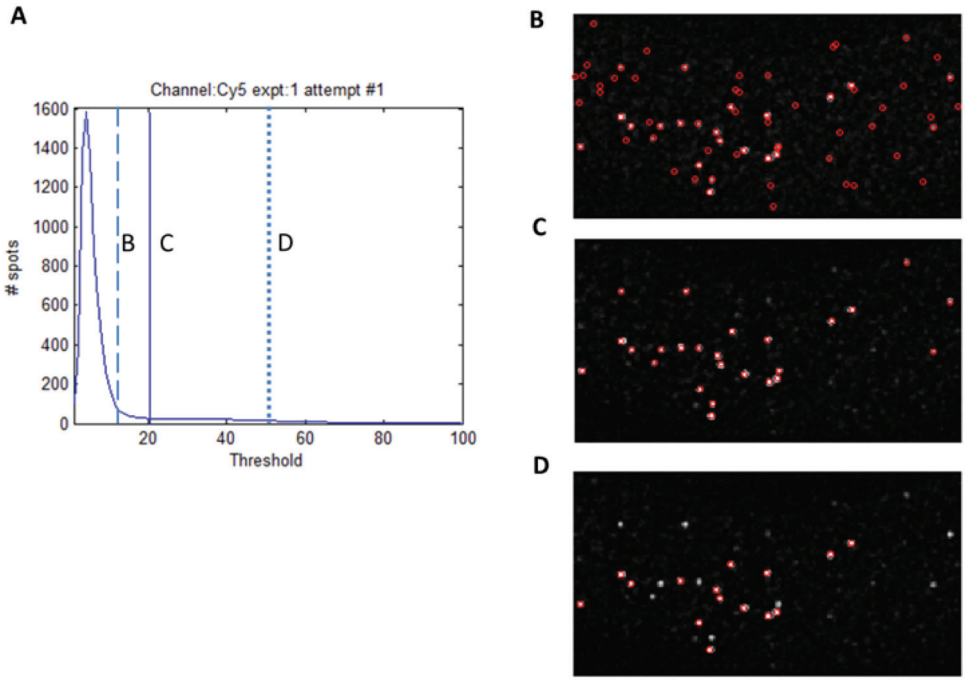

Figure 5. Choice of threshold for automatic detection of smFISH spots. (**A**) Total spot counts plotted as a function of the pixel intensity threshold. Optimal threshold values are located where the spot count is insensitive to the threshold value (where the "plateau" is). (**B-D**) Maximum intensity projection of the stack of smFISH images analyzed in **A**. Red circles are spots detected by MATLAB-based custom-written software. (**B**) Spot detection when threshold is chosen too low (broken line in **A**). Note many out-of-focus spots and background speckles are mistakenly included as spots. (**C**) Spot detection when an optimal threshold (solid vertical line in **A**) is chosen. Red circles indicate computationally identified spots. Note that out-of-focus spots (faint spots in the background) are not included. (**D**) Spot detection when the threshold is chosen too high (dotted line in **A**). Note the software has failed to recognize several bright spots.

3.8.5 Region-specific spot quantification

Spot quantification within a specific cell or tissue can be conveniently achieved by aligning the results from image segmentation and spot detection. Computationally this can be done by generating a binary map for the region of interest (ROI) and compare this map against the map of spot locations (see Section 3.8.4) to determine the number of spots inside the ROI. In addition to counting, further analyses can be carried out on the location (e.g. detecting co-localized smFISH signal from different fluorescent channels) and intensity (e.g. quantify the intensity of intronic spots) of the smFISH spots.

4. Notes

4.1 Notes referenced in the main text

Note 1: It is desirable to freshly make sodium bicarbonate, or check before use to make sure the pH level is correct.
Note 2: Tween-20 is added to washing solutions to prevent loss of animals or embryos by adherence to the sides of plastic tubes.
Note 3: Dextran sulfate is very difficult to dissolve. It is preferable to add 4 mL of water to the Dextran sulfate, vortex and rotate at RT until all is dissolved (this should take a couple of hours).
Note 4: We have experienced that a formamide concentration of 10% (1 mL) works well in our hands. The formamide concentration can be increased to increase probe binding stringency. This is especially desired for probes having a GC content of >55%. A high formamide concentration can result in low fluorescence signals.
Note 5: Although a confocal microscope can be used for imaging smFISH samples, this will generally lead to accelerated bleaching of the fluorophore and is not recommended.
Note 6: TMR can be hard to dissolve in aqueous solution, so one must first dissolve it in a small volume (<5 µl) of DMSO before adding 50 µl of 0.1 M sodium bicarbonate.
Note 7: Set the detector to monitor DNA absorption (260 nm) and the absorption of the coupled fluorophore (e.g., 555 nm for TMR).
Note 8: Be sure to prevent any light from hitting the probes during the drying process to prevent photo bleaching, especially for photo labile dyes such as Cy5.
Note 9: Be sure to use sufficient animals to form a visible pellet in an micro centrifuge tube.
Note 10: Distilled water can be used instead of M9 buffer in all steps.
Note 11: It is crucial to remove most bacteria and debris from the solution, when in doubt it is recommended to wash a second time.
Note 12: We found that minimizing the amount of supernatant left on the pellet in this and subsequent steps by carefully aspirating will generally lead to a better signal to noise ratio in the end.
Note 13: We use approximately 1 mL of fixation solution for ~10 µL of pellet. Using insufficient amounts of solution may lead to less successful fixation of the animals.
Note 14: A large population of synchronized gravid adults can be obtained by bleaching a mixed population of animals and growing them at 20°C for four/five days.
Note 15: Time used for bleaching should be kept as short as possible and should be determined empirically for each separate strain.
Note 16: We found that minimizing the amount of supernatant left on the embryo pellet in this and subsequent steps by carefully aspirating will generally lead to a better signal to noise ratio in the end.
Note 17: The hybridization buffer should be warmed to room temperature before opening, to prevent oxidation of the formamide.
Note 18: For new probes it is usually best to test these in a dilution series of 1:10, 1:20, 1:50 and 1:100 as stock solutions.
Note 19: By spinning in this fashion, loss of animals by adherence to the sides of the tube is minimized.
Note 20: The sample can be stored in the dark for imaging at 4°C for approximately one

day. We have seen that storage for longer times is possible, but a decline in signal intensity is noticeable.
Note 21: Excess solution is removed to flatten the sample and thereby decreases light scattering. This has to be performed quite securely. Removing too little will increase out of focus light as well as allow the animals to float away. Whereas removing too much will cause the sample to dry out quickly. This step can only be optimized by practice.
Note 22: Optionally, the edges of the cover glass can be covered with nail polish to prevent dehydration of the sample.
Note 23: To save computation time, it is advisable to crop the image and perform image processing only on the segmented ROIs. Table 1 lists several MATLAB functions useful for executing this task.
Note 24: The radius of the region to search for maxima should be set to approximate the radius of a single smFISH spot

4.2 Troubleshooting

Here we describe some common troubleshooting tips for problems that can be encountered when performing smFISH experiments on *C. elegans* or any other species.

Low signal intensity

When testing a new probe it is good to take along a previously tested probe to make sure that all solutions and equipment used are working properly. Low signal intensity can have several causes, some of which are indicated here.

- The probe concentration is too low. Try increasing the concentration of the probe at least two-fold and see whether this helps the signal.
- The formamide concentration in the hybridization buffer is too high. Formamide increases the stringency of the hybridization reaction. Care is to be taken when lowering the formamide concentration though, since this may increase the amount of nonspecifically binding probe.
- The tissue is not well penetrated. *C. elegans* larvae or adults should be incubated in 70% ethanol for ample time, at least 24 hours. We did not experience that incubating for longer times, say 48 hours, is detrimental to the sample.

High fluorescence background

Below we note several causes that can lead to a high background signal.

- The animals used originated from a plate that was too crowded or starved. Care should be taken to use animals that were cultured in ideal conditions.
- The probe concentration is too high or the washing was not thorough enough. This can be solved by lowering probe concentration and/or more frequent and longer washing steps.
- The animals were incubated too long in fixation solution. Fixation time should be kept under an hour to prevent over fixation.

- Light scattering may result in detection of out-of-focus light during the image acquisition. Removing excess liquid from under the coverslip and thereby flattening the animals can usually minimize this problem.
- The probe shows a high degree of nonspecific binding. This can be caused by a high GC content (>55%) of the probe or by a formamide concentration that is too low for this specific probe.

Unexpected spot morphology causes problems with identifying and counting spots

In principle smFISH spots should be of similar sizes and appear circular in a 2D plane. However, if too much liquid remains between the objective and sample, this can interfere with regular spot morphology. Maximally flattening the sample by sucking away liquid can help in reducing this problem. Furthermore, a high concentration of multiple spots in the case of high gene expression can obscure individual signals. This can be solved computationally by identifying local maxima in a connected region of interest.

Non-specific fluorescent signal

Sometimes fluorescent spots can be detected that arise from auto-fluorescence of the sample. In order to identify auto-fluorescent spots it is good to note that they will usually appear across multiple fluorescence detection channels, whereas real smFISH spots only show up in one channel. As a control for persistent auto fluorescence problems a staining could be performed that does not include a coupled smFISH probe. Any spot that does appear now will not be due to a real smFISH signal.

Bleed-through of emission light from one fluorophore into the channel of a second fluorophore can also lead to the detection of non-specific signal. This can occur if genes are very highly expressed (often in the case of highly expressed transgenes) or if optical filters are not optimally separated in their detected spectra. To check for occurring bleed-through of signal one can perform single probe smFISH experiments and identify the underlying cause of the problem.

References

Boulin, T., Etchberger, J.F., and Hobert, O. (2006). Reporter gene fusions. WormBook : the online review of C elegans biology, 1-23.

Gubb, D., Green, C., Huen, D., Coulson, D., Johnson, G., Tree, D., Collier, S., and Roote, J. (1999). The balance between isoforms of the prickle LIM domain protein is critical for planar polarity in Drosophila imaginal discs. Genes & development *13*, 2315-2327.

Harterink, M., Kim, D.H., Middelkoop, T.C., Doan, T.D., van Oudenaarden, A., and Korswagen, H.C. (2011). Neuroblast migration along the anteroposterior axis of C. elegans is controlled by opposing gradients of Wnts and a secreted Frizzled-related protein. Development *138*, 2915-2924.

Huarcaya Najarro, E., and Ackley, B.D. (2013). C. elegans fmi-1/flamingo and Wnt pathway components interact genetically to control the anteroposterior neurite growth of the VD GABAergic neurons. Developmental biology *377*, 224-235.

Raj, A., Rifkin, S.A., Andersen, E., and van Oudenaarden, A. (2010). Variability in gene expression underlies incomplete penetrance. Nature *463*, 913-918.

Raj, A., van den Bogaard, P., Rifkin, S.A., van Oudenaarden, A., and Tyagi, S. (2008). Imaging individual mRNA molecules using multiple singly labeled probes. Nature methods *5*, 877-879.

Sanchez-Alvarez, L., Visanuvimol, J., McEwan, A., Su, A., Imai, J.H., and Colavita, A. (2011). VANG-1 and PRKL-1 cooperate to negatively regulate neurite formation in Caenorhabditis elegans. PLoS genetics *7*, e1002257.

Shakes, D.C., Miller, D.M., 3rd, and Nonet, M.L. (2012). Immunofluorescence microscopy. Methods in cell biology *107*, 35-66.

Tabara, H., Motohashi, T., and Kohara, Y. (1996). A multi-well version of in situ hybridization on whole mount embryos of Caenorhabditis elegans. Nucleic acids research *24*, 2119-2124.

Chapter 7

General discussion

Wnt signaling has been subject to intense investigation since its discovery approximately 30 years ago. Wnts play major roles during the development of the animal body plan and regulate such processes as anteroposterior axis specification, stem cell maintenance, cell specification and differentiation, cell polarity and cell migration. Even during adult life, Wnt signaling is crucial for the maintenance of many types of stem cells and deregulation is a cause for cancer or neurodegenerative diseases (Clevers and Nusse, 2012). It stands to reason that a signaling pathway regulating such a wide array of different developmental processes is inherently complex itself. Indeed, with the identification of no less than 19 Wnt and 11 Frizzled homologues in the vertebrate genome it was recognized that the amount of possible ligand receptor interactions is staggering. This complexity was further enhanced when the originally studied canonical Wnt/ß-catenin pathway was accompanied by a large collection of non-canonical Wnt pathways, all having differing signaling outputs (van Amerongen and Nusse, 2009). It is no wonder then that one of the most important questions in the Wnt field is to ask how Wnts achieve signaling specificity during development.

During the making of this thesis we have attempted to reduce the complexity of the system by choosing a simplified model organism for our studies: the small nematode *Caenorhabditis elegans*. We chose to study the development of the nervous system, which is at all levels heavily controlled by Wnt signaling (introduced in **Chapter 1**). More specifically, we examined how the process of anteroposterior neuronal cell migration is controlled by Wnt signaling. As a model system we turned to the migration of the Q neuroblasts and their descendants during early larval development, as well as a collection of neurons that migrate during embryogenesis. One of the most informative tools we discovered to be the specific staining of single mRNA transcripts using a single molecule fluorescence *in situ* hybridization protocol (smFISH) (Raj et al., 2008). With its use came the realization that much of Wnt signaling pathway specificity and output may be determined by the controlled expression of certain components in the receiving cell. Below our findings concerning the role of Wnt signaling during cell migration in *C. elegans* will be summarized and discussed.

Wnt receptor expression determines downstream signaling response

Previous studies have demonstrated that the anterior migration of the QR neuroblast and its descendants (QR.d) is controlled by a multitude of Wnt ligands and receptors (Harris et al., 1996; Whangbo and Kenyon, 1999; Zinovyeva and Forrester, 2005; Zinovyeva et al., 2008). These results raised the question how the QR.d might integrate this complex information and robustly migrate to their final positions. The various Wnts in *C. elegans* are all expressed in specific, partially overlapping domains along the anteroposterior axis, suggesting that they form directional concentration gradients, as was indeed confirmed for EGL-20/Wnt (Coudreuse et al., 2006; Harterink et al., 2011). Wnts are known to function as morphogens in different systems, exerting concentration dependent effects on the surrounding tissue (Cadigan and Nusse, 1997; Zecca et al., 1996). Indeed, also in *C. elegans* they may act as either repulsive or attractive guiding factors in processes such as anterior migration of the HSN neuron or posterior extension of neurites originating from the RME neuron (Pan et al., 2006; Song et al., 2010). However, data obtained by others as well as by ourselves describing the permissive roles of the EGL-20/Wnt and CWN-1/Wnt during QR.d migration suggested that the precise positioning of the final descendants is most likely not controlled by a ligand concentration dependent effect (Mentink et al., 2014; Whangbo and Kenyon,

1999, see also **Chapter 2**). As it seemed counter-intuitive that a permissive Wnt signal would be sufficient to control QR.d migration, we turned to study more closely the role of the different Wnt receptors involved in QR.d migration. Examination of receptor mRNA expression using smFISH revealed that many *C. elegans* Wnt receptors are expressed in the QR.d in a highly dynamic way, suggesting that this regulation is the prime manner in which the migratory response of the QR.d cells to the Wnt ligand signal is controlled (Figure 1, see also **Chapter 2**).

mom-5/Fz and cam-1/Ror2 cooperate to regulate long range QR.p migration

The long-range migration of QR.p is controlled by two parallel non-canonical Wnt pathways that influence migration speed and directionality via *mom-5/Fz* and *cam-1/Ror2* respectively, both of which are also expressed in QR.p. How could the QR.p neuroblast be coordinating the different signals sent by both these pathways, resulting in its anterior migration?

Even though we found that *cwn-1* is in the same genetic pathway as *mom-5*, while *egl-20* signals via the *cam-1* receptor, previous research has found that CAM-1 is also able to bind to CWN-1 (Green et al., 2007). It has been shown that competition of Wnt ligands for surface receptors expressed on the receiving cell may be instrumental in determining the cell's downstream response (Grumolato et al., 2010). It will be interesting to determine whether a similar ligand competition is occurring in QR.p and to which extent this is required for a proper migratory response. Perhaps the different expression dynamics of both receptors, with *mom-5* expression quickly increasing after QR.p has started its migration, ensure that it is able to bind *cwn-1* more readily than the *cam-1* receptor (Figure 1). Of course, the lag between mRNA expression and protein translation has to be considered, as well as the amount of receptor that may already be present due to expression in the QR neuroblast and that will be segregated - perhaps asymmetrically - to both QR.a and QR.p.

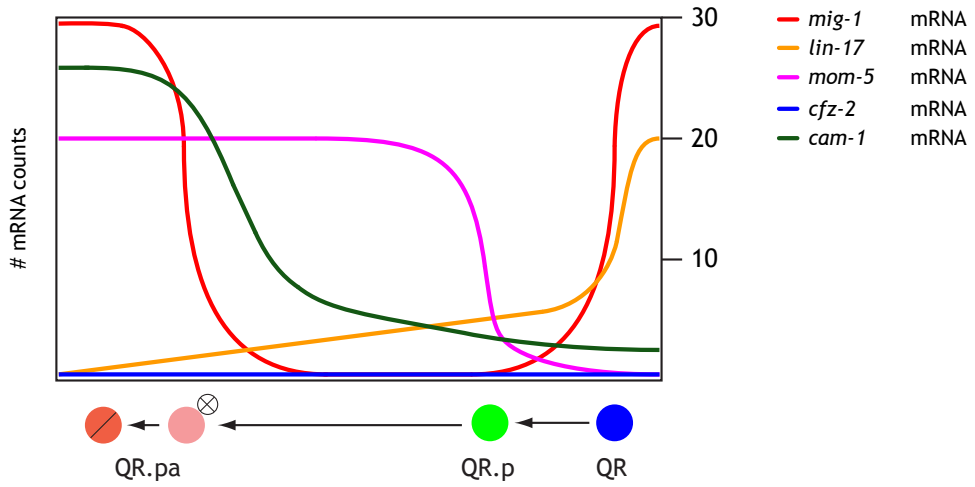

Figure 1. Wnt receptors show highly dynamic expression patterns in the QR descendants. Schematic overview of the number of transcript counts of the four Frizzleds (*mig-1*, *lin-17*, *mom-5* and *cfz-2*) and *cam-1/Ror2* in QR (blue), QR.p (green) and QR.pa (pink) during their posterior (right) to anterior (left) migration.

Another way in which Wnts can activate distinct pathways within a cell is by differential receptor internalization. Using cell culture studies, it was found that Wnt5A can induce clathrin-mediated endocytosis of its receptor Ror2, whereas Wnt3A was found in intracellular vesicles containing its co-receptor LRP6, as well as caveolin (Sakane et al., 2012; Sato et al., 2010). This work supported a growing body of literature describing the specific activation of downstream pathways by Wnts through the use of a distinct internalization route (Kikuchi et al., 2009). It will therefore be interesting to study the intracellular localization of both *mom-5* and *cam-1* in QR.p using fluorescent reporters and determine to which extent they use different trafficking routes and if so, how this is instrumental for downstream pathway activation.

Such a mechanism could perhaps serve to recruit specific downstream factors required for migration, e.g. the Dishevelleds (Dvl / Dsh in invertebrates) *dsh-2* and *mig-5*. We found that both these factors are required for anterior migration, but we were unable to genetically associate them with either the *mom-5* or *cam-1* pathway (Mentink et al., 2014, see also **Chapter 2**). Examining Dsh mutants for defects in QR.p polarity or migration speed could serve to distinguish their involvement, perhaps resulting in the conclusion that they function in both pathways. This would not be entirely unexpected, as Dsh is often found to have a role in multiple signaling pathways (Gao and Chen, 2010). For example, canonical Wnt/ß-catenin signaling drives convergence and extension (CE) in *Xenopus* through Dvl (Kuhl et al., 2001). However, this process is counteracted by Wnt/Ca^{2+} signaling that phosphorylates Dvl via PKC activity, a modification that prevents it from acting in the canonical pathway (Kuhl et al., 2001). Although looking at specific post-translational modifications of Dsh proteins might be challenging in *C. elegans*, studying Dsh localization and/or co-localization with MOM-5 or CAM-1 receptors may give additional insight.

MIG-1/Fz acts in a canonical Wnt/ß-catenin pathway to stop QR.pa migration

We found that at the end of its migration the QR.p neuroblast divides and generates the QR.pa neuroblast, as well as QR.pp, an apoptotic corpse. This is accompanied by a cell intrinsic, time-dependent, exponential increase in the expression of *mig-1/Fz*, which results in the activation of a *bar-1/ß-catenin* dependent pathway that in turn instructs the QR.pa cell to terminate its anterior migration (Mentink et al., 2014, see also **Chapter 2**). Our results raised many questions concerning how precisely this mechanism operates.

Such as: how does upregulation of *mig-1* lead to a switch in signaling activity from the non-canonical Wnt pathway driving anterior migration to a canonical Wnt pathway that terminates migration? During QL neuroblast initial migration *mig-1* is, together with *lin-17/Fz*, the Wnt receptor required for activation of canonical Wnt signaling, leading to expression of the Hox gene *mab-5* and posterior migration (Ji et al., 2013, see also **Chapter 4**). A simple model could therefore be that *mig-1* and *lin-17* have a similar function in the QR lineage and that their expression leads to activation of canonical Wnt signaling in QR.pa. However, considering that both *mom-5* and *cam-1* are still expressed at the time of *mig-1* upregulation (Figure 1), we could think of a more elaborate model where *mig-1* competes with these receptors for Wnt ligands, resulting in a change in pathway activation. It is however difficult to show involvement of Wnts in this second stage of QR.d migration, as they are also involved during the first stage, which may confound the eventual read out. Furthermore, to investigate this model it would be very helpful to possess data on the binding affinities of *egl-20* and *cwn-1* with all three receptors, something that is currently

only available to some extent for the *cam-1* receptor (Green et al., 2007). A third possibility could be that *cam-1* and/or *mom-5* are also involved in the canonical pathway that terminates migration and that the increased amount of *mig-1* receptor alters their signaling activity. Perhaps *mig-1* is able to form a heterodimeric receptor complex with either the *cam-1* or *mom-5* receptor. Heterodimeric Wnt receptor complexes have been suggested to regulate the strength of muscle synapse signaling in *C. elegans* (Jensen et al., 2012). Both *lin-17/Fz* and *cam-1* are required to localize acetylcholine receptors to postsynaptic muscle sites and fluorescently labeled LIN-17 and CAM-1 colocalize in neuromuscular junctions (Jensen et al., 2012).

We may also ask how the activation of canonical Wnt signaling leads to the termination of QR.pa migration i.e. which target genes are activated/repressed by *bar-1*? One might envision that *bar-1* mediated transcription leads to the upregulation of gene products that enhance cellular adhesion to the extracellular matrix (ECM) or neighboring cells, causing the cell to slow and eventually stop. Our finding that QR.p cells migrate faster in the collagen mutant *emb-9*, as well as slower in the integrin mutant *ina-1*, suggests that interactions with the ECM are important to control the extent of migration (Mentink et al., 2014, see also **Chapter 2**). Furthermore, we have shown that constitutive activation of canonical Wnt signaling in the *pry-1/Axin* mutant leads to a marked decrease in the speed of QR.p migration, without affecting the polarity of the cell. Since the speed of QR.p migration is regulated in parallel by both the *mom-5* pathway and cellular adhesion through the integrin *ina-1*, the *pry-1* mutant phenotype suggests that canonical Wnt signaling counteracts migration via either of these pathways (Mentink et al., 2014, see also **Chapter 2**). Although not much is known about *bar-1* target genes in *C. elegans*, save for its role in activating the expression of the Hox genes *lin-39*, *mab-5* and *egl-5* (Sawa and Korswagen, 2013), studies performed in vertebrate model systems demonstrate that ß-catenin mediated transcription may influence ECM adhesion by controlling the expression of ECM components or proteins that regulate integrin activity (Gradl et al., 1999; Heuberger and Birchmeier, 2010; Hlubek et al., 2004; Wu et al., 2014). It may be that *C. elegans bar-1* shares similar target genes. Detailed live imaging of QR.pa migration in both wild type and *bar-1* mutants, combined with markers for ECM or integrin dynamics could aid in identifying if and how the canonical Wnt pathway influences this process.

Finally, an important question is how the sudden increase in *mig-1* transcription is controlled. We have shown that a time-dependent, cell intrinsic mechanism is responsible for the upregulation by demonstrating that it is not dependent on the anteroposterior position of the migrating QR.p and QR.pa cells (Mentink et al., 2014, see also **Chapter 2**). Since the increase in *mig-1* expression seems correlated with the division of QR.p into QR.pa (Figure 1), the possibility exists that it is also dependent on this very division. An experiment where the cell cycle of QR.p is either inhibited or delayed will have to determine whether such a link indeed exists. Remarkably, previous work on the relation between cell cycle and gene transcription in *C. elegans* demonstrated that in the intestinal and muscle lineages, initiation of transcription can be uncoupled from cell division (Nair et al., 2013). This leads to an altered number of cells expressing a similar number of transcripts when the cell cycle is delayed (Nair et al., 2013). These results indicate that certain clock-like mechanisms exist that are coupled to developmental time and regulate gene transcription irrespective of cell type. An attractive model would be that, during QR.p migration, the progressive or timed degradation of a transcriptional repressor or the removal of a repressive histone

modification would allow expression of *mig-1* at a predetermined moment, causing QR.pa to stop migration at the correct time. Such a system could be analogous to the timed transcriptional regulation of the circadian clock (Hardin and Yu, 2006). In *C. elegans*, the heterochronic genes that control the developmental timing of molting cycles can be seen as a primitive form of the rhythmic circadian clock (Monsalve and Frand, 2012). However, since the complete process of QR.d migration occurs between molting cycles during the L1 stage, involvement of the heterochronic pathway seems unlikely.

Migrating embryonic neurons each express their own specific "set" of Wnt receptors
It is possible that the use of different Wnt receptors to control specific aspects of the migration process, which we identified in the QR.d, similarly plays a role in controlling the migration of four bilateral neurons during *C. elegans* embryogenesis. In **Chapter 5** we have shown that the HSN, ALM, BDU and CAN neurons all express their own repertoire of Wnt receptors. Although it is more challenging to study cell migration in the *C. elegans* embryo, it will be interesting to determine what the contribution of each of these receptors is to the migration process. Furthermore, besides the repulsive role of EGL-20 in HSN migration (Pan et al., 2006), it is unknown whether the different Wnts act instructively or permissively during these migrations. Ectopic expression of Wnts through heat shock or alternative promoters will provide insight into this question. In a dream experiment, one would be able to reverse the Wnt gradients, as well as the receptor expression in for example ALM and HSN, and observe whether they now still migrate in a similar fashion.

Dynamically expressed receptors control Wnt pathway activation
Wnt receptor expression has increasingly become recognized as an important mechanism to control specificity in pathway activation (van Amerongen and Nusse, 2009). For example, Wnt5A inhibits canonical Wnt signaling in the presence of the Ror2 receptor, but may activate the same pathway when Fz4 is provided (Mikels and Nusse, 2006). Furthermore, overexpression of Wnt5A in *Xenopus* causes defects in convergence and extension, a non-canonical Wnt signaling response (Du et al., 1995; Moon et al., 1993). However, when Wnt5A is expressed together with Fz5 axis duplication is observed, which is the result of canonical Wnt signaling (He et al., 1997; Holmen et al., 2002). A more detailed *in vivo* study in mice revealed that Wnt5A activates both types of pathways depending on receptor expression context in different tissues (van Amerongen et al., 2012).

Our data on *mig-1* expression in the QR.d corroborates these findings and shows that indeed the presence of a different receptor can alter the downstream response to the Wnt ligand. In addition, we have shown that the timed expression of *mig-1* is important to control the precise positioning of the QR.d. These results may give insight into how analogous processes are regulated in vertebrate systems. For example, during midline crossing of callosal axons between the two hemispheres of the brain, outgrowth of precrossing axons is dependent on Wnt signaling through the Fz3 receptor, whereas Ryk controls their fasciculation (Keeble et al., 2006; Wang et al., 2002; Wang et al., 2006). In contrast, the outgrowth of postcrossing axons is highly dependent on Ryk (Keeble et al., 2006). These results show that two receptors control different aspects of axon outgrowth, depending on whether they have crossed the midline or not. It is possible that changes in receptor expression contribute to the differential requirements for these receptors.

Wnt signaling crosstalk may influence pathway activation

In addition to the role that receptors have in determining which Wnt pathway is activated, an important way to achieve signaling specificity is through protein-protein interactions between components of different pathways. Often, such interactions converge on the cytoplasmic Dvl protein, which has also been termed "the hub of Wnt signaling" (Gao and Chen, 2010). Dvl is composed of three different protein domains, the N-terminal DIX domain, a central PDZ domain and a C-terminal DEP domain (Wong et al., 2000). The DIX domain is important for Dvl polymerization and canonical Wnt signaling, whereas the DEP domain is crucial for Wnt/PCP signaling (Boutros et al., 1998; Schwarz-Romond et al., 2005; Smalley et al., 2005; Tada and Smith, 2000). The PDZ domain mediates protein-protein interactions, plays a role during both canonical and non-canonical signaling and has therefore been proposed to distinguish between Wnt pathways by forming pathway-specific protein complexes (Moon and Shah, 2002; Wharton, 2003; Wong et al., 2003). Some illustrative examples exist of proteins that mediate specificity of Wnt signaling through interaction with Dvl. For instance, the mammalian homologue of the intracellular *Drosophila* protein *naked cuticle* (mNkd) binds to Dvl, resulting in inhibition of canonical signaling, as well as stimulation of non-canonical JNK signaling (Yan et al., 2001). The vertebrate protein Inversin binds to Dvl1 and targets it for degradation, inhibiting canonical Wnt signaling, while at the same time it promotes Wnt/PCP signaling, by assisting the interaction of Dvl2 with Fz (Lienkamp et al., 2010; Simons et al., 2005). Perhaps the distinction that Inversin makes between different Dvls is crucial for determining downstream pathway activation, as there is a differential capacity of homologous mammalian Dvls to potentiate canonical Wnt signaling (Lee et al., 2008).

In **Chapter 3** of this thesis, we propose that *vang-1*, the *C. elegans* homologue of the PCP protein Van Gogh, increases the threshold for activation of the canonical Wnt pathway in the QR.d through its interaction with *mig-5*/*Dsh*, effectively lowering its signaling capacity. Our data confirmed the role of Van Gogh as a negative regulator of canonical signaling, that had been suggested previously from overexpression and morpholino studies (Angonin and Van Raay, 2013; Li et al., 2011; Park and Moon, 2002). We propose that the transmembrane protein VANG-1 binds and recruits the MIG-5 protein either to the plasma membrane, or perhaps to intracellular vesicles, which causes it to be unavailable for Fz mediated canonical Wnt signaling.

In **Chapter 2** we described that later during QR.d migration, *vang-1* is involved in controlling the dorsoventral positioning of the QR.paa and QR.pap cells. The PCP homologue *prkl-1* is also required for this migration phase, while it does not play a role during the inhibition of canonical Wnt signaling by *vang-1*. The multiple roles of *vang-1* as well as the differential requirements for *prkl-1* pose an interesting problem: how could such a process be regulated? Putatively, the dynamic expression pattern of *prkl-1* – no expression in QR.p and high expression in QR.pa and QR.paa – could account for its involvement only during the later dorsoventral phases of migration, granted that the PRKL-1 protein product follows the same dynamics as its mRNA template. Another possibility is that the differential activation of downstream pathways is primarily regulated via the VANG-1 protein. VANG-1 could function in a way similar to the Inversin protein, which distinguishes between Dvls to both inhibit canonical Wnt signaling and activate non-canonical Wnt signaling (Lienkamp et al., 2010; Simons et al., 2005). This would require for the PCP-like signaling pathway that

controls dorsoventral migration of QR.paa and QR.pap to be mediated via one of the other *C. elegans* Dshs, either *dsh-1* or *dsh-2*. A previous study has demonstrated that *vang-1*, *prkl-1* and *dsh-1* function together to prevent ectopic neurite formation in the vulval motor neurons VC4 and VC5 (Sanchez-Alvarez et al., 2011). Perhaps these genes share a similar genetic relationship during the dorsoventral migration of QR.paa and QR.pap.

Feedback control of Wnt signaling components modulates the response

In addition to the upstream events that determine Wnt pathway activation, such as Wnt binding to a specific receptor leading to the recruitment of Dvl and specific interaction partners, downstream transcriptional feedback mechanisms can be used to modulate the cell's response. Target genes that respond to canonical Wnt signaling are both numerous and cell- or context-specific (Logan and Nusse, 2004; MacDonald et al., 2009). Some of these target genes comprise components of the Wnt/ß-catenin pathway itself. For example, transcriptional upregulation of vertebrate Axin2 and *Drosophila* Naked by ß-catenin/TCF constitute negative feedback loops that may dampen the activity of Wnt/Wg signaling (Jho et al., 2002; Rousset et al., 2001). Positive feedback loops are known to exist as well, since both R-spondin – a secreted Wnt agonist that may enhance an existing Wnt signal - and TCF/LEF may serve as target genes of canonical Wnt signaling (Hovanes et al., 2001; Kamata et al., 2004; Nam et al., 2006). Some feedback interactions result in more complex effects: in *Drosophila* for example, Wg signaling downregulates the expression of *Fz* and *Dfz2* receptors, resulting in reduced signaling output (Cadigan et al., 1998; Muller et al., 1999). However, the lowered levels of high-affinity Wg receptors in turn influence the spreading and range of the Wg gradient, again altering signaling strength. Related to this, we have shown that in *C. elegans* LIN-17 limits the extent of the EGL-20 gradient, presumably by acting as a ligand sink (see **Addendum I**).

In **Chapter 4** of this thesis we demonstrate that an intricate network of interlocked negative and positive feedback loops is required for robust activation of *mab-5*/*Hox* transcription in the QL neuroblast in response to canonical Wnt signaling. Initially, pathway activation is mediated via the highly transcribed *mig-1* receptor, which is subsequently downregulated by the Wnt signal through a negative feedback loop. At the same time *mab-5* transcription is upregulated, a Hox transcription factor that induces expression of a second Fz receptor, *lin-17,* which in turn induces *mab-5* expression through a positive feedback loop. Finally, a negative feedback loop of *mab-5* inhibiting its own transcription ensures that *mab-5* is fine-tuned to a stable level, resulting in posterior migration of the QL.d (Ji et al., 2013).

We speculate that these extensive transcriptional feedback loops operate to reinforce the difference in intracellular signaling response to EGL-20 between QL and QR. Normally, during initial posterior migration of QL and anterior migration of QR, QL activates a canonical Wnt/ß-catenin pathway, while QR activates a non-canonical pathway (Korswagen, 2002). Overexpression of the EGL-20 ligand causes the QR neuroblasts to activate canonical signaling as well, indicating that QR has a higher activation threshold (Whangbo and Kenyon, 1999). Our theory is that the posterior polarization and migration of QL causes it to encounter higher levels of the posteriorly secreted EGL-20 ligand, leading to high enough expression of *mab-5* to overcome its self-regulatory negative feedback and initiate the positive feedback loop that upregulates expression of *lin-17*. In contrast, the QR neuroblast will migrate away

from the EGL-20 source and fail to initiate high enough *mab-5* expression to upregulate *lin-17*. This idea is reinforced by the fact that, initially, the average amount of *mab-5* and *mig-1* transcript counts in QR is identical to those found in QL and that *mig-1* is subsequently downregulated with similar dynamics (data not shown). A caveat to this proposed model is that ectopic EGL-20 expression from the anterior is able to rescue migration of both QL and QR and their descendants in an *egl-20* mutant background (Whangbo and Kenyon, 1999, our own observations). This indicates that EGL-20 may function permissively during initial migration and that therefore matters may be more complex.

Our findings concerning the transcriptional regulation of Wnt signaling components in QL beg the question whether a similar feedback system might exist in the QR neuroblast and its descendants. The highly dynamic expression of Wnt receptors in QR.p and QR.pa that we describe in **Chapter 2** does suggest that extensive transcriptional regulation may exist in these cells. Future studies that utilize a similar approach as was taken in **Chapter 4** will have to determine whether there is some merit to these thoughts.

Concluding remarks

Our analysis of the Wnt signaling mechanisms that control cell migration in *C. elegans* has revealed that a considerable amount of regulation occurs, leading to activation of different downstream pathways. Our work has raised many new questions about the specifics of each of these different processes, as has been discussed above and in the different chapters. We have shown that *C. elegans* may serve as a valuable model organism to study many different aspects of the Wnt signaling machinery and its role in migration; we are confident that it will continue to provide a platform to interrogate important questions in this field for many years to come.

References

Angonin, D., and Van Raay, T.J. (2013). Nkd1 functions as a passive antagonist of Wnt signaling. PloS one *8*, e74666.

Boutros, M., Paricio, N., Strutt, D.I., and Mlodzik, M. (1998). Dishevelled activates JNK and discriminates between JNK pathways in planar polarity and wingless signaling. Cell *94*, 109-118.

Cadigan, K.M., Fish, M.P., Rulifson, E.J., and Nusse, R. (1998). Wingless repression of Drosophila frizzled 2 expression shapes the Wingless morphogen gradient in the wing. Cell *93*, 767-777.

Cadigan, K.M., and Nusse, R. (1997). Wnt signaling: a common theme in animal development. Genes & development *11*, 3286-3305.

Clevers, H., and Nusse, R. (2012). Wnt/beta-catenin signaling and disease. Cell *149*, 1192-1205.

Coudreuse, D.Y., Roel, G., Betist, M.C., Destree, O., and Korswagen, H.C. (2006). Wnt gradient formation requires retromer function in Wnt-producing cells. Science *312*, 921-924.

Du, S.J., Purcell, S.M., Christian, J.L., McGrew, L.L., and Moon, R.T. (1995). Identification of distinct classes and functional domains of Wnts through expression of wild-type and chimeric proteins in Xenopus embryos. Molecular and cellular biology *15*, 2625-2634.

Gao, C., and Chen, Y.G. (2010). Dishevelled: The hub of Wnt signaling. Cellular signalling *22*, 717-727.

Gradl, D., Kuhl, M., and Wedlich, D. (1999). The Wnt/Wg signal transducer beta-catenin controls fibronectin expression. Molecular and cellular biology *19*, 5576-5587.

Green, J.L., Inoue, T., and Sternberg, P.W. (2007). The C. elegans ROR receptor tyrosine kinase, CAM-1, non-autonomously inhibits the Wnt pathway. Development *134*, 4053-4062.

Grumolato, L., Liu, G., Mong, P., Mudbhary, R., Biswas, R., Arroyave, R., Vijayakumar, S., Economides, A.N., and Aaronson, S.A. (2010). Canonical and noncanonical Wnts use a common mechanism to activate completely unrelated coreceptors. Genes & development *24*, 2517-2530.

Hardin, P.E., and Yu, W. (2006). Circadian transcription: passing the HAT to CLOCK. Cell *125*, 424-426.

Harris, J., Honigberg, L., Robinson, N., and Kenyon, C. (1996). Neuronal cell migration in C. elegans: regulation of Hox gene expression and cell position. Development *122*, 3117-3131.

Harterink, M., Kim, D.H., Middelkoop, T.C., Doan, T.D., van Oudenaarden, A., and Korswagen, H.C. (2011). Neuroblast migration along the anteroposterior axis of C. elegans is controlled by opposing gradients of Wnts and a secreted Frizzled-related protein. Development *138*, 2915-2924.

He, X., Saint-Jeannet, J.P., Wang, Y., Nathans, J., Dawid, I., and Varmus, H. (1997). A member of the Frizzled protein family mediating axis induction by Wnt-5A. Science *275*, 1652-1654.

Heuberger, J., and Birchmeier, W. (2010). Interplay of cadherin-mediated cell adhesion and canonical Wnt signaling. Cold Spring Harbor perspectives in biology *2*, a002915.

Hlubek, F., Spaderna, S., Jung, A., Kirchner, T., and Brabletz, T. (2004). Beta-catenin activates a coordinated expression of the proinvasive factors laminin-5 gamma2 chain and MT1-MMP in colorectal carcinomas. International journal of cancer *108*, 321-326.

Holmen, S.L., Salic, A., Zylstra, C.R., Kirschner, M.W., and Williams, B.O. (2002). A novel set of Wnt-Frizzled fusion proteins identifies receptor components that activate beta -catenin-dependent signaling. The Journal of biological chemistry *277*, 34727-34735.

Hovanes, K., Li, T.W., Munguia, J.E., Truong, T., Milovanovic, T., Lawrence Marsh, J., Holcombe, R.F., and Waterman, M.L. (2001). Beta-catenin-sensitive isoforms of lymphoid enhancer factor-1 are selectively expressed in colon cancer. Nature genetics *28*, 53-57.

Jensen, M., Hoerndli, F.J., Brockie, P.J., Wang, R., Johnson, E., Maxfield, D., Francis, M.M., Madsen, D.M., and Maricq, A.V. (2012). Wnt signaling regulates acetylcholine receptor translocation and synaptic plasticity in the adult nervous system. Cell *149*, 173-187.

Jho, E.H., Zhang, T., Domon, C., Joo, C.K., Freund, J.N., and Costantini, F. (2002). Wnt/beta-catenin/Tcf signaling induces the transcription of Axin2, a negative regulator of the signaling pathway. Molecular and cellular biology *22*, 1172-1183.

Ji, N., Middelkoop, T.C., Mentink, R.A., Betist, M.C., Tonegawa, S., Mooijman, D., Korswagen, H.C., and van Oudenaarden, A. (2013). Feedback control of gene expression variability in the Caenorhabditis elegans Wnt pathway. Cell *155*, 869-880.

Kamata, T., Katsube, K., Michikawa, M., Yamada, M., Takada, S., and Mizusawa, H. (2004). R-spondin, a novel gene with thrombospondin type 1 domain, was expressed in the dorsal neural tube and affected in Wnts mutants. Biochimica et biophysica acta *1676*, 51-62.

Keeble, T.R., Halford, M.M., Seaman, C., Kee, N., Macheda, M., Anderson, R.B., Stacker, S.A., and Cooper, H.M. (2006). The Wnt receptor Ryk is required for Wnt5a-mediated axon guidance on the contralateral side of the corpus callosum. The Journal of neuroscience : the official journal of the Society for Neuroscience *26*, 5840-5848.

Kikuchi, A., Yamamoto, H., and Sato, A. (2009). Selective activation mechanisms of Wnt signaling pathways. Trends in cell biology *19*, 119-129.

Korswagen, H.C. (2002). Canonical and non-canonical Wnt signaling pathways in Caenorhabditis elegans: variations on a common signaling theme. BioEssays : news and reviews in molecular, cellular and developmental biology *24*, 801-810.

Kuhl, M., Geis, K., Sheldahl, L.C., Pukrop, T., Moon, R.T., and Wedlich, D. (2001). Antagonistic regulation of convergent extension movements in Xenopus by Wnt/beta-catenin and Wnt/Ca2+ signaling. Mechanisms of development *106*, 61-76.

Lee, Y.N., Gao, Y., and Wang, H.Y. (2008). Differential mediation of the Wnt canonical pathway by mammalian Dishevelleds-1, -2, and -3. Cellular signalling *20*, 443-452.

Li, S., Esterberg, R., Lachance, V., Ren, D., Radde-Gallwitz, K., Chi, F., Parent, J.L., Fritz, A., and Chen, P. (2011). Rack1 is required for Vangl2 membrane localization and planar cell polarity signaling while attenuating canonical Wnt activity. Proceedings of the National Academy of Sciences of the United States of

America *108*, 2264-2269.

Lienkamp, S., Ganner, A., Boehlke, C., Schmidt, T., Arnold, S.J., Schafer, T., Romaker, D., Schuler, J., Hoff, S., Powelske, C., *et al.* (2010). Inversin relays Frizzled-8 signals to promote proximal pronephros development. Proceedings of the National Academy of Sciences of the United States of America *107*, 20388-20393.

Logan, C.Y., and Nusse, R. (2004). The Wnt signaling pathway in development and disease. Annual review of cell and developmental biology *20*, 781-810.

MacDonald, B.T., Tamai, K., and He, X. (2009). Wnt/beta-catenin signaling: components, mechanisms, and diseases. Developmental cell *17*, 9-26.

Mentink, R.A., Middelkoop, T.C., Rella, L., Ji, N., Chung, Y.T., Betist, M.C., van Oudenaarden, A., and Korswagen, H.C. (2014). Cell intrinsic modulation of Wnt signaling controls neuroblast migration in C. elegans. Developmental cell *in press*.

Mikels, A.J., and Nusse, R. (2006). Purified Wnt5a protein activates or inhibits beta-catenin-TCF signaling depending on receptor context. PLoS biology *4*, e115.

Monsalve, G.C., and Frand, A.R. (2012). Toward a unified model of developmental timing: A "molting" approach. Worm *1*, 221-230.

Moon, R.T., Campbell, R.M., Christian, J.L., McGrew, L.L., Shih, J., and Fraser, S. (1993). Xwnt-5A: a maternal Wnt that affects morphogenetic movements after overexpression in embryos of Xenopus laevis. Development *119*, 97-111.

Moon, R.T., and Shah, K. (2002). Developmental biology: signalling polarity. Nature *417*, 239-240.

Muller, H.A., Samanta, R., and Wieschaus, E. (1999). Wingless signaling in the Drosophila embryo: zygotic requirements and the role of the frizzled genes. Development *126*, 577-586.

Nair, G., Walton, T., Murray, J.I., and Raj, A. (2013). Gene transcription is coordinated with, but not dependent on, cell divisions during C. elegans embryonic fate specification. Development *140*, 3385-3394.

Nam, J.S., Turcotte, T.J., Smith, P.F., Choi, S., and Yoon, J.K. (2006). Mouse cristin/R-spondin family proteins are novel ligands for the Frizzled 8 and LRP6 receptors and activate beta-catenin-dependent gene expression. The Journal of biological chemistry *281*, 13247-13257.

Pan, C.L., Howell, J.E., Clark, S.G., Hilliard, M., Cordes, S., Bargmann, C.I., and Garriga, G. (2006). Multiple Wnts and frizzled receptors regulate anteriorly directed cell and growth cone migrations in Caenorhabditis elegans. Developmental cell *10*, 367-377.

Park, M., and Moon, R.T. (2002). The planar cell-polarity gene stbm regulates cell behaviour and cell fate in vertebrate embryos. Nature cell biology *4*, 20-25.

Raj, A., van den Bogaard, P., Rifkin, S.A., van Oudenaarden, A., and Tyagi, S. (2008). Imaging individual mRNA molecules using multiple singly labeled probes. Nature methods *5*, 877-879.

Rousset, R., Mack, J.A., Wharton, K.A., Jr., Axelrod, J.D., Cadigan, K.M., Fish, M.P., Nusse, R., and Scott, M.P. (2001). Naked cuticle targets dishevelled to antagonize Wnt signal transduction. Genes & development *15*, 658-671.

Sakane, H., Yamamoto, H., Matsumoto, S., Sato, A., and Kikuchi, A. (2012). Localization of glypican-4 in different membrane microdomains is involved in the regulation of Wnt signaling. Journal of cell science *125*, 449-460.

Sanchez-Alvarez, L., Visanuvimol, J., McEwan, A., Su, A., Imai, J.H., and Colavita, A. (2011). VANG-1 and PRKL-1 cooperate to negatively regulate neurite formation in Caenorhabditis elegans. PLoS genetics *7*, e1002257.

Sato, A., Yamamoto, H., Sakane, H., Koyama, H., and Kikuchi, A. (2010). Wnt5a regulates distinct signalling pathways by binding to Frizzled2. The EMBO journal *29*, 41-54.

Sawa, H., and Korswagen, H.C. (2013). Wnt signaling in *C. elegans*. WormBook : the online review of C elegans biology, 1-30.

Schwarz-Romond, T., Merrifield, C., Nichols, B.J., and Bienz, M. (2005). The Wnt signalling effector Dishevelled forms dynamic protein assemblies rather than stable associations with cytoplasmic vesicles. Journal of cell science *118*, 5269-5277.

Simons, M., Gloy, J., Ganner, A., Bullerkotte, A., Bashkurov, M., Kronig, C., Schermer, B., Benzing, T., Cabello, O.A., Jenny, A., *et al.* (2005). Inversin, the gene product mutated in nephronophthisis type II, functions as a molecular switch between Wnt signaling pathways. Nature genetics *37*, 537-543.

Smalley, M.J., Signoret, N., Robertson, D., Tilley, A., Hann, A., Ewan, K., Ding, Y., Paterson, H., and Dale, T.C. (2005). Dishevelled (Dvl-2) activates canonical Wnt signalling in the absence of cytoplasmic puncta. Journal of cell science *118*, 5279-5289.

Song, S., Zhang, B., Sun, H., Li, X., Xiang, Y., Liu, Z., Huang, X., and Ding, M. (2010). A Wnt-Frz/Ror-Dsh pathway regulates neurite outgrowth in Caenorhabditis elegans. PLoS genetics *6*.

Tada, M., and Smith, J.C. (2000). Xwnt11 is a target of Xenopus Brachyury: regulation of gastrulation movements via Dishevelled, but not through the canonical Wnt pathway. Development *127*, 2227-2238.

van Amerongen, R., Fuerer, C., Mizutani, M., and Nusse, R. (2012). Wnt5a can both activate and repress Wnt/beta-catenin signaling during mouse embryonic development. Developmental biology *369*, 101-114.

van Amerongen, R., and Nusse, R. (2009). Towards an integrated view of Wnt signaling in development. Development *136*, 3205-3214.

Wang, Y., Thekdi, N., Smallwood, P.M., Macke, J.P., and Nathans, J. (2002). Frizzled-3 is required for the development of major fiber tracts in the rostral CNS. The Journal of neuroscience : the official journal of the Society for Neuroscience *22*, 8563-8573.

Wang, Y., Zhang, J., Mori, S., and Nathans, J. (2006). Axonal growth and guidance defects in Frizzled3 knock-out mice: a comparison of diffusion tensor magnetic resonance imaging, neurofilament staining, and genetically directed cell labeling. The Journal of neuroscience : the official journal of the Society for Neuroscience *26*, 355-364.

Whangbo, J., and Kenyon, C. (1999). A Wnt signaling system that specifies two patterns of cell migration in C. elegans. Molecular cell *4*, 851-858.

Wharton, K.A., Jr. (2003). Runnin' with the Dvl: proteins that associate with Dsh/Dvl and their significance to Wnt signal transduction. Developmental biology *253*, 1-17.

Wong, H.C., Bourdelas, A., Krauss, A., Lee, H.J., Shao, Y., Wu, D., Mlodzik, M., Shi, D.L., and Zheng, J. (2003).

Direct binding of the PDZ domain of Dishevelled to a conserved internal sequence in the C-terminal region of Frizzled. Molecular cell *12*, 1251-1260.

Wong, H.C., Mao, J., Nguyen, J.T., Srinivas, S., Zhang, W., Liu, B., Li, L., Wu, D., and Zheng, J. (2000). Structural basis of the recognition of the dishevelled DEP domain in the Wnt signaling pathway. Nature structural biology *7*, 1178-1184.

Wu, X., Wang, J., Jiang, H., Hu, Q., Chen, J., Zhang, J., Zhu, R., Liu, W., and Li, B. (2014). Wnt3a activates beta1-integrin and regulates migration and adhesion of vascular smooth muscle cells. Molecular medicine reports *9*, 1159-1164.

Yan, D., Wallingford, J.B., Sun, T.Q., Nelson, A.M., Sakanaka, C., Reinhard, C., Harland, R.M., Fantl, W.J., and Williams, L.T. (2001). Cell autonomous regulation of multiple Dishevelled-dependent pathways by mammalian Nkd. Proceedings of the National Academy of Sciences of the United States of America *98*, 3802-3807.

Zecca, M., Basler, K., and Struhl, G. (1996). Direct and long-range action of a wingless morphogen gradient. Cell *87*, 833-844.

Zinovyeva, A.Y., and Forrester, W.C. (2005). The C. elegans Frizzled CFZ-2 is required for cell migration and interacts with multiple Wnt signaling pathways. Developmental biology *285*, 447-461.

Zinovyeva, A.Y., Yamamoto, Y., Sawa, H., and Forrester, W.C. (2008). Complex network of Wnt signaling regulates neuronal migrations during Caenorhabditis elegans development. Genetics *179*, 1357-1371.

Addendum

The Frizzled receptor *lin-17* may non-autonomously antagonize Wnt signaling through sequestration of the EGL-20/Wnt ligand

Remco A. Mentink and Hendrik C. Korswagen

Hubrecht Institute, Royal Netherlands Academy of Arts and Sciences and University Medical Center Utrecht, The Netherlands.

Abstract

In *C. elegans,* the migration of the Q neuroblast descendants is dependent on Wnt signaling through the EGL-20 Wnt ligand. EGL-20 is expressed in the animal posterior and forms a posterior to anterior secretion gradient. Previous studies have found that Wnt receptors are able to shape the Wnt gradient, presumably by binding and/or internalization of the Wnt ligand. Interestingly, we found that the mRNA expression pattern of the *lin-17*/*Fz* receptor coincides strongly with the extent of the EGL-20 secretion gradient, suggesting it may have a role in its spreading. Visualization of the EGL-20 gradient demonstrated that its intensity and range are extended in a *lin-17* mutant background, arguing for a role of *lin-17* in antagonizing *egl-20* signaling by acting as a Wnt sink. We propose that *C. elegans* may serve as a useful model system to study the role of Wnt receptors in shaping the Wnt gradient.

Introduction

The migration of the Q neuroblast descendants in *C. elegans* larvae serves as a powerful model system to study the effect of both canonical and non-canonical Wnt signaling pathways on cell migration. Immediately after hatching, two Q neuroblasts are located on the left (QL) and right (QR) lateral sides of the animal. After completion of their initial migration, posteriorly secreted EGL-20/Wnt activates a canonical Wnt/β-catenin pathway in QL, resulting in the expression of the hox gene *mab-5* and subsequent posterior migration of its descendants (QL.d), whereas the QR.d migrate anteriorly under the control of non-canonical Wnt signaling (Coudreuse et al., 2006; Harris et al., 1996; Ji et al., 2013; Korswagen et al., 2002; Korswagen et al., 2000; Maloof et al., 1999; Salser and Kenyon, 1992; Sulston and Horvitz, 1977; Zinovyeva et al., 2008). Failure to activate *mab-5* expression, such as in mutants for the canonical Wnt pathway, causes the QL.d to migrate anteriorly instead. An inherent difference in sensitivity to EGL-20 ensures that only QL activates the canonical Wnt pathway leading to *mab-5* expression and posterior migration (Whangbo and Kenyon, 1999). However, EGL-20 is not only involved in activation of canonical Wnt signaling in QL, but also controls the extent of anterior migration of the QR.d (Harris et al., 1996; Whangbo and Kenyon, 1999).

Previous studies have shown that the CAM-1/Ror2 receptor non-autonomously counteracts EGL-20 signaling in a variety of Wnt dependent developmental processes, including migration of the Q descendants (Forrester et al., 2004; Green et al., 2007; Kim and Forrester, 2003). It was suggested that CAM-1 might act as a sink for EGL-20, effectively lowering its signaling output (Green et al., 2007). Indeed, in an elegant study Modzelewska et al. showed that CAM-1, which is expressed on a posteriorly extended axon, originating from the CAN neuron, sequesters the EGL-20 ligand in discrete punctae (Modzelewska et al., 2013). Additionally, our findings presented in chapter 5 of this thesis demonstrated that the Frizzled receptors *mig-1, lin-17, mom-5* and *cfz-2* may also act non-autonomously in controlling the migration of HSN, ALM, CAN and BDU neurons during *C. elegans* embryogenesis.

We then noticed that the mostly posterior expression pattern of *lin-17* mRNA coincides very closely with the reported posterior to anterior EGL-20 secretion gradient (Coudreuse et al., 2006; Ji et al., 2013). LIN-17 functions, together with MIG-1/Fz, as a receptor for EGL-20 in QL to activate the canonical Wnt pathway that results in posterior migration (Forrester et al., 2004; Harris et al., 1996; Ji et al., 2013). However, *lin-17* mutants display a lowly penetrant QL.d reversal phenotype, which could hypothetically be due to removal of *lin-17* leading to increased EGL-20 levels, which may then in turn signal through the MIG-1 receptor to suppress the phenotype (Figure 1C). We therefore tested whether removal of *lin-17* would result in a more pronounced gradient of EGL-20.

Results and discussion

The EGL-20 secretion gradient can be visualized by immunostaining of a transgenic protein A tagged version of EGL-20, expressed from its own promoter (Coudreuse et al., 2006). Staining with a fluorescently coupled Igg antibody reveals a punctate expression pattern of the tagged EGL-20 protein, originating from the producing cells in the posterior and declining towards the anterior (Figure 1A). We compared the EGL-20 gradient in wild type animals to *lin-17* mutants and observed a more intense staining in the *lin-17* mutant

background (Figure 1A). Quantification of the fluorescent signal using a "Wormshop v2.0" MATLAB algorithm revealed that indeed a stronger signal is observed upon removal of *lin-17*, consistent with our hypothesis and suggesting that it could act as a sink for EGL-20, similar to CAM-1 (Figure 1B). Based on these results we predicted that exogenous expression of *lin-17* throughout the animal might result in ectopic EGL-20 sequestration and give rise to phenotypes associated with loss of *egl-20*. Indeed, expression of *lin-17* from the hypodermal *dpy-7* promoter in the *lin-17* mutant background resulted in an increased amount of QL.d reversals and shifted the position of the QR.d posteriorly (Figure 1C). Both these phenotypes can be correlated to lowered EGL-20 levels and confirm that LIN-17 can indeed act as a sink for EGL-20.

Remarkably, previous studies in *Drosophila* have shown that *Dfz2* exerts the opposite effect on levels of Wg, as it was shown to stabilize Wg upon overexpression, resulting in an extended Wg gradient (Cadigan et al., 1998). A later study showed that, contrary to expectations, a removal of *Dfz2* does not result in a reduced Wg gradient, but rather leads to increased extracellular levels of Wg as well (Han et al., 2005). This was shown to be due to loss of *Dfz2* leading to increased *Dlp* expression, a protein important for Wg spreading (Han et al., 2005). Furthermore, expression of *Dfz2* itself is negatively regulated by Wg signaling (Cadigan et al., 1998). These results argue that signaling feedback mechanisms may confound studying the effect of signal transduction receptors on spreading of their ligand. We propose that *C. elegans* may serve as a simplified model system to study the effect of Wnt receptors on Wnt gradient formation.

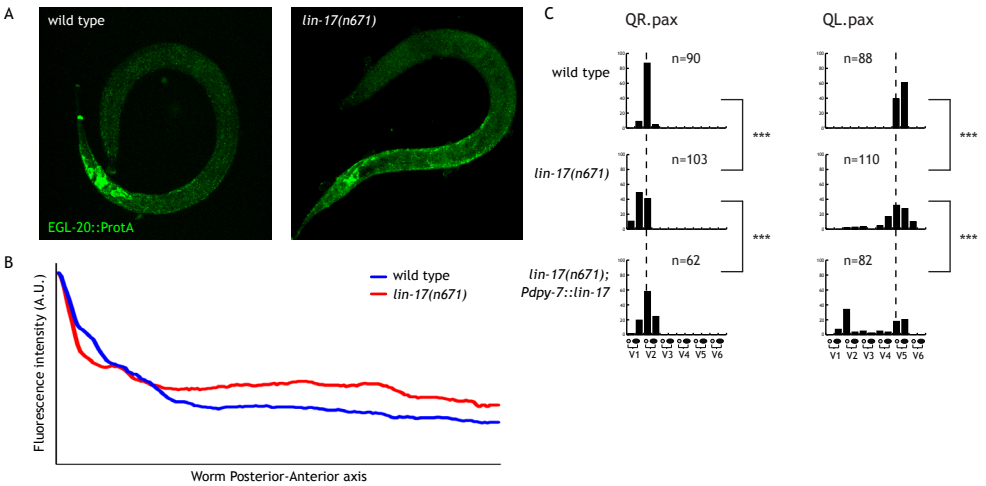

Figure 1. The Frizzled receptor *lin-17* dampens the activity of the Wnt signaling pathways controlling Q neuroblast migration by sequestering EGL-20/Wnt. (**A**) EGL-20::ProtA gradient (green) visualized in wild type and *lin-17* mutant animals by staining L1 larvae carrying the *hulS60* transgene with rabbit-anti-goat-Alexa647. (**B**) Quantification of the EGL-20::ProtA gradient along the anterior-posterior axis of the worm in wild type (blue) and *lin-17* mutant (red) animals. Each line shows the average fluorescence intensity quantified in 3 experiments, using n>10 worms per experiment. (**C**) Final positions of the Q cell descendants Q.pax with respect to the seam cells V1.a to V6.p (open circles indicate Vn.a and closed circles Vn.p cells, n>50 for all genotypes). Statistical significance was calculated using Fisher's Exact Test (*** p<0.0001). Dashed line indicates average wild type Q descendant final positions.

Experimental procedures

C. elegans strains and culture

General methods for *C. elegans* strain culture and maintenance were as previously described. Animals were cultured at 20°C using standard conditions (Lewis and Fleming, 1995). Bristol N2 was used as the wild type control. Mutant alleles and transgenes used in this study were: LGI: *lin-17(n671)*; LGV: *huIs60[Pegl-20::egl-20::ProtA; dpy-20(+)]*. Extrachromosomal transgenes used were: *huEx302, huEx303, huEx305, huEx306[Pdpy-7::lin-17::gfp; Pmyo-2::mtomato]*.

Molecular biology

The *lin-17* coding sequence was PCR amplified from total cDNA using primers containing attB1 and attB2 gateway recombination sites. The PCR fragment was then recombined with pDNR221 to yield a gateway entry vector. A 500 bp *dpy-7* promoter sequence was PCR amplified from a Pdpy::lin-6::mCherry vector (Wildwater, personal communication) using primers containing attB4 and attB1R gateway recombination sites. The PCR fragment was then recombined with pDNRP4-P1R to generate an entry clone. The final Pdpy-7::lin-17::gfp construct was generated by recombining both entry clones with a 3' gfp entry clone in the pCFJ150 expression vector. The constructs was injected at 5 ng/µl with 7 ng/µl co-injection marker and supplemented with pBluescriptII to 150 ng/µl. Injected animals were grown on GFP RNAi food to prevent transgene toxicity.

Scoring of Q descendant final positions, EGL-20::ProtA staining and microscopy

Final positions of Q cell descendants QR.pax and QL.pax were determined using DIC microscopy in late L1 larvae as previously described (Coudreuse et al., 2006). Staining of the EGL-20::ProtA gradient in animals carrying the *huIs60[Pegl-20::egl-20::protA; dpy-20(+)]* transgene was performed as previously described (Coudreuse et al., 2006). Z-stacks of 0.5µm slice thickness were acquired using a Leica TCS SPE confocal microscope (63x objective, 1x zoom, 59% 635 nm laser power). Images were obtained using LASAF software and subsequently analyzed using ImageJ v1.43. Maximum projections were made for each Z-stack and quantified using the "Wormshop v2.0" algorithm written in the MATLAB code. The antibody used was rabbit-anti-goat-Alexa647 (Life Technologies).

Statistical analysis

Statistical analysis of Q descendant position was performed using Fisher's exact test. A Monte Carlo approximation, iterated 10.000 times using SPSS version 20, was used to estimate significance. Results were considered statistically significant if $p<0.05$.

References

Cadigan, K.M., Fish, M.P., Rulifson, E.J., and Nusse, R. (1998). Wingless repression of Drosophila frizzled 2 expression shapes the Wingless morphogen gradient in the wing. Cell *93*, 767-777.

Coudreuse, D.Y., Roel, G., Betist, M.C., Destree, O., and Korswagen, H.C. (2006). Wnt gradient formation requires retromer function in Wnt-producing cells. Science *312*, 921-924.

Forrester, W.C., Kim, C., and Garriga, G. (2004). The Caenorhabditis elegans Ror RTK CAM-1 inhibits EGL-20/Wnt signaling in cell migration. Genetics *168*, 1951-1962.

Green, J.L., Inoue, T., and Sternberg, P.W. (2007). The C. elegans ROR receptor tyrosine kinase, CAM-1, non-autonomously inhibits the Wnt pathway. Development *134*, 4053-4062.

Han, C., Yan, D., Belenkaya, T.Y., and Lin, X. (2005). Drosophila glypicans Dally and Dally-like shape the extracellular Wingless morphogen gradient in the wing disc. Development *132*, 667-679.

Harris, J., Honigberg, L., Robinson, N., and Kenyon, C. (1996). Neuronal cell migration in C. elegans: regulation of Hox gene expression and cell position. Development *122*, 3117-3131.

Ji, N., Middelkoop, T.C., Mentink, R.A., Betist, M.C., Tonegawa, S., Mooijman, D., Korswagen, H.C., and van Oudenaarden, A. (2013). Feedback control of gene expression variability in the Caenorhabditis elegans Wnt pathway. Cell *155*, 869-880.

Kim, C., and Forrester, W.C. (2003). Functional analysis of the domains of the C elegans Ror receptor tyrosine kinase CAM-1. Developmental biology *264*, 376-390.

Korswagen, H.C., Coudreuse, D.Y., Betist, M.C., van de Water, S., Zivkovic, D., and Clevers, H.C. (2002). The Axin-like protein PRY-1 is a negative regulator of a canonical Wnt pathway in C. elegans. Genes & development *16*, 1291-1302.

Korswagen, H.C., Herman, M.A., and Clevers, H.C. (2000). Distinct beta-catenins mediate adhesion and signalling functions in C. elegans. Nature *406*, 527-532.

Lewis, J.A., and Fleming, J.T. (1995). Basic culture methods. Methods in cell biology *48*, 3-29.

Maloof, J.N., Whangbo, J., Harris, J.M., Jongeward, G.D., and Kenyon, C. (1999). A Wnt signaling pathway controls hox gene expression and neuroblast migration in C. elegans. Development *126*, 37-49.

Modzelewska, K., Lauritzen, A., Hasenoeder, S., Brown, L., Georgiou, J., and Moghal, N. (2013). Neurons refine the Caenorhabditis elegans body plan by directing axial patterning by Wnts. PLoS biology *11*, e1001465.

Salser, S.J., and Kenyon, C. (1992). Activation of a C. elegans Antennapedia homologue in migrating cells controls their direction of migration. Nature *355*, 255-258.

Sulston, J.E., and Horvitz, H.R. (1977). Post-embryonic cell lineages of the nematode, Caenorhabditis elegans. Developmental biology *56*, 110-156.

Whangbo, J., and Kenyon, C. (1999). A Wnt signaling system that specifies two patterns of cell migration in C. elegans. Molecular cell *4*, 851-858.

Zinovyeva, A.Y., Yamamoto, Y., Sawa, H., and Forrester, W.C. (2008). Complex network of Wnt signaling regulates neuronal migrations during Caenorhabditis elegans development. Genetics *179*, 1357-1371.

Addendum II

Nederlandse samenvatting
Dankwoord
Curriculum Vitae
List of scientific publications

Nederlandse samenvatting

Wnt signalering

Om tijdens de embryonale ontwikkeling vanuit een enkele eicel een compleet organisme te vormen zijn talloze mechanismen nodig, die cellen in staat stellen om alle individuele weefsels en organen op te bouwen. Cellen kunnen zich uiteindelijk specialiseren in een unieke rol, bijvoorbeeld als spier-, zenuw- of darmcel. Celdeling en het afsterven van cellen moet gecontroleerd worden om tot het juiste aantal cellen in een enkel weefsel te komen. Cellen kunnen zich polariseren en een verschil creëren tussen hun boven- en onderkant om bijvoorbeeld het grensgebied aan te geven tussen de buiten- en binnenkant van een orgaan.

In de kern van elke cel ligt een kopie van het erfelijke materiaal, het genoom, dat bestaat uit DNA. Dit enorme molecuul wordt gevormd uit een lange reeks van vier verschillende basen - A, T, C en G - welke coderen voor de grote variëteit aan eiwitten (in het menselijke genoom ongeveer 25.000 verschillende) die cellen gebruiken om alle processen die zij ondergaan, aan te sturen. Niet al het DNA codeert voor eiwitten en om deze uiteindelijk te produceren is nog een “tussenkopie” van een specifiek stuk DNA vereist, genaamd RNA. Dit fungeert als een soort negatief van het DNA en de uiteindelijke blauwdruk voor het eiwit. De productie van RNA vereist op zijn beurt ook weer allerlei verschillende eiwitten.

Individuele cellen in het lichaam maken veelvuldig gebruik van zogenaamde eiwit signaleringsroutes om elkaar specifieke informatie te sturen. Hierbij wordt vaak een eiwit gemaakt in een bepaalde cel, dat vervolgens uitgescheiden wordt en verderop in het lichaam kan binden aan een receptor eiwit dat zich bevindt op de oppervlakte van een andere cel. Dit zorgt voor een cascade aan reacties in de ontvangende cel en kan leiden tot bijvoorbeeld verhoogde celdeling, celspecialisatie of zelfs beweging van de cel.

Voor een van deze signaleringsroutes zijn de uitgescheiden Wnt eiwitten de drager van informatie en deze route staat dan ook bekend als Wnt signalering, welke vele verschillende functies vervult tijdens de embryonale ontwikkeling en in volwassenen. Wnt signalering is in volwassenen o.a. nodig om de hernieuwbare binnenlaag van de darmen steeds weer van nieuwe cellen te voorzien. Hierbij is het belangrijk dat er een juiste signaleringssterkte optreedt, omdat te actieve Wnt signalering kan leiden tot teveel celdeling en uiteindelijk de vorming van darmkanker. In het embryo is Wnt signalering o.a. bij de vorming van het centrale zenuwstelsel nodig voor de aanleg van de neurale buis, waarbij fouten in Wnt signalering uiteindelijk kunnen leiden tot een open ruggetje (spina bifida) bij de geborene. Verder speelt het een belangrijke rol bij de verplaatsing van zenuwcellen tijdens de ontwikkeling en bij het leggen van verbindingen tussen verschillende zenuwcellen door middel van dendrieten en axonen.

Om deze verschillende processen te sturen gebruiken Wnt eiwitten een tweetal belangrijke signaal transductie routes. Beide routes worden aangezet door binding van Wnt aan een receptor op het celoppervlak. De eerste route is afhankelijk van de activiteit van het eiwit ß-catenine, dat kan zorgen voor de productie van specifieke RNA moleculen (transcriptie). Deze RNA’s coderen vaak voor eiwitten die belangrijk zijn voor processen als celdeling of celspecialisatie. Het is tevens de route die belangrijk is bij de regulatie van celdeling in de volwassen darm. De tweede route is eigenlijk een verzameling aan verschillende routes, die verenigd worden door het feit dat ze juist geen gebruik maken van het eiwit ß-catenine. Belangrijke functies van deze routes zijn het reguleren van de polariteit en beweging van

cellen, processen die ook nodig zijn bij de vorming van het zenuwstelsel.

Caenorhabditis elegans en Q cel migratie

Een groot probleem in het onderzoek naar de rol van Wnt signalering bij de vorming van het zenuwstelsel van gewervelden is dat er vele verschillende Wnt eiwitten (19) en receptoren (10) worden gecodeerd in hun DNA. Dit maakt het moeilijk om te onderscheid te maken tussen de verschillende functies van elke eiwit.

Het is om deze reden dat in onze onderzoeksgroep de kleine (ongeveer 1 mm lange) nematode *Caenorhabditis elegans* gebruikt wordt als een vereenvoudigd systeem om de rol van Wnt signalering tijdens de ontwikkeling van het zenuwstelsel te bestuderen. *C. elegans* bestaat uit slechts 959 cellen, is volledig transparant, heeft een zeer korte levenscyclus en een klein genoom, waarin een bescheiden aantal van 5 Wnt eiwitten en 6 receptoren gecodeerd staan.

Voor mijn onderzoek heb ik de functie van Wnt signalering bij de beweging (migratie) van de QL en QR neuroblasten en hun dochtercellen (QL.d) tot in meer detail onderzocht. Wanneer de *C. elegans* larve uit het ei kruipt, liggen er twee neuroblasten aan zowel de linker- (QL) als de rechter- (QR) zijde van de worm, middenin een rij epithele huidcellen. Tijdens het eerste larvale stadium migreren beide cellen langs de lengteas van de worm, terwijl zij ook een aantal keer delen om uiteindelijk ieder een drietal neuronen te generen op verschillende plekken langs de lengteas. De QL.d migreren naar achteren onder invloed van een ß-catenine afhankelijke Wnt route, terwijl de QR.d naar voren migreren via een ß-catenine onafhankelijke Wnt route. De voorste dochtercel van beide Q neuroblasten (Qx.a) migreert de grootste afstand en ontwikkelt zich uiteindelijk aan beide uiteinden van de worm tot een zuurstof waarnemend neuron (QL.ap, oftewel PQR en QR.ap oftewel AQR). De achterste dochtercel (Qx.p) migreert een kleinere afstand en deelt uiteindelijk zo, om een interneuron (QL.pap, oftewel SDQL en QR.pap, oftewel SDQR) en een motorneuron (QL. paa, oftewel PVM en QR.paa, oftewel AVM) aan beide uiteinden van de worm te vormen. Ik heb vooral de migratie van de Qx.p dochtercellen bestudeerd, omdat de Qx.a dochtercellen te midden van vele andere neuronen migreren, waardoor zij minder goed te zien zijn.

Samenvatting van de verschillende hoofdstukken

Mijn onderzoek naar Q cel migratie in *C. elegans* is uiteindelijk onder te verdelen in enkele hoofdlijnen, die elk in hun eigen experimentele hoofdstuk beschreven staan in dit proefschrift.

In **Hoofdstuk 2** beschrijf ik hoe drie verschillende Wnt signalering routes na elkaar nodig zijn om de voorwaartse migratie van de QR.d zeer precies te sturen. Voor de eerste, lange afstand, fase van de migratie van QR.p zijn twee ß-catenine onafhankelijke Wnt signaleringsroutes vereist, via de receptoren MOM-5/Frizzled en CAM-1/Ror. Deze reguleren in parallel respectievelijk de snelheid en de polariteit van de migrerende cel en in hun afwezigheid migreert de QR.p cel dan ook significant minder ver. Vervolgens deelt de QR.p cel en vormt de QR.pa cel, welke slechts een korte afstand naar voren migreert. In deze cel is een ß-catenine afhankelijke Wnt route via de receptoren MIG-1/Fz en LIN-17/Fz nodig om de cel op tijd te stoppen, aangezien in hun afwezigheid de QR.pa cel te ver door migreert. Tenslotte deelt de QR.pa cel in twee cellen (QR.paa en QR.pap), die nu niet meer langs de lengteas, maar langs de dorsoventrale (rug-buik) as migreren. Om dit laatste deel van de migratie te reguleren, zijn de eiwitten VANG-1/Vangl en PRKL-1/Prickle nodig. Deze

eiwitten zijn verwant aan eiwitten die in fruitvliegen betrokken zijn bij een ß-catenine onafhankelijke Wnt route die de groeirichting van vleugelhaartjes controleert. Hier lijken ze dus echter celmigratie, een heel ander proces, te sturen.

Een belangrijke ontdekking is dat de QR.pa cel voor de overgang van de MOM-5 en CAM-1 Wnt routes naar de ß-catenine afhankelijke Wnt route de transcriptie van *mig-1/Fz* mRNA sterkt verhoogt via een tijdsgebonden mechanisme. Dit laat zien dat de cel zelf de overgang van de ene naar de andere signaleringsroute kan regelen, door middel van het tot expressie brengen van een andere receptor. Dit is een nieuw inzicht dat kan leiden tot een beter begrip van Wnt gereguleerde celmigratie in andere systemen.

Hoofdstuk 3 laat zien dat VANG-1, naast de rol die het speelt tijdens de dorsoventrale migratie van QR.paa en QR.pap, ook een functie heeft tijdens de lange afstand migratie van de QR.p cel. VANG-1 is nodig om de ß-catenine afhankelijke Wnt route die zorgt voor achterwaartse migratie in de QL.d cellen, te blokkeren in de QR.p cel. Om ectopische activatie van ß-catenine afhankelijke Wnt signalering in de QR.p cel te krijgen (en dus achterwaartse migratie van de QR.d), moeten zowel VANG-1 als SFRP-1, een uitgescheiden eiwit dat Wnt signalering remt, uitgeschakeld worden. Dit duidt erop dat deze functie van VANG-1 waarschijnlijk niet zijn belangrijkste is, maar meer geldt als een soort buffermechanisme voor wanneer andere mechanismen wegvallen.

De mogelijkheid van Vangl-achtige eiwitten om ß-catenine afhankelijke Wnt signalering te remmen, wordt al een tijd vermoed. In dit hoofdstuk laat ik duidelijk zien dat in ieder geval de *C. elegans* versie van dit eiwit, VANG-1, zeker deze eigenschap heeft.

Hoofdstuk 4 betreft, in tegenstelling tot de vorige twee hoofdstukken die vrijwel uitsluitend QR.d migratie bestuderen, het proces van QL.d migratie. Voor de activatie van het ß-catenine afhankelijke Wnt signaal en achterwaartse migratie van de QL.d is het nodig dat het Wnt eiwit EGL-20 gebonden wordt door de MIG-1 en LIN-17 receptoren. Hier laten we zien dat de activatie van het Wnt signaal niet alleen leidt tot transcriptie van *mab-5/Hox* mRNA, de translatie waarvan nodig is voor achterwaartse migratie. Het leidt tevens tot transcriptionele terugkoppeling op beide receptoren, die op hun beurt weer terugkoppelen op de transcriptie van *mab-5* mRNA. Dit alles vormt samen een transcriptioneel netwerk van zowel positieve als negatieve terugkoppeling, dat ervoor zorgt dat er altijd precies genoeg *mab-5* mRNA geproduceerd wordt. Waneer delen van het netwerk weggehaald worden, dan zal een deel van de QL.d cellen niet achterwaarts migreren, omdat zij onvoldoende *mab-5* transcriberen. Door te modelleren laten we zien dat de bijdrage van elke component aan het netwerk kwantitatief te bepalen is en dat alleen het volledige netwerk tot een robuust aantal *mab-5* transcripten zal leiden.

In het laatste experimentele **Hoofdstuk 5** laat ik zien dat Wnt signalering ook de migratie van enkele andere neuronen (de CAN, HSN, ALM en BDU neuronen) tijdens embryogenese stuurt. Door te kijken naar de expressie van de vier Frizzled receptoren en de enkele Ror receptor, wordt duidelijk dat elk van deze cellen zijn eigen “set” aan Wnt receptoren bevat. Dit komt vrij goed overeen met het feit dat elke cel andere receptoren nodig heeft voor zijn migratie, wanneer we het fenotype van receptor mutanten beschouwen. Verder blijkt dat de Wnt receptoren niet alleen nodig zijn in de migrerende neuronen zelf (cel autonoom), maar ook in andere celtypes (cel niet-autonoom).

Hoofdstuk 6 tenslotte beschrijft het protocol dat we gebruikt hebben om “single molecule mRNA fluorescence *in situ* hybridization” uit te voeren. Dit is een methode waarmee men enkele mRNA moleculen een detecteerbaar fluorescent signaal kan laten uitzenden. Oftewel,

het wordt mogelijk om enkele mRNA moleculen te tellen in elke cel. Deze methode is van groot belang geweest bij het tot stand komen van elk van de experimentele hoofdstukken beschreven in dit proefschrift.

Met ons onderzoek in *C. elegans* hebben we een aantal nieuwe inzichten verkregen die zouden kunnen helpen bij het begrijpen van vergelijkbare processen in mensen. Celmigratie is in mensen niet alleen van belang bij bijvoorbeeld de vorming van het centrale zenuwstelsel, maar speelt ook een rol bij de vorming van metastases vanuit primaire tumoren. Onze resultaten vertellen meer over hoe Wnt eiwitten celmigratie reguleren en kunnen misschien helpen bij het herkennen van aangeboren afwijkingen aan het zenuwstelsel of bij het voorkomen van kanker.

Dankwoord

Na bijna 5 jaar is dan eindelijk mijn proefschrift voltooid. Het waren een vijftal bevlogen jaren en, zoals velen mij al hadden benadrukt toen ik aan mijn promotietraject begon, zijn ze werkelijk omgevlogen. Ik heb zeer veel geleerd en ben gegroeid als mens en wetenschapper. Ik ben zeker ook heel blij met het uiteindelijke resultaat, maar dit alles was nooit tot stand gekomen zonder de directe en indirecte bijdragen van vele mensen om mij heen. Vandaar dat ik hier dan ook de ruimte neem om deze mensen te bedanken.

Ik wil graag beginnen met Rik te bedanken, mijn directe begeleider, dat ik mocht werken in je lab aan het fascinerende onderwerp van cel migratie in *C. elegans*. Ik heb erg veel van je geleerd over dit onderwerp, maar ik ben ook gegroeid als wetenschapper door je begeleiding, onder andere ook doordat je iedereen in je lab altijd veel vrijheid gunt. Ook heb ik veel opgestoken op het gebied van wetenschappelijk tekstschrijven en presenteren; een tekst of presentatie is eigenlijk nooit helemaal af. Verder wil ik je bedanken dat ik een flink aantal congressen heb kunnen bezoeken, onder andere in Los Angeles. Ik ben ervan overtuigd dat ik de perfecte bagage heb meegekregen voor mijn verdere carrière! Door de samenwerking de je had opgezet met Alexander hebben we grote stappen kunnen zetten in ons wormenonderzoek. I would like to thank Alexander and Ni Ji for a great experience and collaboration that played a big part in most, if not all, of the research written in this thesis.

Dan wil ik natuurlijk de andere leden die het Korswagen lab door de jaren heen gekend heeft bedanken: Marco, Reinoud, Teije en Martin, met jullie was het vaak goed mogelijk om even afleiding van het werk te vinden in iets luchtigs, er is een enorme hoeveelheid koffie doorheen gegaan! Martin en (in het bijzonder) Teije wil ik ook bedanken voor het aanbieden van een slaapplaats voor wanneer er geen trein meer terug naar Arnhem ging (geweldig, die strenge winters ;-)) of wanneer ik toch wel graag dat feestje wilde meemaken. Teije, ook bedankt voor al onze experimentele samenwerkingen en de leuke ervaringen op alle meetings waar we samen naar toe zijn geweest. Reinoud, je hebt me vaak geholpen met celkweek experimenten, bedankt voor al je lessen en tevens de vele levensfilosofieën die je gedeeld hebt. Marco, bedankt voor al die vroege ochtenden in het lab die we samen hebben doorgebracht en al je wormenwijsheid. Ik vind het echt leuk dat je mijn paranimf wil zijn! Chung en Niels, jullie waren allebei geweldige studenten waar ik graag mee heb samen gewerkt. Jullie hebben uiteindelijk mooie projecten afgeleverd, waar ik en het lab zeker mee verder konden! Magdalena, when I started you were the experienced postdoc and I was happy to learn a lot from you. Annabel en Sophie, jullie brachten een hoop licht in onze donkere ˝mancave˝, veel dank daarvoor! Lorenzo and Euclides, I'm sure you guys will do great and discover amazing things about our mysterious *C. elegans* and its enigmatic Q cells. I really enjoyed our trip to the worm meeting in Berlin.

Niet alleen collega's van het Hubrecht hebben een bijdrage geleverd aan de bewerkstelliging van dit boekje. Ik wil graag ook mijn vriendengroep uit (oorspronkelijk) Apeldoorn bedanken. Ook al wonen we allemaal niet meer in de buurt, onze online multiplayersessies in het weekend waren een welkome afwisseling! En wanneer we dan toch wel bij elkaar komen, is het er niet minder gezellig om! Jorrit, Alexander, Stefan en Michiel, bedankt voor alle "dude" middagen en avonden waarin vele kaarten zijn gelegd, characters gebouwd, films

en café's bezocht en gewoon lol gemaakt! Tevens wil ik mijn studie vrienden uit Wageningen bedanken. Pascal, Marre en Leon, bedankt voor alle nerdkennis en de (soms erg lange) spelletjesavonden. Leon, je vertelde dat je het naar je zin hebt in Australië, dat klinkt helemaal goed! Pascal en Marre, onze trip naar Graspop dit jaar was zeker voor herhaling vatbaar!

Als laatste wil ik natuurlijk ook nog mijn familie bedanken. Ruud en Dinie, pa en ma, jullie hebben me altijd vrijgelaten in al mijn keuzes en zonder jullie onvoorwaardelijke steun had ik hier nu niet gezeten, bedankt daarvoor! Thomas en Pauliene, Laura en David, ook jullie ontzettend bedankt voor alle interesse en gezelligheid. Thomas, hartstikke leuk dat je mijn paranimf wil zijn! En natuurlijk wil ik ook mijn schoonfamilie niet vergeten: Ineke, Theo, Rob, Marloes, Aerent en Helle, bedankt voor alle gezellige uitjes en Sinterklazen.

Ten slotte kan ik natuurlijk één persoon al helemaal niet vergeten: Eline, jij bent de afgelopen jaren absoluut mijn grootste steun en toeverlaat geweest. Ik heb van jou ontzettend veel geleerd en ben daardoor een beter mens geworden. Ontzettend bedankt daarvoor en ik voorzie voor ons nog vele mooie jaren in de toekomst!

Curriculum Vitae

Remco Mentink is geboren op 10 februari 1986 te Apeldoorn. Hij heeft in 2004 zijn VWO voltooid aan het Stedelijk Gymnasium Apeldoorn en is vervolgens Moleculaire (Levens) Wetenschappen gaan studeren in Wageningen. Tijdens zijn master heeft hij gedurende een periode van anderhalf jaar twee afstudeervakken en een stage van elk zes maanden voltooid. Zijn eerste afstudeervak betrof de studie van receptor kinase interacties in *Arabidopsis* protoplasten in het Biochemie laboratorium te Wageningen onder begeleiding van dr. Jan Willem Borst en prof. dr. Sacco de Vries. Daarna heeft hij tijdens zijn tweede afstudeervak gewerkt aan de purificatie van glycopeptiden uit *Arabidopsis* in de Planten Fysiologie groep van prof. dr. Sander van der Krol, tevens in Wageningen. Zijn stage vond plaats in het Cancer Research UK instituut in Cambridge, waar hij onder begeleiding van Esther Arwert en prof. dr. Fiona Watt het mechanisme van papilloma vorming in de huid van een transgene muis bestudeerde. In 2009 studeerde hij met de specialisatie “Biological Chemistry” af aan de Wageningen Universiteit en is hij begonnen aan zijn promotietraject in de groep van prof. dr. Rik Korswagen in het Hubrecht Instituut te Utrecht. De resultaten van zijn promotieonderzoek staan beschreven in dit proefschrift.

List of scientific publications

Mentink RA, Betist MC, Korswagen HC. *The planar cell polarity protein VANG-1/Vangl negatively regulates β-catenin dependent Wnt signaling in C. elegans.* Manuscript submitted.

Mentink RA, Middelkoop TC, Ji N, Tang CY, Betist MC, van Oudenaarden A, Korswagen HC. *Cell intrinsic modulation of Wnt signaling controls neuroblast migration in C. elegans.* Developmental Cell. *in press*

Mentink RA*, Ji N*, van Oudenaarden A, Korswagen HC. *Quantitative single molecule mRNA fluorescent in situ hybridization in C. elegans.* Neuromethods. *in press*

Bhambhani C, Ravindranath AJ, **Mentink RA**, Chang MV, Betist MC, Yang YX, Koushika SP, Korswagen HC, Cadigan KM. *Distinct DNA binding sites contribute to the TCF transcriptional switch in C. elegans and Drosophila.* PLoS Genet. 2014 Feb 6;10(2):e1004133

Ji N*, Middelkoop TC*, **Mentink RA**, Betist MC, Tonegawa S, Mooijman D, Korswagen HC, van Oudenaarden A. *Feedback control of gene expression variability in the Caenorhabditis elegans Wnt pathway.* Cell. 2013 Nov 7;155(4):869-80

Song W, **Mentink RA**, Henquet MG, Cordewener JH, van Dijk AD, Bosch D, America AH, van der Krol AR. *N-glycan occupancy of Arabidopsis N-glycoproteins.* J Proteomics. 2013 Nov 20;93:343-55.

Tan RZ, Ji N, **Mentink RA**, Korswagen HC, van Oudenaarden A. *Deconvolving the roles of Wnt ligands and receptors in sensing and amplification.* Mol Syst Biol. 2013 Jan 8;9(1):631.

Arwert EN*, **Mentink RA***, Driskell RR, Hoste E, Goldie SJ, Quist S, Watt FM. *Upregulation of CD26 expression in epithelial cells and stromal cells during wound-induced skin tumour formation.* Oncogene. 2012 Feb 23;31(8):992-1000

Song W, Henquet MG, **Mentink RA**, van Dijk AJ, Cordewener JH, Bosch D, America AH, van der Krol AR. *N-glycoproteomics in plants: perspectives and challenges.* J Proteomics. 2011 Aug 12;74(8):1463-74

*These authors contributed equally to this work.